

Stochastic Framework for Catchment-Scale Reactive Transport Simulations

Dissertation

der Mathematisch-Naturwissenschaftlichen Fakultät

der Eberhard Karls Universität Tübingen

zur Erlangung des Grades eines

Doktors der Naturwissenschaften

(Dr. rer. nat.)

vorgelegt von

Matthias Loschko

aus

Herrenberg

Tübingen

2018

Gedruckt mit der Genehmigung der Mathematisch-Naturwissenschaftlichen Fakultät der Eberhard Karls Universität Tübingen.

Tag der mündlichen Qualifikation:	24.08.2018
Dekan:	Prof. Dr. Wolfgang Rosenstiel
1. Berichterstatter:	Prof. Dr.-Ing. Olaf A. Cirpka
2. Berichterstatter:	Dr.-Ing. Thomas Wöhling
3. Berichterstatter:	Prof. Dr. David L. Rudolph

Abstract

Quantitative understanding of pollutant fluxes from diffuse sources from the land surface and turnover of pollutants at catchment scale requires process-based numerical models that can explain observed time series of heads, fluxes, and concentrations under current conditions and predict future states under changing conditions. The uncertainty of forcing, parameters, and conceptual assumptions as well as the unresolved internal variability entails a stochastic framework, predicting probabilities of reactive-species concentrations rather than deterministically derived concentration values. Due to the high computational effort, such evaluations cannot be done with a fully coupled, multi-dimensional, spatially explicit reactive-transport model overarching both the surface and subsurface of the hydrological system. Conceptual simplifications are needed, keeping spatially explicit calculations whenever needed and computationally manageable, but simplifying reactive-transport computations without sacrificing mechanistic system understanding.

This dissertation presents a probabilistic modeling approach to assess metrics of water quality at catchment scale. The approach expresses a paradigm shift from deterministic to probabilistic models even for complex (i.e. highly heterogeneous) reactive-transport systems. The reactive transport description is based on a travel-time formulation. However, the framework presented in this thesis goes beyond considering exclusively travel- or exposure times because it takes the reactive properties of the aquifers matrix into account. In doing so, a reactivity-weighted travel-time, the so called cumulative relative reactivity, replaces the travel time in the reactive transport equations in a spatially non-explicit framework. Numerical methods that require solving partial differential equations for reactive transport become redundant. The computational effort as well as the computational time are strikingly reduced, such that a stochastic framework using Monte Carlo simulations becomes feasible. The uncertain knowledge about the aquifer geometry, internal structures, chemical inputs or land use can be accounted for [Loschko *et al.*, 2016].

The modeling framework is extended to account for the decreasing reaction potential of the aquifer, namely the steady decrease of electron donors in the matrix as a result of usage by (bio)chemical

reactions. By introducing travel-time increments and updating the concentrations of reactants for every increment, the spatially explicit decreasing reaction potential can be implemented into the spatially non-explicit framework of cumulative relative reactivity [Loschko *et al.*, 2018a]. Finally, the cumulative reaction potential helps to predict the breakthrough of contaminants at a receptor, such as a pumping well, once the reaction potential of the aquifer is used up [Loschko *et al.*, 2018b].

The methods derived in this thesis help to better understand pollutant fluxes and turnover at the catchment scale and to quantify the remaining time of the decreasing reaction potential of an aquifer.

Kurzfassung

Das quantitative Verständnis von Schadstoffflüssen aus diffusen Eintragsquellen von der Landoberfläche und der Umsatz von Schadstoffen im Einzugsgebietsmaßstab erfordern prozessorientierte numerische Modelle, die die beobachteten Zeitreihen von Grundwasserständen, Stoffflüssen und Konzentrationen unter den aktuellen Bedingungen beschreiben und zukünftige Zustände unter sich ändernden Bedingungen vorhersagen können. Die Unsicherheiten in Bezug auf die verwendeten Parameter und konzeptionellen Annahmen, sowie die nicht aufgelöste interne Variabilität, erfordert eine probabilistische Betrachtungsweise, welche Wahrscheinlichkeitsverteilungen von reaktiven Stoffkonzentrationen vorhersagt, anstatt einzelner deterministisch hergeleiteter Konzentrationswerte. Aufgrund des hohen Rechenaufwandes können solche Auswertungen nicht mit einem vollständig gekoppelten, mehrdimensionalen, räumlich expliziten reaktiven Transportmodell durchgeführt werden, welches alle Kompartimente umfasst. Konzeptionelle Vereinfachungen sind erforderlich, die räumlich explizite Berechnungen verwenden wann immer dies nötig und rechnerisch umsetzbar ist, aber die reaktive Transportberechnung vereinfachen, ohne dabei das mechanistische Systemverständnis zu opfern.

Die vorliegende Dissertation hat zum Ziel, einen probabilistischen Modellierungsansatz zu entwickeln, um die Wasserqualität im Einzugsgebietsmaßstab zu quantifizieren. Der Ansatz führt zu einem Paradigmenwechsel von deterministischen hin zu probabilistischen Modellen, auch für komplexe reaktive Transportsysteme (z.B. solche mit einer hohen Heterogenität). Der reaktive Transport basiert dabei auf einer Fließzeitformulierung. Der Ansatz in dieser Arbeit geht jedoch über die Betrachtung von Fließ- beziehungsweise Expositionszeiten hinaus, indem die reaktiven Eigenschaften des Grundwasserleiters mit berücksichtigt werden. Eine reaktivitätsgewichtete Fließzeit, die so genannte kumulative relative Reaktivität, ersetzt die Fließzeit in den reaktiven Transportgleichungen in einem räumlich nicht expliziten Ansatz. Numerische Methoden, die das Lösen partieller Differentialgleichungen für den reaktiven Stofftransport erfordern, werden überflüssig. Der rechnerische Aufwand, sowie die Rechenzeit sind deutlich geringer. Ein

stochastischer Ansatz unter Verwendung von Monte-Carlo-Simulationen wird möglich. Die Unsicherheiten bezüglich der Geometrie des Grundwasserleiters, der internen Struktur, des Stoffeintrags sowie der Landnutzung können berücksichtigt werden [Loschko *et al.*, 2016].

Der Ansatz wird erweitert, indem das stetig abnehmende Reaktionspotential des Grundwasserleiters, namentlich die Reduktion eines Elektronendonators in der Matrix aufgrund (bio)chemischer Reaktionen, berücksichtigt wird. Durch die Einführung von Fließzeitinkrementen und der Aktualisierung der Stoffkonzentrationen für jedes Inkrement, kann das räumlich explizit abnehmende Reaktionspotential in den räumlich nicht expliziten Ansatz der kumulativen relativen Reaktivität aufgenommen werden [Loschko *et al.*, 2018a]. Schließlich hilft das kumulative Reaktionspotential, den Durchbruch von Kontaminationen an einem Rezeptor, z. B. einem Pumpbrunnen, vorherzusagen, sobald das Reaktionspotential des Grundwasserleiters aufgebraucht ist [Loschko *et al.*, 2018b].

Die Methoden, die in dieser Dissertation hergeleitet werden, helfen dabei, ein besseres Verständnis von Schadstoffflüssen und deren Umsatz im Einzugsgebietsmaßstab zu erhalten, sowie das mit der Zeit nachlassende Reaktionspotential eines Grundwasserleiters zu quantifizieren.

Acknowledgments

There are a few persons I would like to thank. Without them this thesis wouldn't have been possible.

- My supervisor Olaf Cirpka who besides his busy schedule always had time for meetings. His infectious enthusiasm and his great ideas are part of this work.
- My co-supervisor Thomas (Eddy) Wöhling who was always available, either in Tübingen, Dresden, or the other side of the world.
- My co-supervisor David Rudolph for hosting me in Waterloo and many valuable meetings in person and on Skype. His more practical point of view gave me many insights and helped to improve this work.
- All colleagues from the (I)RTG and Keplerstraße 17. Thanks for your help and the good times in the office, and outside the office. And maybe I was able to infect some of you with the VfB virus.
- Monika Jekelius and all the administrative staff of Hölderlinstraße 12 for helping me to not get lost in the jungle of German bureaucracy.
- The German Research Foundation (DFG) for funding this work within the research training group “Integrated Hydrosystem Modeling”.
- All colleagues at BoSS Consult for giving me the opportunity to finish the thesis.
- My family that was often uncertain on what I am actually doing all day but nonetheless supported me all the time. And last, but definitely not least, Denise. Danke für deine uneingeschränkte Unterstützung!

Contents

List of Figures	xii
List of Tables	xiv
List of Acronyms	xv
1 Introduction	1
2 State of the Art	4
2.1 Reactive Transport Modeling at the Catchment-Scale	4
2.2 Stochastic Methods for Subsurface Characterization	8
2.3 Denitrification	9
2.3.1 Factors controlling denitrification	10
2.3.2 The Role of Organic Carbon in Denitrification	12
3 Objectives & Contributions	15
4 General Concept	18
4.1 Cumulative Relative Reactivity	18
4.2 Decreasing Reaction Potential	21
4.3 Cumulative Reaction Potential	22
5 Test of Approaches	24
5.1 Numerical Implementation	25
5.2 Cumulative Relative Reactivity: Test of Approaches	28
5.2.1 Two-Dimensional Benchmark Test on the Validity of the Cumulative Relative Reactivity	28

5.2.2	Three-Dimensional Test Case on the Applicability of the Cumulative Relative Reactivity	32
5.3	Decreasing Reaction Potential: Test of Approaches	38
5.3.1	One-Dimensional Benchmark Test on the Relation between Relative Reactivity and NOM	38
5.3.2	Two-Dimensional Benchmark Test on the Validity of the Decreasing Reaction Potential	43
5.3.3	Three-Dimensional Test Case on the Applicability of the Decreasing Reaction Potential	46
5.4	Cumulative Reaction Potential: Test of Approaches	52
5.4.1	Two-Dimensional Benchmark Test on the Validity of the Cumulative Reaction Potential	53
6	Discussion	57
6.1	Cumulative Relative Reactivity	58
6.2	Decreasing Reaction Potential	59
6.3	Cumulative Reaction Potential	61
7	Conclusions and Outlook	63
	Bibliography	65
	List of Publications	76
	Publications	77

List of Figures

2.1	Schematic figure of aerobic and anaerobic zone in an aquifer with natural denitrification potential.	12
2.2	Conceptual model of oxidants and reductants in water-filled pore-spaces of an aquifer.	14
4.1	Comparison of two contamination scenarios with contamination input at the land surface.	19
5.1	Schematic code procedure of the three-dimensional test cases.	26
5.2	Comparison of the run-time of 3-D steady state particle tracking simulations on the Central Processing Unit and the Graphical Processing Unit.	28
5.3	Hydraulic conductivity, relative reactivity, and flow net of the two-dimensional test case n the validity of the cumulative relative reactivity.	29
5.4	Comparison of the spatially explicit model results and the corresponding one-dimensional model results mapped on the 2-D domain for the cumulative relative reactivity.	31
5.5	Schematic plan view and side view of the three-dimensional test case to test the applicability of the concept of cumulative relative reactivity.	33
5.6	Relative Reactivity of the three-dimensional test case of cumulative relative reactivity.	34
5.7	Cumulative relative reactivity and steady-state concentration distribution of nitrate and dissolved oxygen for the three-dimensional test case on the applicability of the cumulative relative reactivity.	37
5.8	Relationship between natural-organic-matter concentration and relative reactivity.	42
5.9	Two-dimensional test case on the validity of the decreasing reaction potential. .	44
5.10	Comparison of the two-dimensional test case on the validity of the decreasing reaction potential.	45

List of Figures

5.11 Schematic plan view and side view of the three-dimensional test case to test the applicability of the decreasing denitrification potential.	47
5.12 Parameter distribution in a single realization of the three-dimensional test case on the applicability of the decreasing reaction potential.	48
5.13 Length profiles of concentrations along a single streamline for the three-dimensional test case on the applicability of the decreasing reaction potential. .	52
5.14 Two-dimensional test case of the validity of the cumulative reaction potential. .	54
5.15 Breakthrough curves of nitrate and oxygen of the spatially explicit model. . . .	56
5.16 Cumulative distribution functions travel time, concentration of NOM, and cumulative reaction potential.	56

List of Tables

6.1 Comparison between state of the art reactive transport models on the catchment-scale and the concept of cumulative relative reactivity. 57

List of Acronyms

cdf	Cumulative Density Function
CPU	Central Processing Unit
CUDA	Compute Unified Device Architecture
DO	Dissolved Oxygen
DOC	Dissolved Organic Carbon
GPU	Graphics Processing Unit
MC	Monte Carlo
NOM	Natural Organic Matter
OC	Organic Carbon
pde	Partial Differential Equation
pdf	Probability Density Function

1 Introduction

Groundwater is an indispensable resource for public drinking water. Up to 70% of the total amount of drinking water in Germany is produced from groundwater and natural spring water. Some federal states even depend completely on the supply of groundwater [*Bundesministerium für Umwelt, Naturschutz und Reaktorsicherheit*, 2008]. These numbers underline the importance of groundwater as water resource. An operative water supply system would not be possible without groundwater. It is inevitable to protect and preserve groundwater resources. However, intensive agriculture, growing industry, denser settlement areas and expansion of infrastructure threaten the quality of groundwater resources. Especially with the intensification of agriculture in the 1960s and 1970s, the total exposure of groundwater to agricultural contaminants has increased [*Galloway et al.*, 2004]. Of national and international concern is the increase in nitrogen load to aquifers due to the enhanced use of mineral fertilizers and manure [*Bouraoui et al.*, 2011]. Excess nitrate and other fertilizers and nutrients, which are not taken up by the plants, lost through volatilization or removed through runoff of surface water, is transported with the infiltrating water from the root zone into the saturated zone and may reach the drinking water wells of water suppliers.

Even though there are numerous laws and regulations concerning the protection of groundwater resources like the European Framework for Community Action in the Field of Water Policy and the Directive on Protection of Groundwater against Pollution and Deterioration [*European Union*, 2000, 2007], the leaching of pollutants such as nitrate into the subsurface can not be fully prevented or prohibited. Nitrate concentrations in groundwater recharge have remained at elevated levels in regions of intensive agriculture worldwide [*Strebel et al.*, 1989; *Pacheco et al.*, 2001; *Wakida and Lerner*, 2005]. In Germany more than 14 percent of all groundwater monitoring wells indicate a nitrate concentration above the drinking water standard of 50 mg/L total nitrate [*Bundesministerium für Umwelt, Naturschutz und Reaktorsicherheit*, 2013]. Nonetheless, the nitrate concentrations in pumping wells and also monitoring wells have often not increased

to the same extent as the concentrations in groundwater recharge. However, other substances originating from artificial fertilizers (e.g., chloride) were found in those wells which indicates an anthropogenic influence [Wisotzky, 2012]. This demonstrates that some aquifers naturally degrade and transform nitrate by denitrification.

Numerical models can help to quantify the fate of pollutants in the subsurface and to quantify denitrification processes. As many agricultural pollutants are introduced over a large area and are transported over long distances, the analysis has to be done on the catchment-scale, which is also relevant for management practices. For reactive transport on the catchment-scale it is a well-known conceptual and computational challenge to deal with this spatial variability and uncertainty [Carrera, 1993; Thorsen *et al.*, 2001]. Conventional numerical models for reactive solute transport require a spatially explicit representation of all physical states and system parameters. Denitrification, groundwater flow and contaminant transport are controlled and affected by many factors and parameters. All of these factors are to some degree uncertain and spatially variable. This can be due to insufficient knowledge or because of unpredictable and immeasurable dynamics of forcing and unresolved subscale variability.

To account for subscale variability and uncertainty of the model parameters, a stochastic framework using Monte Carlo (MC) simulations may be applied. In MC simulations, random realizations of parameter fields (e.g., hydraulic conductivity) are generated and the flow-and-transport problem is solved for each realization to generate an ensemble of dependent variable values [Dagan, 2002]. Within a stochastic framework, predictions of the fate of a contaminant are expressed in terms of probabilities rather than single values. For catchment-scale, fully coupled, multi-dimensional, non-linear, spatially explicit, multi-component reactive-transport models that exhibit rather large model run-times, MC simulations or other stochastic techniques beyond linear error propagation are typically prohibitive. Hence, conceptual simplifications are necessary, keeping spatially explicit calculations whenever needed and computationally manageable, but simplifying reactive-transport computations without sacrificing mechanistic understanding.

The streamline approach is a specific type of simplification which is followed in this work. It is based on a Lagrangian viewpoint that tracks travel times of water parcels [e.g., Jury, 1982; Feyen *et al.*, 1998; Luo, 2012]. Streamline approaches restrict solute transport to the direction of flow. Dispersion is addressed by the consideration of transit- or travel-time distributions at any time and location, rather than deterministic values. Instead of evaluating reactive transport in the entire domain, the streamline approach calculates it along pathlines. Due to the reduced dimensionality

of the reactive transport problem and the associated reduction of computational effort, a stochastic framework using MC simulations becomes possible. Previous studies using streamline approaches replaced the spatial coordinates required in the fully explicit three-dimensional reactive-transport models by groundwater travel time or exposure time [*Cvetkovic and Dagan, 1994; Cvetkovic et al., 1996; Dagan and Nguyen, 1989; Feyen et al., 1998; Simmons, 1982; Shapiro and Cvetkovic, 1988*]. However, geochemical properties of the subsurface are also spatial variable and uncertain. In the case of denitrification, the decay rate of nitrate varies within different hydrogeological facies. When considering travel or exposure times only, it is not possible to account for the heterogeneity and spatial variability of the reactivity within the aquifer. Also the reaction partner in the matrix (an electron donor in case of denitrification) is used up over time. Travel-time based approaches are not able to account for such a depletion of reactivity as this is a spatially explicit problem and streamline approaches follow a non-spatially explicit framework.

The main contribution of this thesis is a framework to better assess and quantify the propagation of contaminants (with a focus on nitrate) on the catchment-scale. The proposed framework is designed to deal with the inherent uncertainty of insufficient knowledge of subsurface characteristics, unpredictable dynamics of forcing and unresolved subscale variability of both hydraulic and geochemical properties. The framework is based on a streamline approach that goes beyond mere travel or exposure time formulations. To demonstrate the potential of the proposed framework, it is applied to multi-component, nonlinear reactive transport. Moreover, it is extended to account for the spatially explicit decreasing reaction potential of an aquifer. With the help of an electron balance, the lasting time of the reaction potential is estimated.

2 State of the Art

2.1 Reactive Transport Modeling at the Catchment-Scale

One of the biggest challenges in reactive transport modeling on the catchment-scale is the heterogeneous nature of an aquifer and its associated parameters. Not only the boundary conditions (e.g., recharge, values of fixed heads) but also the hydraulic and geochemical parameters are spatially variable and uncertain. Also the reactive properties of subsurface materials (e.g., grains, rocks) play a crucial role in solute transport [Seeboonruang and Ginn, 2006].

Different types of catchment models have been developed in the past. The simplest approach is based on so called conceptual hydrological models, where a catchment is described as a series of interlinked reservoirs with exchange rules [Arnold *et al.*, 1998; Bergström *et al.*, 1992]. These types of models consider conservation of mass only. In conceptual hydrological models, solute transport is often addressed by the consideration of travel-time distributions within each reservoir. These travel-time distributions have to be estimated additionally to the water fluxes [Rinaldo *et al.*, 2006; Botter *et al.*, 2010; Hrachowitz *et al.*, 2010].

Spatially Explicit Models

The conventional approach of solving catchment-scale reactive transport are numerical models that solve the advection-dispersion-reaction equation [Schäfer and Therrien, 1995; Therrien and Sudicky, 1996; Mayer *et al.*, 2002; Prommer *et al.*, 2001]. These models are based on partial differential equations (pdes) that can account for relevant flow and transport processes

2.1. REACTIVE TRANSPORT MODELING AT THE CATCHMENT-SCALE

such as dispersion, diffusion, and transverse mixing. The classical advection-dispersion-reaction equation for the concentration c_i [ML^{-3}] of a dissolved compound i is:

$$\frac{\partial c_i}{\partial t} + \mathbf{v} \cdot \nabla c_i - \nabla \cdot (\mathbf{D} \nabla c_i) = r_i(\mathbf{c}(\mathbf{x}), \mathbf{x}, t) \quad (2.1)$$

in which t [T] is time, $\mathbf{v} = \frac{\mathbf{q}}{n_f}$ [LT^{-1}] denotes the linear average velocity, which is the quotient of specific discharge \mathbf{q} [LT^{-1}] and flow-effective porosity n_f [-], \mathbf{D} [L^2T^{-1}] is the dispersion tensor, and r_i is the reaction rate of compound i depending on the vector of all concentrations \mathbf{c} , the location \mathbf{x} , and potentially time.

These models can also use a fully hydromechanic description of water flow in the subsurface [Goderniaux *et al.*, 2009; Refsgaard, 1997; Kollet and Maxwell, 2006]. Reactive transport simulations with these models is straightforward as the standard advection-dispersion-equation requires spatially distributed velocity fields that are readily computed by pde-based flow models [Schäfer and Therrien, 1995; Therrien and Sudicky, 1996]. In theory, spatially explicit models may facilitate the most complete and accurate description of flow and reactive transport currently available. However, they also require a spatially explicit representation of all physical states and system characteristics at every location in the model domain including the specification of hydraulic parameters, parameters for solute transport, and reactive parameters. In practice these parameters are impossible to obtain. Because they are hard to measure at the required temporal and spatial resolution and because they are subject to unpredictable dynamics of forcing. The high data demand typically stays in stark contrast to the amount of data that can be obtained. On the catchment-scale, pde-based models suffer from a too high computational effort, a too high demand of parameters, and also numerical issues, such as numerical dispersion.

Travel-Time based Models

Considering large-scale solute transport along flow pathlines leads to so called streamtube and streamline approaches which can be based on travel and exposure times [Jury, 1982]. Travel-time based models make use of the fact, that reactive-species concentrations can be associated with travel times or times of exposure to certain reactive facies [Jury, 1982; Feyen *et al.*, 1998; Luo, 2012]. The advective travel time, or kinematic groundwater age, is obtained by integration of the

inverse velocity along a particle trajectory:

$$\tau_{adv}(\mathbf{x}) = \int_{\mathbf{x}_0}^{\mathbf{x}} \frac{d\mathbf{x}_p}{\|\mathbf{v}(\mathbf{x}_p)\|} = \int_{\mathbf{x}_0}^{\mathbf{x}} \frac{\theta}{q(\mathbf{x}_p)} d\mathbf{x}_p \quad (2.2)$$

in which \mathbf{x}_p [L] is the position vector of a particle along its trajectory from starting point \mathbf{x}_0 [L] to the observation point \mathbf{x} [L], \mathbf{v} [LT^{-1}] is the seepage velocity, θ [-] is porosity, and q [LT^{-1}] is the absolute value of the specific discharge vector.

Streamtube and streamline approaches describe solute transport only in the direction of flow. Dispersion is addressed by the consideration of transit- or travel-time distributions, rather than individual values at a point. The travel time of a water parcel is defined as the time needed from entering the model domain to the outlet or observation point. The exposure time is defined as the time that the water parcel is exposed to certain facies with specific chemical or other environmental characteristics facilitating a desired reaction [Rubin *et al.*, 1994]. Thus, exposure time is typically smaller or at maximum equal to travel time. The use of exposure time rather than travel time can be useful if an investigated chemical process only takes place in certain facies of the aquifer. Exposure-time models provide good approximations of nonlinear bio-reactive transport when transverse mixing is not the overall controlling process [Sanz-Prat *et al.*, 2016a].

Previous studies have shown that it is important to distinguish between travel and exposure times because the mineralogical composition of the matrix and the biogeochemical conditions are commonly non-uniformly distributed in an aquifer [Lohse *et al.*, 2009; Reich *et al.*, 2006; Ocampo *et al.*, 2006; Frei and Peiffer, 2016].

Travel-time analysis, that follows a Lagrangian approach, was introduced by Todorovic [1970] and further developed by Shapiro and Cvetkovic [1988]. Instead of evaluating reactive transport in the entire domain, as it is done in the conventional pde-based approach, it is calculated along a pathline. The spatial coordinates, that are required in the equations for reactive transport in fully explicit three dimensional models, are replaced by groundwater travel time (Eq. 2.2) [Feyen *et al.*, 1998]. The reactive transport equations thus become one-dimensional with a uniform travel time “velocity” of one. To solve them, a single one-dimensional simulation in travel-time coordinates is sufficient if the inflow concentration is uniform along the entire inflow boundary and if reaction constants are uniform within the domain. Streamline approaches are likely to

2.1. REACTIVE TRANSPORT MODELING AT THE CATCHMENT-SCALE

be appropriate if the input of contaminants is diffusive (i.e., spread over large areas) so that transverse macroscopic mixing processes may be neglected, as this is, for example, the case for nitrate leaching from agricultural soils into groundwater [Sanz-Prat *et al.*, 2015]. In contrast, when a contaminant plume is developing from a continuous point, the fate of the contaminant will most likely be subject to transverse mixing processes, that require explicit reactive transport models [Cirpka *et al.*, 1999c].

In previous studies investigating streamline and streamtube approaches, dispersive mixing has often been neglected altogether, which leads to a pure advective transport regime [Atchley *et al.*, 2013; Ginn *et al.*, 1995]. An exchange between streamtubes, that are considered as independent one-dimensional systems, is not considered. Travel-time based models that consider random advection only are known as stochastic-convective reactive models [Dagan and Nguyen, 1989; Cvetkovic *et al.*, 1996; Simmons *et al.*, 1995; Atchley *et al.*, 2013] and have been applied to groundwater hydrology in numerous studies [Simmons, 1982; Cvetkovic and Dagan, 1994; Cvetkovic *et al.*, 1996; Ginn, 2002]. Mixing controlled reactions cannot be addressed by these models. However, effective longitudinal mixing and pore scale dispersion may be accounted for in stream tube approaches by using an appropriate longitudinal dispersion coefficient [Cirpka and Kitanidis, 2000; Luo and Cirpka, 2011].

The stochastic-convective reaction models have been extended to nonlinear multi-component reactive transport and multi-phase flow problems [Cvetkovic and Dagan, 1994; Dagan and Cvetkovic, 1996; Kaluarachchi *et al.*, 2000; Yabusaki *et al.*, 1998; Malmström *et al.*, 2004] under the premise that solute mixing can be neglected. Travel-time based non-linear reactive-transport schemes are also a good method for describing a continuous input of reactants undergoing microbial degradation [Sanz-Prat *et al.*, 2015, 2016b].

One of the biggest advantages of travel-time based models is that the computational effort of solving reactive transport is very small [Atchley *et al.*, 2014; Gong *et al.*, 2011; Diem *et al.*, 2013]. Thus a stochastic framework accounting for variability and uncertainty of model parameters becomes possible. Such a stochastic framework can account for internal variability of spatially distributed parameters, uncertainty in zonation and in spatially uniform parameters. However, for all streamtube- and streamline based models, it is still inevitable to solve spatially explicit flow and conservative transport but no multi-dimensional reactive transport simulations are necessary.

2.2 Stochastic Methods for Subsurface Characterization

Real-world aquifers and porous media are heterogeneous. In corresponding model applications, all hydraulic and chemical parameters are uncertain, either because of lacking knowledge or because of unpredictable dynamics. Hence, reactive transport at the catchment-scale may require a stochastic framework to account for the uncertainty of forcings, model parameters, and conceptual assumptions [e.g., *Jury, 1982; Shapiro and Cvetkovic, 1988; Yabusaki et al., 1998; Cirpka and Kitanidis, 2000; Luo, 2012*]. Because the quantity of interest (e.g., nitrate concentration) depends on the model parameters in a nonlinear way, the use of linear uncertainty propagation methods most likely is not sufficient, and techniques based on multiple model runs representing multiple possible realizations of parameter fields are needed. The simplest but computationally most expensive approach to account for subscale variability and uncertainty of the model parameters are Monte Carlo (MC) simulations. Even though more efficient nonlinear uncertainty quantification techniques exist [e.g., *Xiu and Hesthaven, 2005; Nobile et al., 2008*], all techniques of uncertainty quantification that do not rely on linearization imply that a large number of model runs have to be performed, which corresponds to a high computational demand. Direct approaches, where there is no need to generate multiple realizations of a certain variable or parameter field also suffer from high computational costs and are usually more complex to set up and handle than MC simulations [*Neumann and Orr, 1993; Guadagnini and Neuman, 1999*]. An example for such a direct method are integro-differential moment equations that have been developed for flow and transport in porous media [*Zhang, 2001*].

The main idea behind Monte Carlo simulations in hydrogeology is to generate numerous equally likely and independent random realizations of the parameter fields and averaging the results [*Zhang, 2001*]. These fields (e.g., field of hydraulic conductivity) are a random variation over space. Values at different locations, however, may be correlated. The statistics of the random parameter fields (e.g., mean hydraulic value) are drawn randomly from a distribution function. The flow-and-transport problem is then solved for each realization to generate an ensemble of dependent variable values [*Dagan, 2002*], which implies that a prohibitively large number of model runs is performed. The randomness of each realization represents the uncertainty of the model parameters (e.g., field of hydraulic conductivity). Field data to estimate these parameters are often scarce and permit for a parameter estimation in statistical terms only. The obtained probability density function (pdf) serves then as input for the stochastic model resulting in stochastic (differential) equations for dependent variables. Therefore these variables can also only

2.3. DENITRIFICATION

be characterized in a statistical manner by the corresponding pdf. The hydraulic conductivity field of a single realization, for example, may belong to an ensemble of realizations that are all compatible with observations.

Monte Carlo simulations are often chosen because of the conceptual simplicity and comprehensive characteristics of solutions. It can be applied to a broad range of linear and nonlinear flow problems. It is also not necessary to change or adapt the model used, because the multiple model runs are performed independently with different input parameters. With such a framework, predictions of the fate of a contaminant are expressed in terms of probabilities rather than single values. However, because of the associated computational effort such a probabilistic framework cannot be performed using a fully coupled, multi-dimensional, non-linear, spatially explicit, multi-component reactive-transport model.

2.3 Denitrification

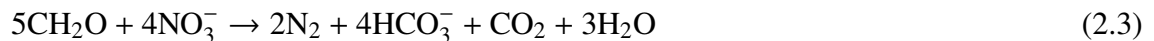
Nitrate is one of the most prominent and wide-spread contaminants of groundwater worldwide. With an increasing use of agricultural fertilizer in the 1960s and 1970s, the exposure of groundwater to nitrate and other agricultural contaminants has increased [Galloway *et al.*, 2004]. Excess nitrate, that is not taken up by plants for their metabolism, may be transported with the percolating water through the root and vadose zone into the saturated zone, which leads to groundwater contamination and potentially to surface water contamination as well [Puckett *et al.*, 2010]. Nitrate can be a hazard to humans and to the environment. In the human body nitrate can be reduced to nitrite, which can cause methemoglobinemia of infants [Wolfe and Patz, 2002]. Other studies were able to link elevated nitrate concentrations in drinking water to a higher cancer risk [Ward *et al.*, 2005; Weyer *et al.*, 2001]. In surface waters nitrate can lead to eutrophication. This process induces growth of weeds and algae and due to the high biomass, may result in oxygen depletion of the water body [Hickel *et al.*, 1993; Smolders *et al.*, 2010].

Even though nitrate is a regulated compound (drinking-water standards: 50 mg/L total nitrate in the European Union, 10 mg/L nitrate-N = 44mg/L total nitrate in the U.S.), the release of nitrate and other pollutants into the subsurface can not fully be prevented or prohibited by regulations or laws because the ever-growing need for higher yields to feed the planet requires the application of fertilizer to satisfy the crop nutrient requirements. Especially in regions with intensive agriculture

2.3. DENITRIFICATION

the nitrate levels remain at elevated levels [Strebel *et al.*, 1989; Pacheco *et al.*, 2001; Wakida and Lerner, 2005].

Many aquifers, that are exposed to an increasing input of nitrate, however, have the natural capability to degrade nitrate. Nitrate concentrations of polluted groundwater can be remarkably reduced by the natural ability of aquifers to break down nitrate [Green and Bekins, 2010; Wisotzky, 2012]. This process is called denitrification and is defined as the microbial reduction of one or both of the ionic nitrogen oxides nitrate (NO_3^-), and nitrite (NO_2^-) respectively, to the gaseous oxides nitric oxide (NO), and nitrous oxide (N_2O), which may be further reduced to molecular nitrogen (N_2) [Knowles, 1982]. Denitrification is a major process in the global nitrogen balance and a common process in the root zone and the saturated zone of an aquifer. The net stoichiometry heterotrophic-chemoorganotrophic denitrification, where organic carbon (OC) acts as electron donor, is:



in which CH_2O denotes the simplified chemical composition of the organic matter, NO_3^- is the nitrate anion, N_2 is molecular nitrogen, HCO_3^- is bicarbonate, CO_2 is carbon dioxide, and H_2O is water.

2.3.1 Factors controlling denitrification

Potential for denitrification to occur exists in most natural environments. However, denitrification rates vary widely depending on a variety of conditions that are subsequently described.

Microorganisms

Denitrification is not possible without the presence of specialized microorganisms. Bacteria capable of denitrification are commonly found in many subsurface environments, even when denitrification is not actively occurring [Ghiorse and Wilson, 1988]. The denitrification process is catalyzed by either heterotrophic or autotrophic microorganisms that derive their energy requirements by the oxidation of organic and inorganic material, respectively. However, most denitrifying bacteria are heterotrophic and are able to utilize a wide range of carbon compounds as

2.3. DENITRIFICATION

of electron donors [Hiscock *et al.*, 1991]. *Pseudomonas* is the most common isolated denitrifying bacteria from soils and sediments [Gamble *et al.*, 1977; Heitzer and Ottow, 1976]. It is the most active denitrifier in natural environments.

Microbial communities can adapt to changing and unfavorable conditions without becoming extinct [Mellage *et al.*, 2015]. Experiments showed that microorganisms can remain dormant for extended periods of time and then regain their full biodegradation potential within few hours after the starvation period. Under anaerobic conditions, facultative denitrifiers are able to switch from oxygen as an electron acceptor to nitrogen within a period of 40 minutes to three hours [Payne and Riley, 1969; Payne *et al.*, 1971; Williams *et al.*, 1978].

Oxygen

Another important factor controlling denitrification is the dissolved oxygen concentration as nitrogen oxide reductases are repressed by oxygen. When the availability of oxygen is limited, aerobic respiration is replaced by anaerobic respiration, during which oxygen is replaced by an alternative electron acceptor. Denitrification is thermodynamically less favorable than the reduction of dissolved oxygen (DO) [Rivett *et al.*, 2008]. Oxygen is therefore the preferred electron acceptor in presence of dissolved oxygen, nitrate and organic carbon. However, denitrification has been observed at “bulk” O₂ concentrations of up to 2 mg/l [Smith and Duff, 1988], suggesting anaerobic conditions at microsites. Because of the heterogeneity of the aquifer and the geometry of the oxygen diffusion path, there is frequently an interaggregate airfilled porosity surrounding intraaggregate waterfilled pores, that can then become anaerobic, leading to denitrification [Smith, 1980]. Taking organic matter as the electron donor, the net stoichiometry of aerobic respiration is:



in which O₂ denotes molecular oxygen.

Denitrifying bacteria are able to use nitrogen oxides as electron acceptors instead of oxygen when exposed to anaerobic conditions (Eq. 2.3). After the consumption of oxygen, denitrifiers rely on nitrate to generate energy via cellular respiration [Foth *et al.*, 1991].

2.3. DENITRIFICATION

Figure 2.1 shows the typical stratification in a reducing aquifer. The oxidants DO and NO_3^- percolate with the recharge water through the unsaturated zone into groundwater. In shallow aerobic groundwater, microorganisms consume DO until it is depleted. In the following anaerobic zone microorganisms deplete NO_3^- as nitrate is the first compound to be reduced after oxygen depletion. If there are enough reductants the nitrate will be entirely consumed.

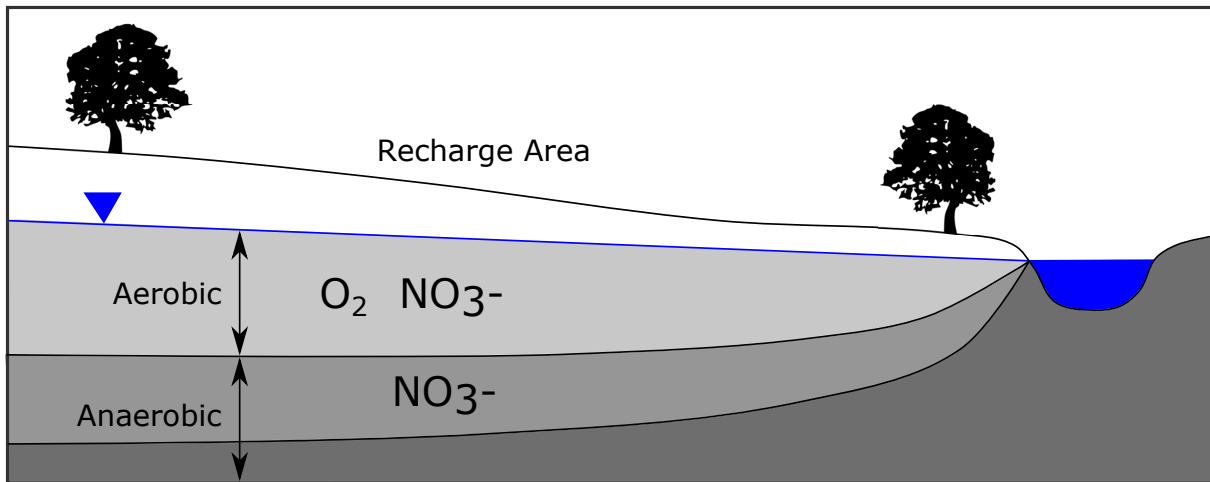


Figure 2.1: Schematic figure of aerobic and anaerobic zone in an aquifer with natural denitrification potential.

Other Factors

Denitrification is also related to pH with an optimum in the range of pH 7.0-8.0 [Delwiche and Bryan, 1976; Wijler and Delwiche, 1954]. Temperature is also a significant factor, as at high temperatures the oxygen solubility is smaller [Stanford *et al.*, 1975]. Other factors controlling denitrification are the presence of nitrogen oxides and the presence of inhibitors like acetylene (C_2H_2) or azide (N_3^-) [Knowles, 1982] or other inhibiting compounds like sulphur compounds. Most of these factors play only a minor role in the natural denitrification process and thus can be neglected when modelling the denitrification process.

2.3.2 The Role of Organic Carbon in Denitrification

As state above and depicted in Eq. 2.3, an electron donor needs to be present for denitrification to occur. The most prominent and wide-spread electron donor in aquifers worldwide is organic carbon. The availability of electrons in organic carbon compounds is one of the most important

2.3. DENITRIFICATION

factors controlling the activity of the denitrifying heterotrophic bacteria. Previous studies showed, that denitrification rates are directly related to organic carbon contents [Van Kessel, 1978]. Even though organic carbon is the most common electron donor for the denitrification process, the electron donors are not limited to organic materials. Reduced sulfur compounds, ferrous iron (Fe^{2+}), molecular hydrogen, assimilating dissolved CO_2 , or pyrite (FeS_2) can act as electron donor and lead to denitrification. For stimulated in-situ denitrification in aquifers that lack appropriate natural electron donors, acetate (CH_3CO_2^-) or granular iron is injected to enhance denitrification processes [Critchley *et al.*, 2014; Devlin *et al.*, 2000].

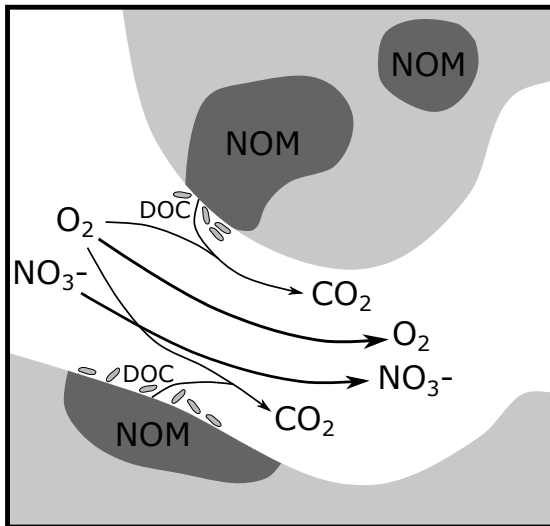
Organic material in aquifers is mostly of sedimentary origin and consists of the remains of plants in terrestrial sediments, supplemented by plankton and animal residues in the case of marine and lacustrine sediments. The most abundant source of sedimentary organic matter is plant material, consisting mainly of lignin and polysaccharides. In the root zone, the pool of organic material is replenished by dying off plant material, such as leaves, roots, and wood, or by infiltration of solutions with high concentrations of dissolved organic carbon. In the saturated zone, by contrast, the organic material is mostly of geogenic origin and is not replenished [Appelo and Postma, 2004]. Aquifers can lose their natural denitrification potential as organic carbon or other electron donors are used up by the denitrification process over typically large time-scales.

The organic carbon content is commonly low in sand deposits and limestones but higher in clays and silts. Generally, the degradation of organic matter is very slow. Older aquifer systems generally contain organic matter that reacts more slowly than younger organic matter, although the reactivity of organic matter depends on the diagenetic history. The organic matter reactivity is ultimately the engine that drives most redox reactions, including denitrification.

Figure 2.2 shows a conceptual model of oxidants and reductants in water-filled pore-scales of an aquifer for (A) aerobic and (B) anaerobic conditions. While oxygen is present (aerobic conditions) denitrification is inhibited and only DO is consumed by microorganisms. The natural organic matter (NOM) in the solid aquifer material acts as an electron donor and enables the aerobic respiration. Once all DO is consumed (anaerobic conditions) microorganisms consume NO_3^- . Because of the limited availability of reductants, some NO_3^- does not react and passes farther into the anaerobic zone. Also, not all NOM is bioavailable. That means that only a part of the total organic carbon of the aquifer matrix is readily available to microorganisms.

2.3. DENITRIFICATION

A: Aerobic Conditions



B: Anaerobic Conditions

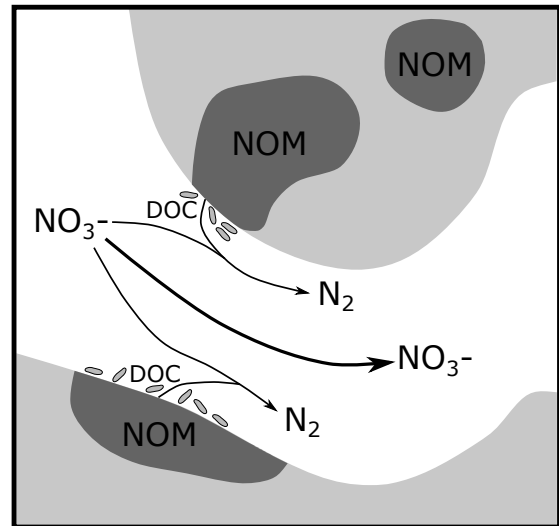


Figure 2.2: Conceptual model of oxidants and reductants in water-filled pore-spaces of an aquifer. (A) Aerobic conditions, (B) anaerobic conditions.

3 Objectives & Contributions

This thesis presents a stochastic framework for catchment-scale reactive transport simulations. The following three research questions are addressed:

1. How can reactive transport on the catchment-scale be simplified that stochastic simulations become possible without only considering travel or exposure times?
2. How can the decreasing reaction potential be accounted for without returning to a fully spatial explicit modeling framework?
3. How can the time of the decreasing reaction potential be predicted without solving reactive transport?

The main objective of this thesis is the development of a stochastic modeling framework for reactive transport on the catchment-scale. The framework will help to assess metrics of water quality on the catchment-scale. The modeling framework is based on the following principles:

- It should be as mechanistic as necessary to account for the spatial structure of the hydrogeological system and for the major processes determining water-quality metrics.
- It should be as efficient as possible to reduce computational effort and to enable Monte Carlo runs for a subsurface flow model accounting for variability and uncertainty of forcing, internal hydraulic variability, internal geochemical variability, and uncertainty in geological zonation.

Corresponding to the three research questions postulated above, the thesis is structured into three parts:

Part 1: Cumulative Relative Reactivity In the first part of the thesis I derived a general stochastic framework for catchment-scale reactive transport simulations. For this purpose, I identified and described the relevant and important processes of reactive transport on the catchment-scale. Processes that have only a small influence on the system and on reactive transport were identified and then simplified or neglected altogether, as their contribution was relatively small compared to the overall error and uncertainty of the reactive transport model. The proposed approach goes beyond exclusively considering travel or exposure times and considers the reactivity of the aquifer matrix. The simplifications of the newly developed framework were tested against a spatially explicit “virtual truth” and were applied on a three-dimensional test case to show the applicability of the approach [Loschko *et al.*, 2016].

Part 2: Decreasing Reaction Potential In the second part of this thesis I improved and updated the derived framework by implementing a method that accounts for the decreasing reaction potential of the aquifer. In natural systems the reaction potential of aquifers decreases over time if the reaction partner in the matrix is not replenished. In case of denitrification, the electron donor in the saturated zone is used up over time which leads eventually to a break-through of nitrate concentrations in pumping wells or other receptors. This important feature cannot be reproduced by state-of-the-art travel- or exposure-time based models. The challenge for this implementation was the spatially explicit process of the decreasing reaction potential in the spatially non-explicit modeling framework. By discretizing the streamlines into travel-time increments, the decreasing denitrification potential was accounted for without returning to a fully spatially explicit model description and without losing the computational efficiency of the approach. The decreasing denitrification potential of an artificial aquifer was calculated for a three-dimensional steady-state test case over 200 years in an ensemble of 200 members. In these simulations, different scales of observations were evaluated [Loschko *et al.*, 2018a].

Part 3: Cumulative Reaction Potential In the third part of the thesis I derived the concept of the cumulative reaction potential as a predictor for contaminant breakthrough at a receptor (such as a pumping well). This prediction is possible using the concept of the cumulative reaction potential without solving reactive transport equations altogether. For this purpose, the consideration of travel times and the content of electron donors or another reaction partner in the matrix is sufficient. With that new concept, the estimation of the breakthrough of a contaminant is computationally even less expensive. The predictive ability of the cumulative reaction potential

was tested against a spatially explicit model on a heterogeneous two-dimensional test case [Loschko *et al.*, 2018b].

Contributions The stochastic framework for catchment-scale reactive transport simulations is a crucial enhancement of existing travel- and exposure-time based modeling frameworks. Simulations of the reactivity of aquifers is now feasible within a stochastic framework. Different reactive zones and their internal variability can be addressed. With the implementation of the decreasing denitrification potential it is possible to account for this spatially explicit process without losing the computational efficiency of the proposed approach. The derived principles can also be applied to other travel-time based modeling frameworks. Finally, the cumulative reaction potential is used as a predictor for breakthrough of contaminants without solving any reactive transport equations.

4 General Concept

4.1 Cumulative Relative Reactivity

The starting point of the analysis is the assumption of advective-reactive transport, in which dispersive mixing is neglected altogether. Figure 4.1 depicts two different contamination scenarios to illustrate under which conditions such an assumption may be acceptable. Both setups show groundwater recharge from the top, an extraction well, and a river at the right-hand side of the domain. In Figure 4.1a, the contaminant is introduced by a point source and reacts with a solute in the ambient solution. This is the typical scenario of a contaminant plume, the reaction of which is controlled by transverse mixing, so that neglecting dispersion is strictly prohibited [e.g., *Cirpka and Valocchi, 2007; Cirpka et al., 2012*]. Another scenario, in which dispersive mixing controls the overall reaction behavior, is when the solution containing one non-sorbing reactant is replaced by the solution containing the other, also non-sorbing reaction partner [e.g., *Le Borgne et al., 2014; de Anna et al., 2014*]. In contrast to such cases, Figure 4.1b depicts the scenario for which the present framework is developed. Here, the contaminant (e.g., nitrate) enters the model domain as diffuse input spread over the entire land surface, as is typical for agricultural pollution. The solute of interest reacts with constituents of the aquifer matrix, which are non-uniformly distributed within the domain. In Figure 4.1b, zones with high contents of solid-phase reactants (e.g., NOM) are shown as green inclusions, whereas the white background reflects essentially non-reactive zones. In this scenario, the chemical reaction is controlled by mass transfer from the aquifer matrix to the aqueous solution and takes place only during the transit of water and solutes through the reactive zones. While one cannot totally exclude an influence of dispersive mixing on the overall reactive-transport behavior, it is not the major factor controlling the reaction.

4.1. CUMULATIVE RELATIVE REACTIVITY

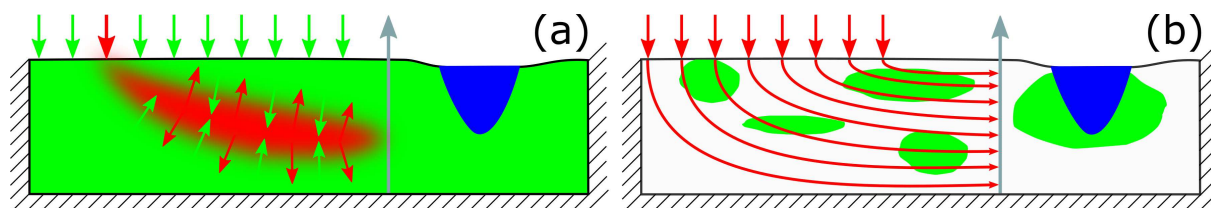


Figure 4.1: Comparison of two contamination scenarios with contamination input (red) at the land surface. A: point-source contamination requiring a reaction partner (green) introduced in parallel, leading to a plume controlled by transverse dispersive mixing; B: diffusive contamination reacting with compounds released by the matrix (reactive zones shown as green patches). The proposed method is only valid for scenario B.

In the proposed framework, the existing advective-reactive transport model is extended by introducing the dimensionless relative reactivity $f(\mathbf{x}) [-]$, which parametrizes the intensity of a the considered reaction at every location in the domain, in relation to a reference reaction rate for the same concentrations of dissolved compounds. A high relative reactivity ($f > 1$) amplifies the reference reaction rates, whereas a low relative reactivity ($f < 1$) dampens them. The relative reactivity reflects spatial differences of reaction intensity in the aquifers matrix. For the chemical reduction of solutes, the relative reactivity is thus related to the electron donor supply by the matrix (e.g., from natural organic matter, pyrite, or biotite). For chemical oxidation of solutes, by contrast, the relative reactivity parametrizes the electron acceptor supply (e.g., from ferric iron oxides). In a practical setting, the relative reactivity will be related to different geological facies. The internal chemical variability within individual units can be addressed by spatial variation of the relative reactivity, e.g., by treating it as a random space function.

The key assumption of using the relative reactivity is that the supply of reaction partners from the matrix controls the overall reaction, and that the microbial communities, catalyzing the reactions, adapt quickly to the reactive-solute concentrations and the reaction-partner supply by the matrix. The abundance of microbes itself is not explicitly accounted for since populations adapt quickly to ambient conditions, whereas potentially non-linear dependencies on reactive-solute concentrations remain. As such, the concept stands somewhere between a comprehensive description of the reaction network, including explicit modeling of microbial dynamics, and approaches reducing all reactions to apparent first-order decay laws.

In the proposed reactive transport framework, the key Lagrangian premise of following water parcels along their trajectories through the domain is pursued. Two integral quantities along a

4.1. CUMULATIVE RELATIVE REACTIVITY

travel path are calculated: (1) the travel time or kinematic age, allowing to compute when a water parcel, that is observed in the aquifer at a given time, has entered the subsurface via the land surface; and (2) the cumulative relative reactivity $F(\mathbf{x})$ [T], which is the time integral of the local relative reactivity experienced by the moving water parcel. Under steady state flow conditions the cumulative relative reactivity is computed by:

$$F(\mathbf{x}) = F(\tau(\mathbf{x}) | \mathbf{x}_0(\mathbf{x})) = \int_0^{\tau} f(\mathbf{x}(\tau_* | \mathbf{x}_0)) d\tau_* \quad (4.1)$$

in which τ [T] is travel time, and \mathbf{x}_0 [L] is the starting location.

The composition of reactive solutes changes while the water parcel moves through zones of different reactivity. This may be seen as an aging of the water parcel with associated change in chemical composition. However, the clock by which the water ages ticks quicker in zones of high relative reactivity than in those of low relative reactivity, so that the cumulative relative reactivity F may be interpreted as a reaction-relevant age.

In the presented approach with application to denitrification reaction, the concentrations of oxygen and nitrate at a given location and time can be computed from (1) the origin and travel time of the water parcel, determining the initial concentrations of oxygen and nitrate when the water parcel entered the system, and (2) the cumulative relative reactivity that the water parcel has experienced while passing through the aquifer along its flow path. Origin, travel time, and cumulative relative reactivity can easily be evaluated by particle tracking methods. For the reaction equations, time is replaced by cumulative relative reactivity. Thus, with a finite set of initial-concentration values, one reaction equation evaluation per initial condition, and the information from particle tracking, concentrations of the electron acceptors can be computed at all times and locations, without reducing the reactions to single-compound descriptions. This approach significantly reduces the computational effort of reactive-transport simulations.

The proposed modeling approach for aquifer-scale reactive transport using the concept of cumulative relative reactivity consists of the following steps:

1. Calculate the groundwater velocity field with a spatially explicit pde-based model.
2. Determine particle trajectories to obtain the travel time and the cumulative relative reactivity, which are time-independent in case of steady-state flow (Eq. 4.1).

4.2. DECREASING REACTION POTENTIAL

3. Solve a set of ordinary differential equations for reactive transport and all occurring inflow concentrations.
4. Map travel time and cumulative relative reactivity to reactive-species concentrations.

4.2 Decreasing Reaction Potential

So far, I assumed that the relative reactivity remains constant over time, indicating an infinite supply of reaction partners from the aquifer matrix. In the theoretical considerations described in Chapter 4.1, the relative reactivity was considered to be time independent. However, the pool of reaction partners in real-world systems is limited. To account for a decreasing reaction potential of the aquifer, a time dependent relative reactivity is considered. The approach is based on the conceptual simplifications introduced in the first part (Chapter 4.1), namely on the concept of cumulative relative reactivity. This way, the framework remains computationally efficient and a stochastic analysis using Monte Carlo simulations is still possible without relying on unrealistic first-order decay of nitrate in aquifers. Streamlines are discretized in identical travel-time increments with variable content of reaction partners in the matrix. For every travel-time increment, the cumulative relative reactivity and the concentrations of dissolved oxygen, nitrate and NOM are updated regularly. This scheme results in breakthrough curves of reactive-species concentrations.

The proposed modeling approach for aquifer-scale reactive transport using the cumulative relative reactivity including a decreasing reaction potential consist of the following steps:

1. Solve a set of ordinary differential equations for all inflow concentrations occurring, resulting in the function dependence $\mathbf{c}(F, \mathbf{c}_{in})$.
2. Evaluate steady-state flow.
3. Construct streamlines leading to observation points, extraction wells, or control planes of interest by backward particle tracking.
4. Discretize all streamlines by identical travel-time increments and average the concentration of the reaction partner in the matrix in all streamline-increments.
5. Set total time to zero.

4.3. CUMULATIVE REACTION POTENTIAL

6. Compute the relative reactivity of each streamline-increment from the concentration of the reaction partner in the aquifer matrix.
7. Compute the cumulative relative reactivity for all streamlines.
8. Compute the reactive species concentrations.
9. Reconstruct the reaction rate in all streamline-time increments.
10. Update the concentration of the reaction partner in the matrix.
11. Increase the time by the time of a travel-time increment and go back to step 6, unless the time exceeds the end time of simulation.

4.3 Cumulative Reaction Potential

Considering the electron balance along a flow path in the subsurface, the primary cause of uncertainty should be the uncertainty of the total NOM mass in the streamtube leading to the observation point, well, river or lake. To analyze the influence of the uncertainty of hydraulic conductivity, and therefore the uncertainty of the coupled total natural organic matter (NOM) mass, I introduce the cumulative reaction potential τ_{pot} [T]. The cumulative reaction potential is defined as the time that is needed for an instantaneous reaction of all solutes (e.g., nitrate and dissolved oxygen) and the reaction partner in the aquifer matrix (e.g., NOM). Reaction kinetics are neglected. If the reactions were instantaneous, there would be a breakthrough of the inflow concentration after time τ_{pot} . The cumulative reaction potential at an observation point \mathbf{x}_{obs} can be calculated by:

$$\tau_{pot}(\mathbf{x}_{obs}) = \frac{1}{\gamma_{DO} \cdot c_{in,DO} + \gamma_{Nit} \cdot c_{in,Nit}} \cdot \int_0^{\tau(\mathbf{x}_{obs})} \frac{\rho_b \cdot c_{NOM}^*}{\theta} d\tau \quad (4.2)$$

in which γ_{DO} [$\text{mol}_C \text{mol}_{DO}^{-1}$] and γ_{Nit} [$\text{mol}_C \text{mol}_{Nit}^{-1}$] are the stoichiometric coefficients between DOC and the electron acceptors oxygen and nitrate respectively, $c_{in,DO}$ [$\text{mol}_{DO} \text{L}^{-3}$] and $c_{in,Nit}$ [$\text{mol}_{Nit} \text{L}^{-3}$] are the inflow concentrations of oxygen and nitrate, c_{NOM}^* [$\text{mol}_C \text{M}_{soil}^{-1}$] denotes

4.3. CUMULATIVE REACTION POTENTIAL

the mass-related concentration of the NOM in the aquifer, $\rho_b [M_{\text{soil}}L^{-3}]$ is the dry bulk mass density of the aquifer material and $\theta [-]$ the volumetric water content.

The cumulative reaction potential along a particular flow line depends on the hydraulics of the aquifer, the distribution of the NOM mass, and the electron-acceptor load in the inflow. As hydraulic and geochemical properties of aquifers are spatially variable and uncertain, the cumulative reaction potential at an observation point, well, or plane is also uncertain. For a spatially distributed observation in a well or plane, τ_{pot} is a distribution rather than a single value even without uncertainty because different streamlines leading to the same target have been exposed to a different NOM mass over a different time.

The proposed modeling approach for the estimation of contaminant breakthrough at a receptor with the cumulative reaction potential consist of the following steps:

1. Calculate the groundwater velocity field with a spatially explicit pde-based model.
2. Determine particle trajectories to obtain the travel time and the cumulative NOM content.
3. Determine the initial concentrations of all solute compounds.
4. Calculate the cumulative reaction potential at a receptor (Eq. 4.2).

The modeling approach using the cumulative reaction potential can handle a heterogeneous distribution of hydraulic conductivity and a heterogeneous distribution of the NOM, respectively.

5 Test of Approaches

To test the the theoretical considerations and assumptions made in Chapter 4 I developed the following test cases for the three parts of the thesis:

Part 1: Cumulative Relative Reactivity

- **Two-dimensional benchmark test on the validity of the concept of cumulative relative reactivity**

This model compares steady-state concentration distributions of a spatially explicit virtual truth, accounting for dispersive mixing, with the approximation based on the proposed new concept of cumulative relative reactivity. The validity of the concept of cumulative relative reactivity is shown.

- **Three-dimensional model on the efficiency of the concept of cumulative relative reactivity**

This model demonstrates the efficiency of the concept of cumulative relative reactivity for strictly advective transport on a three-dimensional conceptual aquifer. The efficiency and applicability of the concept of cumulative relative reactivity is shown.

Part 2: Decreasing Reaction Potential

- **One-dimensional benchmark test on the relation between relative reactivity and NOM**

In this test case with a highly detailed description of the reactions I derive an empirical relationship between the bioavailable organic-carbon content and the relative reactivity which is needed in all models using the concept of cumulative relative reactivity.

- **Two-dimensional benchmark test on the validity of the decreasing reaction potential**
In this test case I show the validity of the new concept of cumulative relative reactivity including travel-time increments by comparing the concept to a spatially explicit model.
- **Three-dimensional model on the applicability of the decreasing reaction potential**
For this proof of concept a simplified model based on the concept of cumulative relative reactivity including travel-time increments is used to calculate the decreasing denitrification potential of an artificial aquifer in an ensemble of 200 members.

Part 3: Cumulative Reaction Potential

- **Two-dimensional benchmark test on the validity of the cumulative reaction potential**
In this test case I compare results from a two-dimensional spatially explicit model against the cumulative reaction potential. The validity of the concept of the cumulative reaction potential is shown.

5.1 Numerical Implementation

All presented test cases were implemented in Matlab. For the numerical implementation of the presented three-dimensional approaches additional tools like the groundwater flow model MODFLOW-NWT [Niswonger *et al.*, 2011] and parallel computation techniques using NVIDIA CUDA programming were used. The reactive-transport modeling framework was exclusively implemented within Matlab, all other software packages were linked to Matlab. The schematic code procedure of the three-dimensional test cases can be seen in Figure 5.1. The groundwater heads are calculated using MODFLOW-NWT. Matlab acts as a wrapper and is used to generate random spatial fields of hydraulic conductivity and relative reactivity. Matlab scripts then (re)write the MODFLOW-NWT input files. Other parameters like recharge, extraction rates, and boundary conditions can also be changed within the Matlab script. After MODFLOW-NWT finishes with the calculation of the hydraulic heads, the generated output files, like the binary hydraulic head files, are imported into Matlab. The Matlab scripts reading in and creating the MODFLOW-NWT files are based on mFLab, an open-source scripting environment [Olsthoorn, 2013]. While MODFLOW-NWT runs, the Matlab script pauses. The velocity information are then used as input for particle tracking. The particle tracking is conducted within Matlab using

5.1. NUMERICAL IMPLEMENTATION

Pollock's semianalytical method [Pollock, 1988] in parallel on the Graphics Processing Unit (GPU). Also the reactive transport is calculated partly on the GPU. To solve the set of ordinary differential equations, Matlabs build-in ode15s solver was used [Shampine and Reichelt, 1997].

In case of a stochastic analysis, the Matlab script performs Monte Carlo loops. For every MC simulation, the input parameters (hydraulic conductivity, relative reactivity, boundary conditions, etc.) can be randomly changed. The results of each MC realization are stored separately on the hard disk for later analysis.

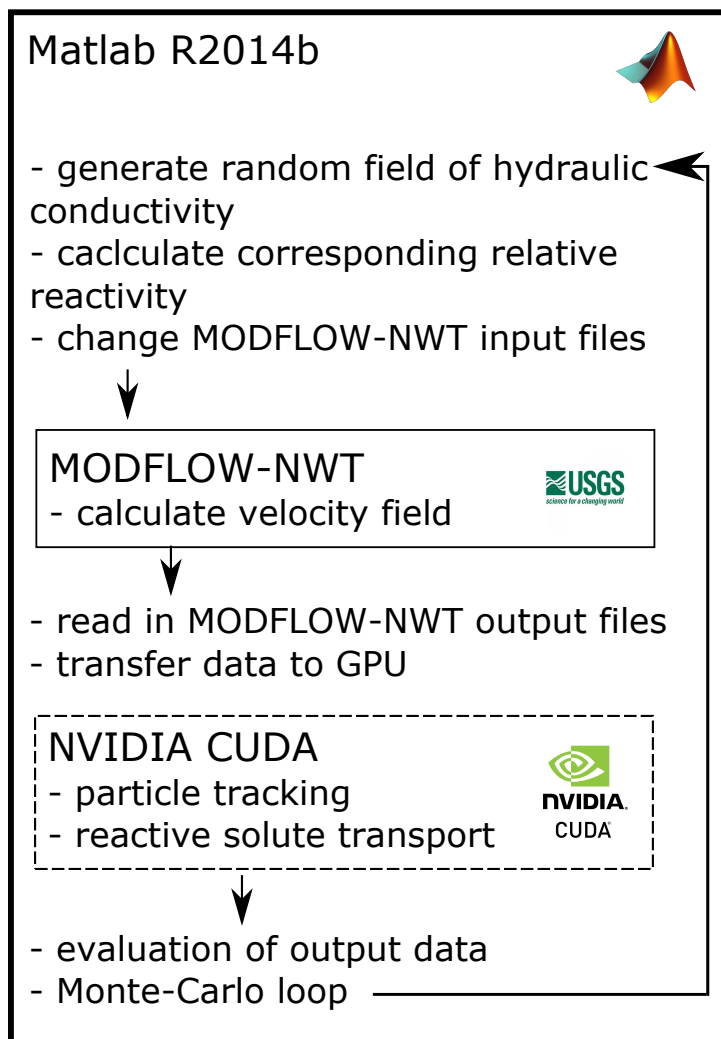


Figure 5.1: Schematic code procedure of the three-dimensional test cases.

GPU Programming

Recent advancements in Graphic Processing Units (GPUs), and in programming tools designed for utilizing their power, makes performing scientific calculations on a GPU an increasingly attractive option compared to classical Central Processing Unit (CPU) calculations. For GPU programming, NVIDIA's Compute Unified Device Architecture (CUDA) platform was used. CUDA is a parallel computing platform and application programming interface model. It allows the use of a CUDA-enabled GPU for general purpose processing. The CUDA platform is a software layer that gives direct access to the GPU's virtual instruction set and parallel computational elements and is designed to work with the programming language Matlab. With the available GPU-features of Matlab, parallel computing becomes feasible, as no deeper understanding of GPU programming is necessary. For the presented test cases a NVIDIA GeForce-GTX 970 graphics card was used.

Particle Tracking

Since particle tracking was identified as one of the remaining bottlenecks of the model runs with respect to a relatively large CPU run-time demand, the particle tracking scheme is implemented using a GPU based code to speed up the calculations. A particle tracking benchmark run on a synthetic three-dimensional aquifer with steady-state flow showed that significant speedups can be achieved compared to computation on the Central Processing Unit (see also *Erdal and Cirpka* [2015]). Figure 5.2 shows the tremendous speedup of the GPU-based particle tracking method for a test case similar to the one used in the test case of cumulative relative reactivity (rectangular synthetic test case with 1.5 million computational cells). The \log_{10} number of particles is plotted on the x-axis, and the \log_{10} simulation time is plotted on the y-axis. For more than 1,000 particles the GPU based particle tracking method outruns the CPU based method. When tracking one million particles the run-time on the CPU is about one hour and twenty minutes, whereas the run-time on the GPU is only about 11 seconds. This shows the immense speed up factor of the approach used in this work.

Reactive Transport

Similar to the particle tracking, the reactive transport along individual streamlines can be computed in parallel. Therefore the reactive transport calculations were also partly performed

5.2. CUMULATIVE RELATIVE REACTIVITY: TEST OF APPROACHES

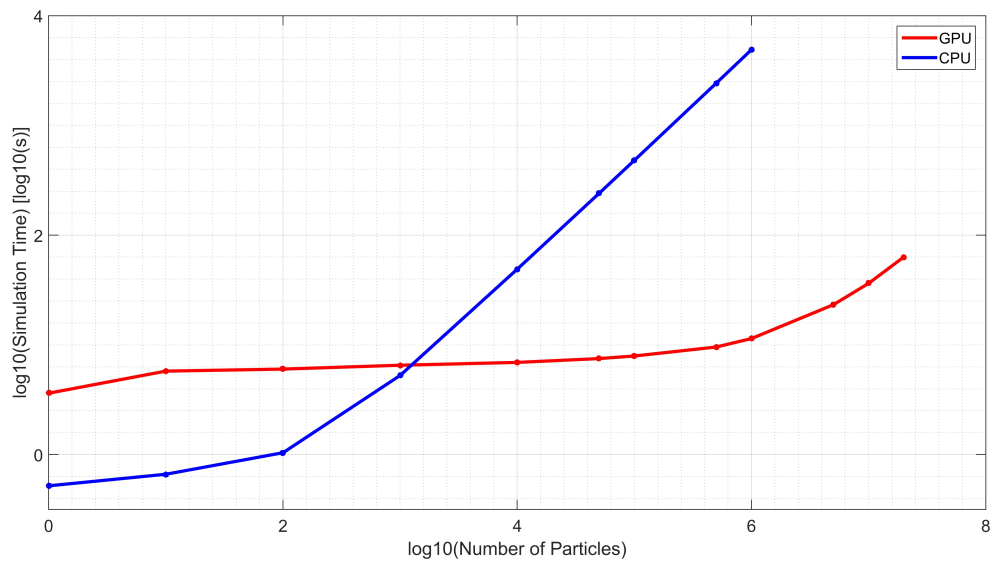


Figure 5.2: Comparison of the run-time of 3-D steady state particle tracking simulations with different numbers of particles on the Central Processing Unit (CPU) and the Graphical Processing Unit (GPU).

using NVIDIA's CUDA platform.

5.2 Cumulative Relative Reactivity: Test of Approaches

To show the validity and applicability of the new concept of cumulative relative reactivity I developed the following two test cases.

5.2.1 Two-Dimensional Benchmark Test on the Validity of the Cumulative Relative Reactivity

Set Up

To test the validity of the proposed concept of cumulative relative reactivity, a two-dimensional study in a $50\text{ m} \times 50\text{ m}$ domain with a $0.1\text{ m} \times 0.1\text{ m}$ resolution was performed. A pattern of two different materials was set up and filled by independent multi-Gaussian fields. Zone 1 had a

5.2. CUMULATIVE RELATIVE REACTIVITY: TEST OF APPROACHES

geometric mean of hydraulic conductivity of 10^{-4} m/s and a geometric mean of relative reactivity of 2, whereas the geometric means of hydraulic conductivity and relative reactivity in zone 2 were 10^{-3} m/s and 0.1, respectively. That is, on a larger scale log-hydraulic conductivity and log-relative reactivity are anti-correlated, whereas the local deviations are not correlated at all. The variance of $\ln(K)$ was 1.0 in both zones, and that of $\ln(f)$ was 0.25. Figure 5.3A shows the log-conductivity field, and Figure 5.3B the log-relative reactivity field for an arbitrarily chosen single realization. Figure 5.3C depicts the resulting flow net.

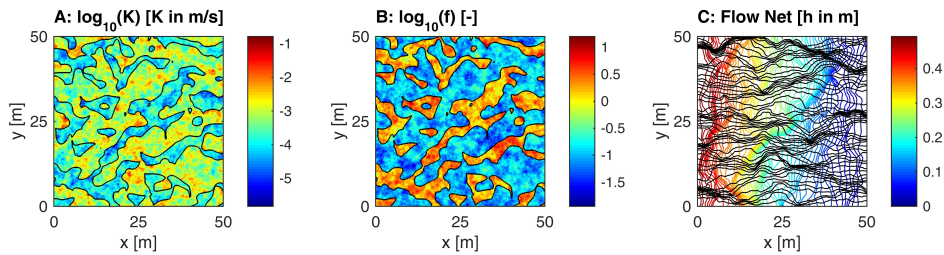


Figure 5.3: A: \log_{10} hydraulic conductivity, B: \log_{10} relative reactivity, and C: Flow net of the two-dimensional test case.

Results

Figure 5.4 compares the concentrations computed by solving the 2-D spatially explicit advection-dispersion-reaction model (“true”) to the concentrations computed by mapping the cumulative relative reactivity to reactive-species concentrations. The virtually true concentration distributions of oxygen (Figure 5.4A) and nitrate (Figure 5.4H) are shown in the first column. The concentration distributions obtained by mapping the cumulative relative reactivity to reactive-species concentrations are shown in the second column. The residual errors are shown in the third column, and the right column shows the *cdfs* of nitrate and dissolved oxygen concentrations in the outflow. All concentrations are normalized by the corresponding inflow concentrations.

As can be seen from Figures 5.4A, 5.4B, 5.4E and Figures 5.4H, 5.4I, 5.4L, respectively, the spatial patterns of oxygen and nitrate concentrations hardly differ among the different approaches. The biggest residual errors occur along the elongated stripes where old and young water mix by transverse dispersion. This holds not only for the mapping approach for strictly advective transport (Figures 5.4F & 5.4M), but also for the mapping approach based on the mean cumulative relative reactivity of advective-dispersive transport (Figures 5.4C & 5.4J). Figures 5.4D & 5.4G

5.2. CUMULATIVE RELATIVE REACTIVITY: TEST OF APPROACHES

show the *cdfs* of the normalized dissolved-oxygen concentration in the outflow, and Figures 5.4K & 5.4N show the *cdfs* of the normalized nitrate concentration. Differences in the *cdfs*, particularly a tendency to overestimate the occurrence of zero oxygen concentrations are apparent. Overall, the error introduced by neglecting (transverse) mixing seems to be acceptable, at least for the case of diffuse contamination controlled by reactions with the aquifer matrix considered here. These findings are in agreement with results of previous analyses on using exposure time as proxy for reactive transport [Sanz-Prat *et al.*, 2016a].

5.2. CUMULATIVE RELATIVE REACTIVITY: TEST OF APPROACHES

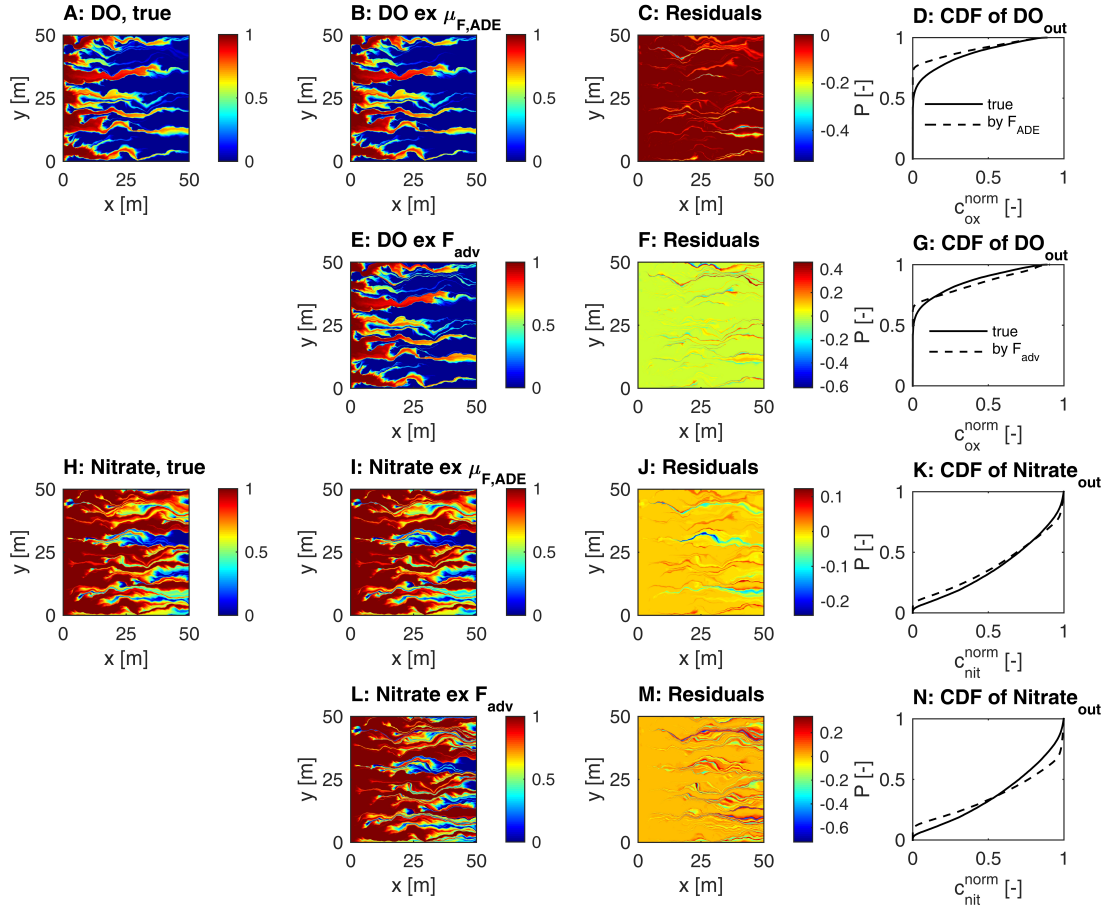


Figure 5.4: Comparison of the spatially explicit model results and the corresponding one-dimensional model results mapped on the 2-D domain. Left column: normalized concentrations of dissolved oxygen (DO) and nitrate obtained by the spatially explicit advective-dispersive-reactive model (true); second column: normalized concentrations of DO and nitrate computed by mapping the cumulative relative reactivity to dissolved-oxygen and nitrate concentrations (“by $\mu_{F, ADE}$ ”: using the mean cumulative relative reactivity F for advective-dispersive transport, “by F_{adv} ”: using the cumulative relative reactivity F for strictly advective transport); third column: residual errors; right column: comparison of *cdfs* at the outflow (solid lines: virtual truth; dashed lines: approximations based on mapping F). The first three columns are for a single realization, the last one averaged over 100 realizations.

5.2.2 Three-Dimensional Test Case on the Applicability of the Cumulative Relative Reactivity

Set Up

I designed a relatively simple three-dimensional test case to demonstrate the efficiency of approximating reactive transport using the cumulative relative reactivity for strictly advective transport. The model domain represents an aquifer that is drained by a river.

Figure 5.5A depicts the conceptual aquifer in plan view and Figure 5.5B in side view at the cross-section $y = 750m$ (see cutting line in Figure 5.5A). The model domain is a cuboid with a length of 2.5 kilometers, a width of 1.5 kilometers, and a depth of 50 meters. Three sides, as well as the bottom are assigned no-flow boundaries. On the remaining side, a constant-head boundary representing a river, is set down to a depth of 20 meters from the top, whereas the bottom 30 meters are considered a no-flow boundary. The head of the river is three meters below the model's top elevation. An extraction well is located at $x_{well} = 1,800m$, $y_{well} = 750m$ and constantly pumps at a rate of $5\ell/s$.

At the top boundary of the model, the spatial distribution of recharge as well as the nitrate and oxygen concentrations in the recharge are defined. It is assumed that the nitrate leaching into the groundwater has already passed the unsaturated zone. This implies that nitrate concentrations represent conditions in the infiltrating water below the root depth. Spatial variability in recharge as well as nitrate and oxygen concentrations in the inflow is expressed as auto-correlated multi-Gaussian random space functions. For dissolved oxygen, I account for a maximum concentration in the infiltrating water, set to $10.92\text{ mg}/\ell$ which is the saturation concentration of oxygen at 10°C in equilibrium to the atmosphere.

5.2. CUMULATIVE RELATIVE REACTIVITY: TEST OF APPROACHES

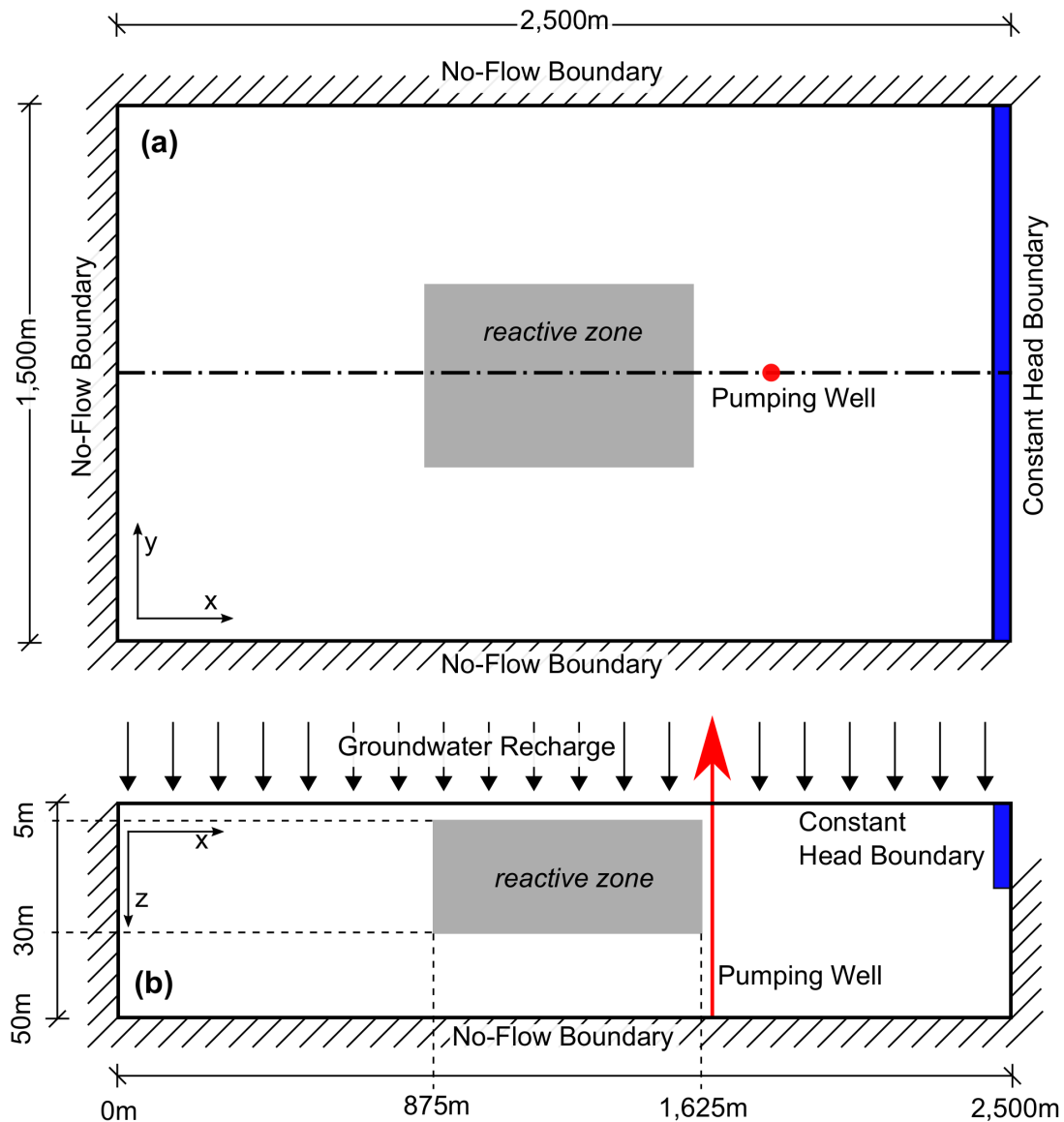


Figure 5.5: Schematic (a) plan view and (b) side view of the three-dimensional test case to test the applicability of the concept of cumulative relative reactivity.

As illustrated in Figure 5.5, the model contains a single reactive inclusion which is located in the center of the aquifer. The dimensions of the reactive zone are $750\text{m} \times 500\text{m} \times 25\text{m}$. Only in this reactive zone, aerobic respiration and denitrification take place. The inclusion may resemble a peat lens or carbonaceous limestone with a strong reduction potential. In the surrounding non-reactive zones the relative reactivity f is set to zero.

A three-dimensional, blockwise stationary multi-Gaussian random field with mean 1, variance

5.2. CUMULATIVE RELATIVE REACTIVITY: TEST OF APPROACHES

0.25, correlation lengths of $500m \times 500m \times 25m$, and integral scales of $760m \times 500m \times 25m$ in the x -, y -, and z -direction, following a Gaussian covariance function was generated to obtain the values for log-relative reactivity within the inclusion. This ensures that values for the relative reactivity are non-negative and spatially correlated. The realization of the reactive zone for this study is shown in detail in Figure 5.6. Isolines of relative reactivity show the changing relative reactivity throughout the reactive zone. In the upper left corner of the domain, f reaches values of up to three. The values of f decrease in the x -direction. The reactive and non-reactive zones also differ in hydraulic conductivity. For better visualization and comprehensibility of the results, hydraulic conductivity is set uniform within the reactive ($10^{-3} m/s$) and non-reactive zones ($10^{-4} m/s$).

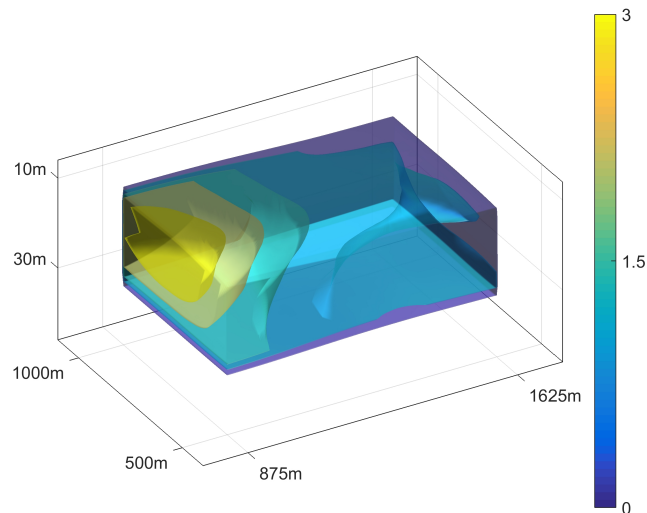


Figure 5.6: Relative Reactivity of the three-dimensional test case of cumulative relative reactivity.

Reactive System

In this test case, it is assumed that the microbial turnover over oxygen and nitrate depends on the solute concentrations and the release of electron donors from the aquifer matrix. The chemical processes of aerobic respiration and denitrification are modeled using standard Michaelis-Menten kinetics. On larger scales, like in the present application, Michaelis-Menten laws may be seen as effective expressions, leading to a specific type of concentration dependence without agreeing

5.2. CUMULATIVE RELATIVE REACTIVITY: TEST OF APPROACHES

with strictly enzymatic reactions. In particular, aerobic metabolism is known to be practically independent of the dissolved-oxygen concentration over a wide range of concentrations [e.g., *Diem et al.*, 2013] so that the main purpose of the (small) Michaelis-Menten coefficient of oxygen is to smooth the zero-order reaction law at low concentrations, rather than to reflect the actual strength of oxygen-enzyme binding. Michaelis-Menten coefficients of nitrate are typically higher than those of oxygen, expressing less efficiency of the bacteria to process nitrate in comparison to oxygen.

Neither the electron-donor concentration nor the biomass concentrations, which are both assumed to be at steady-state, are explicitly calculated. Instead, the effects of these concentrations are parametrized by the relative reactivity f . For thermodynamics reasons, it is assumed that oxygen is consumed first. If there is hardly any oxygen left, the reduction of nitrate starts. This is expressed by a non-competitive inhibition term in the kinetic rate laws as follows:

$$r_{0,DO} = \frac{dc_{DO}}{dF} = -\frac{c_{DO}}{c_{DO} + K_{DO}} \cdot r_{max}^{aer} \quad (5.1)$$

$$r_{0,Nit} = \frac{dc_{Nit}}{dF} = -\frac{c_{Nit}}{c_{Nit} + K_{Nit}} \cdot \frac{K_{DO}^{inh}}{K_{DO}^{inh} + c_{DO}} \cdot r_{max}^{Nit} \quad (5.2)$$

in which c_{DO} [ML⁻³] is the concentration of dissolved oxygen, c_{Nit} [ML⁻³] is the nitrate concentration, K_i [ML⁻³] is the Michaelis-Menten constant of terminal electron acceptor i , r_{max}^{aer} [ML⁻³T⁻¹] and r_{max}^{Nit} [ML⁻³T⁻¹] are the maximum reaction rates of oxygen and nitrate, respectively, for a relative reactivity of one, and K_{DO}^{inh} [ML⁻³] is the inhibition constant of oxygen in denitrification.

Results

For each location of the domain, particle tracking has led to unique values of travel time, cumulative relative reactivity, and origin. The origin and travel time yields the concentrations of the reactive species in the infiltrating water, whereas the cumulative relative reactivity yields the progress in reducing the electron acceptors. With the mapping procedure, a transfer to

5.2. CUMULATIVE RELATIVE REACTIVITY: TEST OF APPROACHES

the reactive-species concentrations obtained from solving the ODE system of equation to the spatial distribution of reactive-species concentrations is possible. For Figure 5.7, 1,000 ODE calculations were performed. They cover a wide range of inflow values. From these 1,000 ODE runs, the nitrate and oxygen concentration at all points (in this case 1.5 million cell centers) by interpolation in the c_{0,Nit^-} , F^- , and $c_{0,DO}$ -dimensions could be determined.

Figure 5.7A depicts the cumulative relative reactivity $F(\mathbf{x})$. Only when the reactive zone is reached values for the cumulative relative reactivity are non-zero. They rise until they reach the downstream end of the reactive zone and stay constant after that. Figures 5.7B & 5.7C shows the resulting spatial concentration distributions of nitrate and oxygen for the case presented in Figure 5.5 for uniform input at the land surface (nitrate: $40 \text{ mg}/\ell$; oxygen: $10 \text{ mg}/\ell$). The influence of the reactive zone can be seen. The concentrations of nitrate and oxygen decrease significantly while passing the reactive zone. Among other features, Figure 5.7 shows the effect that denitrification is inhibited at elevated oxygen levels. As long as oxygen is present in the system (Figures 5.7C), nitrate concentrations stay comparatively high. Only when all oxygen is consumed, the denitrification process starts and nitrate is degraded.

5.2. CUMULATIVE RELATIVE REACTIVITY: TEST OF APPROACHES

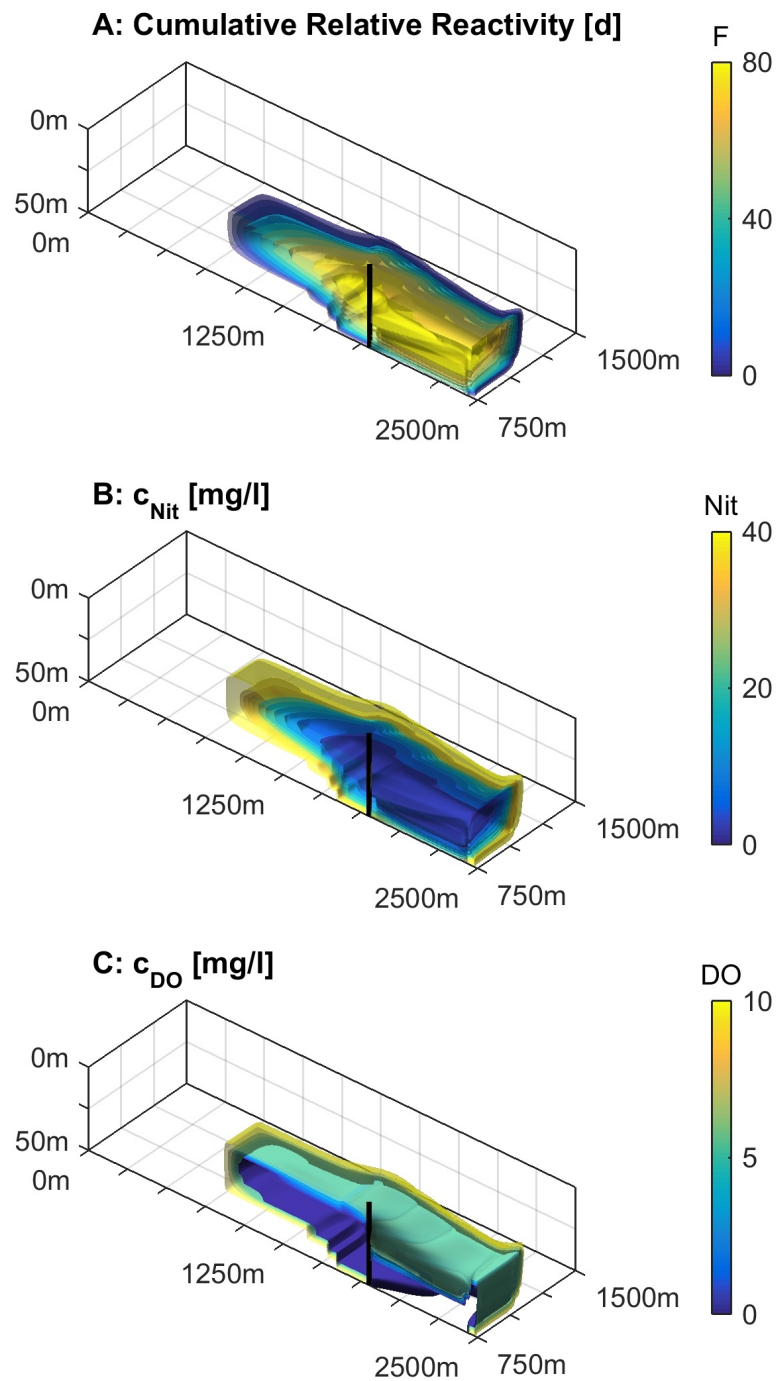


Figure 5.7: Cumulative relative reactivity (A) and steady-state concentration distribution of nitrate (B) and dissolved oxygen (C) isosurfaces according to the proposed mapping procedure applied to the three-dimensional test case for uniform input at the land surface (nitrate: $40 \text{ mg}/\ell$; oxygen: $10 \text{ mg}/\ell$). Black line: extraction well.

5.3 Decreasing Reaction Potential: Test of Approaches

To show the validity and applicability of the concept of cumulative relative reactivity including travel-time increments, as well as a relation between relative reactivity and NOM, I developed the following two test cases.

5.3.1 One-Dimensional Benchmark Test on the Relation between Relative Reactivity and NOM

Set Up

The length of the modeling domain was chosen to be 50 m. The linear average velocity of 1 m/d was assumed to be uniform and constant. The model accounts for advection, dispersion, biomass growth and decay with associated turnover of nitrate, oxygen, and dissolved organic carbon, as well as the release of dissolved organic carbon (DOC) from NOM in the matrix. Three solutes (nitrate, dissolved oxygen, dissolved organic carbon) and two immobile constituents (natural organic matter, biomass) were considered. The constant inflow concentration of nitrate (50 mg/ℓ) and dissolved oxygen (10 mg/ℓ) represent typical values. The initial organic carbon content of the aquifer material was set to a uniform value of 45 mg_C/kg_{soil}. The initial biomass concentration was set to 4.5×10^{-5} mol_C/kg_{soil} and the maximal biomass concentration was specified at 0.045 mol_C/kg_{soil}. In the model, the natural organic matter in the aquifer matrix cannot directly be used by the microorganisms.

Reactive System

For this test case a highly detailed description of the reactions is considered. The one-dimensional model considers the dynamic biomass of an immobile facultative anaerobic microbial culture, dissolved organic carbon, nitrate and oxygen as solutes, and natural organic matter as electron-donor pool in the matrix. The rate of change r_i of the respective compound i and can be described as [adapted from *Sanz-Prat et al.*, 2015]:

5.3. DECREASING REACTION POTENTIAL: TEST OF APPROACHES

$$r_{DO} = -\frac{\mu_{DO}}{Y_{DO}} \cdot \frac{\varrho_b}{\theta} \cdot c_{bio}^* \quad (5.3)$$

$$r_{Nit} = -\frac{\mu_{Nit}}{Y_{Nit}} \cdot \frac{\varrho_b}{\theta} \cdot c_{bio}^* \quad (5.4)$$

$$r_{DOC} = r_{DOC}^{rel} - \left(\frac{\mu_{DO}}{Y_{DO}} + \frac{5}{4} \frac{\mu_{Nit}}{Y_{Nit}} \right) \cdot \frac{\varrho_b}{\theta} \cdot c_{bio}^* \quad (5.5)$$

$$r_{NOM}^* = -\frac{\theta}{\varrho_b} \cdot r_{DOC}^{rel} \quad (5.6)$$

$$r_{bio}^* = \left((\mu_{DO} + \mu_{Nit}) \cdot \left(1 - \frac{c_{bio}}{c_{bio}^{max}} \right) - k_{dec} \right) \cdot c_{bio}^*(x) \quad (5.7)$$

with:

$$\mu_{DO} = \frac{c_{DO}}{c_{DO} + K_{DO}} \cdot \frac{c_{DOC}}{c_{DOC} + K_{DOC}} \cdot \mu_{max}^{aer} \quad (5.8)$$

$$\mu_{Nit} = \frac{c_{DOC}}{c_{DOC} + K_{DOC}} \cdot \frac{c_{Nit}}{c_{Nit} + K_{Nit}} \cdot \frac{K_{DO}^{inh}}{K_{DO}^{inh} + c_{DO}} \cdot \mu_{max}^{Nit} \quad (5.9)$$

in which $c_{DO}(\mathbf{x}, t)$ [$\text{mol}_{\text{DO}}\text{L}^{-3}$], $c_{Nit}(\mathbf{x}, t)$ [$\text{mol}_{\text{Nit}}\text{L}^{-3}$], and $c_{DOC}(\mathbf{x}, t)$ [$\text{mol}_{\text{C}}\text{L}^{-3}$] are the concentrations of dissolved oxygen, nitrate and dissolved organic carbon, respectively, whereas $c_{bio}^*(\mathbf{x}, t)$ [$\text{mol}_{\text{C}}\text{M}_{\text{soil}}^{-1}$] denotes the mass-related concentration of the immobile biomass in the aquifers matrix. ϱ_b [$\text{M}_{\text{soil}}\text{L}^{-3}$] and θ [-] are the dry bulk mass density of the aquifer material and the volumetric water content, respectively. $\mu_{DO}(\mathbf{x}, t)$ [T^{-1}] and $\mu_{Nit}(\mathbf{x}, t)$ [T^{-1}] are the specific growth rates due to aerobic respiration and denitrification, respectively, whereas μ_{max}^{aer} [T^{-1}] and μ_{max}^{Nit} [T^{-1}] are the corresponding maximum specific growth rates. Y_{DO} [$\text{mol}_{\text{C}}\text{mol}_{\text{DO}}^{-1}$] and Y_{Nit} [$\text{mol}_{\text{C}}\text{mol}_{\text{Nit}}^{-1}$] are the yield coefficients of aerobic respiration and denitrification, respectively, K_i [molL^{-3}] denotes the Monod constant of compound i , and K_{DO}^{inh} [molL^{-3}] is the inhibition constant of oxygen in denitrification. c_{bio}^{max} [$\text{mol}_{\text{C}}\text{M}_{\text{soil}}^{-1}$] is the maximum biomass concentration, and k_{dec} [T^{-1}] denotes the rate coefficient of biomass decay. Finally, $r_{DOC}^{rel}(\mathbf{x}, t)$ [$\text{mol}_{\text{C}}\text{T}^{-1}\text{L}^{-3}$] denotes the release rate of dissolved organic carbon from the aquifer matrix, which I model as a

5.3. DECREASING REACTION POTENTIAL: TEST OF APPROACHES

first-order mass-transfer process:

$$r_{DOC}^{rel} = k_{DOC}^{rel,eff} \cdot (c_{DOC}^{sat} - c_{DOC}) \quad (5.10)$$

with

$$k_{DOC}^{rel,eff} = k_{DOC}^{rel,max} \cdot \left(\frac{c_{NOM}^*}{c_{NOM}^{*init}} \right)^{\frac{2}{3}}. \quad (5.11)$$

in which $k_{DOC}^{rel,eff}$ [T⁻¹] is the effective rate coefficient of DOC release with its maximum of $k_{DOC}^{rel,max}$ [T⁻¹], obtained at the initial concentration c_{NOM}^{*init} [mol_CL⁻³] of NOM, c_{DOC}^{sat} [mol_CL⁻³] denotes the saturation concentration of DOC, and $c_{NOM}^*(\mathbf{x}, t)$ [mol_CM_{soil}⁻¹] is the mass-related concentration of the natural organic matter in the aquifers matrix. The release rate of DOC changes with changing concentration of NOM. At early times, the microorganisms can utilize the easily available NOM. With progressing dissolution of NOM, the surface area of bioavailable NOM decreases. Assuming spherical NOM particles and a release rate that is proportional to the surface area, one arrives at the power-law dependence of the release rate to the NOM concentration with an exponent of 2/3 in equation 5.11. The dissolved organic carbon has an upper limit of 10 mg/l.

In order to test the concept of the relative reactivity, the reaction rates of equations 5.3 and 5.4 are split into equations that only depend on the dissolved-oxygen and nitrate concentrations:

$$r_{0,DO} = -\frac{c_{DO}}{c_{DO} + K_{DO}} \cdot \frac{\mu_{max}^{aer}}{Y_{DO}} \cdot c_{bio}^{max}, \quad (5.12)$$

$$r_{0,Nit} = -\frac{c_{Nit}}{c_{Nit} + K_{Nit}} \cdot \frac{K_{DO}^{inh}}{K_{DO}^{inh} + c_{DO}} \cdot \frac{\mu_{max}^{Nit}}{Y_{Nit}} \cdot c_{bio}^{max}, \quad (5.13)$$

5.3. DECREASING REACTION POTENTIAL: TEST OF APPROACHES

and a factor containing the DOC and biomass concentrations:

$$f = \frac{c_{DOC}}{c_{DOC} + K_{DOC}} \cdot c_{bio}^* \cdot \left(1 - \frac{k_{dec}}{(\mu_{max}^{Nit} + \mu_{max}^{DO})} \right). \quad (5.14)$$

The factor defines the relative reactivity for the given problem. Because the DOC and biomass concentrations are dynamic state variables, it cannot be expected a priori that the relative reactivity f as calculated by equation 5.14 depends purely on the NOM-concentration in the matrix as implied by the simplified reaction scheme.

Results

With the results obtained by the detailed bioreactive transport model I computed the relative reactivity according to equation 5.14. Figure 5.8 shows the relationship between the calculated organic carbon content in the aquifer c_{NOM} and the relative relative reactivity f restricted to time points with noticeable reactions. I observed a monotonic relationship in which the relative reactivity increases rapidly with the organic-carbon content and then reaches its maximum rate once the organic-carbon is at saturation. Figure 5.8 also includes the following parametric fit $g(c_{NOM})$ to the data as dashed line:

$$g(c_{OC}) = \frac{(c_{NOM})^a}{(c_{NOM})^a + K_{NOM,f}^a} \quad (5.15)$$

in which $c_{NOM} [\text{molCM}_{\text{soil}}^{-1}]$ is the concentration of organic carbon in the aquifer and $K_{NOM,f} [\text{molCM}_{\text{soil}}^{-1}]$ is the half-reactivity concentration, whereas $a [-]$ is a fitting exponent. The fitting parameters a , and $K_{NOM,f}$ depend on the type of reactive material and the reactive system. In the present application, I obtained the following values:

5.3. DECREASING REACTION POTENTIAL: TEST OF APPROACHES

$$a = 0.5$$
$$K_{NOM,f} = 0.5$$

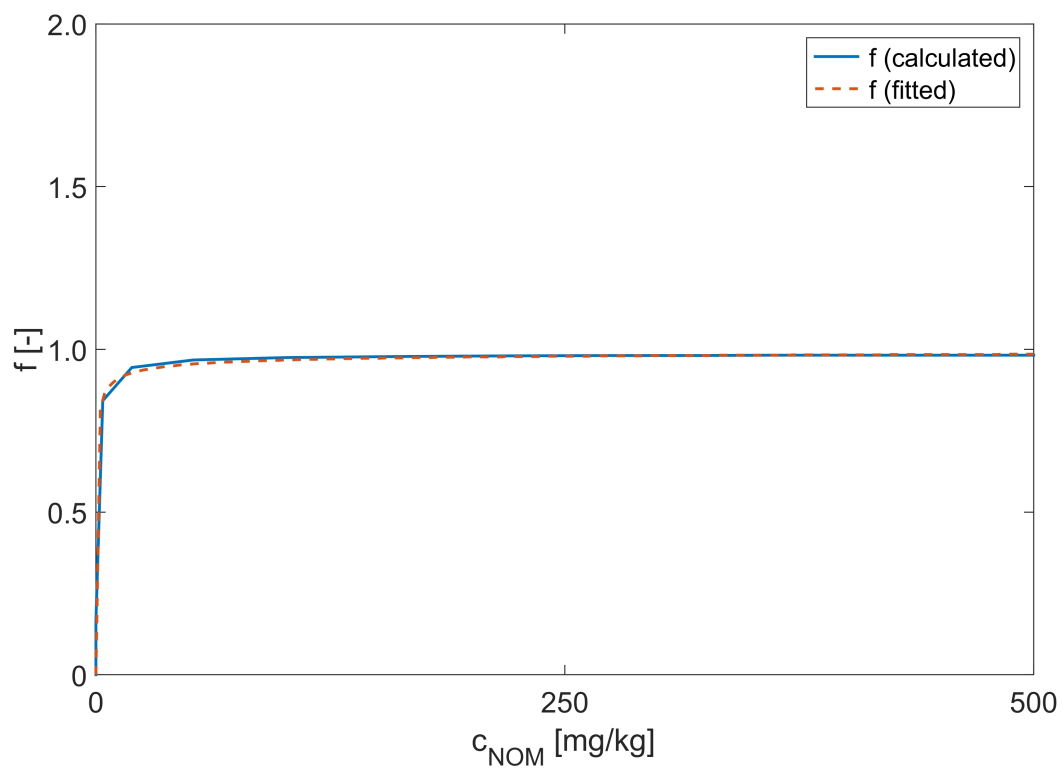


Figure 5.8: Relationship between natural-organic-matter concentration and relative reactivity f , calculated by equation 5.14, in the one-dimensional domain. Line: simulation results of the model with detailed reaction kinetics, markers: parametric fit according to equation 5.15.

5.3.2 Two-Dimensional Benchmark Test on the Validity of the Decreasing Reaction Potential

Set Up

To test the validity of the presented approach of the decreasing reaction potential using the cumulative relative reactivity and travel-time increments, I set up a two-dimensional heterogeneous test case. The study domain is $50\text{ m} \times 25\text{ m}$ with a resolution of $0.1\text{ m} \times 0.1\text{ m}$. The hydraulic conductivity was randomly generated using an exponential covariance model field with variance of 1.0 and a geometric mean of 10^{-3} m/s . The spatially distribution of NOM concentration was generated by adding a multi-Gaussian random field to the generated hydraulic conductivity with variance of 0.25, correlation length of 5 in both directions and a mean NOM concentration of $0.05\text{ mol}_C/\text{kg}$. Figure 5.9(A) shows the log hydraulic conductivity field, Figure 5.9(D) the spatial distribution of NOM. A correlation can be seen. High values of hydraulic conductivity tend to have lower concentration of NOM and vice versa. For the spatially explicit model the longitudinal dispersivity was set to $\alpha_l = 0.01\text{ m}$, the transverse dispersivity $\alpha_t = 0.001\text{ m}$, and the molecular diffusion coefficient to $D_m = 10^{-9}\text{ m}^2/\text{s}$.

The top and the bottom of the domain were assigned no-flow boundaries, whereas the left and right side were assigned fixed-head boundaries. The head difference was set to 0.2 m . Groundwater flow was solved by the finite element method with bilinear elements. I generated a streamline-oriented grid with 250×500 elements by solving for stream function values [Cirpka *et al.*, 1999b]. The resulting flow net is depicted in Figure 5.9(C). I solved steady state transport on the streamline-oriented grid using the cell-centered finite volume method for spatial discretization [Cirpka *et al.*, 1999a]. After that I computed the mean travel time distribution for strictly advective transport with the mean groundwater-age equation from Goode [1996] and the mean cumulative relative reactivity for strictly advective transport. Figure 5.9(B) shows the advective travel times and Figure 5.9(E) shows the cumulative relative reactivity.

5.3. DECREASING REACTION POTENTIAL: TEST OF APPROACHES

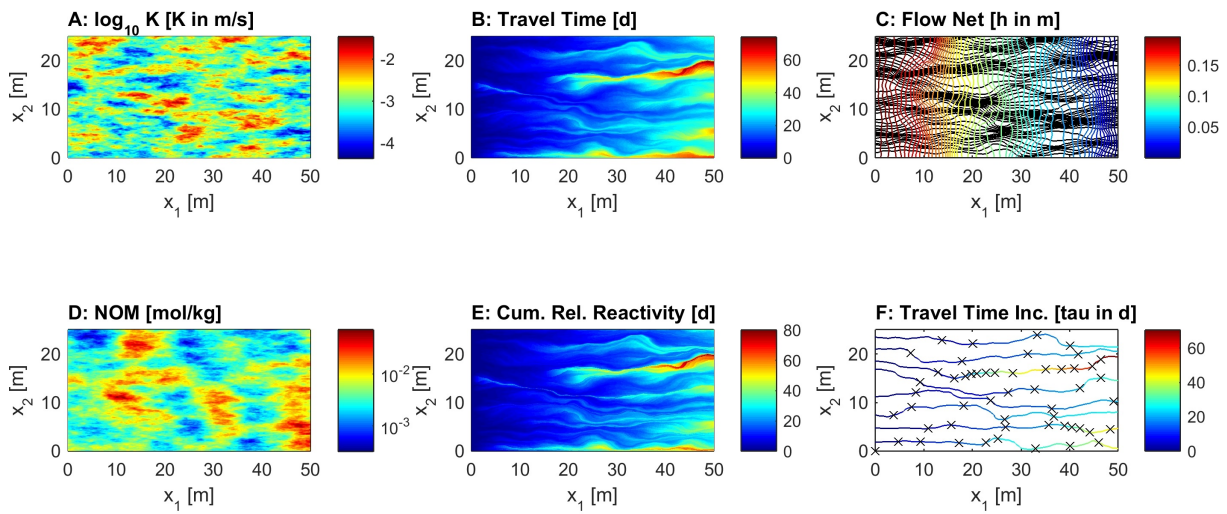


Figure 5.9: Two-dimensional test case on the validity of the decreasing reaction potential.. (A) Spatial distribution of log-hydraulic conductivity; (B) mean groundwater age for strictly advective transport; (C) flow net (colored lines: heads; black lines: streamlines); (D) Spatial distribution of NOM; (E) mean cumulative relative reactivity for strictly advective transport; (F) selected streamlines with travel-time increments (colored lines: streamlines with travel time; crosses: travel-time increments of five days).

Reactive System

I simulated aerobic respiration and denitrification with two different models. The inflow concentrations were constant (8 mg/l for dissolved oxygen and 62 mg/l for nitrate). The first model uses the spatially explicit advection-dispersion-reaction equation for steady state flow with a fully implicit approach using Newton-Raphson iterations. The second model is the simplified model using cumulative relative reactivity and travel-time increments. The reactive system of aerobic respiration and denitrification for the simplified model is the same than in the previous one-dimensional test case (Chapter 5.3.1). Figure 5.9(F) shows selected streamlines colored with travel time. The marks indicate the travel-time increments. The influence of the travel time on the spatial discretization can be seen. Whereas streamlines with a low travel time have less travel-time increments (e.g. the fifth streamline from the top), streamlines with a high travel time have also a higher spatial discretization (e.g. the third streamline from the top). In this case the travel-time increments were set to five days. The simulation time was 100 years. For the computation of the relative reactivity I used equation 5.15.

Result

Figure 5.10 shows the breakthrough curves of dissolved oxygen (blue) and nitrate (red) for the spatially explicit model (dashed lines) and the simplified model (solid lines) for a single realization shown in Figure 5.9. The concentration of nitrate show a good agreement. The simplified model is able to predict the breakthrough of nitrate at the outflow. For dissolved oxygen, the simplified model overestimates the concentration. In both cases the NOM concentration of the artificial aquifer is totally depleted after 100 years. In the simplified model the resulting concentration profiles are not as smooth as in the spatially explicit model. This is due to the discretization into travel-time increments. The concentrations are updated for every $\Delta\tau$.

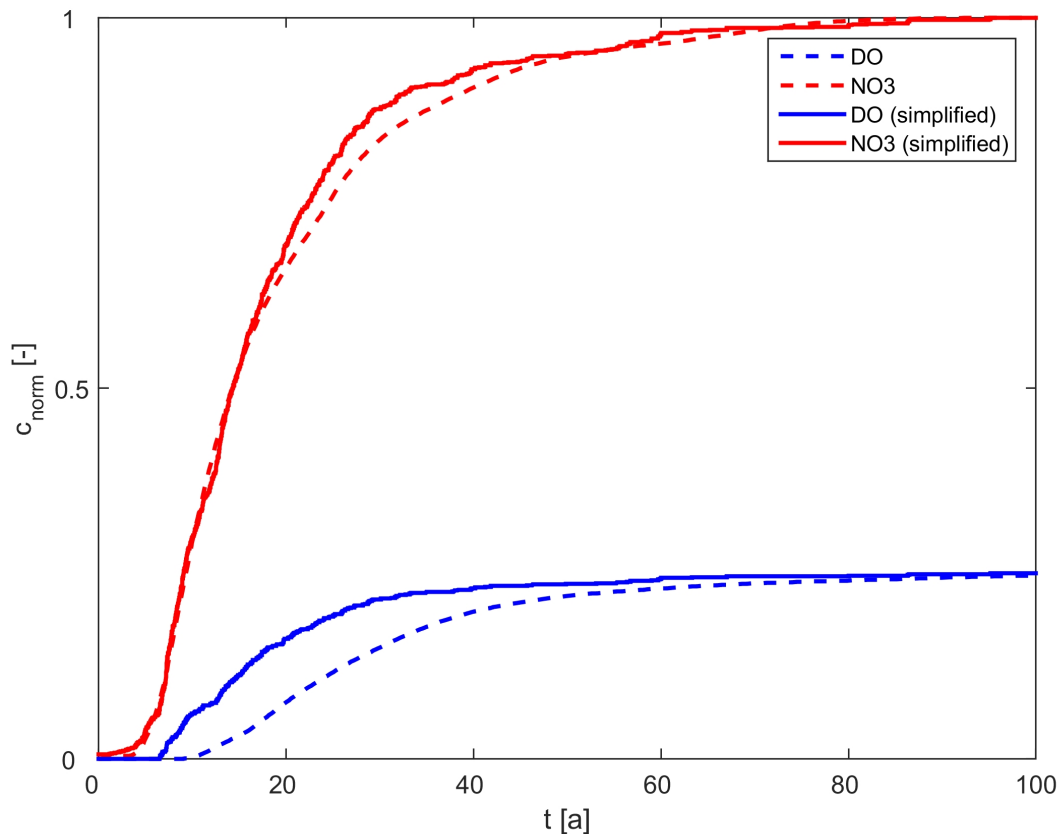


Figure 5.10: Comparison of the two-dimensional test case on the validity of the decreasing reaction potential. Breakthrough curves of dissolved oxygen and nitrate concentrations at the outflow for a single realization over 100 years. Dashed lines: spatially explicit advective-dispersive-reactive model. Solid lines: simplified model using cumulative reactive reactivity with travel-time increments.

5.3.3 Three-Dimensional Test Case on the Applicability of the Decreasing Reaction Potential

Set Up

The rectangular three-dimensional domain, depicted in Figure 5.11, resembles a small aquifer. The model considers only the saturated zone, thus leaving out the intricate feedback between surface water hydrology, vegetation, as well as water movement and nutrient cycling in the vadose zone. Flow is introduced from the top by groundwater recharge with a constant rate of 450 mm a^{-1} , and from the left side, where a constant head boundary down to a depth of 2 meters represents an infiltrating river. The remaining left side is considered to be a no flow boundary. At the right side I consider a constant head boundary. The remaining sides are no flow boundary conditions. Figure 5.11 shows a plan view (A) and a vertical cross-section (B) of the three-dimensional domain.

Two extraction wells are located at $(x_{well,1}, y_{well,1}) = (2000\text{m}, 900\text{m})$ and $(x_{well,2}, y_{well,2}) = (1610\text{m}, 470\text{m})$. The first well is screened over the entire depth of the aquifer, whereas the second well is screened only in the upper sediment layer to a depth of 10m . The fully screened well has a pumping rate of $30 \ell \text{ s}^{-1}$, the partially penetrating well has an assigned pumping rate of $15 \ell \text{ s}^{-1}$. Two groundwater observation wells are located upstream of the two pumping wells at $(x_{obs,1}, y_{obs,1}) = (1800\text{m}, 900\text{m})$ and $(x_{obs,2}, y_{obs,2}) = (1400\text{m}, 470\text{m})$, respectively.

Like in the previous three-dimensional models, nitrate and oxygen concentrations are introduced by groundwater recharge from the top and by bank infiltration at the left side of the model domain. The recharging water is assumed to have already passed the unsaturated zone above the aquifer. The nitrate and oxygen concentrations in groundwater recharge were set to $50 \text{ mg}(\text{NO}_3^-) \ell^{-1}$ and $10 \text{ mg}(\text{O}_2) \ell^{-1}$, respectively. The nitrate and oxygen concentrations of the infiltrating river water were set to $30 \text{ mg}(\text{NO}_3^-) \ell^{-1}$ and $7 \text{ mg}(\text{O}_2) \ell^{-1}$.

5.3. DECREASING REACTION POTENTIAL: TEST OF APPROACHES

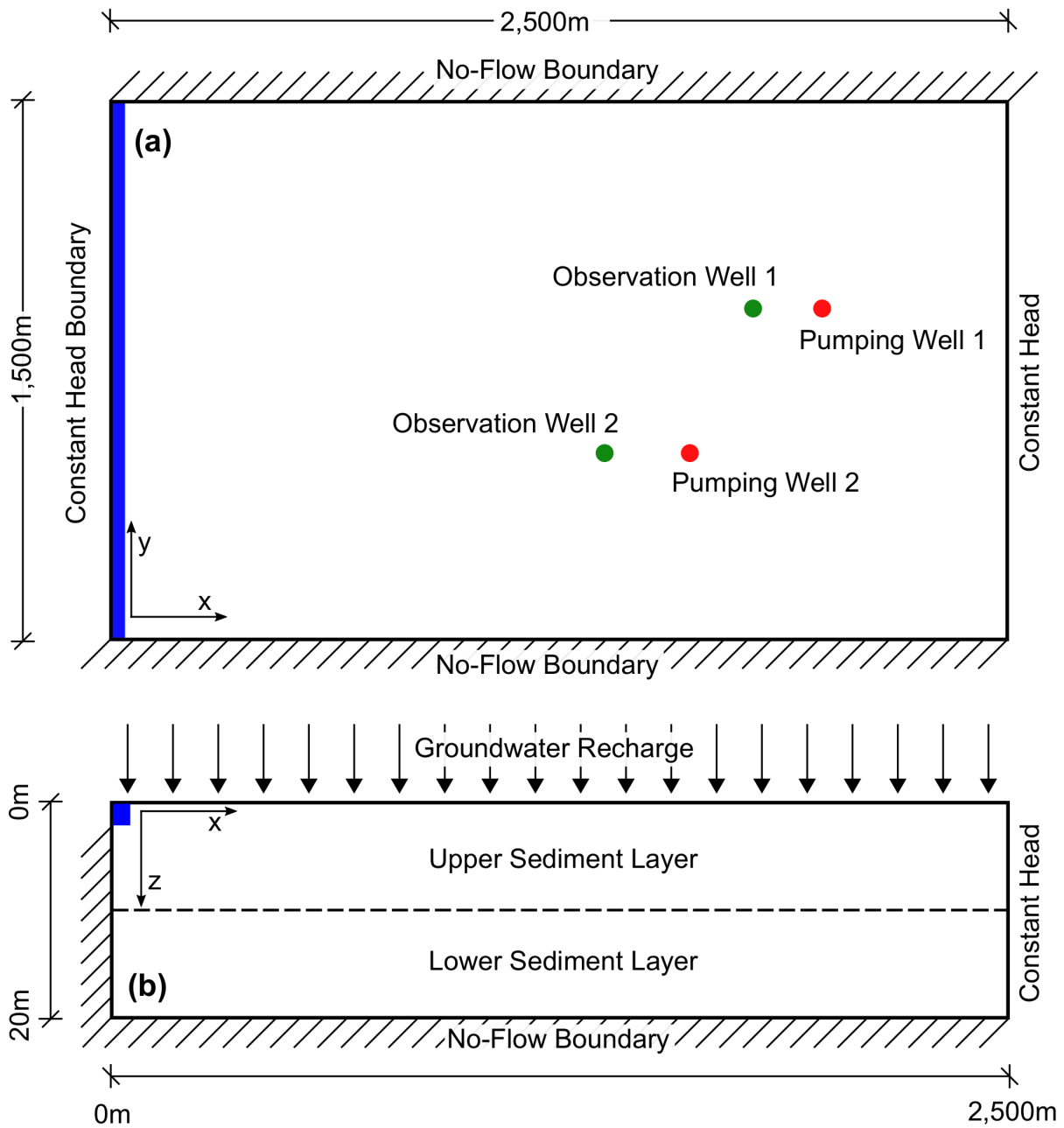


Figure 5.11: Schematic (a) plan view and (b) side view of the three-dimensional test case to test the applicability if the decreasing denitrification potential.

The aquifer consists of two heterogeneous sediment layers. They differ in their mean hydraulic conductivity and NOM-content, which also implies differences in their denitrification potential. The upper sediment layer extends from the top of the model domain to a depth of 10 meters,

5.3. DECREASING REACTION POTENTIAL: TEST OF APPROACHES

the lower from a depth of 10 meters to 20 meters, where the aquifer is underlain by impervious material. The log-hydraulic conductivity in the two layers is assumed to be independent, auto-correlated, multi-Gaussian random-space functions.

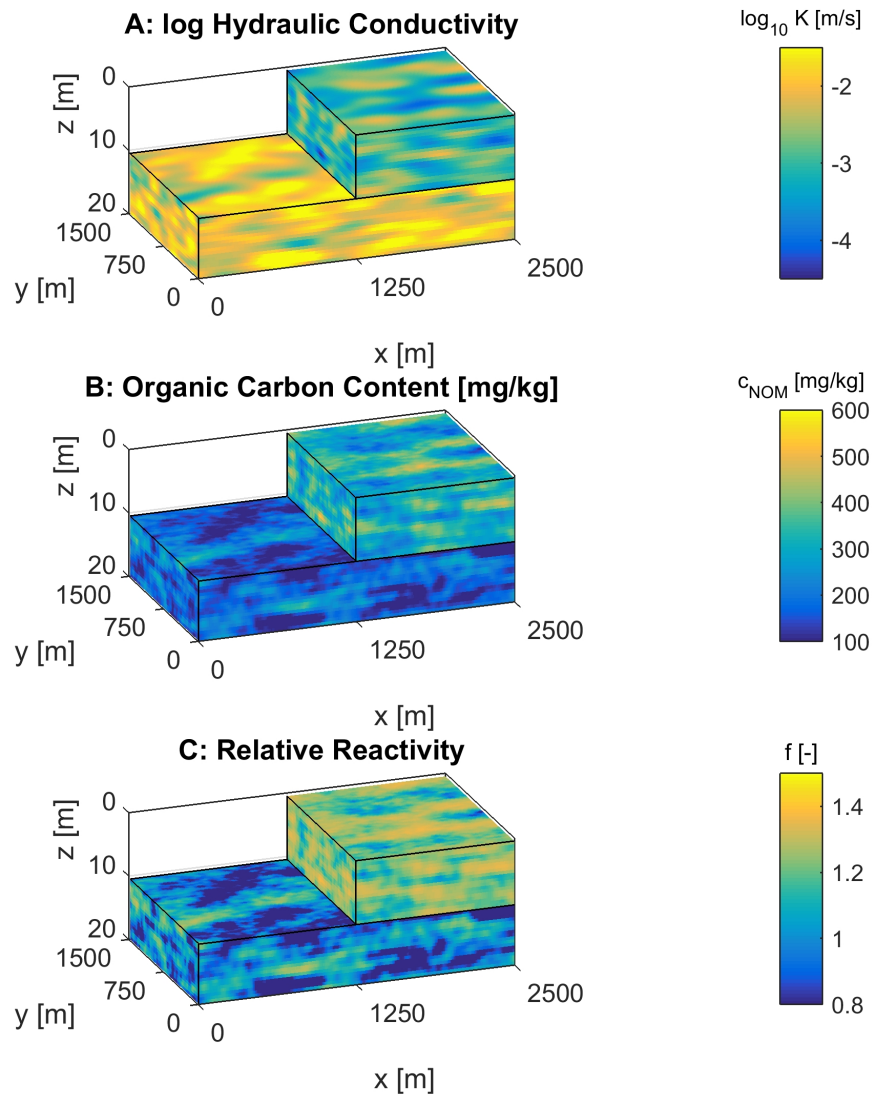


Figure 5.12: Parameter distribution in a single realization of the three-dimensional domain: A: log-hydraulic conductivity; B: organic-carbon content ; C: relative reactivity.

The organic-carbon content is assumed to be correlated to the hydraulic conductivity. Areas with a high hydraulic conductivity are assigned a low organic-carbon content, whereas areas with a low

5.3. DECREASING REACTION POTENTIAL: TEST OF APPROACHES

hydraulic conductivity are assigned a high organic-carbon content, following the rationale that fines have higher natural-organic-matter concentrations. The organic-carbon content is computed by:

$$c_{NOM} = (\log_{10}(K) + \xi) \cdot A \quad (5.16)$$

in which c_{NOM} is the NOM concentration [$M_C M_{soil}^{-1}$], K [LT^{-1}] is the hydraulic conductivity, ξ is an independent multi-Gaussian random field with zero mean, variance of 0.025, and correlation lengths of 30m, 20m, and 2m in the x -, y -, and z -direction, respectively. $A = -50$ [$mol_C m_{soil}^{-3}$] is a scaling parameter. Figure 5.12 visualizes the spatially distributed material properties of a single realization. Figure 5.12A shows the log-hydraulic conductivity, Figure 5.12B the organic-carbon content, and Figure 5.12C the corresponding relative reactivity according to Equation 5.15. The difference in the two sediment layers can be clearly seen. The upper layer is more reactive and has a lower hydraulic conductivity, whereas the lower sedimentary layer has a higher hydraulic conductivity and a lower reactivity.

Reactive System

The detailed model given above involves many states and parameters that are difficult to determine in practical applications. Based on the findings in the previous test cases, the system can be simplified with the following assumptions:

1. Except for the initial establishment of a microbial anaerobic community, there may be no need to simulate the abundances of microbes explicitly. Also, the presence of microbes does not influence the hydraulic conductivity.
2. The dissolved assimilable organic carbon adapts quickly to the environmental conditions and does not need to be simulated explicitly. The content of natural organic matter or other electron donors in the matrix, by contrast, exhibits a major control on aerobic respiration and denitrification [Bradley *et al.*, 1992; D'haene *et al.*, 2003; Drury *et al.*, 1991; Hiscock *et al.*, 1991; Smith, 1980]. This is addressed by relating the relative reactivity to the natural-organic-matter content of the aquifer, which is depleted over time by the reactions.

5.3. DECREASING REACTION POTENTIAL: TEST OF APPROACHES

3. The inhibition constant K_{DO}^{inh} of oxygen in denitrification is typically so low that even the smallest dissolved-oxygen concentration can be considered inhibitory for denitrification.
4. The Monod constant K_{DO} of oxygen is typically so low that aerobic respiration can be considered to exhibit zero-order kinetics.
5. The Monod constant K_{nit} of nitrate, by contrast, is typically so high that a first-order dependence of denitrification rates on nitrate becomes valid.

With these simplifications, the reaction rates of oxygen and nitrate for a relative reactivity f of unity, become:

$$r_{0,DO} = -r_{0,DO}^{max} H(c_{ox}) \quad (5.17)$$

$$r_{0,nit} = -k_{0,nit} c_{nit} \cdot (1 - H(c_{ox})) \quad (5.18)$$

with the zero-order reaction rate $r_{0,DO}^{max}$ [$\text{mol}_{\text{DO}}\text{L}^{-3}\text{T}^{-1}$] under standard conditions, the first-order decay coefficient $k_{0,nit}$ [T^{-1}] of nitrate under standard conditions, and the Heaviside function $H(\cdot)$.

With this definition of the reaction rates, the solution of the system of ordinary differential equations is:

$$c_{ox}(F, \mathbf{c}_{in}) = \max(c_{in,DO} - F \cdot r_{0,DO}^{max}, 0) \quad (5.19)$$

$$c_{nit}(F, \mathbf{c}_{in}) = \begin{cases} c_{in,nit} & \text{if } F < \frac{c_{in,DO}}{r_{0,DO}^{max}} \\ c_{in,nit} \exp\left(-k_{0,nit} \left(F - \frac{c_{in,DO}}{r_{0,DO}^{max}}\right)\right) & \text{otherwise} \end{cases} \quad (5.20)$$

The stoichiometric coefficients between the NOM in the matrix and the dissolved reactants are:

5.3. DECREASING REACTION POTENTIAL: TEST OF APPROACHES

$$\gamma_{DO} = \frac{\theta}{\rho_b} \quad (5.21)$$

$$\gamma_{nit} = \frac{5}{4} \frac{\theta}{\rho_b} \quad (5.22)$$

To close the system in the simplified modeling approach, the functional relationship between the relative reactivity f and the NOM-concentration c_{NOM}^* in the matrix from the one-dimensional highly detailed model is used (see Section 5.3.1).

Results

Figure 5.13 shows spatial profiles of concentrations along a single streamline. The individual lines represent time points that are 25 years apart from each other. Figures 5.13A, 5.13B, 5.13C depict the organic-carbon content, the dissolved oxygen, and the nitrate concentration, respectively. The gray lines in each plot indicate the travel-time increments. It can be seen that the organic-carbon content is gradually used up with time along the streamline. The first-order rate coefficient of nitrate under reference conditions is so small that at even at early times already $\approx 10 \text{mg } \ell^{-1}$ nitrate reaches the well, implying NOM depletion along the entire streamline. Oxygen, by contrast, can only be observed up to a certain distance along the streamline which changes over time.

Note that Figure 5.13 shows spatial profiles rather than profiles with respect to travel time. The velocity in the first 200 meters is particularly slow so that it appears as if the oxygen front is not moving for the first 75 years, when the NOM-concentration in the first section is permanently decreasing. Over this time period, the nitrate profile changes little, too. Once the oxygen front has passed the first low-velocity zone, it moves more quickly along the streamline and the nitrate concentrations in the well starts increasing. There is a second low-velocity region between $\approx 1000\text{m}$ and $\approx 1500\text{m}$ in this realization. At the time when the oxygen front reaches this zone, however, the NOM concentration has already been significantly decreased due to denitrification so that the dissolved-oxygen front is not retarded as strongly as in the initial section. After about 200 years, the bioavailable organic carbon is almost completely gone along the entire streamline, and dissolved oxygen breaks through at the extraction well. The full breakthrough of nitrate is about 25 years earlier. That is, for this particular streamline, the time series of nitrate in the

5.4. CUMULATIVE REACTION POTENTIAL: TEST OF APPROACHES

well is characterized by 75 years of almost constant low values, followed by 100 years of steady increase.

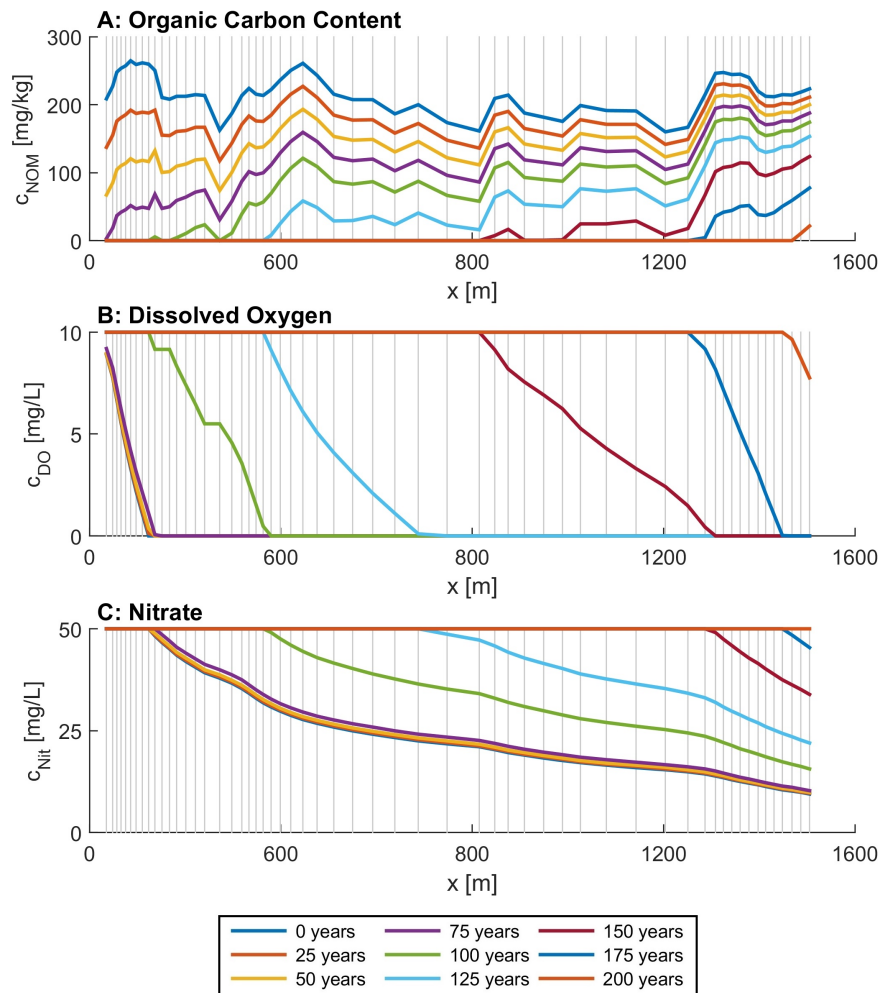


Figure 5.13: Length profiles of concentrations along a single streamline. A: natural organic matter in the aquifer matrix ; B: dissolved oxygen concentration; C: nitrate concentration. One concentration profile per 25 years is shown. Gray lines indicate travel-time increments of one month.

5.4 Cumulative Reaction Potential: Test of Approaches

To show the validity of the new concept of cumulative reaction potential I developed the following test case.

5.4.1 Two-Dimensional Benchmark Test on the Validity of the Cumulative Reaction Potential

Set Up

To test the validity of the cumulative reaction potential I set up a two-dimensional spatially explicit test case in which steady-state reactive transport of aerobic respiration and denitrification is simulated by solving the spatially explicit advection-dispersion-reaction equation.

The two-dimensional test case has a domain of 50m × 25m with a resolution of 0.1m × 0.1m. Top and bottom boundaries were no-flow boundaries, whereas the left and the right side were assigned a fixed head with a head difference of 0.2 m. The longitudinal dispersivity was set to $\alpha_l = 0.01$ m and the transverse dispersivity to $\alpha_t = 0.001$ m. The pore diffusion coefficient was $D_p = 3 \times 10^{-10}$ m²/s. For each realization, one random hydraulic conductivity field with an exponential covariance function of log(K) and a geometric mean of 10⁻³ m/s was generated. The variance of ln(K) was set to 1.0 the correlation length was 4 m in the x-direction and 1 m in the y-direction. The NOM content is correlated with hydraulic conductivity. High values of hydraulic conductivity result in low values of NOM and vice versa. The geometric mean NOM concentration was set to $c_{NOM,g} = 0.05$ mol_C/kg. The concentration of NOM was then calculated by:

$$c_{NOM} = \left(\frac{K}{K_g} \right)^{(-0.5 \cdot R_{NOM} \cdot c_{NOM,g})} \quad (5.23)$$

in which K is the field of hydraulic conductivity, K_g is the geometric mean of hydraulic conductivity, and R_{NOM} is a multi-Gaussian random field with a geometric mean of 1, correlation length of 5 m in both directions, and a variance of 0.25. Figure 5.14A shows the hydraulic conductivity and Figure 5.14C the distribution of NOM for a single realization. The resulting head is depicted in Figure 5.14B.

I then solved for stream function values, and generated streamline-oriented grids with 250 streamtubes and 500 sections per streamtube [Frind and Matanga, 1985; Cirpka et al., 1999b].

5.4. CUMULATIVE REACTION POTENTIAL: TEST OF APPROACHES

Figure 5.14D shows the resulting flow net of a single realization. Transport was calculated on the streamline-oriented grid using a cell-centered finite volume method for spatial discretization [Cirpka *et al.*, 1999a].

Reactive transport was solved using a fully implicit approach with Newton-Raphson iterations. Cumulative reaction potentials were calculated for every streamline. For a more robust comparison 100 fields of hydraulic conductivity were simulated and the spatially explicit reactive transport simulation was performed for each of them.

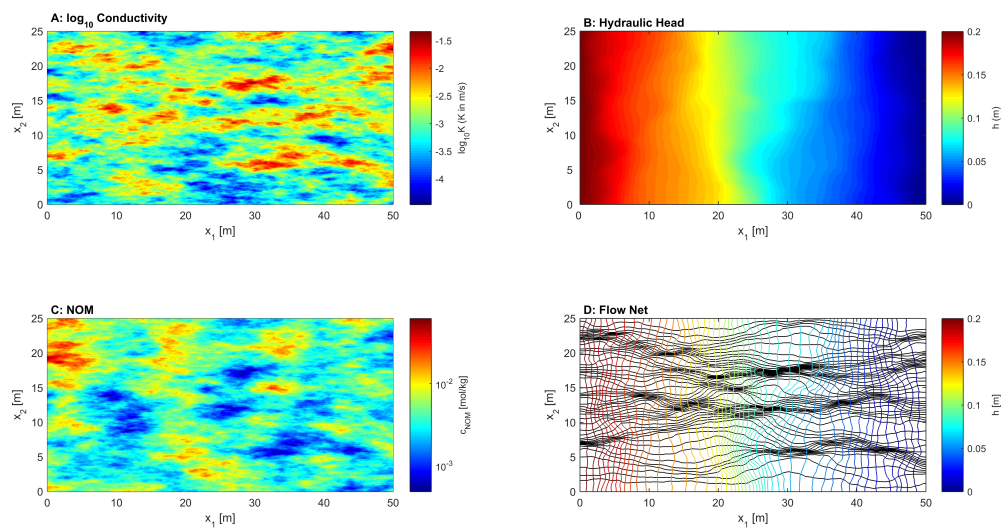


Figure 5.14: Two-dimensional test case. (A) Spatial distribution of log-hydraulic conductivity; (B) spatial distribution of hydraulic head; (C) spatial distribution of NOM concentration; (D) flow net (colored lines: heads; black lines: streamlines). All figures are for a single realization.

Reactive System

The reactive system of the two-dimensional test case was analogous to the detailed model in Section 5.3.3.

Results

Figure 5.15 shows the breakthrough curves of oxygen in blue and nitrate in red of 100 realizations of the spatially explicit model. The light blue and light red areas show the 2%-98% and the

5.4. CUMULATIVE REACTION POTENTIAL: TEST OF APPROACHES

16%-84% quantile, respectively, whereas the bold lines are the medians overall realizations. The dotted black line indicates the point of intersection between the mean cumulative reaction potential and the mean breakthrough curve of nitrate. In the given example the average cumulative reaction potential relates to 92% breakthrough of nitrate in the aquifer. Figure 5.15B shows the same breakthrough curves now scaled with the mean cumulative reaction potential of each individual run. Scaling the breakthrough curves makes clear that the distribution of the scaled breakthrough curves is narrower, indicating that the cumulative reaction potential is a good predictor for the timing of the breakthrough of a contaminant.

Figure 5.16A and B depict the cumulative distribution function (*cdf*) of the travel time and the log-NOM concentration respectively. The dashed lines are derived from the 100 model realizations of the two-dimensional model. The travel-time distribution was fitted with a log-normal distribution with a mean of 0.0944 years and a standard deviation of 0.0322 years. The logarithmic NOM concentration was fitted with a normal distribution with a mean of $-3.0571 \text{ mol}_C/\text{kg}$ and a standard deviation of $0.6541 \text{ mol}_C/\text{kg}$. The fitted distributions are plotted as blue solid lines in Figure 5.16A and B respectively. With those two distribution functions, and neglecting potential correlations between NOM and travel times, the *cdf* of the cumulative reaction potential, shown as blue solid line in Figure 5.16C, can easily be computed. To do so one million random numbers from each of the two fitted distributions were drawn. For comparison the *cdf* of the cumulative reaction potential from the 100 model runs is shown as dashed line. The mean cumulative reaction potential, estimated from the pdfs of travel time and NOM, is 32.33 years whereas the mean cumulative reaction potential of 100 model realizations of the two-dimensional test case is 35.75 years.

5.4. CUMULATIVE REACTION POTENTIAL: TEST OF APPROACHES

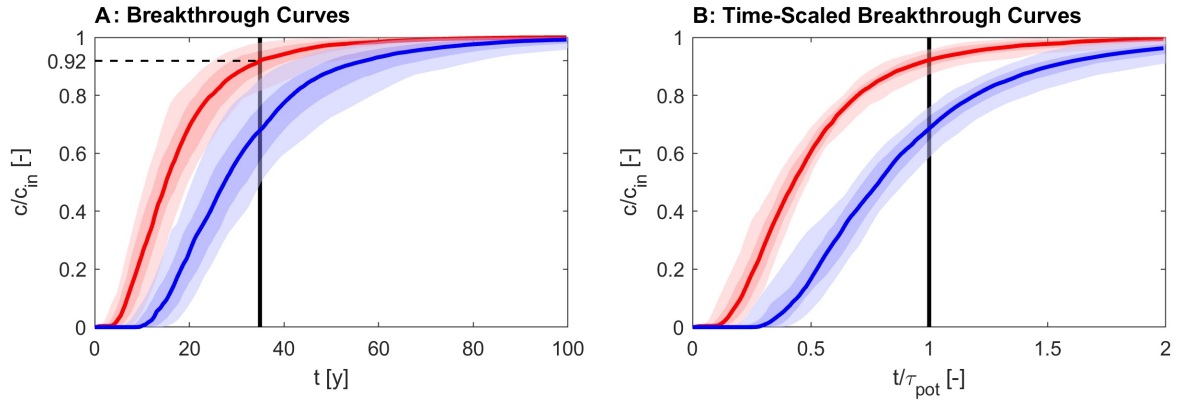


Figure 5.15: Median breakthrough curves of nitrate (red) and oxygen (blue) for 100 realizations of the spatially explicit model scaled with the inflow concentrations. A: as function of time; B: every curve scaled by the mean cumulative reaction potential of the corresponding simulation. Light red and blue areas show the 2%-98% and the 16%-84% quantile, respectively. Thick black line in A: mean cumulative reaction potential of all realizations.

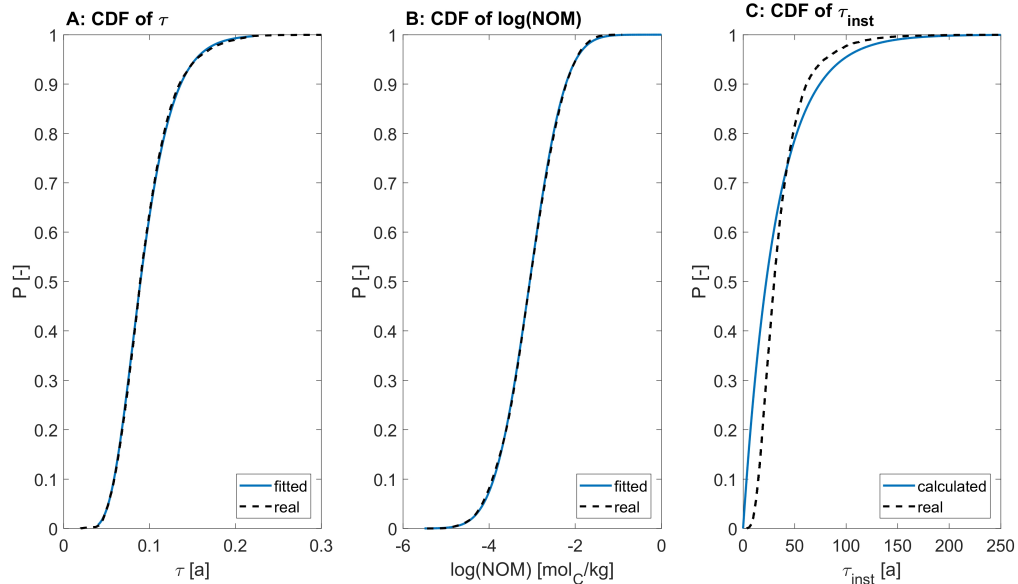


Figure 5.16: Cumulative distribution functions (*cdf*) of (A) travel time; (B) log concentration of NOM; and (C) cumulative reaction potential. The solid lines refer to the fitted and calculated *cdf*, respectively. The dashed lines are the *cdf*s derived from 100 realizations of the two-dimensional test case.

6 Discussion

In this thesis I derived a stochastic framework for catchment-scale reactive transport simulations. The new concept of cumulative relative reactivity adds important features to the existing travel-time based models for reactive transport. It is now possible to account for the chemical heterogeneity of an aquifer. With the addition of travel-time increments the depletion of a reaction partner in the aquifers matrix becomes possible, making travel-time based models more realistic and precise. Table 6.1 compares the existing models with the concepts developed in this thesis. And finally, for an estimate of the lasting time of the natural reaction potential of an aquifer, the cumulative reaction potential can be determined.

	State of the Art		
	PDE-based	Travel-time	Cum. Rel. React.
spatially explicit	yes	no	no
approach	Eulerian	Lagrangian	Lagrangian
(transverse) mixing	yes	no*	no
chemical heterogeneity	yes	no**	yes
depletion of reaction partner	yes	no	yes
computational effort	high	low	low

Table 6.1: Comparison between state of the art reactive transport models on the catchment-scale and the concept of cumulative relative reactivity. *streamline based models that account for mixing by an exchange coefficient between streamlines; **exposure-time based models can account for chemical heterogeneity in a binary way.

6.1 Cumulative Relative Reactivity

The first part of the thesis deals with the concept of cumulative relative reactivity [Loschko *et al.*, 2016]. The proposed framework solves efficiently reactive transport in large-scale applications. In comparison to a spatially explicit approach, the simplified approach of solving reactive solute transport along trajectories is computationally so inexpensive that Monte Carlo simulations with a large number of model runs are possible. The proposed framework differs from approaches in which reactive transport is restricted to first-order degradation. In particular, inhibition of denitrification is accounted for by the presence of dissolved oxygen, which is known to be a major control of denitrification. The framework can be applied to reactive transport in groundwater using computational domains with a large number of computational cells, and is not restricted to simple model geometries. It is also not restricted to denitrification but can be applied to any other non-mixing controlled reaction, where the reaction partner is present in the aquifers matrix (either as an electron donor or an electron acceptor). The core of the modeling framework does not change if other reactions are considered.

The validity of the concept of cumulative relative reactivity has been shown by comparing a spatially explicit advective-dispersive-reactive transport model in a heterogeneous two-dimensional domain to the results obtained by mapping reactive-species concentrations based on local values of the cumulative relative reactivity (Chapter 5.2.1). Due to the computational effort of the spatially explicit model, this benchmark study was performed in 2-D. The results showed an excellent match of the mean reactive-species concentrations in the outflow, a good match in the standard deviation, and some deviations in the full *cdf*. The predictive capabilities are higher for the estimation of the reactive-species mass flux integrated over a control plane or by a well than for values at true point observations. Evaluating the mean cumulative relative reactivity for advective-dispersive transport rather than for strictly advective transport does not really pay off.

The presented simple three-dimensional test case is chosen to explain the concept of relative reactivity in a comprehensive way (Chapter 5.2.2) and to show the applicability on the large scale. Boundary conditions, such as groundwater recharge and the concentrations in the inflow, are addressed independently. To account for uncertainty and variability of the model parameters (hydraulic conductivity, recharge, initial concentrations) random realizations of the parameter fields are implemented. Statistics for those could also be obtained from measurements or already available data. Moreover, the model could be conditioned at measurement locations, reducing

6.2. DECREASING REACTION POTENTIAL

the variability and uncertainty of the parameter fields. The distribution of reactive zones as well as the assignment of values for relative reactivities have been conducted by a stochastic approach. The transfer of the model concept to a real catchment is possible. While the flow field in the given test case is at steady state, transient runs are also possible as travel time and cumulative relative reactivity are computed by integration along particle trajectories which can be computed also in transient flow.

Like fully explicit three-dimensional reactive transport models, the concept of cumulative relative reactivity suffers from data requirements. Especially data for the distribution of reactive zones and the relative reactivity are difficult to obtain and to assign. In contrast to these methods, however, the approach allows explicitly addressing this uncertainty, because it makes catchment-scale reactive transport computationally so inexpensive that it becomes accessible for stochastic simulation.

In the first part of the thesis the reaction partner in the matrix is assumed to be an infinite supply of electron donors. This is acceptable for short times but unrealistic for larger simulation periods. The challenge of implementing the spatially explicit problem of a decreasing supply of reaction partners in the non-spatially explicit framework of cumulative relative reactivity is addressed in the second part of this thesis.

6.2 Decreasing Reaction Potential

The second part of this thesis deals with the implementation of the consumption of reaction partners in the aquifer matrix [Loschko *et al.*, 2018a]. The approach is based on the conceptual simplifications introduced in the first part, namely on the concept of cumulative relative reactivity and introduces the additional concept of travel-time increments. The framework remains computationally efficient while not relying on unrealistic first-order decay of nitrate in aquifers.

In a two-dimensional test case I was able to demonstrate both, the validity of travel and exposure-time-based models as well as of the concept of cumulative relative reactivity for bioreactive transport in heterogeneous media (Chapter 5.3.2). Due to the associated high computational effort of the pde-based model, the comparative test case study was performed on a two-dimensional test case.

6.2. DECREASING REACTION POTENTIAL

The three-dimensional test case was chosen to show the applicability of the concept of cumulative relative reactivity including travel-time increments. Results from the three-dimensional test case show that the predictive capabilities are higher at pumping wells or at the outflow of the domain than at single observation points, because reactive-species concentrations observed in pumping wells and in the outflow plane of the model domain, are flux integrated (Chapter 5.3.3). For the case of the observation well, where mixing should not be neglected, a spatially explicit modeling framework might be the better choice and other techniques to account for uncertainties in the model domain need to be applied. But when performing multiple model executions within a stochastic framework, I still assess travel-time based models as a useful modeling strategy.

The travel-time based approach of accounting for a decreasing reaction potential of the aquifer matrix requires that the spatial pattern of flow paths and thus travel times does not change during the simulation. This requirement is met if flow is at steady state or when a time-invariant velocity field is multiplied with a spatially uniform transient multiplier [Selroos *et al.*, 2013; Sanz-Prat *et al.*, 2016b]. If this simplification is not appropriate for the real-world system under consideration, the model problem can only be solved using a spatially fully explicit framework, which comes at higher computational costs and may involve issues of numerical dispersion. Accounting for dynamic changes of inflow concentrations, by contrast, poses no challenge to the proposed framework.

In the second part of the thesis, also a simple relation between organic carbon content and relative reactivity is derived for the case of aerobic respiration and denitrification (Chapter 5.3.1). This is an essential problem because values for relative reactivity need to be assigned in the proposed framework (and for that matter also in spatially explicit models). Here, a possible relation between the bioavailable NOM-content in the aquifers matrix and the relative reactivity has been derived. However, aquifers may contain other electron donors (e.g. pyrite, biotite) suitable for denitrification that are likely to have a different degradation behavior and will lead to other values of relative reactivity for identical electron content. Thus, the relationship between the electron donor content of the matrix and the relative reactivity needs to be calibrated for every specific application. The proposed approach serves as one possible option to determine the relation between the concentration of the reaction partner in the matrix and the relative reactivity. But as noted before, the framework is not restricted to aerobic respiration and denitrification and can be adapted to other types of reactions that are not controlled by mixing and where the reaction partner is in the matrix.

6.3. CUMULATIVE REACTION POTENTIAL

Similar to the first part, I see the biggest challenges in obtaining sufficient data about the characteristics of the aquifer. Apart from the hydraulic parameters, such as hydraulic conductivity, groundwater recharge, and other boundary conditions, the content of the reaction partner in the matrix has to be estimated and linked to the relative reactivity. Data for these parameters are often scarce and difficult to gather at the required scale. Several modeling studies have assessed the potential interplay between physical and chemical heterogeneity using educated guesses regarding the chemical heterogeneity and the potential correlation to its physical counterpart. Clearly more field data are needed on the chemical heterogeneity to be expected in certain geological settings. If uncertainty bounds and correlation scales are known, however, the presented stochastic framework can be used to propagate these uncertainties to distributions of reactive-species concentrations.

6.3 Cumulative Reaction Potential

In the third part of this thesis, I proposed the new concept of the cumulative reaction potential [Loschko *et al.*, 2018b]. It is essentially the time during which the aquifer has still some capability for reactions given a defined input concentration. It shows a good correlation with the breakthrough of nitrate at an observation plane (Chapter 5.4.1). This leads to the conclusion that the cumulative reaction potential is a good predictor for the breakthrough of a contaminant at a observation point or plane. Especially with regard to the computational effort, the cumulative reaction potential τ_{pot} is a fast and easy applicable tool to estimate the time of the remaining natural reaction potential of an aquifer. A stochastic analysis can be performed fast. As no reaction equations are solved when evaluating τ_{pot} , no reactive parameters are needed and no knowledge about their non-uniform distribution is necessary.

For the calculation of the cumulative reaction potential only the travel time and the distribution of a reaction partner in the aquifer matrix is necessary. The travel time can be easily obtained by simple particle tracking, also on the catchment-scale and in a three-dimensional domain. If no numerical model is present, travel-time distributions can often be estimated or are known from tracer tests.

Also, the cumulative concentration of organic carbon, or other relevant reaction partners in the aquifers matrix, is needed. If a distribution of travel times and NOM concentrations can be

6.3. CUMULATIVE REACTION POTENTIAL

estimated, the cumulative reaction potential can be computed without any numerical model at all. Cumulative concentrations are often easier to predict as a spatially explicit description. A mean value for a sedimentary layer can be a good estimate. There is no need to spatially resolve the geochemical heterogeneity, which was identified as one of the limiting factors of numerical models, as data about the chemical heterogeneity of aquifers are often scarce. It was demonstrated in the third part of this thesis that without any numerical model it was possible to predict the *cdf* for the instantaneous reaction time fairly well compared to a fully spatially explicit model.

However, the cumulative reaction potential τ_{pot} is not able to replace a numerical model as its validity is limited to the decreasing reaction potential. However, it can be seen as a quick and easy to implement tool for the estimation of the lasting decreasing reaction potential of a contaminated aquifer, without solving any numerical or reactive models. Water suppliers, for example, could use the cumulative reaction potential to predict the lasting time of the natural denitrification potential of their aquifer. As input they would need the distributions of travel time, NOM, and nitrate loading.

7 Conclusions and Outlook

The framework of cumulative relative reactivity and the decreasing reaction potential using travel-time increments is an essential and important extension to the existing travel-time based models. By simplifying reactive transport, it is possible to perform large numbers of model runs that allow a stochastic analysis of reactive transport on the catchment-scale beyond a pure consideration of travel- or exposure times only. With the cumulative relative reactivity, the natural reaction potential of the aquifer can also be accounted for. This is important as chemical and hydraulic properties of natural aquifers are heterogeneous and the framework is not restricted to first-order degradation. Previous travel-time based models were also not able to account for the spatially explicit consumption of a reaction partner in the aquifer matrix. This is possible with the implementation of travel-time increments into the framework of cumulative relative reactivity. The approach can readily be implemented also in other models that solve reactive transport along trajectories.

The cumulative reaction potential can serve as a tool for water suppliers or other stakeholders to quickly estimate the time of breakthrough of a contaminant at a receptor. It may not replace a numerical model and its predictive capabilities, but can serve as an easy-to-implement assessment tool. Especially for non-modelers the cumulative reaction potential can be a handy approach as no knowledge about numerical reactive transport models is necessary and distributions of travel times and reaction partner contents in the matrix are sufficient to make a prediction.

For practical applications, I see the biggest difficulties in assigning a representative distribution of reactive zones or statistics thereof and attribute values for relative reactivities to those zones. All presented approaches require data about the chemical heterogeneity of the aquifer. Assessing the spatial distribution of reactive zones in an aquifer is not trivial, because in many formations the internal structure is not or only poorly known. A clear distinction between reactive and non-reactive zones is challenging, but not actually needed as the relative reactivity can take any non-negative value. Further research and field investigations are necessary to obtain justifiable

statistics for relative reactivities. However, this is not a sole requirement of the framework of cumulative relative reactivity or other travel-time based models but is also valid for spatially explicit modeling approaches. In contrast to these methods, the approach presented in this thesis allows explicitly addressing the uncertainty of chemical heterogeneity, because it makes catchment-scale reactive transport computationally so inexpensive that it becomes accessible for stochastic ensemble runs.

Another challenge that still remains is the relation between the relative reactivity and the particular reactive component. In this thesis, a relation between the bioavailable NOM and the relative reactivity is derived. The relationship depends on conceptual and parameter choices used for its calibration. For field applications, experimental data would be highly beneficial that can be used to derive the dependence of the NOM's reactivity on its content in the aquifer matrix. Of course, aquifers may contain other electron donors (e.g., ferrous-iron bearing minerals such as pyrite, biotite, siderite, or magnetite) suitable for denitrification that are likely to have a different degradation behavior and will lead to other values of relative reactivity for identical electron content. Thus, the relationship between the electron-donor content of the matrix and the relative reactivity needs to be evaluated in every specific application for every specific compound.

In an ongoing DFG funded project (CRC 1253 CAMPOS - Catchments as Reactors: Metabolism of Pollutants on the Catchment Scale) the concept of cumulative relative reactivity will be implemented in a broader stochastic modeling framework for catchment-scale reactive transport, including the uncertain classification of soil types and land use and the uncertain soil-vegetation-atmosphere-solute transport. To simulate the strong feedbacks between soils and vegetation at the land-surface, a fully coupled one dimensional, vertical soil-crop models will be set up which is coupled to an underlying three dimensional flow model of the deeper subsurface and streamline-based models of reactive transport, potentially using the framework of cumulative relative reactivity. The model framework will be adapted to the fate of nitrate in the Ammer catchment in south-western Germany.

Bibliography

- Appelo, C. A. J., and D. Postma, *Geochemistry, groundwater and pollution*, CRC press, doi:10.1201/9781439833544, 2004.
- Arnold, J. G., R. Srinivasan, R. S. Muttiah, and J. R. Williams, Large area hydrologic modeling and assessment part i: Model development1, doi:10.1111/j.1752-1688.1998.tb05961.x, 1998.
- Atchley, A. L., R. M. Maxwell, and A. K. Navarre-Sitchler, Using streamlines to simulate stochastic reactive transport in heterogeneous aquifers: Kinetic metal release and transport in co 2 impacted drinking water aquifers, *Advances in Water Resources*, 52, 93–106, doi: 10.1016/j.advwatres.2012.09.005, 2013.
- Atchley, A. L., A. K. Navarre-Sitchler, and R. M. Maxwell, The effects of physical and geochemical heterogeneities on hydro-geochemical transport and effective reaction rates, *Journal of Contaminant Hydrology*, 165, 53–64, doi:10.1016/j.jconhyd.2014.07.008, 2014.
- Bergström, S., J. Harlin, and G. Lindström, Spillway design floods in sweden: I. new guidelines, *Hydrological Sciences Journal*, 37(5), 505–519, doi:10.1080/02626669209492615, 1992.
- Botter, G., E. Bertuzzo, and A. Rinaldo, Transport in the hydrologic response: Travel time distributions, soil moisture dynamics, and the old water paradox, *Water Resources Research*, 46(3), doi:10.1029/2009WR008371, 2010.
- Bouraoui, F., B. Grizzetti, and A. Aloe, Long term nutrient loads entering european seas, european commission joint research centre, *Institute for Environment and Sustainability, Ispra, Italy*, 2011.
- Bradley, P., M. Fernandez Jr, and F. Chapelle, Carbon limitation of denitrification rates in an anaerobic groundwater system, *Environmental science & technology*, 26(12), 2377–2381, doi:10.1021/es00036a007, 1992.

Bibliography

- Bundesministerium für Umwelt, Naturschutz und Reaktorsicherheit, Grundwasser in Deutschland, Referat Öffentlichkeitsarbeit, 11055 Berlin, 2008.
- Bundesministerium für Umwelt, Naturschutz und Reaktorsicherheit, Wasserwirtschaft in Deutschland, Postfach 12 06 29, 53048 Bonn, 2013.
- Carrera, J., An overview of uncertainties in modelling groundwater solute transport, *Journal of Contaminant Hydrology*, 13(1), 23–48, doi:10.1016/0169-7722(93)90049-X, 1993.
- Cirpka, O. A., and P. K. Kitanidis, An advective-dispersive stream tube approach for the transfer of conservative-tracer data to reactive transport, *Water Resources Research*, 36(5), 1209–1220, doi:10.1029/1999WR900355, 2000.
- Cirpka, O. A., and A. J. Valocchi, Two-dimensional concentration distribution for mixing-controlled bioreactive transport in steady state, *Advances Water Resour.*, 30(6-7), 1668–1679, doi:10.1016/j.advwatres.2006.05.022, 2007.
- Cirpka, O. A., E. O. Frind, and R. Helmig, Numerical methods for reactive transport on rectangular and streamline-oriented grids, *Advances in Water Resources*, 22(7), 711–728, doi:10.1016/S0309-1708(98)00051-7, 1999a.
- Cirpka, O. A., E. O. Frind, and R. Helmig, Streamline-oriented grid generation for transport modelling in two-dimensional domains including wells, *Advances in Water Resources*, 22(7), 697–710, doi:10.1016/S0309-1708(98)00050-5, 1999b.
- Cirpka, O. A., E. O. Frind, and R. Helmig, Numerical simulation of biodegradation controlled by transverse mixing, *Journal of Contaminant Hydrology*, 40(2), 159–182, doi:10.1016/S0169-7722(99)00044-3, 1999c.
- Cirpka, O. A., M. Rolle, G. Chiogna, F. P. J. de Barros, and W. Nowak, Stochastic evaluation of mixing-controlled steady-state plume lengths in two-dimensional heterogeneous domains, *Journal of Contaminant Hydrology*, 138-139, 22–39, doi:10.1016/j.jconhyd.2012.05.007, 2012.
- Critchley, K., D. Rudolph, J. Devlin, and P. Schillig, Stimulating in situ denitrification in an aerobic, highly permeable municipal drinking water aquifer, *Journal of Contaminant Hydrology*, 171, 66–80, 2014.

Bibliography

- Cvetkovic, V., and G. Dagan, Transport of kinetically sorbing solute by steady random velocity in heterogeneous porous formations, *Journal of Fluid Mechanics*, 265, 189–215, doi:10.1017/S0022112094000807, 1994.
- Cvetkovic, V., H. Cheng, and X.-H. Wen, Analysis of nonlinear effects on tracer migration in heterogeneous aquifers using lagrangian travel time statistics, *Water Resources Research*, 32(6), 1671–1680, doi:10.1029/96WR00278, 1996.
- Dagan, G., An overview of stochastic modeling of groundwater flow and transport: From theory to applications, *EOS, Transactions American Geophysical Union*, 83(53), 621–625, doi:10.1029/2002EO000421, 2002.
- Dagan, G., and V. Cvetkovic, Reactive transport and immiscible flow in geological media. i. general theory, in *Proceedings of the Royal Society of London A: Mathematical, Physical and Engineering Sciences*, vol. 452, pp. 285–301, The Royal Society, doi:10.1098/rspa.1996.0016, 1996.
- Dagan, G., and V. Nguyen, A comparison of travel time and concentration approaches to modeling transport by groundwater, *Journal of Contaminant Hydrology*, 4(1), 79–91, doi:10.1016/0169-7722(89)90027-2, 1989.
- de Anna, P., M. Dentz, A. Tartakovsky, and T. Le Borgne, The filamentary structure of mixing fronts and its control on reaction kinetics in porous media flows, *Geophysical Research Letters*, 41(13), 4586–4593, doi:10.1002/2014GL060068, 2014.
- Delwiche, C., and B. A. Bryan, Denitrification, *Annual Reviews in microbiology*, 30(1), 241–262, doi:10.1146/annurev.mi.30.100176.001325, 1976.
- Devlin, J., R. Eedy, and B. Butler, The effects of electron donor and granular iron on nitrate transformation rates in sediments from a municipal water supply aquifer, *Journal of Contaminant Hydrology*, 46(1), 81–97, doi:10.1016/S0169-7722(00)00126-1, 2000.
- D’haene, K., E. Moreels, S. De Neve, B. C. Daguilar, P. Boeckx, G. Hofman, and O. Van Cleemput, Soil properties influencing the denitrification potential of flemish agricultural soils, *Biology and fertility of soils*, 38(6), 358–366, doi:10.1007/s00374-003-0662-x, 2003.
- Diem, S., O. A. Cirpka, and M. Schirmer, Modeling the dynamics of oxygen consumption upon riverbank filtration by a stochastic–convective approach, *Journal of Hydrology*, 505, 352–363, doi:10.1016/j.jhydrol.2013.10.015, 2013.

Bibliography

- Drury, C., D. McKenney, and W. Findlay, Relationships between denitrification, microbial biomass and indigenous soil properties, *Soil Biology and Biochemistry*, 23(8), 751–755, doi:10.1016/0038-0717(91)90145-A, 1991.
- Erdal, D., and O. A. Cirpka, Simple implementations of particle-tracking and groundwater-flow model on graphic cards, *Water Resources Research*, (submitted), 2015.
- European Union, Directive 2000/60/EC of the European Parliament and of the Council of 23 October 2000 establishing a framework for Community action in the field of water policy, 2000.
- European Union, Directive 2006/118/EC of the European Parliament and of the Council of 12 December 2006 on the protection of groundwater against pollution and deterioration, 2007.
- Feyen, J., D. Jacques, A. Timmerman, and J. Vanderborght, Modelling water flow and solute transport in heterogeneous soils: A review of recent approaches, *Journal of Agricultural Engineering Research*, 70(3), 231–256, doi:10.1006/jaer.1998.0272, 1998.
- Foth, H. D., et al., *Fundamentals of soil science.*, Ed. 8, John Wiley and Sons, Inc., 1991.
- Frei, S., and S. Peiffer, Exposure times rather than residence times control redox transformation efficiencies in riparian wetlands, *Journal of Hydrology*, doi:10.1016/j.jhydrol.2016.02.001, 2016.
- Frind, E. O., and G. B. Matanga, The dual formulation of flow for contaminant transport modeling 1. review of theory and accuracy aspects, *Water Resources Research*, 21(2), 159–169, doi:10.1029/WR021i002p00159, 1985.
- Galloway, J. N., et al., Nitrogen cycles: past, present, and future, *Biogeochemistry*, 70(2), 153–226, doi:10.1007/s10533-004-0370-0, 2004.
- Gamble, T. N., M. R. Betlach, and J. M. Tiedje, Numerically dominant denitrifying bacteria from world soils, *Applied and Environmental Microbiology*, 33(4), 926–939, 1977.
- Ghiorse, W. C., and J. T. Wilson, Microbial ecology of the terrestrial subsurface, *Advances in Applied Microbiology*, 33, 107, doi:10.1016/S0065-2164(08)70206-5, 1988.

Bibliography

- Ginn, T., C. Simmons, and B. Wood, Stochastic-convective transport with nonlinear reaction: Biodegradation with microbial growth, *Water Resources Research*, 31(11), 2689–2700, doi:10.1029/95WR02179, 1995.
- Ginn, T. R., A travel time approach to exclusion on transport in porous media, *Water Resources Research*, 38(4), 12–1, doi:10.1029/2001WR000865, 2002.
- Goderniaux, P., S. Brouyère, H. J. Fowler, S. Blenkinsop, R. Therrien, P. Orban, and A. Dassargues, Large scale surface–subsurface hydrological model to assess climate change impacts on groundwater reserves, *Journal of Hydrology*, 373(1), 122–138, 2009.
- Gong, R., et al., Estimating reaction rate coefficients within a travel-time modeling framework, *Groundwater*, 49(2), 209–218, doi:10.1111/j.1745-6584.2010.00683.x, 2011.
- Goode, D. J., Direct simulation of groundwater age, *Water Resources Research*, 32(2), 289–296, doi:10.1029/95WR03401, 1996.
- Green, C. T., and B. A. Bekins, Sustainability of natural attenuation of nitrate in agricultural aquifers, *Tech. rep.*, US Geological Survey, 2010.
- Guadagnini, A., and S. P. Neuman, Nonlocal and localized analyses of conditional mean steady state flow in bounded, randomly nonuniform domains: 1. theory and computational approach, *Water Resources Research*, 35(10), 2999–3018, 1999.
- Heitzer, R., and J. Ottow, New denitrifying bacteria isolated from red sea sediments, *Marine Biology*, 37(1), 1–10, 1976.
- Hickel, W., P. Mangelsdorf, and J. Berg, The human impact in the german bight: Eutrophication during three decades (1962–1991), *Helgoländer Meeresuntersuchungen*, 47(3), 243, doi: 10.1007/BF02367167, 1993.
- Hiscock, K., J. Lloyd, and D. Lerner, Review of natural and artificial denitrification of groundwater, *Water Research*, 25(9), 1099–1111, doi:10.1016/0043-1354(91)90203-3, 1991.
- Hrachowitz, M., C. Soulsby, D. Tetzlaff, I. Malcolm, and G. Schoups, Gamma distribution models for transit time estimation in catchments: Physical interpretation of parameters and implications for time-variant transit time assessment, *Water Resources Research*, 46(10), 2010.

Bibliography

- Jury, W. A., Simulation of solute transport using a transfer function model, *Water Resources Research*, 18(2), 363–368, doi:10.1029/WR018i002p00363, 1982.
- Kaluarachchi, J. J., V. Cvetkovic, and S. Berglund, Stochastic analysis of oxygen-and nitrate-based biodegradation of hydrocarbons in aquifers, *Journal of Contaminant Hydrology*, 41(3), 335–365, doi:10.1016/S0169-7722(99)00072-8, 2000.
- Knowles, R., Denitrification., *Microbiological Reviews*, 46(1), 43, 1982.
- Kollet, S. J., and R. M. Maxwell, Integrated surface–groundwater flow modeling: A free-surface overland flow boundary condition in a parallel groundwater flow model, *Advances in Water Resources*, 29(7), 945–958, 2006.
- Le Borgne, T., T. R. Ginn, and M. Dentz, Impact of fluid deformation on mixing-induced chemical reactions in heterogeneous flows, *Geophys. Res. Lett.*, 41(22), 7898–7906, doi:10.1002/2014GL062038, 2014.
- Lohse, K. A., P. D. Brooks, J. C. McIntosh, T. Meixner, and T. E. Huxman, Interactions between biogeochemistry and hydrologic systems, *Annual Review of Environment and Resources*, 34, 65–96, doi:10.1146/annurev.environ.33.031207.111141, 2009.
- Loschko, M., T. Wöhling, D. L. Rudolph, and O. A. Cirpka, Cumulative relative reactivity: A concept for modeling aquifer-scale reactive transport, *Water Resources Research*, 52(10), 8117–8137, doi:10.1002/2016WR019080, 2016.
- Loschko, M., T. Wöhling, D. L. Rudolph, and O. A. Cirpka, Accounting for the decreasing reaction potential of heterogeneous aquifers in a stochastic framework of aquifer-scale reactive transport, *Water Resources Research*, 54(1), 442–463, 2018a.
- Loschko, M., T. Wöhling, D. L. Rudolph, and O. A. Cirpka, An electron-balance based approach to predict the decreasing denitrification potential of an aquifer, *Groundwater (in review)*, 2018b.
- Luo, J., Travel-time based reactive transport modeling for in situ subsurface reactor, in *Delivery and Mixing in the Subsurface*, pp. 117–138, Springer, doi:10.1007/978-1-4614-2239-6_5, 2012.
- Luo, J., and O. A. Cirpka, How well do mean breakthrough curves predict mixing-controlled reactive transport?, *Water Resources Research*, 47(2), doi:10.1029/2010WR009461, 2011.

Bibliography

- Malmström, M. E., G. Destouni, and P. Martinet, Modeling expected solute concentration in randomly heterogeneous flow systems with multicomponent reactions, *Environmental science & technology*, 38(9), 2673–2679, doi:10.1021/es030029d, 2004.
- Mayer, K. U., E. O. Frind, and D. W. Blowes, Multicomponent reactive transport modeling in variably saturated porous media using a generalized formulation for kinetically controlled reactions, *Water Resources Research*, 38(9), doi:10.1029/2001WR000862, 2002.
- Mellage, A., D. Eckert, M. Grösbacher, A. Z. Inan, O. A. Cirpka, and C. Griebl, Dynamics of suspended and attached aerobic toluene degraders in small-scale flow-through sediment systems under growth and starvation conditions, *Environmental science & technology*, doi:10.1021/es5058538, 2015.
- Neumann, S., and S. Orr, Prediction of steady state flow in nonuniform geologic media by conditional moments: exact nonlocal formulation, effective conductivities and weak approximation, *Water Resource Research*, 29(2), 341–364, doi:10.1029/92WR02062, 1993.
- Niswonger, R., S. Panday, and M. Ibaraki, Modflow nwt, a newton formulation for modflow-2005, *U.S. Geological Survey Techniques and Methods*, 6-A37, 44 p., 2011.
- Nobile, F., R. Tempone, and C. G. Webster, A sparse grid stochastic collocation method for partial differential equations with random input data, *SIAM Journal on Numerical Analysis*, 46(5), 2309–2345, doi:10.1137/060663660, 2008.
- Ocampo, C. J., C. E. Oldham, and M. Sivapalan, Nitrate attenuation in agricultural catchments: Shifting balances between transport and reaction, *Water Resources Research*, 42(1), doi:10.1029/2004WR003773, 2006.
- Olsthoorn, T., mflab: Environment for modflow suite groundwater modeling, URL: <http://code.google.com/p/mflab>, 2013.
- Pacheco, J., L. Marín, A. Cabrera, B. Steinich, and O. Escolero, Nitrate temporal and spatial patterns in 12 water-supply wells, yucatan, mexico, *Environmental Geology*, 40(6), 708–715, doi:10.1007/s002540000180, 2001.
- Payne, W. J., and P. Riley, Suppression by nitrate of enzymatic reduction of nitric oxide, *Experimental Biology and Medicine*, 132(1), 258–260, 1969.

Bibliography

- Payne, W. J., P. Riley, and C. Cox, Separate nitrite, nitric oxide, and nitrous oxide reducing fractions from *Pseudomonas perfectomarinus*, *Journal of Bacteriology*, 106(2), 356–361, 1971.
- Pollock, D. W., Semianalytical computation of path lines for finite-difference models, *Groundwater*, 26(6), 743–750, doi:10.1111/j.1745-6584.1988.tb00425.x, 1988.
- Prommer, H., D. Barry, W. Chiang, and C. Zheng, Pht3d-a modflow-mt3dms-based reactive multicomponent transport model, *MODFLOW 2001 and other modeling odysseys*, pp. 477–483, doi:10.1111/j.1745-6584.2003.tb02588.x, 2001.
- Puckett, L. J., A. J. Tesoriero, and N. M. Dubrovsky, Nitrogen contamination of surficial aquifers - a growing legacy, doi:10.1021/es1038358, 2010.
- Refsgaard, J. C., Parameterisation, calibration and validation of distributed hydrological models, *Journal of Hydrology*, 198(1-4), 69–97, 1997.
- Reich, P. B., B. A. Hungate, and Y. Luo, Carbon-nitrogen interactions in terrestrial ecosystems in response to rising atmospheric carbon dioxide, *Annual Review of Ecology, Evolution, and Systematics*, pp. 611–636, doi:10.1146/annurev.ecolsys.37.091305.11003, 2006.
- Rinaldo, A., G. Botter, E. Bertuzzo, A. Uccelli, T. Settin, and M. Marani, Transport at basin scales: 1. theoretical framework, *Hydrology and Earth System Sciences*, 10(1), 19–29, doi:10.5194/hess-10-19-2006, 2006.
- Rivett, M. O., S. R. Buss, P. Morgan, J. W. Smith, and C. D. Bement, Nitrate attenuation in groundwater: a review of biogeochemical controlling processes, *Water Research*, 42(16), 4215–4232, doi:10.1016/j.watres.2008.07.020, 2008.
- Rubin, Y., M. Cushey, and A. Bellin, Modeling of transport in groundwater for environmental risk assessment, *Stochastic Hydrology and Hydraulics*, 8(1), 57–77, doi:10.1007/BF01581390, 1994.
- Sanz-Prat, A., C. Lu, M. Finkel, and O. A. Cirpka, On the validity of travel-time based nonlinear bioreactive transport models in steady-state flow, *Journal of Contaminant Hydrology*, 175, 26–43, doi:10.1016/j.jconhyd.2015.02.003, 2015.

Bibliography

- Sanz-Prat, A., C. Lu, R. T. Amos, M. Finkel, D. W. Blowes, and O. A. Cirpka, Exposure-time based modeling of nonlinear reactive transport in porous media subject to physical and geochemical heterogeneity, *Journal of Contaminant Hydrology*, 192, 35–49, doi:10.1016/j.jconhyd.2016.06.002, 2016a.
- Sanz-Prat, A., C. Lu, M. Finkel, and O. A. Cirpka, Using travel times to simulate multi-dimensional bioreactive transport in time-periodic flows, *Journal of Contaminant Hydrology*, doi:10.1016/j.jconhyd.2016.01.005, 2016b.
- Schäfer, W., and R. Therrien, Simulating transport and removal of xylene during remediation of a sandy aquifer, *Journal of Contaminant Hydrology*, 19(3), 205–236, doi:10.1016/0169-7722(95)00018-Q, 1995.
- Seeboonruang, U., and T. R. Ginn, Upscaling heterogeneity in aquifer reactivity via exposure-time concept: Forward model, *Journal of Contaminant Hydrology*, 84(3), 127–154, doi:10.1016/j.jconhyd.2005.12.011, 2006.
- Selroos, J.-O., H. Cheng, S. Painter, and P. Vidstrand, Radionuclide transport during glacial cycles: Comparison of two approaches for representing flow transients, *Physics and Chemistry of the Earth*, 64, 32–45, doi:10.1016/j.pce.2012.10.003, 2013.
- Shampine, L. F., and M. W. Reichelt, The matlab ode suite, *SIAM journal on scientific computing*, 18(1), 1–22, doi:10.1137/S1064827594276424, 1997.
- Shapiro, A. M., and V. D. Cvetkovic, Stochastic analysis of solute arrival time in heterogeneous porous media, *Water Resources Research*, 24(10), 1711–1718, doi:10.1029/WR024i010p01711, 1988.
- Simmons, C., A stochastic-convective transport representation of dispersion in one-dimensional porous media systems, *Water Resources Research*, 18(4), 1193–1214, doi:10.1029/WR018i004p01193, 1982.
- Simmons, C., T. Ginn, and B. Wood, Stochastic-convective transport with nonlinear reaction: Mathematical framework, *Water Resources Research*, 31(11), 2675–2688, doi:10.1029/95WR02178, 1995.
- Smith, K., A model of the extent of anaerobic zones in aggregated soils, and its potential application to estimates of denitrification¹, *Journal of Soil Science*, 31(2), 263–277, doi:10.1111/j.1365-2389.1980.tb02080.x, 1980.

Bibliography

- Smith, R. L., and J. H. Duff, Denitrification in a sand and gravel aquifer, *Applied and Environmental Microbiology*, 54(5), 1071–1078, 1988.
- Smolders, A. J., E. C. Lucassen, R. Bobbink, J. G. Roelofs, and L. P. Lamers, How nitrate leaching from agricultural lands provokes phosphate eutrophication in groundwater fed wetlands: the sulphur bridge, *Biogeochemistry*, 98(1-3), 1–7, doi:10.1007/s10533-009-9387-8, 2010.
- Stanford, G., S. Dzienia, and R. A. Vander Pol, Effect of temperature on denitrification rate in soils, *Soil Science Society of America Journal*, 39(5), 867–870, doi:10.2136/sssaj1975.03615995003900050024x, 1975.
- Strebel, O., W. Duynisveld, and J. Böttcher, Nitrate pollution of groundwater in western europe, *Agriculture, Ecosystems & Environment*, 26(3-4), 189–214, doi:10.1016/0167-8809(89)90013-3, 1989.
- Therrien, R., and E. Sudicky, Three-dimensional analysis of variably-saturated flow and solute transport in discretely-fractured porous media, *Journal of Contaminant Hydrology*, 23(1), 1–44, doi:10.1016/0169-7722(95)00088-7, 1996.
- Thorsen, M., J. Refsgaard, S. Hansen, E. Pebesma, J. Jensen, and S. Kleeschulte, Assessment of uncertainty in simulation of nitrate leaching to aquifers at catchment scale, *Journal of Hydrology*, 242(3), 210–227, doi:10.1016/S0022-1694(00)00396-6, 2001.
- Todorovic, P., A stochastic model of longitudinal diffusion in porous media, *Water Resources Research*, 6(1), 211–222, doi:10.1029/WR006i001p00211, 1970.
- Van Kessel, J., Gas production in aquatic sediments in the presence and absence of nitrate, *Water Research*, 12(5), 291–297, 1978.
- Wakida, F. T., and D. N. Lerner, Non-agricultural sources of groundwater nitrate: a review and case study, *Water Research*, 39(1), 3–16, doi:10.1016/j.watres.2004.07.026, 2005.
- Ward, M. H., et al., Workgroup report: drinking-water nitrate and health - recent findings and research needs, *Environmental Health Perspectives*, 113(11), 1607, doi:10.1289/ehp.8043, 2005.
- Weyer, P. J., J. R. Cerhan, B. C. Kross, G. R. Hallberg, J. Kantamneni, G. Breuer, M. P. Jones, W. Zheng, and C. F. Lynch, Municipal drinking water nitrate level and cancer

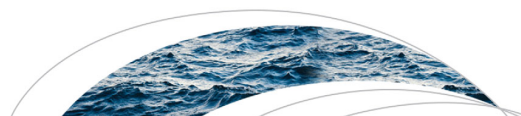
Bibliography

- risk in older women: the iowa women's health study, *Epidemiology*, 12(3), 327–338, doi: 10.1097/00001648-200105000-00013, 2001.
- Wijler, J., and C. Delwiche, Investigations on the denitrifying process in soil, *Plant and Soil*, 5(2), 155–169, 1954.
- Williams, D., J. Rowe, P. Romero, and R. Eagon, Denitrifying pseudomonas aeruginosa: some parameters of growth and active transport., *Applied and Environmental Microbiology*, 36(2), 257–263, 1978.
- Wisotzky, F., *Angewandte Grundwasserchemie, Hydrogeologie und hydrogeochemische Modellierung: Grundlagen, Anwendungen und Problemlösungen*, Springer-Verlag, doi: 10.1007/978-3-642-17813-9, 2012.
- Wolfe, A. H., and J. A. Patz, Reactive nitrogen and human health: acute and long-term implications, *AMBIO: A Journal of the Human Environment*, 31(2), 120–125, doi:10.1579/0044-7447-31.2.120, 2002.
- Xiu, D., and J. S. Hesthaven, High-order collocation methods for differential equations with random inputs, *SIAM Journal on Scientific Computing*, 27(3), 1118–1139, doi:10.1137/040615201, 2005.
- Yabusaki, S. B., C. I. Steefel, and B. Wood, Multidimensional, multicomponent, subsurface reactive transport in nonuniform velocity fields: code verification using an advective reactive streamtube approach, *Journal of Contaminant Hydrology*, 30(3), 299–331, doi:10.1016/S0169-7722(97)00050-8, 1998.
- Zhang, D., *Stochastic methods for flow in porous media: coping with uncertainties*, Elsevier, 2001.

List of Publications

1. Loschko M., Wöhling, T., Rudolph, D.L., Cirpka, O.A. (2016). Cumulative Relative Reactivity: A Concept for Modeling Aquifer-Scale Reactive Transport. *Water Resources Research*, 52(10), 8117-8137.
DOI: 10.1002/2016WR019080
2. Loschko M., Wöhling, T., Rudolph, D.L., Cirpka, O.A. (2018). Accounting for the Decreasing Reaction Potential of Heterogeneous Aquifers in a Stochastic Framework for Aquifer-Scale Reactive Transport. *Water Resources Research*, 54(1), 442-463.
DOI: 10.1002/2017wr021645
3. Loschko M., Wöhling, T., Rudolph, D.L., Cirpka, O.A. (2018). An Electron-Balance Based Approach to Predict the Decreasing Denitrification Potential of an Aquifer. *Groundwater* (in review).
DOI:

Publications



RESEARCH ARTICLE

10.1002/2016WR019080

Key Points:

- Relative reactivity is a spatial variable quantifying the intensity of reactions in comparison to a reference case
- Cumulative relative reactivity allows efficiently solving reactive transport in large-scale applications
- The low computational costs facilitate ensemble simulations of nonlinear, multicomponent, catchment-scale reactive transport

Correspondence to:

O. A. Cirpka,
olaf.cirpka@uni-tuebingen.de

Citation:

Loschko, M., T. Wöhling, D. L. Rudolph, and O. A. Cirpka (2016), Cumulative relative reactivity: A concept for modeling aquifer-scale reactive transport, *Water Resour. Res.*, 52, 8117–8137, doi:10.1002/2016WR019080.

Received 16 APR 2016

Accepted 27 SEP 2016

Accepted article online 29 SEP 2016

Published online 19 OCT 2016

Cumulative relative reactivity: A concept for modeling aquifer-scale reactive transport

Matthias Loschko¹, Thomas Wöhling², David L. Rudolph³, and Olaf A. Cirpka¹

¹Center for Applied Geoscience, University of Tübingen, Tübingen, Germany, ²Department of Hydrology, Technische Universität Dresden, Dresden, Germany, ³Department of Earth and Environmental Sciences, University of Waterloo, Waterloo, Ontario, Canada

Abstract We simulate aquifer-scale reactive transport using an approach based on travel times and relative reactivity. The latter quantifies the intensity of the chemical reaction relative to a reference reaction rate with identical concentrations and can be interpreted as the strength of electron-donor (or electron-acceptor) release by the matrix, scaled by a reference release. In general, the relative reactivity is a spatially variable property reflecting the geology of the formation. In the proposed approach, we track the path of individual water parcels through the aquifer and evaluate the age of the water parcels and the relative reactivity integrated along their trajectories. By switching from spatial discretization to cumulative relative reactivity, advective-reactive transport can be simulated by solving a single system of ordinary differential equations for each combination of concentrations in the inflow. We test the validity of the approach in a two-dimensional test case of steady state groundwater flow and reactive transport involving aerobic respiration and denitrification. Here we compare steady state concentration distributions of the spatially explicit virtual truth, accounting for dispersive mixing, with the approximation based on cumulative relative reactivity and show that the errors introduced by neglecting dispersive mixing are minor if the target quantities are the mass fluxes crossing a control plane or being collected by a well. We further demonstrate the efficiency of the approach in a synthetic three-dimensional case study. The proposed approach is computationally so efficient that ensemble runs to assess statistical distributions of concentration time series of reactive solutes become feasible, which is not practical with a spatially explicit model.

1. Introduction

Quantitative understanding of pollutant fluxes from diffuse input and turnover of pollutants on the catchment scale requires process-based numerical models that can explain observed time series of hydraulic heads and concentrations under current conditions and predict future states under changing ones. For reactive transport on the scale of entire aquifers, conventional numerical methods for reactive solute transport solve the advection-dispersion-reaction equation [e.g., Schäfer and Therrien, 1995; Therrien and Sudicky, 1996; Prommer et al., 2001; Mayer et al., 2002; Steefel, 2009]. These partial differential equation (PDE)-based models require a spatially explicit representation of all physical states and system parameters. Upon the discretization of the spatial parameter fields, many discrete parameters are needed. Groundwater quantity and quality are affected by land use, soil type, vegetation, chemical inputs, geometry of the aquifer, groundwater recharge, and other parameters [e.g., Refsgaard et al., 2014]. All of these are spatially variable and uncertain, either due to insufficient knowledge or because of unpredictable dynamics of forcing and unresolved subscale variability. Dealing with spatial variability and uncertainty in catchment-scale reactive transport is thus a well-known conceptual and computational challenge [Carrera, 1993; Pechlivanidis et al., 2011; Thorsen et al., 2001].

To account for subscale variability and uncertainty of the model parameters, a stochastic framework using Monte-Carlo (MC) simulations may be applied. In MC simulations, random realizations of the parameter fields are generated and the flow and transport problem is solved for each realization to generate an ensemble of dependent variable values [Dagan, 2002]. While more efficient ways of sampling the probability space of the random parameters exist [e.g., Xiu and Hesthaven, 2005; Ganapathysubramanian and Zabaras, 2007; Nobile et al., 2008], all techniques of uncertainty quantification that do not rely on linearization imply that a large number of model runs need to be performed, which increases the computationally

demand dramatically. Uncertainty quantification methods that are based on nonlocal, integro-differential equations to obtain the first two statistical moments also suffer from high computational costs [Neuman and Orr, 1993; Guadagnini and Neuman, 1999]. Within a stochastic framework, predictions of the fate of a contaminant are expressed in terms of probabilities rather than single values. For catchment-scale, fully coupled, multidimensional, nonlinear, spatially explicit, multicomponent reactive transport models that exhibit rather large model run-times, MC simulations or the other mentioned techniques going beyond linear uncertainty propagation are typically prohibitive. Hence, conceptual simplifications are necessary, keeping spatially explicit calculations whenever needed and computationally manageable, but simplifying reactive transport computations without sacrificing mechanistic understanding.

A specific type of simplification, following a Lagrangian framework, is known as the streamline approach which is based on travel times of water parcels [e.g., Jury, 1982; Feyen et al., 1998; Luo, 2012]. Travel time analysis for transport in porous media were first mentioned by Todorovic [1970] and further developed by Shapiro and Cvetkovic [1988]. These models make use of the fact that reactive-species concentrations are strongly associated with travel times or times of exposure to certain reactive facies with specific chemical or other environmental characteristics facilitating a desired reaction [Rubin et al., 1994]. Streamline approaches restrict solute transport to the direction of flow. Dispersion is addressed by the consideration of transit or travel time distributions, rather than individual values at a point.

Instead of evaluating reactive transport in the entire domain, the streamline approach calculates it along pathlines. The spatial coordinates, required in the fully explicit three-dimensional reactive transport models, are replaced by groundwater travel time [Feyen et al., 1998]. The reactive transport equation thus becomes one-dimensional. To solve it, a single one-dimensional simulation in travel time coordinates is sufficient if the inflow concentration is uniform along the entire inflow boundary and if reaction constants are uniform within the domain. Streamline approaches are likely to be valid if the input of contaminants is diffusive (i.e., spread over large areas) so that transverse macroscopic mixing processes may be neglected, as transverse mixing across stream tubes has a minor influence on concentration relative to the concentration changes along the stream tube. This condition is most likely met in the case of nitrate leaching from agricultural soils into groundwater, which is the application of this study. In addition, we assume in the present study that the nitrate loading is uniform over time even though this is not a prerequisite of the approach outlined here. In previous studies investigating streamline approaches, dispersive mixing along stream tubes has often been neglected altogether, which leads to purely advective-reactive transport [Atchley et al., 2013; Ginn et al., 1995]. An exchange between the stream tubes, which are conceptualized as independent one-dimensional systems, is not considered. Travel time-based models that consider random advection are known as stochastic-convective reactive models [Dagan and Nguyen, 1989; Cvetkovic et al., 1996; Simmons et al., 1995; Atchley et al., 2013] and have been applied to groundwater hydrology in numerous studies [e.g., Simmons, 1982; Cvetkovic and Dagan, 1994; Cvetkovic et al., 1996; Ginn, 2002]. Mixing-controlled reactions cannot be addressed by these models. However, effective longitudinal mixing may be accounted for in stream tube approaches by using an appropriate longitudinal dispersion coefficient [Cirpka and Kitanidis, 2000; Sanz-Prat et al., 2015; Luo and Cirpka, 2011]. One of the biggest advantages of travel time-based models is that the computational effort of solving reactive transport is extremely reduced [Atchley et al., 2014; Gong et al., 2011; Diem et al., 2013].

Most studies on catchment-scale reactive transport reduce nonlinear reaction pathways to compartment-dependent first-order terms, coupled to component-specific travel time distributions. In this framework, the travel time distributions of a whole catchment are transferred to probability density functions of concentration using linear reaction equations [Rinaldo and Marani, 1987; Rinaldo et al., 2006; Destouni et al., 2010; Botter et al., 2010]. For systems on large scales, simple relationships between discharge and concentrations of nutrients have been found [e.g., Basu et al., 2010; Törnqvist et al., 2015], but values obtained in monitoring wells can only be explained if the internal aquifer structure (e.g., hydraulic conductivity and reactive zones) is accounted for.

The stochastic-convective framework has been extended to nonlinear multicomponent reactive transport and multiphase flow problems [Cvetkovic and Dagan, 1994; Dagan and Cvetkovic, 1996; Kaluarachchi et al., 2000; Yabusaki et al., 1998; Malmström et al., 2004] under the premise that solute mixing can be neglected. Sanz-Prat et al. [2015] and Sanz-Prat et al. [2016b] tested the validity of travel time-based nonlinear reactive transport schemes considering dispersive mixing, confirming travel time-based methods to be a good basis

for continuous input of reactants undergoing microbial degradation. These authors simulated the simultaneous injection of dissolved organic carbon (DOC), nitrate, and oxygen into an aquifer, transport and turnover of the compounds, and the dynamics of aerobic and denitrifying bacteria. After an initial period, a stable microbial community evolved, and steady state conditions were reached. While in the latter study the electron donor (DOC) was introduced into the subsurface together with the electron acceptors (nitrate and dissolved oxygen), and biomass growth was limited by a predefined carrying capacity, a more typical situation is a stoichiometric imbalance of electron acceptors and donors in groundwater recharge. In regions affected by intensive agriculture, a surplus of nitrate in the recharging water is observed. Here the denitrifying microbial community is limited by lacking assimilable organic carbon or other electron donors (e.g., pyrite) that are typically supplied by the aquifer matrix [e.g., Korom, 1992; Molz *et al.*, 1986].

Previous studies have shown that it is important to distinguish between travel and exposure times because the mineralogical composition of the matrix and the biogeochemical conditions are commonly nonuniformly distributed in an aquifer [Lohse *et al.*, 2009; Reich *et al.*, 2006; Ocampo *et al.*, 2006]. The exposure time is the time that a solute particle has been exposed to particular conditions, whereas the travel time is the total time spent in the domain. Cvetkovic *et al.* [1998] performed first-order stochastic analyses of spatial and temporal moments of solutes. These authors accounted for the spatial variability of sorption parameters and integrated the sorptivity experienced by water parcels while being advected through heterogeneous domains. They could derive first-order analytical expressions for the first two moments of this quantity, from which the spatial and temporal moments of sorbing compounds in mildly heterogeneous domains could be inferred. The results are subject to the limitations of first-order theory (small variability), and the analytical expressions require second-order stationary velocity fields.

Frei and Peiffer [2016] highlighted the importance of distinguishing between residence and exposure times and presented an approach to couple residence and exposure time distributions by Damköhler numbers. However, the approach is computationally expensive and therefore not suitable for a stochastic framework. Seeboonruang and Ginn [2006] also showed that the reactive properties of solid-phase materials play a crucial role in solute transport. These authors combined the stream tube approach presented by Simmons *et al.* [1995] and the exposure time approach by Ginn [1999] to a modified stochastic-convective method. They constructed a stream tube ensemble approach that accommodates the travel time as well as a cumulative reactivity as quantities over which the solute flux is distributed. Here the cumulative reactivity is a structural variable to keep track of the exposure of solutes to specific reactive surfaces. However, the application of the approach was limited to linear, kinetically controlled reactions and the applicability to nonlinear reactions was not tested. Sanz-Prat *et al.* [2016a] showed that exposure time models provide good approximations of nonlinear bio-reactive transport when transverse mixing is not the overall controlling process. In the latter study, the reactive zones considered for the exposure time had identical and uniform reactive parameters. The present work revisits the approach of Seeboonruang and Ginn [2006] and the work of Sanz-Prat *et al.* [2016a] and applies it to multicomponent, nonlinear reactive transport.

In the present work, we simulate groundwater flow in a spatially explicit way, enabling us to account for aquifer heterogeneity. We simulate reactive transport of dissolved oxygen and nitrate along particle trajectories obtained by particle tracking. Note that the presented approach is not limited to this specific reactive system, but can be applied to other, even more complex, reactions. The one-dimensional transport is further simplified by introducing the concept of relative reactivity f [–], which is properly introduced in section 2. As we will show, this approach is computationally so inexpensive that massive Monte-Carlo simulations, which are prohibitive for spatially explicit models, become feasible even though the latter is not in the focus of the present study.

The remainder of the paper is structured as follows. The concept of (cumulative) relative reactivity is explained in detail in section 2, whereas section 3 contains the associated mathematical derivations. In section 4, we introduce the reactive system analyzed in the present study. In section 5, we test the validity of the proposed approach in a two-dimensional test case, in which dissolved oxygen and nitrate are transported through a heterogeneous aquifer and react with the aquifer matrix. Here we compare a spatially explicit model, accounting for dispersive mixing, with the proposed advective-reactive approach based on the cumulative relative reactivity. In section 6, we demonstrate the efficiency of the concept in the application to a three-dimensional synthetic test case representing an aquifer with a single, chemically heterogeneous reactive zone. The paper closes with general conclusions in section 7.

2. General Concept

The starting point of our analysis is the assumption of advective-reactive transport, in which dispersive mixing is neglected altogether. Figure 1 depicts two different contamination scenarios to illustrate under which conditions such an assumption may be acceptable. Both setups show groundwater recharge from the top, an extraction well, and a river at the right-hand side. In Figure 1a, the contaminant is introduced by a point source and reacts with a solute in the ambient solution. This is the typical scenario of a contaminant plume, the reaction of which is controlled by transverse mixing, so that neglecting dispersion is strictly prohibited [e.g., Cirpka and Valocchi, 2007; Cirpka et al., 2012]. Another scenario, in which dispersive mixing controls the overall reaction behavior, is when the solution containing one nonsorbing reactant is replaced by the solution containing the other, also nonsorbing reaction partner [e.g., Le Borgne et al., 2014; de Anna et al., 2014]. In contrast to such cases, Figure 1b depicts the scenario for which the present framework is developed. Here we consider the diffuse input of a reactant at the land surface as it is typical for agricultural pollution (e.g., by nitrate). The solute of interest reacts with constituents of the aquifer matrix, which are nonuniformly distributed within the domain. In Figure 1b, zones with high contents of solid-phase reactants are shown as green inclusions, whereas the white background reflects essentially nonreactive zones. In this scenario, the chemical reaction is controlled by mass transfer from the aquifer matrix to the aqueous solution and takes place only during the transit of water and solutes through the reactive zones. While we cannot totally exclude an influence of dispersive mixing on the overall reactive transport behavior, it is not the major control of the reaction. The validity of this assumption for our reactive system will be tested in section 5.

In the proposed framework, the existing advective-reactive transport model is extended by introducing the dimensionless relative reactivity $f(\mathbf{x}) [-]$, which parameterizes the intensity of a target reaction at every location $\mathbf{x} [L]$ in the domain, in comparison to a reference reaction rate for the same concentrations of dissolved compounds. A high relative reactivity ($f > 1$) amplifies the reference reaction rates, whereas a low relative reactivity ($f < 1$) dampens them. The relative reactivity reflects spatial differences in the solid phases, which are not explicitly described in the model. For the chemical reduction of solutes, the relative reactivity is thus related to the electron-donor supply by the matrix (e.g., from natural organic matter, pyrite, or biotite). For chemical oxidation of solutes, by contrast, the relative reactivity parameterizes the electron-acceptor supply (e.g., from ferric iron oxides). In a practical setting, the relative reactivity will be related to different geological facies. Our application deals with reduction of solutes, where materials with strong reduction potential, such as peat lenses, would be assigned a large relative reactivity ($f > 1$), materials with intermediate reduction potential, such as carbonaceous limestones, would obtain smaller relative reactivity values ($f \approx 1$), and redox-insensitive materials like clean quartz sand would have a relative reactivity of zero ($f = 0$). The internal chemical variability within individual units can be addressed by spatial variation of the relative reactivity, e.g., by treating it as a random space function.

The key assumption of using the relative reactivity is that the supply of reaction partners from the matrix controls the overall reaction and that the microbial communities, catalyzing the reactions, adapt quickly to the reactive-solute concentrations and the reaction-partner supply by the matrix. The abundance of microbes itself is not explicitly accounted for in the remaining model description of the reactions, whereas potentially nonlinear dependencies on reactive-solute concentrations remain. As such, the concept stands somewhere between a comprehensive description of the reaction network, including explicit modeling of microbial dynamics, and approaches reducing all reactions to apparent first-order decay laws. In particular, we want to keep the competition of several solutes for the reaction partner supplied by the matrix in our

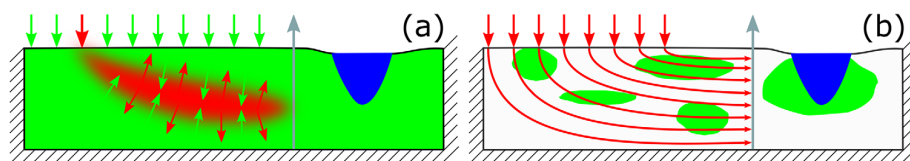


Figure 1. Comparison of two contamination scenarios with contamination input (red) at the land surface. (A) Point-source contamination requiring a reaction partner (green) introduced in parallel, leading to a plume controlled by transverse dispersive mixing; (B) diffusive contamination reacting with compounds released by the matrix (reactive zones shown as green patches). The proposed method is only valid for scenario B.

reaction model. For multicomponent mixtures, the approach requires identical relative reactivities for all reactions considered, implying that the release of the same reactants from the matrix controls all reactions.

For demonstration of our methodology, we choose the case of aerobic respiration and denitrification. The microbial reduction of oxygen and nitrate is assumed to follow standard Michaelis-Menten kinetics with a noncompetitive inhibition term expressing the inhibition of denitrification in the presence of elevated oxygen concentrations. Biomass concentrations, however, are not explicitly modeled, assuming that the establishment and specificity of the microbial community is controlled by the availability of electron donors and acceptors. This seems to be justified by preceding studies. *Mellage et al.* [2015] showed that even a starvation period of several months will not lead to a breakdown of the degradation capacity of a microbial community. The microbes can lie dormant for extended periods of time and then regain their full biodegradation potential within few hours after the end of the starvation period. Other investigations showed that if anaerobic conditions occur, facultative denitrifiers switch from oxygen to nitrate as the electron acceptor within a period of 40 min to 3 h [Payne and Riley, 1969; Payne et al., 1971; Williams et al., 1978]. On the catchment scale, groundwater travel times are generally in the order of several years or decades, and contaminants have been introduced over a long time period so that functionally stable microbial communities have been established, and can be reactivated quickly under dynamic biogeochemical conditions. We are not looking at the first arrival of a nitrate front in a pristine aquifer, where complex growth dynamics of the microbial community may control the overall reaction behavior.

We follow the key Lagrangian premise of following water parcels along their trajectories through the domain. We calculate two integral quantities along a travel path: (1) the travel time or kinematic age $\tau(\mathbf{x})$ [T], allowing to compute when a water parcel, that is observed in the aquifer at a given time, entered the subsurface at the land surface; and (2) the cumulative relative reactivity $F(\mathbf{x})$ [T], which is the time integral of the local relative reactivity experienced by the moving water parcel. In cases where the concentration of the reactive solutes in the inflow varies, we also need to consider the location $\mathbf{x}_0(\mathbf{x})$ [L] where the water parcel entered the domain. Under transient-flow conditions, τ , F , and \mathbf{x}_0 also depend on time.

The composition of reactive solutes changes while the water parcel moves through zones of different reactivity. This may be seen as an aging of the water parcel with associated change in chemical composition. However, the clock by which the water ages ticks quicker in zones of high relative reactivity than in those of low relative reactivity, so that the cumulative relative reactivity F may be interpreted as a reaction-relevant age. As we will derive in section 3, the concentrations of the reactive solutes uniquely depend on the vector of inflow concentrations \mathbf{c}_0 [ML⁻³], the cumulative relative reactivity F , and the reaction law of the reference reaction rates, the latter being a system of ordinary differential equations (ODEs).

In our application, the concentrations of oxygen and nitrate at a given location \mathbf{x} and time t can be computed from (1) the origin \mathbf{x}_0 and travel time τ of the water parcel, determining the initial concentrations \mathbf{c}_0 of oxygen and nitrate when the water parcel entered the system, and (2) the cumulative relative reactivity F that the water parcel has experienced while passing through the aquifer. Origin, travel time, and cumulative relative reactivity can easily be evaluated by particle tracking. For the reactions, ordinary differential equations (ODEs) are solved, in which time is replaced by cumulative relative reactivity. Thus, with a finite set of initial concentration values, one ODE solution per initial condition, and the information from particle tracking, concentrations of the electron acceptors can be computed at all times and locations, without reducing the reactions to single-compound descriptions. This approach significantly reduces the computational effort of reactive transport simulations.

3. Mathematical Framework

3.1. Reactive Transport Equation

We start with the classical advection-dispersion-reaction equation of a dissolved compound i with concentration c_i [ML⁻³]

$$\frac{\partial c_i}{\partial t} + \mathbf{v} \cdot \nabla c_i - \nabla \cdot (\mathbf{D} \nabla c_i) = r_i(\mathbf{c}(\mathbf{x}, t), \mathbf{x}, t), \quad (1)$$

in which t [T] is time, $\mathbf{v} = \frac{\mathbf{q}}{\theta}$ [LT⁻¹] denotes the linear average velocity vector, which is the specific-discharge vector \mathbf{q} [LT⁻¹] divided by flow-effective porosity θ [-], \mathbf{D} [L²T⁻¹] is the dispersion tensor, and

r_i [$\text{ML}^{-3}\text{T}^{-1}$] is the reaction rate of compound i depending on the $n_{comp} \times 1$ vector of all concentrations \mathbf{c} [ML^{-3}], the location \mathbf{x} [L], and potentially time.

We now consider the vector $\mathbf{r}(\mathbf{c}(\mathbf{x}, t), \mathbf{x}, t)$ of all reaction rates. For the time being, we assume that the only influence of time is by the time dependence of the concentrations $\mathbf{c}(\mathbf{x}, t)$. As explained in section 2, we further separate the reaction rate into a concentration-dependent base reaction rate $\mathbf{r}_0(\mathbf{c}(\mathbf{x}, t))$ and a concentration-independent, spatially variable scalar multiplier $f(\mathbf{x})$ [-], denoted relative reactivity

$$\mathbf{r}(\mathbf{c}(\mathbf{x}, t), \mathbf{x}, t) = f(\mathbf{x})\mathbf{r}_0(\mathbf{c}(\mathbf{x}, t)), \quad (2)$$

in which $\mathbf{r}_0(\mathbf{c}(\mathbf{x}, t))$ [$\text{ML}^{-3}\text{T}^{-1}$] is the concentration-dependent $n_{comp} \times 1$ vector of reaction rates of all compounds for a reference reactivity. The parameters of the reference reactivity are assumed uniform. The selected set of reaction parameters refers to a relative reactivity of unity. The key idea of the relative reactivity $f(\mathbf{x})$ is to express spatially variable influences on the reactions that are not caused by the solute concentrations varying in space. As an example, the reaction rate of oxygen at a given location in space and time may be caused by small oxygen concentrations, high nitrate concentrations, or low availability of a reaction partner in the matrix. In our approach, the first two causes are included in $\mathbf{r}_0(\mathbf{c}(\mathbf{x}, t))$, whereas the third belongs to $f(\mathbf{x})$.

Neglecting dispersion, equation (1) becomes

$$\frac{\partial \mathbf{c}}{\partial t} + \mathbf{v} \cdot \nabla \mathbf{c} = f(\mathbf{x})\mathbf{r}_0(\mathbf{c}(\mathbf{x}, t)) \quad (3)$$

for nonsorbing compounds.

3.2. Solving Advective-Reactive Transport Using Cumulative Relative Reactivity

We now change from an Eulerian to a Lagrangian perspective, that is, we follow a water parcel that moves with $\mathbf{v}(\mathbf{x}, t)$ through the domain, where the Lagrangian velocity of the parcel equals the local Eulerian velocity. In the standard forward particle tracking scheme, a water parcel with the starting location \mathbf{x}_0 [L] and the starting time t_0 [T] is followed through the domain over the travel time τ [T]

$$\mathbf{x}(t_0 + \tau | \mathbf{x}_0, t_0) = \mathbf{x}_0 + \int_{t_0}^{t_0 + \tau} \mathbf{v}(\mathbf{x}(\tau_* | \mathbf{x}_0), \tau_*) d\tau_*. \quad (4)$$

The cumulative relative reactivity F [T] is derived in analogy to equation (4) by integrating the local relative reactivity experienced by the water parcel while it is advected through the domain

$$F(t_0 + \tau | \mathbf{x}_0, t_0) = \int_{t_0}^{t_0 + \tau} f(\mathbf{x}(\tau_* | \mathbf{x}_0)) d\tau_*. \quad (5)$$

We can also revert the analysis and determine which starting location $\mathbf{x}_0(\mathbf{x}, t)$ and travel time $\tau(\mathbf{x}, t)$ are associated with an observation at point \mathbf{x} and time t . Then, $F(\mathbf{x}, t) = F(t | \mathbf{x}_0(\mathbf{x}, t), t_0(\mathbf{x}, t))$ is the associated cumulative relative reactivity. We follow this approach in the present study where flow is considered to be at steady state. In case of transient flow, it might be computationally more feasible to introduce particles continuously, track them forward in time, and perform spatial interpolation between the nearest particles when computing $\mathbf{x}_0(\mathbf{x}, t)$, $\tau(\mathbf{x}, t)$, and $F(\mathbf{x}, t)$ at a given point in space and time, because in backward tracking velocity fields at preceding time levels need to be stored.

Revisiting equation (3) in the Lagrangian framework, the vector of reactive-species concentrations in the moving water parcel meets

$$\frac{d\mathbf{c}(\mathbf{x}(t), t)}{dt} = f\mathbf{r}_0(\mathbf{c}(\mathbf{x}(t), t)) \text{ along } \frac{d\mathbf{x}(t)}{dt} = \mathbf{v}(\mathbf{x}(t), t), \mathbf{x}(t_0) = \mathbf{x}_0, \quad (6)$$

subject to

$$\mathbf{c}(\mathbf{x}_0, t_0) = \mathbf{c}_0(\mathbf{x}_0, t_0). \quad (7)$$

Applying the chain rule of differentiation yields

$$\frac{d\mathbf{c}(\mathbf{x}(t), t)}{dt} = \frac{dF(\mathbf{x}(t), t)}{dt} \frac{d\mathbf{c}(\mathbf{x}(t), t)}{dF} \text{ along } \frac{d\mathbf{x}(t)}{dt} = \mathbf{v}(\mathbf{x}(t), t), \mathbf{x}(t_0) = \mathbf{x}_0, \quad (8)$$

in which we need the rate of change of cumulative relative reactivity along the trajectory, which can easily be computed from its definition

$$\frac{dF}{dt} = \frac{dF}{d\tau} = f. \quad (9)$$

Substitution yields

$$\frac{d\mathbf{c}(\mathbf{x}(t), t)}{dt} = f \frac{d\mathbf{c}}{dF} = f \mathbf{r}_0(\mathbf{c}(\mathbf{x}(t), t)). \quad (10)$$

and thus

$$\frac{d\mathbf{c}}{dF} = \mathbf{r}_0(\mathbf{c}) \text{ subject to } \mathbf{c}(t_0) = \mathbf{c}_0(\mathbf{x}_0, t_0). \quad (11)$$

The system of ODEs of equation (11) can be solved for all initial concentrations of oxygen and nitrate $\mathbf{c}_0(t_0)$ occurring in the model problem. Finally, we can evaluate the concentration at any given point in space and time $\mathbf{c}(\mathbf{x}, t)$ by determining the origin $\mathbf{x}_0(\mathbf{x}, t)$, travel time $\tau(\mathbf{x}, t)$, and cumulative reactivity $F(\mathbf{x}, t)$ of the water parcel at that point, and looking up the corresponding inflow concentration $\mathbf{c}_0(\mathbf{x}_0(\mathbf{x}, t), t - \tau(\mathbf{x}, t))$ with its corresponding ODE solution

$$\mathbf{c}(\mathbf{x}, t) = \mathbf{c}_{ode}(F(\mathbf{x}, t), \mathbf{c}_0(\mathbf{x}_0(\mathbf{x}, t), t - \tau(\mathbf{x}, t))) \quad (12)$$

in which $\mathbf{c}_{ode}(F, \mathbf{c}_0)$ is the solution of equation (11) at the cumulative-relative-reactivity value F for the initial value \mathbf{c}_0 .

Equation (12) defines a unique mapping from travel time τ , origin of the water parcel \mathbf{x}_0 , and cumulative relative reactivity F to reactive-species concentrations at location \mathbf{x} and time t . It simplifies the calculation of reactive-solute concentrations even more than standard advective-reactive approaches because the ODE of equation (11) needs to be solved only once for any given combination of concentrations in groundwater recharge. If $F(\mathbf{x}, t)$, $\mathbf{x}_0(\mathbf{x}, t)$, and $\tau(\mathbf{x}, t)$ are considered random variables, the full statistical distribution of $\mathbf{c}(\mathbf{x}, t)$ can be constructed from the joint probability density function of $F(\mathbf{x}, t)$, $\mathbf{x}_0(\mathbf{x}, t)$, and $\tau(\mathbf{x}, t)$. The conceptually simplest approach of doing that would be by Monte-Carlo simulations.

Under steady state flow conditions, the time dependencies in equations (4) and (5) drop out

$$\mathbf{x}(\tau|\mathbf{x}_0) = \mathbf{x}_0 + \int_0^\tau \mathbf{v}(\mathbf{x}(\tau_*|\mathbf{x}_0)) d\tau_*, \quad (13)$$

$$F(\mathbf{x}) = F(\tau(\mathbf{x})|\mathbf{x}_0(\mathbf{x})) = \int_0^\tau f(\mathbf{x}(\tau_*|\mathbf{x}_0)) d\tau_*, \quad (14)$$

and thus also the reverse relationships $\mathbf{x}_0(\mathbf{x})$, and $\tau(\mathbf{x})$ become time independent. Under these conditions, the cumulative relative reactivity can also be evaluated in an Eulerian framework by solving

$$\mathbf{v} \cdot \nabla F = f, \quad (15)$$

subject to

$$F = 0 \text{ on } \Gamma_{in}, \quad (16)$$

in which Γ_{in} denotes an inflow boundary.

If we permit dispersion, the cumulative relative reactivity $F(\mathbf{x})$ at every point becomes a distribution instead of a single value. In analogy to the mean groundwater-age equation of Goode [1996], the mean cumulative relative reactivity μ_F for advective-dispersive transport in steady state flow fields can be described by

$$\mathbf{v} \cdot \nabla \mu_F - \nabla \cdot (\mathbf{D} \nabla \mu_F) = f(\mathbf{x}) \quad (17)$$

subject to

$$\mathbf{n} \cdot (\mathbf{v}\mu_F - \mathbf{D}\nabla\mu_F) = 0 \text{ on } \Gamma_{in}, \quad (18)$$

$$\mathbf{n} \cdot \mathbf{D}\nabla\mu_F = 0 \text{ on } \Gamma_{out} \cup \Gamma_{nf}, \quad (19)$$

in which Γ_{out} and Γ_{nf} denote outflow and no-flow boundaries.

3.3. Modeling Approach

The proposed modeling approach for aquifer-scale reactive transport using the cumulative relative reactivity consists of the following four steps:

1. Calculate the groundwater velocity field with a spatially explicit PDE-based model (in the present application at steady state, but the approach would also work in transient flows).
2. Determine particle trajectories to obtain the travel time $\tau(\mathbf{x}, t)$ and the cumulative relative reactivity $F(\mathbf{x}, t)$, which are time-independent in case of steady state flow. In the 2-D test case presented below, equation (15) was solved for the strictly advective case, and equation (17) for the advective-dispersive case using an Eulerian stream tube approach.
3. Solve the ordinary differential equation (11) for all occurring inflow concentrations \mathbf{c}_0 resulting in $\mathbf{c}_{ode}(F, \mathbf{c}_0)$.
4. Map travel time and cumulative relative reactivity to reactive-species concentrations according to equation (12).

4. Chemical Reactions Considered in This Study

In the present case, we simulate microbial reduction of oxygen and nitrate. We assume that their microbial turnover depends on the solute concentrations and the release of electron donors from the aquifer matrix. These simplifications seem to be justified as the microbial biomass readily approaches quasi steady state values that hardly change in times of starvation [Mellage *et al.*, 2015; Payne *et al.*, 1971]. We consider, however, that denitrification is inhibited in the presence of elevated oxygen concentrations. This corresponds with the well-studied behavior that the depletion of oxygen favors the occurrence of denitrification and that nitrogen reductases are inhibited by elevated oxygen levels [Chan and Campbell, 1980; Payne, 1973].

The chemical processes of aerobic respiration and denitrification are modeled using standard Michaelis-Menten kinetics, which have been developed to model enzymatic reactions [Betlach and Tiedje, 1981; Reddy *et al.*, 1982]. The key idea of Michaelis-Menten kinetics is that the reaction is catalyzed by an enzyme which is available only at small concentrations and to which the reactant readily binds; the reaction rate is assumed proportional to the number of enzyme-reactant complexes. Michaelis-Menten kinetics with various variants are the standard laws to express microbially mediated reactions. On larger scales, like in the present application, Michaelis-Menten laws may be seen as effective expressions, leading to a specific type of concentration dependence without agreeing with strictly enzymatic reactions. In particular, aerobic metabolism is known to be practically independent of the dissolved-oxygen concentration over a wide range of concentrations [e.g., Diem *et al.*, 2013] so that the main purpose of the (small) Michaelis-Menten coefficient of oxygen is to smooth the zero-order reaction law at low concentrations, rather than to reflect the actual strength of oxygen-enzyme binding. Michaelis-Menten coefficients of nitrate are typically higher than those of oxygen, expressing less efficiency of the bacteria to process nitrate in comparison to oxygen.

We implicitly assume that the biomass concentrations of the aerobic and denitrifying microbes, and thus of the associated catalyzing enzymes, have reached a steady state value that is related to the electron-donor release of the matrix. Neither the electron-donor concentration, which is also assumed to be at steady state, nor the biomass concentrations are explicitly calculated. Instead, the effects of these concentrations are parameterized by the relative reactivity f . For thermodynamics reasons, we assume that oxygen is consumed first. If there is hardly any oxygen left, the reduction of nitrate starts. This is expressed by a noncompetitive inhibition term in the kinetic rate laws as follows:

$$r_{0,DO} = \frac{dc_{DO}}{dF} = - \frac{c_{DO}}{c_{DO} + K_{DO}} \cdot r_{max}^{aer}, \quad (20)$$

Table 1. Reactive Parameters Used in This Study

Symbol	Meaning	Value
K_{DO}	Michaelis-Menten constant for oxygen	11.4 $\mu\text{mol/L}$
K_{Nit}	Michaelis-Menten constant for nitrate	70 $\mu\text{mol/L}$
K_{DO}^{inh}	Inhibition constant	10 $\mu\text{mol/L}$
r_{max}^{aer}	Maximal reaction rate of oxygen under reference conditions	15 $\mu\text{mol/L d}$
r_{max}^{Nit}	Maximal reaction rate of nitrate under reference conditions	15 $\mu\text{mol/L d}$

$$r_{0,Nit} = \frac{dc_{Nit}}{dF} = - \frac{c_{Nit}}{c_{Nit} + K_{Nit}} \cdot \frac{K_{DO}^{inh}}{K_{DO}^{inh} + c_{DO}} \cdot r_{max}^{Nit}, \quad (21)$$

in which c_{DO} [ML^{-3}] is the concentration of dissolved oxygen, c_{Nit} [ML^{-3}] is the nitrate concentration, K_i [ML^{-3}] is the Michaelis-Menten constant of terminal electron acceptor i , r_{max}^{aer} [$\text{ML}^{-3}\text{T}^{-1}$] and r_{max}^{Nit} [$\text{ML}^{-3}\text{T}^{-1}$] are the maximum reaction rates of oxygen and nitrate, respec-

tively, for a relative reactivity of one, and K_{DO}^{inh} [ML^{-3}] is the inhibition constant of oxygen in denitrification.

The kinetics of the denitrification inhibition by oxygen may be different in laboratory experiments than in aquifers because small-scale heterogeneity can cause microanaerobic environments facilitating denitrification in the macroscopic presence of dissolved oxygen [Smith, 1980]. However, the basic concept that dissolved oxygen suppresses denitrification remains untouched in the present study.

Table 1 contains the reactive parameters under reference conditions ($f = 1$) applied in the present study. Figure 2 shows the evolution of the oxygen and nitrate concentrations for a water parcel with initial values of 40 mg/L of NO_3^- and 10 mg/L of O_2 as function of the cumulative relative reactivity F . The concentration series are obtained by solving equations (11), (20), and (21) with the ODE-solver ode15s of Matlab, which is based on backward differentiation formulas [Shampine and Reichelt, 1997]. As can be seen, the presence of dissolved oxygen at elevated concentration levels inhibits denitrification. For the given parameters and initial values, dissolved-oxygen concentrations decrease almost linearly with F , indicating essentially zero-order degradation, and the cumulative relative reactivity must exceed a value of approximately 2×10^6 s (≈ 23 days) for significant denitrification to occur. A slight decrease in nitrate concentration can be observed before because the inhibition term is not zero even for high values of the oxygen concentration.

Figure 3 shows the nitrate concentration as a function of the cumulative relative reactivity F , the initial nitrate concentration $c_{0,Nit}$, and the initial concentration of dissolved oxygen $c_{0,DO}$ for the reactive parameters of Table 1. To construct Figure 3, 1000 ODE systems have been solved, systematically scanning the initial concentrations of nitrate and oxygen. As can be seen, the onset of significant denitrification depends on the oxygen concentration in the inflow. The true value in the data plotted in Figure 3 lies in the ability to compute the spatial distribution of reactive-species concentrations by simple mapping according to equation (12). From the origin \mathbf{x}_0 and travel time τ at all points, we can compute the inflow concentrations $c_{0,Nit}$ and $c_{0,DO}$. Together with the cumulative relative reactivity F at the observation point, we can determine the

reactive species concentration by interpolating the numerically determined relationships $c_{Nit}(c_{0,Nit}, F, c_{0,DO})$ (shown in Figure 3) and $c_{DO}(c_{0,Nit}, F, c_{0,DO})$ (not show, but determined together with $c_{Nit}(c_{0,Nit}, F, c_{0,DO})$).

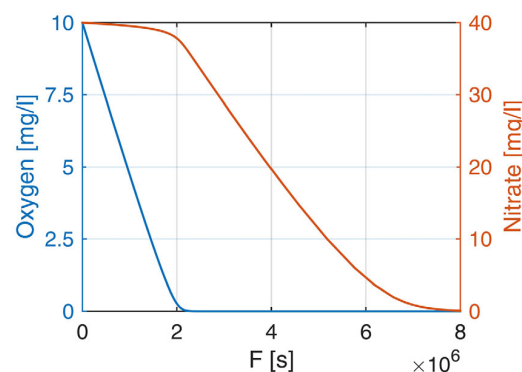


Figure 2. Dependence of dissolved oxygen and nitrate concentrations on cumulative relative reactivity F for reactive parameters given in Table 1 and initial values of 40 mg/L of NO_3^- and 10 mg/L of O_2 . Brown line: nitrate concentration. Blue line: dissolved oxygen concentration.

5. Two-Dimensional Test Case on the Validity of the Approach

5.1. Setup and Methods

To test the validity of the proposed concept, we performed a two-dimensional study in a $50 \text{ m} \times 50 \text{ m}$ domain with a $0.1 \text{ m} \times 0.1 \text{ m}$ resolution. We generated a pattern of two different materials by generating a multi-Gaussian field of an auxiliary variable with an isotropic Gaussian covariance function with correlation length of 3 m and assigning the cells with 30% smallest

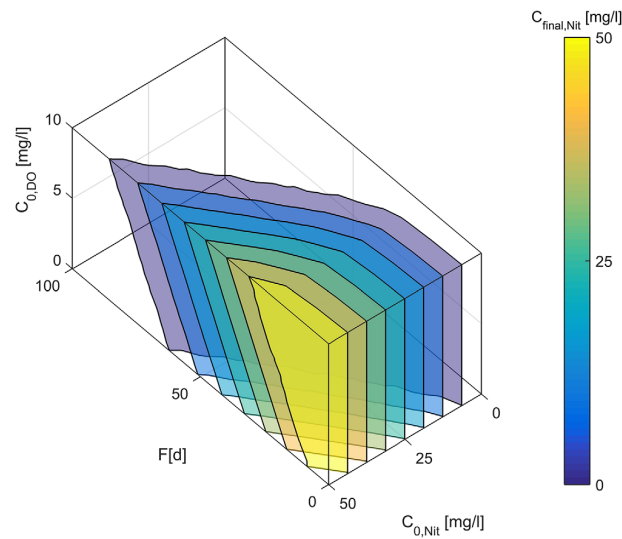


Figure 3. Isosurfaces of resulting nitrate concentration $C_{\text{final,Nit}}(C_{0,\text{Nit}}, F, C_{0,\text{DO}})$ as function of initial nitrate concentration $C_{0,\text{Nit}}$, cumulative relative reactivity F , and initial oxygen concentration $C_{0,\text{DO}}$.

values an indicator value of 1, and the remaining 70% an indicator value of 2. We then generated four independent multi-Gaussian fields with an isotropic exponential covariance function with correlation length of 1 m to fill up the two zones defined by the indicator variable with log-hydraulic conductivity and log-relative reactivity values. Zone 1 had a geometric mean of hydraulic conductivity of 10^{-4} m/s and a geometric mean of relative reactivity of 2, whereas the geometric means of hydraulic conductivity and relative reactivity in zone 2 were 10^{-3} m/s and 0.1, respectively. That is, on a larger scale log-hydraulic conductivity and log-relative reactivity are anti-correlated, whereas the local deviations are not correlated at all. The variance of $\ln(K)$ was 1.0 in both zones, and that of $\ln(f)$ was 0.25. Figure 4A

shows the log conductivity field, and Figure 4B the log-relative reactivity field for an arbitrarily chosen single realization.

For groundwater flow, the top and bottom boundaries were assigned no-flow boundaries, and the left and right boundaries were fixed-head boundaries. The head difference was chosen such that the mean linear velocity v was 1 m/d. Groundwater flow was solved by the finite element method with bilinear elements, written as a Matlab script. We also solved for stream function values, and generated streamline-oriented grids with 500×500 elements [Frind and Matanga, 1985; Cirpka et al., 1999a]. Figure 4C shows the resulting flow net. Steady state transport was solved on the streamline-oriented grids using the cell-centered finite volume method of Cirpka et al. [1999b] for spatial discretization. We computed the mean travel time distribution $\tau(\mathbf{x})$ by solving the mean groundwater-age equation [Goode, 1996] for strictly advective and advective-dispersive transport (longitudinal dispersivity $\alpha_L=0.01$ m, transverse dispersivity $\alpha_T=0.001$ m, pore diffusion coefficient $D_p=4 \times 10^{-10}$ m²/s). We also computed the mean cumulative relative reactivity μ_F according to equations (15) and (17) for strictly advective and advective-dispersive transport.

We simulated steady state reactive transport, using the reactive parameters of Table 1 and inflow concentrations of 40 mg/L for nitrate and 10 mg/L for dissolved oxygen, by three different methods. As virtual truth, we solved the spatially explicit advection-dispersion-reaction (equation (1)), for steady state conditions with a fully implicit approach using Newton-Raphson iterations. This is compared to the mapping approach of equation (12), in which reactive-species concentrations are uniquely defined by local cumulative-relative-reactivity values, according to equation (11) and Figure 2. We tested the method using F values both evaluated for strictly advective and advective-dispersive transport. To determine the accuracy of the two approximations, we analyzed the oxygen and nitrate concentrations in the outflow, normalized by the corresponding inflow concentrations. In particular, we computed the corresponding flux-weighted mean and standard deviation, the cumulative distribution function, and the root mean-square error of the normalized concentrations in the outflow. For a more robust comparison, 100 realizations of relative-reactivity and hydraulic-conductivity fields were generated, followed by flow and reactive transport simulations.

5.2. Travel Time and Cumulative Relative Reactivity

Figure 4D shows the computed mean groundwater age $\mu_{\tau, ADE}$ for advective-dispersive transport. The patterns of kinematic age, or advective travel time τ_{adv} are so similar that we decided to show the difference to $\mu_{\tau, ADE}$ in Figure 4E. Neglecting transverse dispersion leads to elongated stripes in the residuals. While in strictly advective transport spatial variation in hydraulic conductivity can cause very old water to flow side

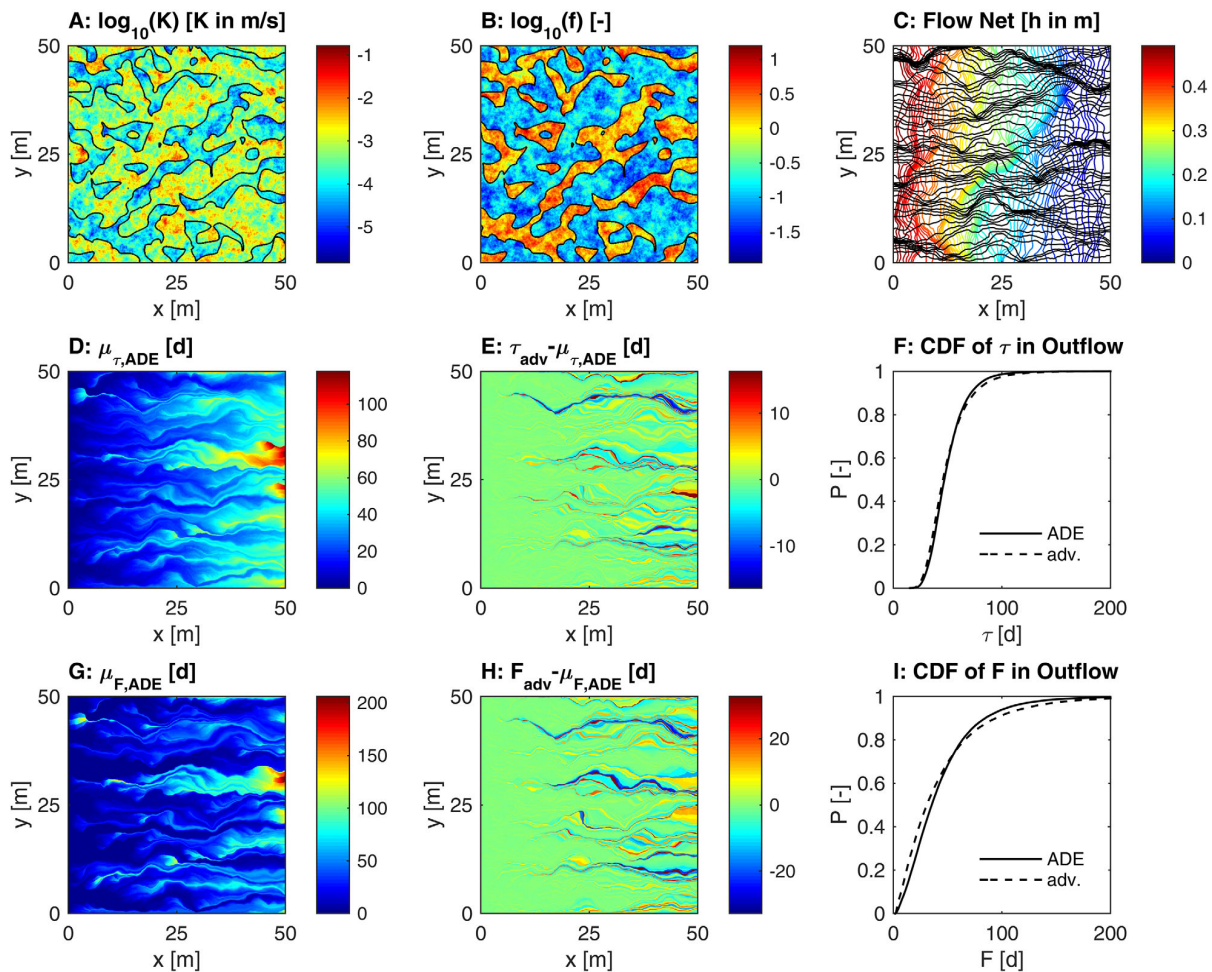


Figure 4. Two-dimensional test case. (A) Spatial distribution of the log-hydraulic conductivity; (B) spatial distribution of log-relative reactivity; (C) flow net (colored lines: heads; black lines: streamlines); (D) mean groundwater age for advective-dispersive transport; (E) difference between groundwater age for strictly advective transport and mean groundwater age of advective-dispersive transport; (F) cumulative distribution function of travel time in the outflow of the domain; (G) mean cumulative relative reactivity for advective-dispersive transport according to equation (17); (H) difference in the cumulative relative reactivity for strictly advective to advective-dispersive transport; (I): cumulative distribution function of cumulative relative reactivity in the outflow. Figures 4A–4E, 4G, and 4H are for a single realization; Figures 4F and 4I are averaged over 100 realizations.

by side to very young water, these differences are smoothed by transverse mixing in advective-dispersive transport. Differences between kinematic age and mean groundwater age have been discussed elsewhere [e.g., Varni and Carrera, 1998]. In particular, we want to note that stagnation points lead to lines or surfaces with infinite kinematic age downstream of the stagnation points, whereas dispersion leads to finite values of the mean groundwater age and a smooth distribution. Figure 4F shows the cumulative distribution functions (CDFs) of mean groundwater age and kinematic age in the outflow of the domain. The two curves are quite similar, with the strictly advective model exhibiting a somewhat stronger spread. That is, while there are local differences in travel time between the advective and the advective-dispersive cases, the statistical distribution is only minor influenced for the given strength of heterogeneity.

Figure 4G shows the mean cumulative relative reactivity $\mu_{F, ADE}$ for advective-dispersive transport according to equation (17) and Figure 4H shows the difference between the cumulative relative reactivity F_{adv} evaluated for strictly advective transport by solving equation (15) and $\mu_{F, ADE}$. Due to the anticorrelation between log conductivity and log-reactivity the spatial patterns of cumulative relative reactivity are more pronounced than the patterns of travel time. Again, neglecting transverse dispersion leads to elongated stripes of residual errors, and the CDFs of F in the outflow, shown in Figure 4I, indicate a minor enhancement of spread by restricting transport to advection only.

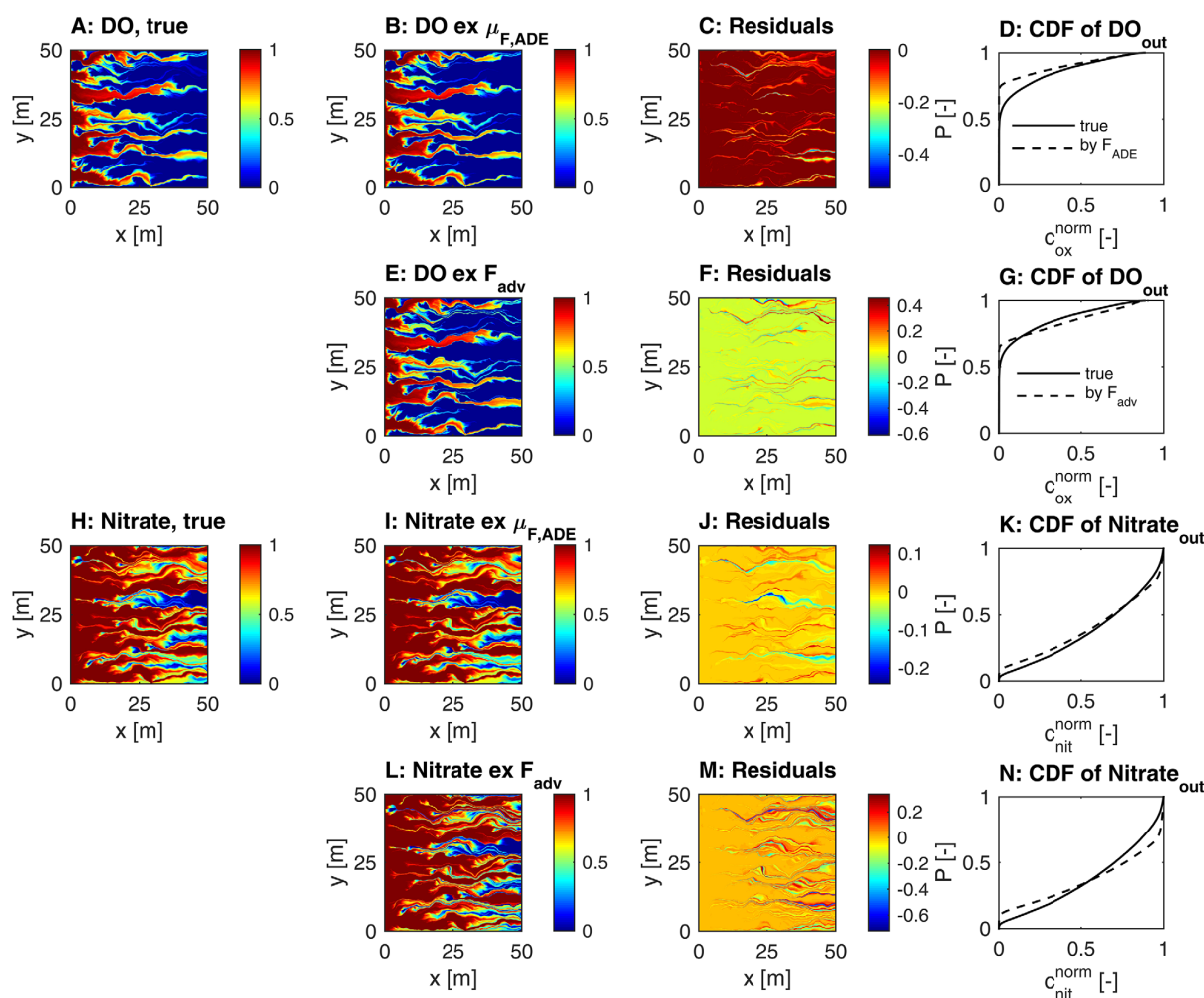


Figure 5. Comparison of the spatially explicit model results and the corresponding one-dimensional model results mapped on the 2-D domain. Left column: normalized concentrations of dissolved oxygen (DO) and nitrate obtained by the spatially explicit advective-dispersive-reactive model (true); second column: normalized concentrations of DO and nitrate computed by mapping the cumulative relative reactivity to dissolved oxygen and nitrate concentrations (“by $\mu_{F,ADE}$ ”: using the mean cumulative relative reactivity F for advective-dispersive transport, “by F_{adv} ”: using the cumulative relative reactivity F for strictly advective transport); third column: residual errors; right column: comparison of CDFs at the outflow (solid lines: virtual truth; dashed lines: approximations based on mapping F). The first three columns are for a single realization, the last one averaged over 100 realization.

5.3. Reactive-Species Concentrations

Figure 5 compares the concentrations computed by solving the 2-D spatially explicit advection-dispersion-reaction model (“true”) to the concentrations computed by mapping the cumulative relative reactivity to reactive-species concentrations. The virtually true concentration distributions of oxygen (Figure 5A) and nitrate (Figure 5H) are shown in the first column. The concentration distributions obtained by mapping the cumulative relative reactivity values shown in Figures 4G and 4H to reactive-species concentrations according to equation (12) are shown in the second column. The residual errors are shown in the third column, and the right column shows the CDFs of nitrate and dissolved oxygen concentrations in the outflow. All concentrations are normalized by the corresponding inflow concentrations.

As can be seen from Figures 5A, 5B, 5E and 5H, 5I, 5L, respectively, the spatial patterns of oxygen and nitrate concentrations hardly differ among the different approaches. The biggest residual errors occur along the elongated stripes where old and young water mix by transverse dispersion. This holds not only for the mapping approach for strictly advective transport (Figures 5F and 5M), but also for the mapping approach based on the mean cumulative relative reactivity of advective-dispersive transport (Figures 5C and 5J). This may be understood by the nonlinear dependence of oxygen and nitrate concentrations on the cumulative

Table 2. Metrics of Reactive-Solute Concentrations in the Outflow of the 2-D Test Case^a

	Mean Normalized Concentration		Normalized Standard Deviation of Concentration		Normalized Root Mean Square Error of Flux-Weighted Concentration	
	Oxygen	Nitrate	Oxygen	Nitrate	Oxygen	Nitrate
True	0.13	0.63	0.21	0.31		
By $\mu_{F, ADE}$	0.09	0.61	0.20	0.35	0.08	0.06
By F_{adv}	0.14	0.64	0.25	0.37	0.09	0.15

^a“True”: spatially explicit advective-dispersive-reactive model, “by $\mu_{F, ADE}$ ”: mapping approach based on mean cumulative relative reactivity F for advective-dispersive transport, “by F_{adv} ”: mapping approach based on cumulative relative reactivity F for strictly advective transport. Results are based on 100 realizations.

reactivity F illustrated in Figure 2: Mixing water with F values smaller and bigger than $\approx 2 \times 10^6$ s may lead to oxygen concentrations significantly larger than zero and nitrate concentrations significantly smaller than the inflow concentration, whereas looking up the corresponding concentration values for the mean F value of 2×10^6 s suggests that oxygen is practically gone and nitrate is still close to the inflow value. While the residual errors based on mapping the advective F values show a larger range, zones of over and underestimation seems to balance better than in the approach mapping the mean advective-dispersive F values.

Figures 5D and 5G show the CDFs of the normalized dissolved-oxygen concentration in the outflow, and Figures 5K and 5N show the CDFs of the normalized nitrate concentration. Differences in the CDFs, particularly a tendency to overestimate the occurrence of zero oxygen concentrations are apparent. Table 2 lists metrics of the normalized concentrations in the outflow. The mean concentrations are met actually better by the mapping approach neglecting mixing than by the one based on $\mu_{F, ADE}$. Standard deviations are somewhat overestimated by the advective mapping approach, and the normalized root mean square error is larger in the latter approach. Overall, however, we would assess the error introduced by neglecting (transverse) mixing as acceptable, at least for the case of diffuse contamination controlled by reactions with the aquifer matrix considered here. These findings are in agreement with results of previous analyses on using exposure time as proxy for reactive transport [Sanz-Prat et al., 2016a].

6. Three-Dimensional Test Case

We designed a relatively simple test case to demonstrate the efficiency of approximating reactive transport using the cumulative relative reactivity for strictly advective transport. The model domain represents an aquifer that is drained by a river. Land use patterns, initial concentrations and groundwater recharge are representative for agricultural landscapes in southwest Germany. In the following, we describe the conceptual model and the numerical implementation.

6.1. Conceptual Model

Figure 6A depicts the conceptual aquifer in plan view and Figure 6B in side view at the cross section $y = 750$ m (see cutting line in Figure 6A). The model domain is a cuboid with a length of 2.5 km, a width of 1.5 km, and a depth of 50 m. Three sides, as well as the bottom are assigned no-flow boundaries. On the remaining side, a constant head boundary representing a river, is set down to a depth of 20 m from the top, whereas the bottom 30 m are considered a no-flow boundary. The head of the river is 3 m below the model’s top elevation. An extraction well is located at $x_{well} = 1800$ m, $y_{well} = 750$ m and constantly pumps at a rate of 5 L/s.

At the top boundary of the model, we define the spatial distribution of recharge as well as the nitrate and oxygen concentrations in the recharge. We assume that the nitrate leaching into the groundwater has already passed the unsaturated zone. This implies that nitrate concentrations represent conditions in the infiltrating water below the root depth. In our model, groundwater recharge as well as the nitrate and oxygen concentrations in the inflow follow a static pattern. This pattern consists of three different types of land use, namely forest, agricultural land, and pasture. For illustration see Figure 6A. Table 3 shows the mean annual recharge rates, the mean nitrate and the mean oxygen concentrations in the recharge for the three different types of land use. Table 3 also includes standard deviations expressing the internal variability.

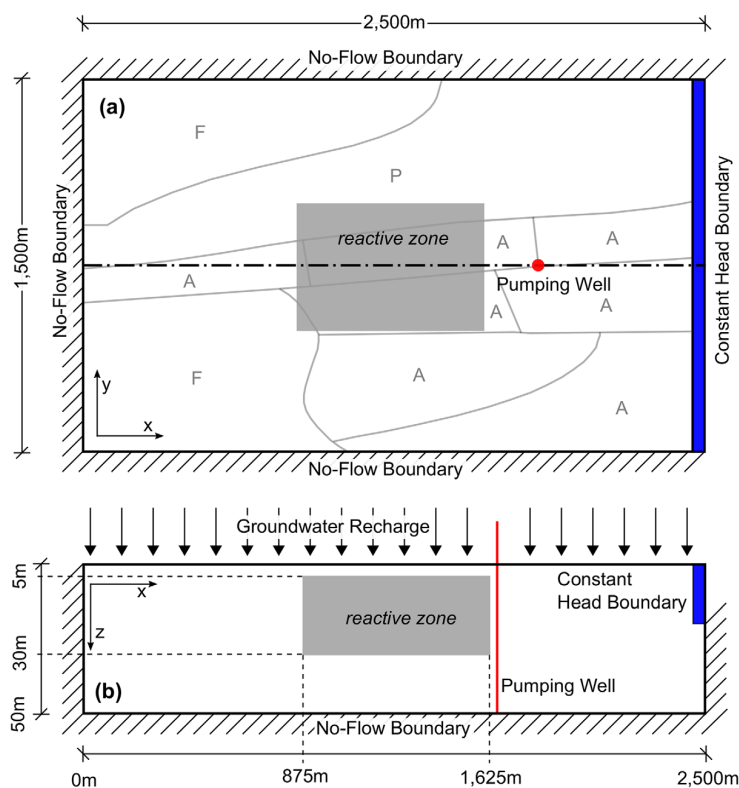


Figure 6. Schematic (a) plan view and (b) side view of the three-dimensional test domain. Three sides and the bottom are no-flow boundaries. Groundwater recharge is applied at the model top. A pumping well at $x_{well}=1800$ m, $y_{well}=750$ m and a constant head boundary at $x_{chb} \geq 2450$ m, -20 m $< z_{chb} < 0$ m are set. A reactive zone is set at 875 m $< x_{reac} < 1625$ m, 500 m $< y_{reac} < 1000$ m, 5 m $< z_{reac} < 30$ m. The static pattern of land use is displayed in light gray, with A = agriculture, F = forest, and P = pasture.

Spatial variability in recharge as well as nitrate and oxygen concentrations in the inflow is expressed as auto-correlated multi-Gaussian random space functions generated with the spectral method of *Dietrich and Newsam* [1993, 1997]. One independent multi-Gaussian field is generated for each type of land use and each variable (recharge, nitrate, and dissolved oxygen concentration in the infiltrating water). Table 4 lists geometric and geostatistical parameters. For dissolved oxygen, we account for a maximum concentration in the infiltrating water, set to 10.92 mg/L which is the saturation concentration of oxygen at 10 °C in equilibrium to the atmosphere.

As illustrated in Figure 6, the model contains a single reactive inclusion which is located in the center of the aquifer. The dimensions of the reactive zone are 750 m \times 500 m \times 25 m. Only in this reactive zone, aerobic respiration and denitrification take place. The inclusion may resemble a peat lens or carbonaceous limestone with a strong reduction potential. In the surrounding nonreactive zones the relative reactivity f is set to zero.

Table 3. Mean Annual Recharge and Concentrations of Nitrate and Oxygen Within Recharge for the Three Different Types of Land Use Used in the 3-D Test Case [Wu, 2014]

	Recharge (mm/a)	Mean \pm SD of Nitrate Concentration		Mean \pm SD Oxygen Concentration	
		(mg/L)	(μ mol/L)	(mg/L)	(μ mol/L)
Forest	250	5.0 \pm 1.5	81 \pm 24	8.0 \pm 2.0	250 \pm 62.5
Agriculture	275	45.0 \pm 10.0	726 \pm 161	10.0 \pm 2.0	313 \pm 62.5
Pasture	300	50.0 \pm 15.0	906 \pm 242	9.0 \pm 2.0	281 \pm 62.5

Table 4. Parameters of the Three-Dimensional Test Case

Symbol	Meaning	Value
<i>Geometric Parameters</i>		
$L \times W \times T$	Length \times width \times depth of domain	2500 m \times 1500 m \times 50 m
$n_x \times n_y \times n_z$	Number of cells in x , y , and z direction	500 \times 300 \times 10
<i>Hydraulic Parameters</i>		
K_{reac}	Hydraulic conductivity of reactive zone	1×10^{-3} m/s
$K_{\text{non-reac}}$	Hydraulic conductivity of nonreactive zone	1×10^{-4} m/s
<i>Geostatistical Parameters</i>		
λ_{NO_3}	Correlation length for nitrate concentration in recharge	250 m
λ_{O_2}	Correlation length for oxygen concentration in recharge	250 m
λ_R	Correlation length for recharge	500 m
λ_f	Correlation lengths for relative reactivity ($x \times y \times z$)	500 m \times 500 m \times 25 m
<i>Transport Parameters</i>		
θ	Porosity	0.35

A three-dimensional, blockwise stationary multi-Gaussian random field with mean 1, variance 0.25, correlation lengths of 500 m \times 500 m \times 25 m, and integral scales of 760 m \times 500 m \times 25 m in the x -, y -, and z -direction, following a Gaussian covariance function was generated to obtain the values for log-relative reactivity within the inclusion. This ensures that values for the relative reactivity are nonnegative and spatially correlated. The realization of the reactive zone for this study is shown in detail in Figure 7C. Isolines of relative reactivity show the changing relative reactivity throughout the reactive zone. In the upper left corner of the domain, f reaches values of up to three. The values of f decrease in the x direction. The reactive and nonreactive zones also differ in hydraulic conductivity (see Table 4). For better visualization and comprehensibility of the results, hydraulic conductivity is set uniform within the reactive and nonreactive zones.

6.2. Implementation and Numerical Methods

The model domain is discretized in 5 m \times 5 m \times 5 m grid cells resulting in 1.5 million cells in total. The modeling framework is implemented in Matlab. Groundwater flow is calculated using MODFLOW-NWT [Niswonger et al., 2011]. Particle tracking is done within Matlab using Pollock's semianalytical method [Pollock, 1988], performing the calculations on the graphics processing unit. The solution of the ordinary differential equations has already been described in section 4. Matlab is also used for the generation of the auto-correlated random fields.

After the calculation of the velocity field, we tracked particles to obtain values of travel time and cumulative relative reactivity. We obtained full spatial coverage of travel time, origin, and cumulative relative reactivity by backward particle tracking. The algebraic sign of the velocity field was reversed, and particles were placed in the center of every cell of the domain, resulting in a total of 1.5 million particle tracks. All particles ended at the top inflow boundary (outflow for reverse particle tracking), resulting in travel times τ , cumulative relative reactivity values F , and locations of origin \mathbf{x}_0 in each cell of the domain. In addition, we show a single particle track obtained by forward tracking, starting at the land surface and ending in the extraction well.

6.3. Results

6.3.1. Hydraulic Head

Figure 7A shows isosurfaces of hydraulic head computed by MODFLOW-NWT and a single representative particle trajectory. For better visualization, the figure is cut at $y_m = 750$ m. The black vertical line at $[x_{\text{well}}, y_{\text{well}}] = [1800 \text{ m}; 750 \text{ m}]$ marks the extraction well. The brown line illustrates a single particle trajectory. The transparent gray box represents the reactive zone. The marked particle enters the domain at $[x_{\text{start}}, y_{\text{start}}, z_{\text{start}}] = [147.5 \text{ m}, 852.5 \text{ m}, 0 \text{ m}]$. It passes the reactive zone and finally ends in the pumping well at $[x_{\text{end}}, y_{\text{end}}, z_{\text{end}}] = [1800 \text{ m}, 755.7 \text{ m}, 39.51 \text{ m}]$. The influence of the hydraulic-conductivity anomaly in the reactive zone and of the extraction well on the head distribution and the velocity field can clearly be seen: The head isosurfaces are bent under the influence of the lens of higher hydraulic conductivity and the depression cone of the well.

6.3.2. Travel Time

Figure 7B shows isosurfaces of the total travel times for the same test case. Like in Figure 7A, the model domain is intersected at $y_m = 750$ m, the extraction well is shown as a black line, and the same particle

trajectory as in Figure 7A is plotted as red line. The main flow direction is from the top of the model domain to the right. Therefore the travel time increases with depth and is higher at the right end of the domain. Particles either end in the well or at the constant head boundary. The disturbance of the travel time isochrones at $x_{well}=1800$ m is due to the extraction well at this location. In the higher conductivity lens, particles are accelerated, leading to larger distances between the isochrones. At the lower right edge, the velocity is zero, implying infinite groundwater age along the right face underneath the outflow face. This is not resolved by the model because travel times are computed at cell centers.

Stagnation points observed in the model can be neglected as all of them were outside the reactive zone. Thus, the large changes in travel time had no impact on the cumulative relative reactivity and reactive transport. To overcome this problem in future applications, multiple particles per cell may be introduced. However, this goes beyond the scope of the current study.

6.3.3. Cumulative Relative Reactivity

Figure 7D shows isosurfaces of cumulative relative reactivity for the same realization used in the Figures 7A and 7B. The cumulative relative reactivity is zero for all positions $x < 875$ m because here the aquifer is defined as nonreactive ($f=0$), and flow is in the positive x direction. The cumulative relative reactivity increases within the reactive zone. In the upstream part of the reactive zone, the relative reactivity is comparatively high, leading to a fast increase in cumulative relative reactivity with distance (see also Figure 7C). In the downstream part of the reactive zone, where relative reactivities are rather low, cumulative relative reactivities are increasing less with distance. This trend is enhanced by the increasing influence of the extraction well, causing higher velocities at the right end of the reactive zone and therefore shorter travel times. After passing the reactive zone ($x_{reac,2}=1625$ m) the cumulative relative reactivity remains constant along each trajectory.

For further illustration, Figure 8 shows four different length profiles along the single particle trajectory selected in Figure 7. The four panels of Figure 8 depict: A: the total travel time τ ; B: the local relative

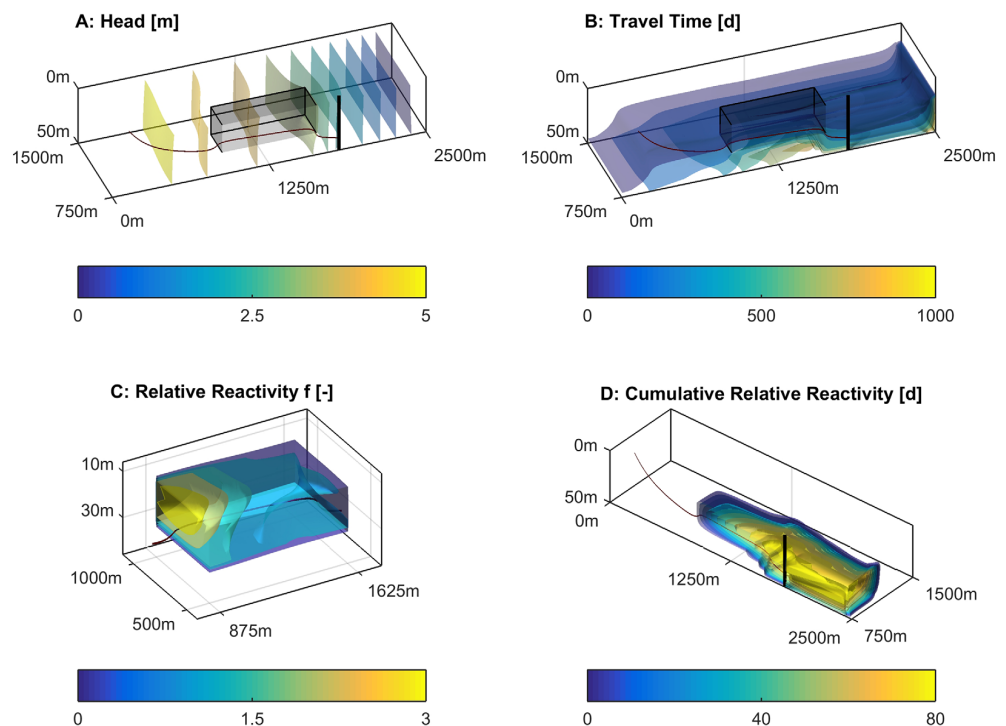


Figure 7. Flow and (cumulative) relative reactivity in the 3-D test case. (A) Isosurfaces of hydraulic head resulting from reverse particle tracking. (B) Isosurfaces of travel time (isochrones) resulting from reverse particle tracking. (C) Isosurfaces of relative reactivity in the reactive zone of the conceptual model presented in Figure 6. (D) Isosurfaces of cumulative relative reactivity (F) resulting from reverse particle tracking. Note that Figures 7A, 7B, and 7D are cut at $y_m = 750$ m. Brown line in all plots: individual particle trajectory. Black line in Figures 7A, 7B, and 7D: extraction well. Gray box in Figures 7A and 7B: reactive zone.

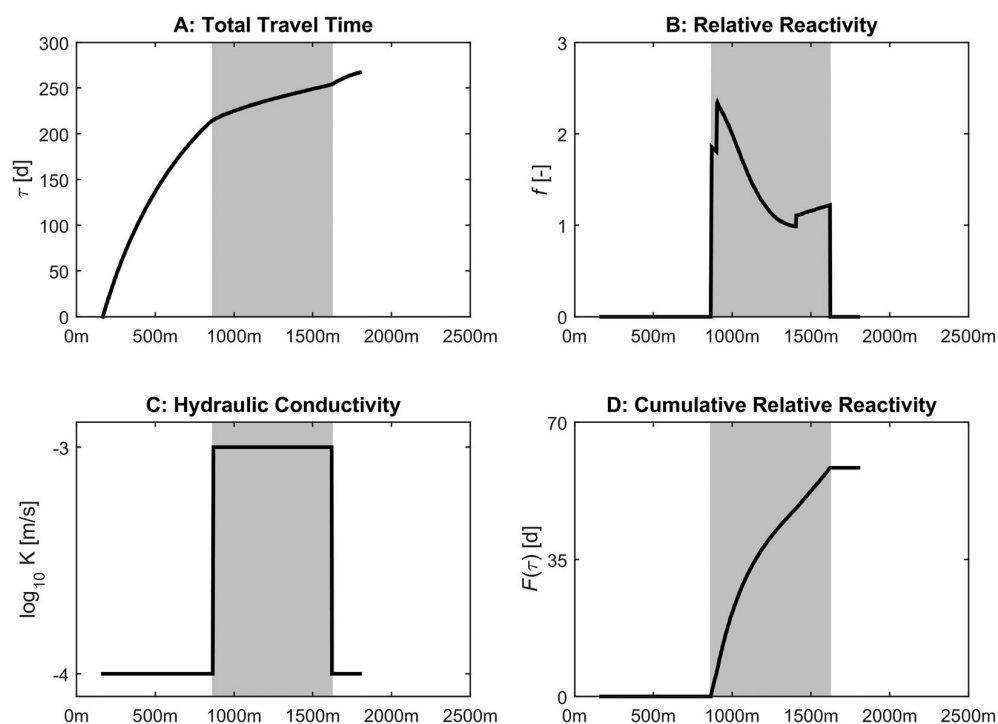


Figure 8. Length profiles along the individual particle trajectory marked in Figure 7. (A) Total travel time τ as function of distance. (B) Relative reactivity f as function of distance. (C) Hydraulic conductivity k_f as function of distance. (D) Cumulative relative reactivity F as function of the x coordinate. Shaded area in all plots: reactive zone ($f > 0$).

reactivity f ; C: the local hydraulic conductivity K ; and D: the cumulative relative reactivity F . All plots are shown as function of distance covered in x direction, which is not the actual travel distance of the particle. The shaded area between $x_{\text{reac},1} = 875$ m and $x_{\text{reac},2} = 1,625$ m illustrates the reactive zone. The influence of hydraulic conductivity K on the travel time τ can be seen in subplots A and C. Once entering the zone of higher hydraulic conductivity, particles speed up, resulting in a smaller slope of total travel time A. The change of relative reactivity can be seen in Figure 8B. The particle enters the reactive zone on the left side where the relative reactivity reaches a value of up to 2.5. While traveling through the reactive zone, the relative reactivity experienced by the particle decreases to values of approximately 1.1. Before and after the reactive zone, the particle travels through a nonreactive zone and the relative reactivity is zero.

Figure 8D shows the cumulative relative reactivity along the trajectory of the particle. After reaching the reactive zone, the cumulative relative reactivity increases fast due to the high value of relative reactivity. When the relative reactivity decreases, the slope of cumulative relative reactivity also decreases. After leaving the reactive zone, the cumulative relative reactivity stays constant.

6.3.4. Reactive Transport

For each location of the domain, particle tracking has led to unique values of travel time $\tau(\mathbf{x})$, cumulative relative reactivity $F(\mathbf{x})$, and origin $\mathbf{x}_0(\mathbf{x})$. The origin and travel time yields the concentrations of the reactive species in the infiltrating water, whereas the cumulative relative reactivity yields the progress in reducing the electron acceptors. With the mapping procedure of equation (12), we could transfer the reactive-species concentrations obtained from solving the ODE system of equation (11) to the spatial distribution of reactive-species concentrations. As outlined in section 4, we have performed 1000 ODE calculations to cover a wide range of inflow values and cumulative relative reactivities. From these 1000 ODE runs, we could determine the nitrate and oxygen concentration at all points (in our case 1.5 million cell centers) by interpolation in the $c_{0,\text{Nit}}$, F , and $c_{0,\text{DO}}$ dimensions. Figures 9A and 9C shows the resulting spatial concentration distributions of nitrate and oxygen for the case presented in Figure 6 and the initial concentration inputs from Table 3. The influence of the reactive zone can be seen. The concentrations of nitrate and oxygen decrease

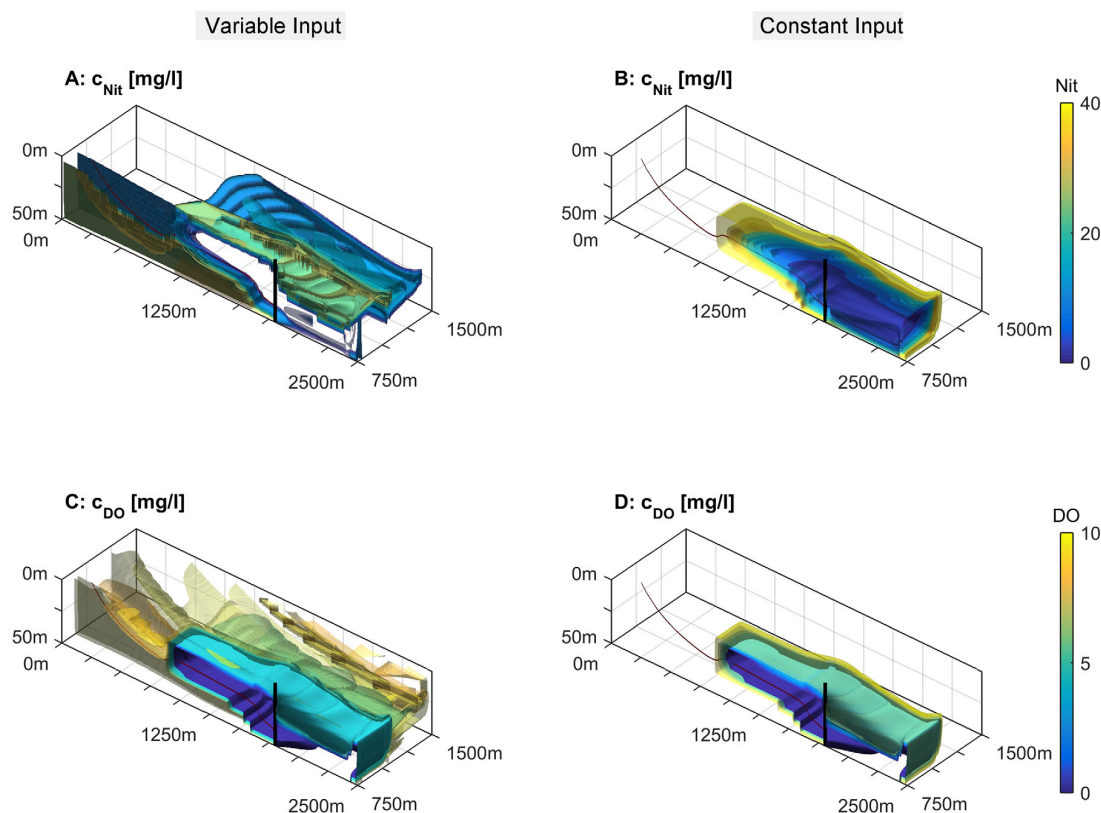


Figure 9. Steady state concentration distribution of nitrate and dissolved oxygen isosurfaces according to the proposed mapping procedure applied to the 3-D test case. (A, B) Nitrate and oxygen concentrations for variable input at the land surface (see Figure 6 and Table 3). (C, D) Nitrate and oxygen concentrations for uniform input at the land surface (nitrate: 40 mg/L; oxygen: 10 mg/L). Black line: extraction well. Brown line: individual particle trajectory.

significantly while passing the reactive zone. Among other features, Figure 9 shows the effect that denitrification is inhibited at elevated oxygen levels. As long as oxygen is present in the system (Figure 9C), nitrate concentrations stay comparatively high. Only when all oxygen is consumed, the denitrification process starts and nitrate is degraded. For a better understandability and ease of visualization Figures 9B and 9D show the steady state concentrations for a uniform inflow concentration of oxygen (10 mg/L) and nitrate (40 mg/L). Here the inhibition of denitrification at elevated oxygen levels can be seen more clearly.

7. Discussion and Conclusions

The concept of relative reactivity allows efficiently solving reactive transport in large-scale applications. With the simplified approach of solving reactive solute transport along a trajectory and the introduction of the concept of relative reactivity, nonlinear reactive transport calculations on aquifer scales are computationally inexpensive (12 min clock time for the given three-dimensional problem, computed on a standard PC with an NVIDIA graphics card). The proposed framework differs from approaches in which reactive transport is restricted to first-order degradation. In particular, we account for inhibition of denitrification by the presence of dissolved oxygen, which we consider a major control in denitrification. The framework can be applied to reactive transport in groundwater using computational domains with a large number of computational cells, and is not restricted to simple model geometries.

We have shown the validity of the proposed approach by comparing a spatially explicit advective-dispersive-reactive transport model in a heterogeneous 2-D domain to the results obtained by mapping reactive-species concentrations based on local values of the cumulative relative reactivity. The results showed an excellent match of the mean reactive-species concentrations in the outflow, a good match in

the standard deviation, and some deviations in the full CDF. The predictive capabilities are higher for the estimation of the reactive-species mass flux integrated over a control plane or by a well than for values at true point observations. Evaluating the mean cumulative relative reactivity for advective-dispersive transport rather than for strictly advective transport does not really pay off. In the case of mild heterogeneity and second-order stationary velocity fields, stochastic-analytical solutions for the cumulative relative reactivity exist [Cvetkovic *et al.*, 1998], even though named differently in the original study. However, we doubt that these analytical expressions are suitable in practicable applications, mainly because the underlying assumptions are fairly restrictive.

The presented simple three-dimensional test case was chosen to explain the concept of relative reactivity in a comprehensive way. Boundary conditions, such as groundwater recharge and the concentrations in the inflow, can be addressed independently. To account for uncertainty and variability of the model parameters (hydraulic conductivity, recharge, initial concentrations) random realizations of the parameter fields can easily be implemented. Statistics for those can be obtained from measurements or already available data. Moreover, the model can be conditioned at measurement locations, reducing the variability and uncertainty of the parameter fields. The distribution of reactive zones as well as the assignment of values for relative reactivities can also be conducted by a stochastic approach. The transfer of the model concept to a real catchment is possible but beyond the scope of the current demonstration study. While the flow field in the given application was at steady state, transient runs are also possible as travel time and cumulative relative reactivity are computed by integration along particle trajectories which can be computed also in transient flow.

For practical applications, we see the biggest difficulties in assigning a representative distribution of reactive zones and especially in attributing values for relative reactivities to those zones. The spatial distribution of reactive zones in an aquifer is not trivial, because in many formations the internal structure of the facies is not or only poorly known. A clear distinction between reactive and nonreactive zones is challenging, but not actually needed as the relative reactivity can take any nonnegative value. Further research and field investigations are necessary to obtain justifiable statistics for relative reactivities. We want to emphasize, however, that fully explicit, 3-D reactive transport models suffer from similar data requirements. In contrast to these methods, our approach allows explicitly addressing this uncertainty, because it makes catchment-scale reactive transport computationally so inexpensive that it becomes accessible for stochastic ensemble runs.

Finally, we assumed in the present study that values of relative reactivity remain constant in time. In natural aquifers, however, a consumption of electron donors over time is observed, thus decreasing the reaction potential. Further research on how to account for this process without returning to a fully explicit description is necessary.

Acknowledgments

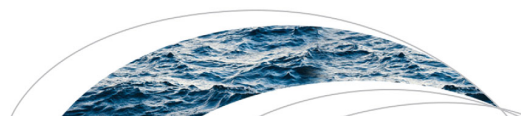
This research was funded by the Deutsche Forschungsgemeinschaft (DFG) in the framework of the International Research Training Group GRK1829 "Integrated Hydrosystem Modeling" of the Universities of Tübingen, Hohenheim, and Waterloo. The authors would like to thank three anonymous reviewers for their meaningful comments helping to improve the paper. The simulation results of the two test cases are available from the first author (matthias.loschko@uni-tuebingen.de) and the corresponding author (olaf.cirpka@uni-tuebingen.de) upon request.

References

- Atchley, A. L., R. M. Maxwell, and A. K. Navarre-Sitchler (2013), Using streamlines to simulate stochastic reactive transport in heterogeneous aquifers: Kinetic metal release and transport in CO₂ impacted drinking water aquifers, *Adv. Water Resour.*, *52*, 93–106, doi:10.1016/j.advwatres.2012.09.005.
- Atchley, A. L., A. K. Navarre-Sitchler, and R. M. Maxwell (2014), The effects of physical and geochemical heterogeneities on hydro-geochemical transport and effective reaction rates, *J. Contam. Hydrol.*, *165*, 53–64, doi:10.1016/j.jconhyd.2014.07.008.
- Basu, N. B., et al. (2010), Nutrient loads exported from managed catchments reveal emergent biogeochemical stationarity, *Geophys. Res. Lett.*, *37*, L23404, doi:10.1029/2010GL045168.
- Betlach, M. R., and J. M. Tiedje (1981), Kinetic explanation for accumulation of nitrite, nitric oxide, and nitrous oxide during bacterial denitrification, *Appl. Environ. Microbiol.*, *42*(6), 1074–1084.
- Botter, G., E. Bertuzzo, and A. Rinaldo (2010), Transport in the hydrologic response: Travel time distributions, soil moisture dynamics, and the old water paradox, *Water Resour. Res.*, *46*, W03514, doi:10.1029/2009WR008371.
- Carrera, J. (1993), An overview of uncertainties in modelling groundwater solute transport, *J. Contam. Hydrol.*, *13*(1), 23–48, doi:10.1016/0169-7722(93)90049-X.
- Chan, Y. K., and N. E. R. Campbell (1980), Denitrification in lake 227 during summer stratification, *Can. J. Fish. Aquat. Sci.*, *37*(3), 506–512, doi:10.1139/f80-065.
- Cirpka, O. A., and P. K. Kitaniadis (2000), An advective-dispersive stream tube approach for the transfer of conservative-tracer data to reactive transport, *Water Resour. Res.*, *36*(5), 1209–1220, doi:10.1029/1999WR900355.
- Cirpka, O. A., and A. J. Valocchi (2007), Two-dimensional concentration distribution for mixing-controlled bioreactive transport in steady state, *Adv. Water Resour.*, *30*(6–7), 1668–1679, doi:10.1016/j.advwatres.2006.05.022.
- Cirpka, O. A., E. O. Frind, and R. Helmig (1999a), Streamline-oriented grid-generation for transport modelling in two-dimensional domains including wells, *Adv. Water Resour.*, *22*(7), 697–710, doi:10.1016/S0309-1708(98)00050-5.

- Cirpka, O. A., R. Helmig, and E. O. Frind (1999b), Numerical methods for reactive transport on rectangular and streamline-oriented grids, *Adv. Water Resour.*, 22(7), 711–728, doi:10.1016/S0309-1708(98)00051-7.
- Cirpka, O. A., M. Rolle, G. Chiogna, F. P. J. de Barros, and W. Nowak (2012), Stochastic evaluation of mixing-controlled steady-state plume lengths in two-dimensional heterogeneous domains, *J. Contam. Hydrol.*, 138–139, 22–39, doi:10.1016/j.jconhyd.2012.05.007.
- Cvetkovic, V., and G. Dagan (1994), Transport of kinetically sorbing solute by steady random velocity in heterogeneous porous formations, *J. Fluid Mech.*, 265, 189–215, doi:10.1017/S0022112094000807.
- Cvetkovic, V., H. Cheng, and X.-H. Wen (1996), Analysis of nonlinear effects on tracer migration in heterogeneous aquifers using Lagrangian travel time statistics, *Water Resour. Res.*, 32(6), 1671–1680, doi:10.1029/96WR00278.
- Cvetkovic, V., G. Dagan, and H. Cheng (1998), Contaminant transport in aquifers with spatially variable hydraulic and sorption properties, *Proc. R. Soc. London, Ser. A*, 454(1976), 2173–2207, doi:10.1098/rspa.1998.0254.
- Dagan, G. (2002), An overview of stochastic modeling of groundwater flow and transport: From theory to applications, *EOS Trans. AGU*, 83(53), 621–625, doi:10.1029/2002EO000421.
- Dagan, G., and V. Cvetkovic (1996), Reactive transport and immiscible flow in geological media. i. General theory, *Proc. R. Soc. London, Ser. A*, 452(1945), 285–301, doi:10.1098/rspa.1996.0016.
- Dagan, G., and V. Nguyen (1989), A comparison of travel time and concentration approaches to modeling transport by groundwater, *J. Contam. Hydrol.*, 4(1), 79–91, doi:10.1016/0169-7722(89)90027-2.
- de Anna, P., M. Dentz, A. Tartakovsky, and T. Le Borgne (2014), The filamentary structure of mixing fronts and its control on reaction kinetics in porous media flows, *Geophys. Res. Lett.*, 41(13), 4586–4593, doi:10.1002/2014GL060068.
- Destouni, G., K. Persson, C. Prieto, and J. Jarsjö (2010), General quantification of catchment-scale nutrient and pollutant transport through the subsurface to surface and coastal waters, *Environ. Sci. Technol.*, 44(6), 2048–2055, doi:10.1021/es902338y.
- Diem, S., O. A. Cirpka, and M. Schirmer (2013), Modeling the dynamics of oxygen consumption upon riverbank filtration by a stochastic-convective approach, *J. Hydrol.*, 505, 352–363, doi:10.1016/j.jhydrol.2013.10.015.
- Dietrich, C. R., and G. N. Newsam (1993), A fast and exact method for multidimensional Gaussian stochastic simulations, *Water Resour. Res.*, 29(8), 2861–2869, doi:10.1029/93WR01070.
- Dietrich, C. R., and G. N. Newsam (1997), Fast and exact simulation of stationary Gaussian processes through circulant embedding of the covariance matrix, *SIAM J. Sci. Comput.*, 18(4), 1088–1107, doi:10.1137/S1064827592240555.
- Feyen, J., D. Jacques, A. Timmerman, and J. Vanderborght (1998), Modelling water flow and solute transport in heterogeneous soils: A review of recent approaches, *J. Agric. Eng. Res.*, 70(3), 231–256, doi:10.1006/jaer.1998.0272.
- Frei, S., and S. Peiffer (2016), Exposure times rather than residence times control redox transformation efficiencies in riparian wetlands, *J. Hydrol.*, doi:10.1016/j.jhydrol.2016.02.001, in press.
- Frind, E. O., and G. B. Matanga (1985), The dual formulation of flow for contaminant transport modeling: 1. Review of theory and accuracy aspects, *Water Resour. Res.*, 21(2), 159–169, doi:10.1029/WR021i002p00159.
- Ganapathysubramanian, B., and N. Zabarar (2007), Sparse grid collocation schemes for stochastic natural convection problems, *J. Comput. Phys.*, 225(1), 652–685, doi:10.1016/j.jcp.2006.12.014.
- Ginn, T. R. (1999), On the distribution of multicomponent mixtures over generalized exposure time in subsurface flow and reactive transport: Foundations, and formulations for groundwater age, chemical heterogeneity, and biodegradation, *Water Resour. Res.*, 35(5), 1395–1407, doi:10.1029/1999WR900013.
- Ginn, T. R. (2002), A travel time approach to exclusion on transport in porous media, *Water Resour. Res.*, 38(4), 1041, doi:10.1029/2001WR000865.
- Ginn, T. R., C. S. Simmons, and B. D. Wood (1995), Stochastic-convective transport with nonlinear reaction: Biodegradation with microbial growth, *Water Resour. Res.*, 31(11), 2689–2700, doi:10.1029/95WR02179.
- Gong, R., et al. (2011), Estimating reaction rate coefficients within a travel-time modeling framework, *Groundwater*, 49(2), 209–218, doi:10.1111/j.1745-6584.2010.00683.x.
- Goode, D. J. (1996), Direct simulation of groundwater age, *Water Resour. Res.*, 32(2), 289–296, doi:10.1029/95WR03401.
- Guadagnini, A., and S. P. Neuman (1999), Nonlocal and localized analyses of conditional mean steady state flow in bounded, randomly nonuniform domains: 1. Theory and computational approach, *Water Resour. Res.*, 35(10), 2999–3018, doi:10.1029/1999WR900160.
- Jury, W. A. (1982), Simulation of solute transport using a transfer function model, *Water Resour. Res.*, 18(2), 363–368, doi:10.1029/WR018i002p00363.
- Kaluvarachchi, J. J., V. Cvetkovic, and S. Berglund (2000), Stochastic analysis of oxygen- and nitrate-based biodegradation of hydrocarbons in aquifers, *J. Contam. Hydrol.*, 41(3), 335–365, doi:10.1016/S0169-7722(99)00072-8.
- Korom, S. F. (1992), Natural denitrification in the saturated zone: A review, *Water Resour. Res.*, 28(6), 1657–1668, doi:10.1029/92WR00252.
- Le Borgne, T., T. R. Ginn, and M. Dentz (2014), Impact of fluid deformation on mixing-induced chemical reactions in heterogeneous flows, *Geophys. Res. Lett.*, 41(22), 7898–7906, doi:10.1002/2014GL062038.
- Lohse, K. A., P. D. Brooks, J. C. McIntosh, T. Meixner, and T. E. Huxman (2009), Interactions between biogeochemistry and hydrologic systems, *Ann. Rev. Environ. Resour.*, 34, 65–96, doi:10.1146/annurev.enviro.33.031207.111141.
- Luo, J. (2012), Travel-time based reactive transport modeling for in situ subsurface reactor, in *Delivery and Mixing in the Subsurface*, pp. 117–138, Springer, N. Y.
- Luo, J., and O. A. Cirpka (2011), How well do mean breakthrough curves predict mixing-controlled reactive transport?, *Water Resour. Res.*, 47, W02520, doi:10.1029/2010WR009461.
- Malmström, M. E., G. Destouni, and P. Martinet (2004), Modeling expected solute concentration in randomly heterogeneous flow systems with multicomponent reactions, *Environ. Sci. Technol.*, 38(9), 2673–2679, doi:10.1021/es030029d.
- Mayer, K. U., E. O. Frind, and D. W. Blowes (2002), Multicomponent reactive transport modeling in variably saturated porous media using a generalized formulation for kinetically controlled reactions, *Water Resour. Res.*, 38(9), 1174, doi:10.1029/2001WR000862.
- Mellage, A., D. Eckert, M. Grösbacher, A. Z. Inan, O. A. Cirpka, and C. Griebler (2015), Dynamics of suspended and attached aerobic toluene degraders in small-scale flow-through sediment systems under growth and starvation conditions, *Environ. Sci. Technol.*, 49(12), 7161–7169, doi:10.1021/es5058538.
- Molz, F. J., M. A. Widdowson, and L. D. Benefield (1986), Simulation of microbial growth dynamics coupled to nutrient and oxygen transport in porous media, *Water Resour. Res.*, 22(8), 1207–1216, doi:10.1029/WR022i008p01207.
- Neuman, S. P., and S. Orr (1993), Prediction of steady state flow in nonuniform geologic media by conditional moments: Exact nonlocal formulation, effective conductivities and weak approximation, *Water Resour. Res.*, 29(2), 341–364, doi:10.1029/92WR02062.
- Niswonger, R. G., S. Panday, and M. Ibaraki (2011), MODFLOW NWT, a newton formulation for MODFLOW-2005, *U.S. Geol. Surv. Tech. Methods*, 6-A37, 44 p.

- Nobile, F., R. Tempone, and C. G. Webster (2008), A sparse grid stochastic collocation method for partial differential equations with random input data, *SIAM J. Numer. Anal.*, *46*(5), 2309–2345, doi:10.1137/060663660.
- Ocampo, C. J., C. E. Oldham, and M. Sivapalan (2006), Nitrate attenuation in agricultural catchments: Shifting balances between transport and reaction, *Water Resour. Res.*, *42*, W01408, doi:10.1029/2004WR003773.
- Payne, W. J. (1973), Reduction of nitrogenous oxides by microorganisms, *Bacteriol. Rev.*, *37*(4), 409–452.
- Payne, W. J., and P. S. Riley (1969), Suppression by nitrate of enzymatic reduction of nitric oxide, *Exp. Biol. Med.*, *132*(1), 258–260, doi:10.3181/00379727-132-34192.
- Payne, W. J., P. S. Riley, and C. D. Cox (1971), Separate nitrite, nitric oxide, and nitrous oxide reducing fractions from pseudomonas perfectomarinus, *J. Bacteriol.*, *106*(2), 356–361.
- Pechlivanidis, I. G., B. M. Jackson, N. R. McIntyre, and H. S. Wheatler (2011), Catchment scale hydrological modelling: A review of model types, calibration approaches and uncertainty analysis methods in the context of recent developments in technology and applications, *Global NEST J.*, *13*(3), 193–214.
- Pollock, D. W. (1988), Semianalytical computation of path lines for finite-difference models, *Groundwater*, *26*(6), 743–750, doi:10.1111/j.1745-6584.1988.tb00425.x.
- Prommer, H., D. A. Barry, W. H. Chiang, and C. Zheng (2001), PHT3D—A MODFLOW-MT3DMS-based reactive multicomponent transport model, in *MODFLOW 2001 and Other Modeling Odysseys*, pp. 477–483, International Groundwater Modeling Center, Colorado School of Mines, Golden, Colo.
- Reddy, K. R., P. S. C. Rao, and R. E. Jessup (1982), The effect of carbon mineralization on denitrification kinetics in mineral and organic soils, *Soil Sci. Soc. Am. J.*, *46*(1), 62–68, doi:10.2136/sssaj1982.03615995004600010011x.
- Refsgaard, J. C., et al. (2014), Nitrate reduction in geologically heterogeneous catchments—A framework for assessing the scale of predictive capability of hydrological models, *Sci. Total Environ.*, *468*, 1278–1288, doi:10.1016/j.scitotenv.2013.07.042.
- Reich, P. B., B. A. Hungate, and Y. Luo, Carbon-nitrogen interactions in terrestrial ecosystems in response to rising atmospheric carbon dioxide (2006), *Ann. Rev. Ecol. Syst.*, *37*, 611–636, doi:10.1146/annurev.ecolsys.37.091305.11003.
- Rinaldo, A., and A. Marani (1987), Basin scale model of solute transport, *Water Resour. Res.*, *23*(11), 2107–2118, doi:10.1029/WR023i011p02107.
- Rinaldo, A., G. Botter, E. Bertuzzo, A. Uccelli, T. Settin, and M. Marani (2006), Transport at basin scales: 1. Theoretical framework, *Hydrol. Earth Syst. Sci.*, *10*(1), 19–29, doi:10.5194/hess-10-19-2006.
- Rubin, Y., M. A. Cushey, and A. Bellin (1994), Modeling of transport in groundwater for environmental risk assessment, *Stochastic Hydrol. Hydraul.*, *8*(1), 57–77, doi:10.1007/BF01581390.
- Sanz-Prat, A., C. Lu, M. Finkel, and O. A. Cirpka (2015), On the validity of travel-time based nonlinear bioreactive transport models in steady-state flow, *J. Contam. Hydrol.*, *175*, 26–43, doi:10.1016/j.jconhyd.2015.02.003.
- Sanz-Prat, A., C. Lu, R. T. Amos, M. Finkel, D. W. Blowes, and O. A. Cirpka (2016a), Exposure-time based modeling of nonlinear reactive transport in porous media subject to physical and geochemical heterogeneity, *J. Contam. Hydrol.*, *192*, 35–49, doi:10.1016/j.jconhyd.2016.06.002.
- Sanz-Prat, A., C. Lu, M. Finkel, and O. A. Cirpka (2016b), Using travel times to simulate multi-dimensional bioreactive transport in time-periodic flows, *J. Contam. Hydrol.*, *187*, 1–17, doi:10.1016/j.jconhyd.2016.01.005.
- Schäfer, W., and R. Therrien (1995), Simulating transport and removal of xylene during remediation of a sandy aquifer, *J. Contam. Hydrol.*, *19*(3), 205–236, doi:10.1016/0169-7722(95)00018-Q.
- Seeboonruang, U., and T. R. Ginn (2006), Upscaling heterogeneity in aquifer reactivity via exposure-time concept: Forward model, *J. Contam. Hydrol.*, *84*(3), 127–154, doi:10.1016/j.jconhyd.2005.12.011.
- Shampine, L. F., and M. W. Reichelt (1997), The matlab ode suite, *SIAM J. Sci. Comput.*, *18*(1), 1–22, doi:10.1137/S1064827594276424.
- Shapiro, A. M., and V. D. Cvetkovic (1988), Stochastic analysis of solute arrival time in heterogeneous porous media, *Water Resour. Res.*, *24*(10), 1711–1718, doi:10.1029/WR024i010p01711.
- Simmons, C. S. (1982), A stochastic-convective transport representation of dispersion in one-dimensional porous media systems, *Water Resour. Res.*, *18*(4), 1193–1214, doi:10.1029/WR018i004p01193.
- Simmons, C. S., T. R. Ginn, and B. D. Wood (1995), Stochastic-convective transport with nonlinear reaction: Mathematical framework, *Water Resour. Res.*, *31*(11), 2675–2688, doi:10.1029/95WR02178.
- Smith, K. A. (1980), A model of the extent of anaerobic zones in aggregated soils, and its potential application to estimates of denitrification, *J. Soil Sci.*, *31*(2), 263–277, doi:10.1111/j.1365-2389.1980.tb02080.x.
- Steeffel, C. I. (2009), *Crunchflow Software for Modeling Multicomponent Reactive Flow and Transport: User Manual*, pp. 12–91, Earth Sci. Div., Lawrence Berkeley, Natl. Lab., Berkeley, Calif.
- Therrien, R., and E. A. Sudicky (1996), Three-dimensional analysis of variably-saturated flow and solute transport in discretely-fractured porous media, *J. Contam. Hydrol.*, *23*(1), 1–44, doi:10.1016/0169-7722(95)00088-7.
- Thorsen, M., J. C. Refsgaard, S. Hansen, E. Pebesma, J. B. Jensen, and S. Kleeschulte (2001), Assessment of uncertainty in simulation of nitrate leaching to aquifers at catchment scale, *J. Hydrol.*, *242*(3), 210–227, doi:10.1016/S0022-1694(00)00396-6.
- Todorovic, P. (1970), A stochastic model of longitudinal diffusion in porous media, *Water Resour. Res.*, *6*(1), 211–222, doi:10.1029/WR006i001p00211.
- Törnqvist, R., J. Jarsjö, J. Thorslund, P. S. C. Rao, N. B. Basu, and G. Destouni (2015), Mechanisms of basin-scale nitrogen load reductions under intensified irrigated agriculture, *PLoS One*, *10*(3), e0120015, doi:10.1371/journal.pone.0120015.
- Varni, M., and J. Carrera (1998), Simulation of groundwater age distributions, *Water Resour. Res.*, *34*(12), 3271–3281, doi:10.1029/98WR02536.
- Williams, D. R., J. J. Rowe, P. Romero, and R. G. Eagon (1978), Denitrifying pseudomonas aeruginosa: Some parameters of growth and active transport, *Appl. Environ. Microbiol.*, *36*(2), 257–263.
- Wu, Y. (2014), Simulation of nitrogen leaching in different soil types and land uses of the Ammer catchment, Master's thesis, Univ. of Tübingen, Tübingen, Germany.
- Xiu, D., and J. S. Hesthaven (2005), High-order collocation methods for differential equations with random inputs, *SIAM J. Sci. Comput.*, *27*(3), 1118–1139, doi:10.1137/040615201.
- Yabusaki, S. B., C. I. Steefel, and B. D. Wood (1998), Multidimensional, multicomponent, subsurface reactive transport in nonuniform velocity fields: Code verification using an advective reactive streamtube approach, *J. Contam. Hydrol.*, *30*(3), 299–331, doi:10.1016/S0169-7722(97)00050-8.



RESEARCH ARTICLE

10.1002/2017WR021645

Key Points:

- We account for the decreasing reaction potential of an aquifer in travel-time-based simulations of reactive transport
- The low computational costs facilitate ensemble simulations within a stochastic framework on the aquifer scale
- The uncertainty in predicting the breakthrough of contaminants in a heterogeneous aquifer decreases with increasing scale of observation

Correspondence to:

O. A. Cirpka,
olaf.cirpka@uni-tuebingen.de

Citation:

Loschko, M., Wöhling, T., Rudolph, D. L., & Cirpka, O. A. (2018). Accounting for the decreasing reaction potential of heterogeneous aquifers in a stochastic framework of aquifer-scale reactive transport. *Water Resources Research*, 54, 442–463. <https://doi.org/10.1002/2017WR021645>



Received 2 AUG 2017

Accepted 30 DEC 2017

Accepted article online 8 JAN 2018

Published online 25 JAN 2018

Accounting for the Decreasing Reaction Potential of Heterogeneous Aquifers in a Stochastic Framework of Aquifer-Scale Reactive Transport

Matthias Loschko¹ , Thomas Wöhling^{2,3}, David L. Rudolph⁴, and Olaf A. Cirpka¹ 

¹Center for Applied Geoscience, University of Tübingen, Tübingen, Germany, ²Department of Hydrology, Technische Universität Dresden, Dresden, Germany, ³Lincoln Agritech Ltd., Ruakura Research Centre, Hamilton, New Zealand, ⁴Department of Earth and Environmental Sciences, University of Waterloo, Waterloo, ON, Canada

Abstract Many groundwater contaminants react with components of the aquifer matrix, causing a depletion of the aquifer's reactivity with time. We discuss conceptual simplifications of reactive transport that allow the implementation of a decreasing reaction potential in reactive-transport simulations in chemically and hydraulically heterogeneous aquifers without relying on a fully explicit description. We replace spatial coordinates by travel-times and use the concept of relative reactivity, which represents the reaction-partner supply from the matrix relative to a reference. Microorganisms facilitating the reactions are not explicitly modeled. Solute mixing is neglected. Streamlines, obtained by particle tracking, are discretized in travel-time increments with variable content of reaction partners in the matrix. As exemplary reactive system, we consider aerobic respiration and denitrification with simplified reaction equations: Dissolved oxygen undergoes conditional zero-order decay, nitrate follows first-order decay, which is inhibited in the presence of dissolved oxygen. Both reactions deplete the bioavailable organic carbon of the matrix, which in turn determines the relative reactivity. These simplifications reduce the computational effort, facilitating stochastic simulations of reactive transport on the aquifer scale. In a one-dimensional test case with a more detailed description of the reactions, we derive a potential relationship between the bioavailable organic-carbon content and the relative reactivity. In a three-dimensional steady-state test case, we use the simplified model to calculate the decreasing denitrification potential of an artificial aquifer over 200 years in an ensemble of 200 members. We demonstrate that the uncertainty in predicting the nitrate breakthrough in a heterogeneous aquifer decreases with increasing scale of observation.

Plain Language Summary Many aquifers can break down nitrate that was introduced into the groundwater by farmers. Unfortunately, this natural ability is lost over time while the reaction takes place. When modelling this process, one faces the difficulty that many parameters are not or only little known. That's why we have to run many models with different parameters. In existing models, the decreasing ability to break down the nitrate could not be accounted for. In our model, we look at the important factors controlling this process. By that, we can account for the decreasing reaction potential. And we are still able to calculate this so fast that many model runs are possible. We believe that this is an important contribution to the existing models because it helps to make better predictions about nitrate in groundwater and to get a better understanding of what is really happening.

1. Introduction

With the intensification of agriculture in the 1960s and 1970s, the total exposure of groundwater to agricultural contaminants has increased (Galloway et al., 2004). Of international concern is the increase in nitrogen load to aquifers due to the enhanced use of mineral fertilizers and manure (Bouraoui et al., 2011). Excess nitrate, which is not taken up by the plants, lost through volatilization or removed through surface water runoff processes, may be transported with the infiltrating water from the root zone into the saturated zone (Sebilo et al., 2013). This leads to an increase of nitrate concentrations in groundwater systems and potentially surface waters (e.g., Puckett et al., 2011). Nitrate is a regulated compound (drinking-water standards: 50 mg/L total nitrate in the European Union, 10 mg/L nitrate-N = 44 mg/L total nitrate in the United States)

because it can be reduced to nitrite in the human body, potentially causing methemoglobinemia of infants (Wolfe & Patz, 2002), and may increase cancer risk (Ward et al., 2005; Weyer et al., 2001).

Despite legislation on agricultural practices designed to reduce fertilizer inputs into groundwater, nitrate concentrations in groundwater recharge has remained at elevated levels in regions of intensive agriculture worldwide (Pacheco et al., 2001; Strebel et al., 1989; Wakida & Lerner, 2005). Nonetheless, the nitrate concentrations in pumping and monitoring wells have often not increased to the same extent as the concentrations in groundwater recharge, even though other substances originating from fertilizers (e.g., chloride) have indicated an anthropogenic influence (Wisotzky, 2012). This demonstrates that some aquifers naturally degrade nitrate through denitrification, which requires the supply of electron donors from the aquifer matrix, most notably in the form of organic carbon and pyrite, and to a smaller extent from other reduced components of the matrix, such as biotite (Korom, 1992). Tesoriero and Puckett (2011) showed that lithologic carbon is a major source of electron donors for aerobic respiration and denitrification, whereas surface-derived sources of dissolved organic carbon is not.

In the unsaturated zone, the pool of organic material is replenished by decaying plant material, such as leaves, roots, and wood, or by infiltration of solutions with high concentrations of dissolved organic carbon. In the saturated zone, by contrast, the organic material is mostly of geogenic origin and is not replenished (Appelo & Postma, 2004). This implies that the denitrification potential of an aquifer decreases over time, that is, a long-time nitrate input leads to a decrease of the natural denitrification potential. Wisotzky (2012) showed the breakthrough curves of nitrate and chloride in a well in the lower Rhine valley in Germany. This author used chloride as a conservative indicator of anthropogenic influenced water assuming that it is introduced at the same time as the nitrate. Wisotzky (2012) observed that nitrate concentrations remained low even though chloride concentrations increased. After several years of pumping the aquifer, a sudden increase of the nitrate concentrations was observed, indicating a decrease of the denitrification potential of the aquifer over time. Also other water suppliers in regions of intensive agriculture, who have relied on the natural denitrification potential of their aquifers over decades of pumping, are now faced with an increase of nitrate concentrations in their wells (Böhlke, 2002; Eschenbach & Well, 2013). This increase may come without any prior warning, cause drinking-water standards to be exceeded, and eventually necessitate the shut-down of pumping wells.

Nitrate or other fertilizers are often introduced over large (agricultural) areas and act as a diffuse contaminant. To address the impact of such a diffuse input and the fate of the pollutant in a watershed, we often rely on numerical models that are able to reproduce observed time series of hydraulic head and concentrations under present conditions and make predictions about the future (Almasri & Kaluarachchi, 2007; Kinzelbach et al., 1991; Middelburg et al., 1996). They should also consider the decrease of the denitrification potential (e.g., Jang et al., 2017) and not assume a constant and endless denitrification capacity after anaerobic conditions are achieved. As an example, Almasri and Kaluarachchi (2007) presented a fairly elaborate model of nitrogen cycling in the unsaturated zone, coupled to transport of nitrate in groundwater accounting for simple first-order decay without depletion of electron donors. If a constant supply of electron donors from the matrix is assumed, the long-term concentration trajectory of nitrate would likely be underestimated, deeming forecasts to be overly optimistic. Also, other studies on the fate of nitrate on the catchment scale do not account for the depletion of reactive pools (e.g., Green et al., 2016; Lasserre et al., 1999; Pätzsch et al., 2003), or put their focus on the unsaturated zone or parts of the aquifer where no substrate limitations occurred (Ledoux et al., 2007; Molenat & Gascuel-Oudou, 2002). Wriedt and Rode (2006) account for the different reactivity of organic matter by introducing a release function simulating transfer from a chemically inert pool of sedimentary organic matter into a pool of dissolved organic matter available for turnover reactions. However, due to the complexity of the modeling approach and the associated model runtimes, implementing this scheme in a stochastic framework appears impractical.

Conventional reactive-transport models solve partial differential equations (*pde's*), considering advection, dispersive mixing, and reactions of multiple constituents in a spatially explicit way (e.g., Jang et al., 2017; Mayer et al., 2002; Prommer et al., 2001; Schäfer & Therrien, 1995). While theoretically the spatially explicit representation of all states (heads and concentrations) and processes may facilitate the most complete and accurate description of flow and reactive transport, it also requires a spatially explicit assessment of all parameters for hydraulics (hydraulic conductivity, specific yield), solute transport (porosity, dispersivities),

and reactions (multiple reactive parameters), including the associated boundary conditions (groundwater recharge, water levels in rivers, concentrations in the inflow, etc.).

In real-world applications, all hydraulic and chemical parameters are uncertain, either because of lacking knowledge or because of unpredictable dynamics. Hence, advanced reactive transport at the catchment scale may require a stochastic framework to account for the uncertainty of forcings, model parameters, and conceptual assumptions (e.g., Cirpka & Kitanidis, 2000; Jury, 1982; Luo, 2012; Shapiro & Cvetkovic, 1988; Yabusaki et al., 1998). Because the quantity of interest (nitrate concentration at a location of compliance) depends on the parameters in a nonlinear way, linear uncertainty propagation most likely is not sufficient, and techniques based on multiple model runs are needed. The simplest approach would be Monte-Carlo (MC) simulations, in which multiple model variants with independent, random realizations of the parameter fields are simulated, resulting in multiple model predictions. Even though more efficient nonlinear uncertainty quantification techniques exist (e.g., Nobile et al., 2008; Xiu & Hesthaven, 2005), they all rely on multiple model runs. Unfortunately, conventional *pde*-based reactive-transport models are computationally so demanding that stochastic methods requiring thousands of model executions are often not feasible. To overcome these problems, conceptual simplifications of reactive transport are needed.

A key simplification for transport in heterogeneous domains is to neglect transverse dispersion, so that transport becomes one-dimensional within independent streamtubes (e.g., Thiele et al., 1996). Such a simplification may be valid for diffuse input of compounds, where either all reactants are introduced jointly or the solutes react with the aquifer matrix (e.g., Sanz-Prat et al., 2015). In some stream-tube approaches, longitudinal mixing within the streamtubes is accounted for, which may parameterize effects of local transverse mixing on macroscopically longitudinal mixing (e.g., Cirpka & Kitanidis, 2000; Ginn, 2001). If longitudinal mixing is also neglected, one arrives at purely convective transport, which may be analyzed best in a Lagrangian framework (e.g., Cvetkovic & Dagan, 1994; Dagan & Bresler, 1979; Shapiro & Cvetkovic, 1988; Simmons, 1982). In these models, transport can be expressed in terms of travel times, that is, the time a water parcel spends traveling between entering and exiting the domain or between entering the domain and reaching an observation point or control plane (e.g., Feyen et al., 1998). In reactive-transport implementations of this framework, the concentrations of a water parcel change due to the reactions while being advected through the domain. If the inflow concentrations and the reactive properties are spatially uniform, the reactive-species concentrations are identical for all locations with identical travel time. That is, reaction fronts align with groundwater isochrones. In stochastic-convective transport, breakthrough curves are averaged over an extended control plane or an ensemble of multiple realizations (Dagan, 2002; Shapiro & Cvetkovic, 1988; Simmons, 1982). As an example of aquifer-scale oxygen and nitrate transport, Green et al. (2016) estimated parametric residence-time distributions of the San Joaquin Valley, nitrate inputs, and zero-order reaction rates of oxygen and nitrate in a stochastic framework. Stochastic-convective models may consider nonlinear reactions (e.g., Cvetkovic & Dagan, 1996; Cvetkovic et al., 1996; Dagan & Cvetkovic, 1996; Simmons et al., 1995), including bioreactions (e.g., Ginn et al., 1995; Kaluarachchi et al., 2000).

In aquifers with chemical heterogeneity, the time that solutes can react most likely differs from the time that a water parcel has spent in the aquifer. Glassley et al. (2002) defined the time that two reactants are in contact to each other as exposure time. Seeboonruang and Ginn (2006) considered the exposure time as independent variable in a modified version of the stochastic-convective-reactive method applied to linear kinetically controlled reactions. Ginn (1999, 2000a, 2000b) introduced the exposure time as an additional dimension in the reactive-transport equations, making a three-dimensional transient problem five-dimensional, whereas Sanz-Prat et al. (2016a), among others, used the exposure time to replace spatial coordinates, thus achieving a reduction of dimensionality in reactive transport. In the latter approach, the exposure to conditions suitable for a reaction was defined as a binary switch: the exposure-time clock stopped in nonreactive zones while it progressed with a constant speed in reactive zones. Frei and Peiffer (2016) defined the exposure time for denitrification as the travel time in which the oxygen concentration was below an inhibitory concentration, thus also using a binary, although dynamic, switch.

The biogeochemical conditions in aquifers are usually heterogeneous and the associated parameters are spatially nonuniform (e.g., Jang et al., 2017; Lohse et al., 2009; Ocampo et al., 2006). The classical exposure-time concept may not address the heterogeneity to the extent necessary, as the reactivity in biogeochemically favorable zones may vary on a continuous scale. In a preceding study, we addressed such variability by introducing a relative reactivity, which quantifies the reaction rate for given solute concentrations scaled by

the reaction rate under reference conditions (Loschko et al., 2016). We further introduced the cumulative relative reactivity, which is the relative reactivity experienced by a water parcel integrated over travel time, and used this as master variable for reactive-transport simulations. We could show that certain cases of nonlinear reactive transport simplify to solving a single system of ordinary differential equations in terms of the cumulative relative reactivity instead of time for all streamlines with identical inflow concentration, thus substantially reducing the computational effort, even when considering nonlinear reaction kinetics. For the application to aerobic respiration and denitrification in aquifers, the relative reactivity parameterizes the supply of a suitable electron donor from the aquifer matrix.

A substantial shortcoming of most exposure time concepts, and also of the approach of Loschko et al. (2016), is that they restrict the analysis to concentrations of dissolved compounds. Concentrations of reaction partners in the aquifer matrix are not considered as dynamic variables, ultimately implying an endless supply, which contradicts the observations made in the field (Wisotzky, 2012). That is, the relative reactivity suggested by Loschko et al. (2016) should decrease due to the depletion of matrix-bound reaction partners. Unfortunately, this is a spatially explicit problem, which cannot be addressed in a spatially fully nonexplicit framework.

In this work, we show how to account for the depletion of matrix-bound reaction partners in the framework of relative reactivity without returning to a fully explicit description. The approach can handle the spatial variability of hydraulic aquifer parameters (denoted “physical heterogeneity”) as well as the spatial variability of the reaction-partner supply from the matrix (denoted “chemical heterogeneity”). We revisit the existing modeling framework of cumulative relative reactivity and add a decreasing reaction potential without losing the computational and conceptual advantages. As before, we do this for the case of nitrate transport, which is a relevant issue of concern for many water suppliers. To estimate the uncertainty of nitrate breakthrough curves caused by chemical and hydraulic heterogeneity, we put the method into a stochastic framework and demonstrate how the observation scale affects uncertainty.

The remainder of this paper is organized as follows: In section 2, we present the governing equations for reactive transport of nitrate, considering both a slightly more detailed description of the reactions and a simplified version that we make use of when applying the framework of relative reactivity. We review and extend this framework to account for a decreasing denitrification potential of the aquifer matrix. In section 3, we perform one-dimensional simulations to test the assumptions underlying the concept of relative reactivity and derive a functional dependence of relative reactivity on the organic-carbon content of the aquifer matrix. In section 4, we apply the proposed simplified framework to a three-dimensional test case in which we perform ensemble runs accounting for correlated hydraulic and chemical heterogeneity by a heterogeneous distribution of natural organic carbon in the matrix. In particular, we show that the uncertainty in the prediction of nitrate breakthrough curves significantly depends on the observation scale. The paper closes with final remarks in section 5. Additionally we present a two-dimensional comparison between model results simulating spatially explicit advective-dispersive-reactive transport, using the more detailed description of reactions, and the simplified, travel-time-based approach.

2. Theory

In this chapter, we revisit the framework of cumulative relative reactivity of Loschko et al. (2016) in which we have introduced the cumulative relative reactivity as master variable for reactive transport simulations in a streamline-based framework. We extend the framework to account for the depletion of immobile reaction partners in the matrix.

2.1. General Approach of Reactive-Transport Calculations

2.1.1. Spatially Explicit Description

The starting point of our analysis is the multidimensional advection-dispersion-reaction equation involving mobile and immobile species, potentially including microbes:

$$\frac{\partial \mathbf{c}}{\partial t} + \mathbf{v} \cdot \nabla \mathbf{c} - \nabla \cdot (\mathbf{D} \nabla \mathbf{c}) = \mathbf{r}(\mathbf{c}(\mathbf{x}, t), \mathbf{c}^*(\mathbf{x}, t)), \quad (1)$$

$$\frac{\partial \mathbf{c}^*}{\partial t} = \mathbf{r}^*(\mathbf{c}(\mathbf{x}, t), \mathbf{c}^*(\mathbf{x}, t)), \quad (2)$$

in which \mathbf{c} [molL^{-3}] and \mathbf{c}^* [$\text{molM}_{\text{soil}}^{-1}$] are the concentration vectors of all dissolved and immobile-phase compounds, respectively, t [T] and \mathbf{x} [L] are time and spatial coordinates, \mathbf{v} [LT^{-1}] is the linear average velocity vector, \mathbf{D} [L^2T^{-1}] denotes the local dispersion tensor, whereas \mathbf{r} [$\text{molL}^{-3}\text{T}^{-1}$] and \mathbf{r}^* [$\text{molM}_{\text{soil}}^{-1}\text{T}^{-1}$] are vectors of reaction rates for the mobile and immobile-phase compounds, respectively.

2.1.2. Simplified Description Using the Relative Reactivity

The reaction terms in equations (1) and (2) can be chosen to accommodate almost any type of reactive system (e.g., Jang et al., 2017, for nitrate transport), but the computational effort is typically very high. In the following, we adapt the concept of cumulative relative reactivity proposed by Loschko et al. (2016). The key ideas are (1) to neglect local dispersion altogether, (2) restrict the analysis to a few dominant solutes, and (3) address spatial variability of immobile compounds by the introduction of a relative reactivity $f(\mathbf{x}, t)$ [-], which parameterizes the supply of reaction partners from the matrix, relative to a reference supply. The relative reactivity is a dimensionless parameter for the intensity of a chemical reaction and is defined at every location in the domain. By this single scalar field, we account for the chemical heterogeneity of an aquifer.

We express advective transport along streamlines in terms of travel time τ [T] rather than spatial coordinates. Under steady-state flow conditions, the travel time meets:

$$\mathbf{v} \cdot \nabla \tau = 1, \quad (3)$$

subject to a value of zero at the boundaries of infiltration. Equation (3) is identical to the mean groundwater-age equation of Goode (1996) for zero dispersion.

With the assumptions specified above, the advection-reaction equation along a streamline is described by:

$$\frac{\partial \mathbf{c}}{\partial t} + \frac{\partial \mathbf{c}}{\partial \tau} = f(\tau, t) \mathbf{r}_0(\mathbf{c}(\tau, t)), \quad (4)$$

in which \mathbf{r}_0 [$\text{molL}^{-3}\text{T}^{-1}$] denotes the reaction-rate vector under reference conditions and $f(\tau, t) = f(\mathbf{x}(\tau), t)$ is the relative reactivity along a streamline expressed as function of travel time rather than spatial coordinates where $\mathbf{x}(\tau)$ is the spatial location along an individual streamline where the travel time equals τ .

To further simplify the calculations, we consider the cumulative relative reactivity F [T], which is the relative reactivity experienced by a water parcel integrated over the time of passage through the aquifer, which meets the following transport equation:

$$\frac{\partial F}{\partial t} + \frac{\partial F}{\partial \tau} = f(\tau, t), \quad (5)$$

in which the partial derivative with respect to time, $\frac{\partial F}{\partial t}$, equals zero if the relative reactivity and the flow field do not change with time.

By considering the material derivative, $\frac{D}{Dt} = \frac{\partial}{\partial t} + \frac{\partial}{\partial \tau}$, and applying the chain-rule of differentiation, we can show that the reactive-species concentrations are uniquely related to the cumulative relative reactivity by a single system of ordinary differential equations:

$$\frac{d\mathbf{c}}{dF} = \mathbf{r}_0(\mathbf{c}(\tau, t)), \quad (6)$$

subject to the inflow concentrations as initial condition. Reactive-species concentrations at a given point in space and time can then be obtained by considering the cumulative reactivity at that point and the concentrations when the observed water parcel was introduced into the aquifer.

Loschko et al. (2016) assumed that the relative reactivity remained constant over time, indicating an infinite supply of reaction partners from the matrix. In the equations above, we have already considered a time-dependent relative reactivity $f(\mathbf{x}, t)$. In the present study, we extend the framework of cumulative relative reactivity to account for the consumption of the reaction partner in the matrix, which in our case is natural organic matter (NOM):

$$\frac{dc_{NOM}^*}{dt} = f(\tau, t) \zeta \cdot \mathbf{r}_0(\mathbf{c}(\tau, t)), \quad (7)$$

in which $c_{NOM}^*(\tau, t)$ [$\text{mol}_C \text{M}_{\text{soil}}^{-1}$] is the immobile natural organic matter content of the soil, and ζ [$\text{mol}_C \text{M}_{\text{soil}}^{-1} \text{L}^3 \text{mol}_{\text{solute}}^{-1}$] is the vector of stoichiometric coefficients between the reaction partner in the matrix (here NOM) and the reactive solutes.

Finally, we assume that the relative reactivity depends on the concentration of the reaction partner in the matrix by a unique monotonic function $g(c_{NOM}^*(x, t))$, yet to be determined:

$$f(\tau, t) = g(c_{NOM}^*(\tau, t)). \quad (8)$$

We summarize the simplified scheme of reactive transport by the following steps and provide details about the system of reaction equations in Section 2.2:

1. Solve the ordinary differential equation (6) for all inflow concentrations \mathbf{c}_{in} [ML^{-3}] occurring, resulting in the function dependence $\mathbf{c}(F, \mathbf{c}_{in})$,
2. Evaluate steady-state flow and obtain the velocity field $\mathbf{v}(\mathbf{x})$,
3. Construct streamlines leading to observation points, extraction wells, or control planes of interest by backward particle tracking,
4. Discretize all streamlines by identical travel-time increments $\Delta\tau$ and average the concentration of the reaction partner in the matrix (here c_{NOM}^*) in all streamline-increments,
5. Set time $t = 0$,
6. Compute the relative reactivity $f(\tau, t)$ of each streamline-increment from the concentration of the reaction partner in the aquifer matrix by equation (8),
7. Compute the cumulative relative reactivity $F(\tau, t + \Delta\tau)$ for all streamlines by equation (5), Compute the reactive species concentrations $\mathbf{c}(\tau, t + \Delta\tau) = \mathbf{c}(F(\tau, t + \Delta\tau), \mathbf{c}_{in}(t + \Delta\tau - \tau))$,
8. Reconstruct the reaction rate $f(\tau, t + \Delta\tau) \mathbf{r}_0(\mathbf{c}(\tau, t + \Delta\tau))$ in all streamline-time increments,
9. Update the concentration of the reaction partner in the matrix by equation (7),
10. Increase t by $\Delta\tau$ and go back to step 6, unless time t exceeds the end time of simulation.

This scheme results in breakthrough curves of reactive-species concentrations. For extraction wells and control planes, the breakthrough curves of multiple streamlines need to be averaged applying flux weighting. To address uncertainty, multiple realizations of parameter fields can be considered, resulting in an ensemble of breakthrough curves for each observation point, well, or plane.

The applicability of the approach depends on the validity of the assumption to neglect local dispersion, which we have discussed in previous studies (Sanz-Prat et al., 2015, 2016a, 2016b). In these studies, we compared two-dimensional, heterogeneous, spatially explicit model results of the advection-dispersion-reaction equation to results in which reactive-species concentrations were computed in one-dimensional domains and the results were mapped to the 2-D domain based on travel and exposure times. The travel and exposure-time-based results agreed very well with the spatially explicit simulations of the advection-dispersion-reaction equation. The second key assumption is that a single scalar relative-reactivity field $f(\mathbf{x}, t)$ can be defined for a simplified set of reaction equations. We will test this assumption by simulating a somewhat more elaborate reactive-transport model with dynamic biomass and an explicit description of reaction-partner supply from the matrix and comparing it to the simplified model. The detailed model forms the basis for deriving the simplified reaction scheme using the relative reactivity (see section 3). In this context, we also need to determine the functional dependence of the relative reactivity on the concentration of the reaction partner in the matrix. The reactive system chosen in this study contains aerobic respiration and denitrification. For the case with an infinite electron-donor supply by the matrix, we have tested the validity of the cumulative-relative-reactivity approach by comparisons between the simplified method and two-dimensional spatially explicit simulations (Loschko et al., 2016), showing that the error introduced by simplifying reactive transport are minor if the target quantities are the mass fluxes crossing a control plane or being collected by a well. We have added yet another comparison of this type for the reactive system applied in this study in the Appendix A.

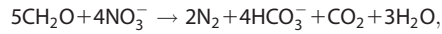
2.2. Reactive System

2.2.1. Denitrification and Aerobic Respiration

Natural denitrification, which is the microbially catalyzed reduction of nitrate via nitrite and nitrous oxide to molecular nitrogen, is the most important process reducing the nitrate load in groundwater. It is coupled to

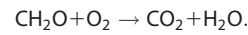
the oxidation of an electron donor, which in aquifers is typically provided by the aquifer matrix. Natural organic matter is the most dominant electron donor in aquifers worldwide, but other reduced constituents such as pyrite may also be present and can be oxidized by the denitrification process (e.g., Jang et al., 2017). In the following, we restrict the analysis to natural organic matter.

Disregarding intermediate steps and the impact of biomass growth to the stoichiometry, the simplified net stoichiometry of heterotrophic-chemoorganotrophic denitrification, where organic carbon acts as electron donor, is:



in which CH_2O denotes the simplified chemical composition of the organic matter. The reduction process involves several intermediates, but dissolved nitrogen gas is the predominant reaction product. The availability of the organic material depends in general on two factors: the microorganisms need to have access to the organic material, and the reactive material needs to be processable by the enzymes. While the steps involved in making natural organic matter of the aquifer matrix bioavailable can be quite complex and are the topic of current biogeochemical research, we simply assume here that a certain fraction of natural organic matter is bioavailable and disregard the refractory components altogether.

Denitrification stands in competition to aerobic respiration. Taking organic matter as the electron donor, the simplified net stoichiometry of aerobic respiration is:



Denitrification is thermodynamically less favorable than aerobic respiration, and elevated oxygen concentrations inhibit the nitrogen oxide reductases (Rivett et al., 2008). Hence, oxygen is the preferred electron acceptor in the presence of dissolved oxygen, nitrate, and organic carbon. This has to be accounted for by oxygen-inhibition terms in the rate laws of denitrification.

The gradual decrease of oxygen and nitrate with depth indicates that oxygen and nitrate reduction rates are slow compared to the rate of vertical water transport. The reactivity of organic matter or other electron donors is probably the overall controlling factor. For reactive-transport simulations, this implies that reaction kinetics needs to be considered.

2.2.2. Detailed Reaction Model

As reference, we start with a moderately detailed model of aerobic respiration and denitrification, considering the dynamic biomass of an immobile facultative anaerobic microbial culture, dissolved organic carbon (DOC), nitrate and oxygen as solutes, and natural organic matter as electron-donor pool in the matrix. In this model, the rate of change r_i of the respective compound i is described as (adapted from Sanz-Prat et al., 2015):

$$r_{DO} = -\frac{\mu_{DO}}{Y_{DO}} \cdot \frac{Q_b}{\theta} \cdot c_{bio}^* \quad (9)$$

$$r_{Nit} = -\frac{\mu_{Nit}}{Y_{Nit}} \cdot \frac{Q_b}{\theta} \cdot c_{bio}^* \quad (10)$$

$$r_{DOC} = r_{DOC}^{rel} - \left(\frac{\mu_{DO}}{Y_{DO}} + \frac{5\mu_{Nit}}{4Y_{Nit}} \right) \cdot \frac{Q_b}{\theta} \cdot c_{bio}^* \quad (11)$$

$$r_{NOM}^* = -\frac{\theta}{Q_b} \cdot r_{DOC}^{rel} \quad (12)$$

$$r_{bio}^* = \left((\mu_{DO} + \mu_{Nit}) \cdot \left(1 - \frac{c_{bio}}{c_{bio}^{max}} \right) - k_{dec} \right) \cdot c_{bio}^*(x) \quad (13)$$

with:

$$\mu_{DO} = \frac{c_{DO}}{c_{DO} + K_{DO}} \cdot \frac{c_{DOC}}{c_{DOC} + K_{DOC}} \cdot \mu_{max}^{aer} \quad (14)$$

$$\mu_{Nit} = \frac{c_{DOC}}{c_{DOC} + K_{DOC}} \cdot \frac{c_{Nit}}{c_{Nit} + K_{Nit}} \cdot \frac{K_{DO}^{inh}}{K_{DO}^{inh} + c_{DO}} \cdot \mu_{max}^{Nit} \quad (15)$$

in which $c_{DO}(\mathbf{x}, t)$ [$\text{mol}_{\text{DO}}\text{L}^{-3}$], $c_{Nit}(\mathbf{x}, t)$ [$\text{mol}_{\text{Nit}}\text{L}^{-3}$], and $c_{DOC}(\mathbf{x}, t)$ [$\text{mol}_{\text{C}}\text{L}^{-3}$] are the concentrations of dissolved oxygen, nitrate, and dissolved organic carbon, respectively, whereas $c_{bio}^*(\mathbf{x}, t)$ [$\text{mol}_{\text{C}}\text{M}_{\text{soil}}^{-1}$] denotes the

mass-related concentration of the immobile biomass in the aquifers matrix. ρ_b [$M_{soil}L^{-3}$] and θ [-] are the dry bulk mass density of the aquifer material and the volumetric water content, respectively. $\mu_{DO}(\mathbf{x}, t)$ [T^{-1}] and $\mu_{Nit}(\mathbf{x}, t)$ [T^{-1}] are the specific growth rates due to aerobic respiration and denitrification, respectively, whereas μ_{max}^{aer} [T^{-1}] and μ_{max}^{Nit} [T^{-1}] are the corresponding maximum specific growth rates. Y_{DO} [$mol_C mol_{DO}^{-1}$] and Y_{Nit} [$mol_C mol_{Nit}^{-1}$] are the yield coefficients of aerobic respiration and denitrification, respectively, K_i [$molL^{-3}$] denotes the Monod constant of compound i , and K_{DO}^{inh} [$molL^{-3}$] is the inhibition constant of oxygen in denitrification. c_{bio}^{max} [$mol_C M_{soil}^{-1}$] is the maximum biomass concentration, and k_{dec} [T^{-1}] denotes the rate coefficient of biomass decay. Finally, $r_{DOC}^{rel}(\mathbf{x}, t)$ [$mol_C T^{-1} L^{-3}$] denotes the release rate of dissolved organic carbon from the aquifer matrix, which we model as a first-order mass-transfer process:

$$r_{DOC}^{rel} = k_{DOC}^{rel,eff} \cdot (c_{DOC}^{sat} - c_{DOC}), \tag{16}$$

with

$$k_{DOC}^{rel,eff} = k_{DOC}^{rel,max} \cdot \left(\frac{c_{NOM}^*}{c_{NOM}^{*init}} \right)^{\frac{2}{3}}, \tag{17}$$

in which $k_{DOC}^{rel,eff}$ [T^{-1}] is the effective rate coefficient of DOC release with its maximum of $k_{DOC}^{rel,max}$ [T^{-1}], obtained at the initial concentration c_{NOM}^{*init} [$mol_C L^{-3}$] of NOM, c_{DOC}^{sat} [$mol_C L^{-3}$] denotes the saturation concentration of DOC, and $c_{NOM}^*(\mathbf{x}, t)$ [$mol_C M_{soil}^{-1}$] is the mass-related concentration of the natural organic matter in the aquifers matrix. The release rate of DOC changes with changing concentration of NOM. At early times, the microorganisms can utilize the easily available NOM. With progressing dissolution of NOM, the surface area of bioavailable NOM decreases. Assuming spherical NOM particles and a release rate that is proportional to the surface area, we arrive at the power-law dependence of the release rate to the NOM concentration with an exponent of 2/3 in equation (17).

It may be worth noting that much more elaborate models of microbial activity in general and denitrification in particular exist. Among the processes neglected are: (1) the transport, attachment, detachment, and straining of mobile biomass, (2) the consideration of several bacterial strains including obligatory aerobic and anaerobic bacteria, (3) biomass dormancy, (4) the production of extracellular enzymes by microbes to foster hydrolysis of NOM, (5) more elaborate dependence of DOC-release rates on NOM content in the matrix that do not build upon spherical NOM particle, (6) sorption of DOC, and (7) pH changes by the reactions with potential feedbacks on the microbial activity, and most likely other possible influences not mentioned. The presented, slightly more detailed model mainly follows assumptions in standard bioreactive transport models. The purpose of this model is not to be as exhaustive as possible in the process description, we simply take it as a reference model for the simplified approach based on the cumulative relative reactivity.

In order to test the concept of the relative reactivity, we split the reaction rates of equations (9) and (10) into equations that only depend on the dissolved-oxygen and nitrate concentrations:

$$r_{0,DO} = - \frac{c_{DO}}{c_{DO} + K_{DO}} \cdot \frac{\mu_{max}^{aer}}{Y_{DO}} \cdot c_{bio}^{max}, \tag{18}$$

$$r_{0,Nit} = - \frac{c_{Nit}}{c_{Nit} + K_{Nit}} \cdot \frac{K_{DO}^{inh}}{K_{DO}^{inh} + c_{DO}} \cdot \frac{\mu_{max}^{Nit}}{Y_{Nit}} \cdot c_{bio}^{max}, \tag{19}$$

and a factor containing the DOC and biomass concentrations:

$$f = \frac{c_{DOC}}{c_{DOC} + K_{DOC}} \cdot c_{bio}^* \cdot \left(1 - \frac{k_{dec}}{(\mu_{max}^{Nit} + \mu_{max}^{DO})} \right). \tag{20}$$

The factor defines the relative reactivity (see equation (4)) for the given model problem. Because the DOC and biomass concentrations are dynamic state variables, we cannot expect a priori that the relative reactivity f as calculated by equation (20) depends purely on the NOM-concentration in the matrix as implied by our simplified reaction scheme. But we can test whether the error introduced by this assumption is significant.

2.2.3. Simplified Reaction Model

The detailed model given above involves many states and parameters that are difficult to determine in practical applications. Based on the experience of previous studies, we believe that we can simplify the system with the following assumptions:

1. Microbes adapt to changing conditions on time scales that are shorter than the typical time scale of changes in aquifer-scale nitrate transport. Intermediate periods of starvation may be overcome by dormancy (e.g., Mellage et al., 2015). Except for the initial establishment of a microbial anaerobic community, there may be no need to simulate the abundances of microbes explicitly. In short terms: if the abiotic conditions are favorable, a stable active microbial community establishes on time scales that are negligible for seasonal or multiyear studies. Also, the presence of microbes does not influence the hydraulic conductivity.
2. The dissolved assimilable organic carbon also adapts quickly to the environmental conditions and does not need to be simulated explicitly. The content of natural organic matter or other electron donors in the matrix, by contrast, exhibits a major control on aerobic respiration and denitrification (Bradley et al., 1992; D'Haene et al., 2003; Drury et al., 1991; Hiscock et al., 1991; Smith, 1980). We address this by relating the relative reactivity (see Section 2.1.2) to the natural-organic-matter content of the aquifer, which is depleted over time by the reactions.
3. The inhibition constant K_{DO}^{inh} of oxygen in denitrification is typically so low that even the smallest dissolved-oxygen concentration can be considered inhibitory for denitrification.
4. The Monod constant K_{DO} of oxygen is typically so low that aerobic respiration can be considered to exhibit conditional zero-order kinetics.
5. The Monod constant K_{nit} of nitrate, by contrast, is typically so high that a first-order dependence of denitrification rates on nitrate becomes valid.

With these simplifications, the reaction rates of oxygen and nitrate for a relative reactivity f of unity, become:

$$r_{0,DO} = -r_{0,DO}^{max} H(c_{ox}) \tag{21}$$

$$r_{0,nit} = -k_{0,nit} c_{nit} \cdot (1 - H(c_{ox})) \tag{22}$$

with the zero-order reaction rate $r_{0,DO}^{max}$ [$\text{mol}_{DO} \text{L}^{-3} \text{T}^{-1}$] under standard conditions, the first-order decay coefficient $k_{0,nit}$ [T^{-1}] of nitrate under standard conditions, and the Heaviside function $H(\cdot)$.

With this definition of the reaction rates, the solution of the system of ordinary differential equations (6) is:

$$c_{ox}(F, \mathbf{c}_{in}) = \max\left(c_{in,DO} - F \cdot r_{0,DO}^{max}, 0\right) \tag{23}$$

$$c_{nit}(F, \mathbf{c}_{in}) = \begin{cases} c_{in,nit} & \text{if } F < \frac{c_{in,DO}}{r_{0,DO}^{max}} \\ c_{in,nit} \exp\left(-k_{0,nit} \left(F - \frac{c_{in,DO}}{r_{0,DO}^{max}}\right)\right) & \text{otherwise} \end{cases} \tag{24}$$

The stoichiometric coefficients between the NOM in the matrix and the dissolved reactants (equation (7)) are:

$$\gamma_{DO} = \frac{\theta}{\varrho_b} \tag{25}$$

$$\gamma_{nit} = \frac{5}{4} \frac{\theta}{\varrho_b} \tag{26}$$

To close the system in the simplified modeling approach, we still need the functional relationship between the relative reactivity f and the NOM-concentration c_{NOM}^* in the matrix. In real-world applications, this relationship has to be determined by experiments with aquifer material. Here we will explore the relationship between the NOM-concentration c_{NOM}^* in the matrix and the aquifer reactivity in the analysis of the more detailed reactive-transport model (Section 3).

3. One-Dimensional Test on the Applicability of the Relative-Reactivity Concept

The key purpose of the one-dimensional test simulation is to analyze whether the underlying assumptions of the relative-reactivity concept proposed by Loschko et al. (2016) are reasonable. In particular, we want to

see whether the reaction rates of dissolved oxygen and nitrate in the complex bioreactive model of section 2.2.2 can be expressed as product of reference rates, which depend only on the electron-acceptor concentrations, with the relative reactivity that, in theory, only depends on the electron-donor supply. We want to assess the potential dependence of the relative reactivity for aerobic respiration and denitrification on the natural-organic-matter concentration in the matrix. For this purpose, a one-dimensional domain for detailed reactive-transport calculations is sufficient. The functional dependence of the relative reactivity on the NOM-content in the matrix derived in this section depends on the assumptions and parameter choices of the moderately detailed model and are not general in a quantitative sense. They demonstrate, however, that assuming such a dependency is reasonable in a qualitative sense.

3.1. Model Setup and Implementation

The length of the domain was chosen to be 50 m. The linear average velocity of 1 m/d was assumed to be uniform and constant. The model accounts for advection, dispersion, biomass growth, and decay with associated turnover of nitrate, oxygen, and dissolved organic carbon, as well as the release of DOC from NOM in the matrix. Three solutes (nitrate, dissolved oxygen, dissolved organic carbon) and two immobile constituents (natural organic matter, biomass) were considered. All parameters of the one-dimensional test case are listed in Table 1. The constant inflow concentration of nitrate (50 mg/L) and dissolved oxygen (10 mg/L) represent typical values. The initial organic carbon content of the aquifer material was set to a uniform value of 0.083 mol_C/kg_{soil}. This corresponds well with measured values of organic-carbon contents in aquifers used for drinking-water supply (DVGW, 2015; Eschenbach & Well, 2013; Wisotzky, 2012) The initial biomass concentration was set to a small value of 4.5 × 10⁻⁵ mol_C/kg_{soil} throughout the domain, and the maximal biomass concentration was specified at 0.045 mol_C/kg_{soil}. In the model, the natural organic matter in the aquifer matrix cannot directly be used by the microorganisms. First, the organic carbon must be dissolved, which is parameterized by a first-order mass-transfer law (equation (16)). The dissolved organic carbon has an upper limit of 10 mg/L (Sanz-Prat et al., 2016b).

The model is implemented in Matlab using the Finite Volume Method with upwind differentiation of the advective term for spatial discretization, using 5,000 grid cells to avoid any effects of numerical dispersion on the results. We use a global implicit approach for coupling physical transport and reactive processes. The resulting large system of coupled nonlinear ordinary differential equations is solved with the ODE-solver ode15s, provided by Matlab (Shampine & Reichelt, 1997).

We solved the described problem using the more detailed model (see section 2.2.2) as well as the simplified model (see section 2.2.3). We manually fitted the simple model to the more detailed model. The resulting breakthrough curves are compared in Figure 1.

3.2. Results

Figure 1a shows the breakthrough curves of all solutes (nitrate, dissolved oxygen, and dissolved organic carbon) in the outflow of the domain for the more detailed and simplified models. Figure 1b shows the concentration time-series of biomass and natural organic matter for both, the more detailed and simplified models, in the last model cell. To interpret the plots, it is beneficial to remember that spatial profiles and breakthrough curves are essentially flipped: a late arrival in the breakthrough curve indicates a front lagging behind.

There is a very early peak of nitrate associated with a first peak of biomass in the more detailed model. This is an artifact of the initial condition. At very early times, the biomass concentrations are low throughout the domain so that a first pulse of electron acceptors can reach the outflow of the domain with little decay. Following this first pulse, more or less stable bioreaction fronts are established. Two such

Table 1
Parameters of the One-Dimensional Test Case

Symbol	Meaning	Value		
Hydraulic parameters				
L	Length of domain	50 m		
Δx	Grid spacing	0.01 m		
θ	Volumetric water content = porosity	0.3		
ρ_b	Dry bulk density	1,855 kg/m ³		
v	Linear average velocity	1 m/d		
α	Dispersivity	0.01 m		
D_p	Pore-diffusion coefficient	3 × 10 ⁻¹⁰ m ² /s		
Reactive parameters				
μ_{max}^{aer}	Maximal specific growth rate using oxygen	15 $\frac{1}{d}$		
μ_{max}^{Nit}	Maximal specific growth rate using nitrate	15 $\frac{1}{d}$		
K_{DO}	Monod constant for oxygen	11.4 $\frac{\mu mol}{L}$		
K_{Nit}	Monod constant for nitrate	70 $\frac{\mu mol}{L}$		
K_{DOC}	Monod constant for DOC	20 $\frac{\mu mol}{L}$		
K_{DO}^{inh}	Inhibition constant of oxygen in denitrification	10 $\frac{\mu mol}{L}$		
Y_{DO}	Yield coefficient of oxygen	0.25		
Y_{Nit}	Yield coefficient of nitrate	0.25		
K_{dec}	Rate coefficient of biomass decay	0.05/d		
C_{bio}^{max}	Maximum biomass concentration	1 $\frac{mg}{L}$		
$K_{sub}^{rel,max}$	Maximum rate coefficient of DOC release	2/d		
C_{sub}^{sat}	Saturation concentration of DOC	10 $\frac{mg}{L}$		
Inflow and initial concentrations				
	Nitrate	Oxygen	NOM	Biomass
Inflow	50 mg/L	10 mg/L		
Initial	0 mg/L	0 mg/L	1,000 mg/kg	1 × 10 ⁻³ mg/L

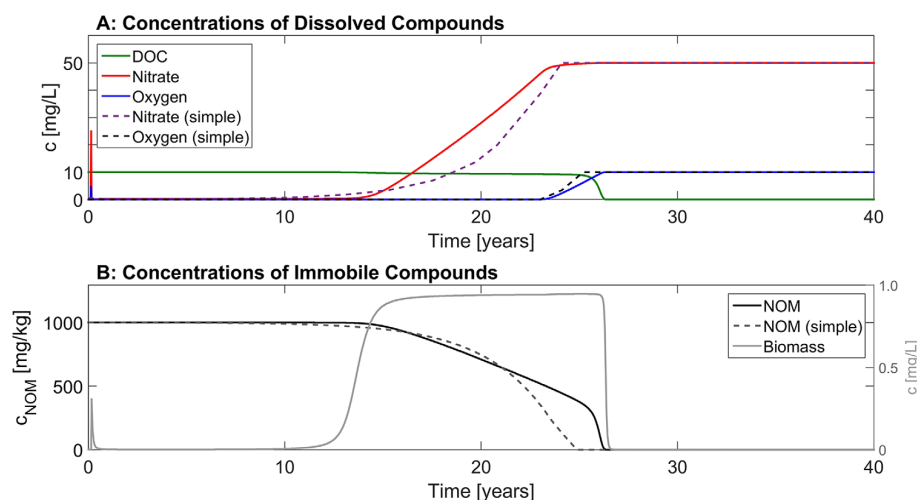


Figure 1. Time series of concentrations at the end of the one-dimensional domain for the detailed reaction model (solid lines) and the simplified reaction model (dashed lines). (a) Dissolved compounds (nitrate, dissolved oxygen, and dissolved organic carbon), (b) Immobile components (biomass and natural organic matter).

fronts can be observed. The more slowly moving front, arriving at the downstream end of the domain after about 9,000 days, involves the complete consumption of the bioavailable NOM by aerobic respiration. When this front arrives at the outflow of the domain, the biomass concentration drops because of lacking electron donors. Where NOM is available, the oxygen is not depleted immediately because the biomass growth is limited by the maximum biomass concentration. That is why we observe a gradual change of oxygen. At the leading edge of the front, arriving early, the DOC has practically reached its saturation concentration.

Nitrate penetrates deeper into the domain than oxygen, implying earlier breakthrough. In the zones where oxygen concentrations change, the nitrate concentrations are almost constant because of the strong inhibition of denitrification by dissolved oxygen. The nitrate front is fairly extended (about 3,000 days from zero to maximal values). In this zone we observe quasi steady-state behavior of NOM and nitrate depletion at the stoichiometric ratio. The biomass concentration is almost constant.

At the leading edge of the nitrate front, biomass is established. This takes some time because growth under denitrifying conditions is slow in comparison to growth under aerobic conditions. Also, the biomass is assumed to be completely immobile. That is, the biomass concentration has undergone first-order decay for some time until the nitrate front arrives. In a more elaborate model accounting for transport of biomass, the aquifer would have been inoculated by floating cells prior to the arrival of the nitrate front, causing a more rapid increase of biomass concentration than in the current model (e.g., Mellage et al., 2015). However, the modeled time of establishing the biomass is only about 2 weeks at the inlet of the domain, which is small in comparison to the approximately eleven years of biomass being close to the maximal concentration.

After the first nitrate pulse, the electron-acceptor concentrations remain close to zero for more than eight years, followed by approximately 8 years of steadily increasing nitrate concentrations. If we chose a longer 1-D domain, the time of practically no nitrate would extend whereas the time increment to reach maximal nitrate concentrations would stay about the same. Such a behavior is known as a traveling-wave solution and has been observed in many reactive-transport applications in the past. The steady increase of nitrate after a time period much larger than a pore volume agrees with observations made in the field (Wisotzky, 2012). A different initial concentration of organic carbon would shift the breakthrough curves of nitrate and oxygen in time but would not change their shape. A higher initial NOM content would lead to a later breakthrough, whereas a lower initial NOM content would lead to an earlier breakthrough.

The differences in the more detailed and simplified models are due to the assumptions made in the simplified model description (see also section 2.2.3). The simplified model does not account for the decay and

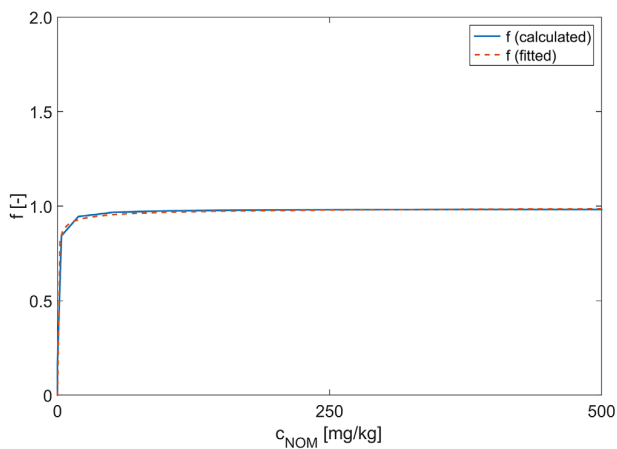


Figure 2. Relationship between immobile natural-organic-matter concentration and relative reactivity f , calculated by equation (20), in the one-dimensional domain. Line: simulation results of the model with detailed reaction kinetics and markers: parametric fit according to equation (27).

growth of microbial communities. Dissolved assimilable organic carbon is not modeled explicitly, and the reaction laws are simplified. Nonetheless the more detailed model and the simplified model show a good agreement.

With the results obtained by the more detailed bioreactive transport model we can compute the relative reactivity according to equation (20). Figure 2 shows the relationship between the calculated organic carbon content in the aquifer c_{NOM} and the relative reactivity f restricted to time points with noticeable reactions. We observe a monotonic relationship in which the relative reactivity increases rapidly with the organic-carbon content and then reaches its maximum rate once the organic-carbon is at saturation. Figure 2 also includes the following parametric fit $g(c_{NOM}^*)$ to the data as dashed line:

$$g(c_{OC}^*) = \frac{(c_{NOM}^*)^a}{(c_{NOM}^*)^a + K_{NOM,f}^a} \quad (27)$$

in which c_{NOM}^* [mol_CM_{soil}⁻¹] is the concentration of organic carbon in the aquifer and $K_{NOM,f}$ [mol_CM_{soil}⁻¹] is the half-reactivity concentration, which is similar to a Michaelis-Menten or Langmuir constant, whereas

$a[-]$ is a fitting exponent. The fitting parameters a , and $K_{NOM,f}$ depend on the type of reactive material and the reactive system. In our application, we obtained the following values:

$$a=0.5$$

$$K_{NOM,f}=0.5$$

The time series of nitrate, dissolved oxygen, and immobile NOM, obtained by the more detailed bioreactive transport model, can be reproduced fairly well by the simplified model. The breakthrough curves of dissolved oxygen and nitrate calculated by the simplified model can be seen in Figure 1a, and the NOM content calculated by the simplified model is shown in Figure 1b. We obtained the following parameters for the simplified model with a time increment of 0.5 days from fitting the more detailed model: $r_{0,DO}^{max}=0.19$ mol/m³/d, and $k_{0,nit}=0.225$ /d.

4. Three-Dimensional Application of the Simplified Model

In the three-dimensional application, we want to demonstrate how the simplified approach of reactive transport can be used for stochastic analysis of nitrate transport.

4.1. General Setup

The rectangular three-dimensional domain, depicted in Figure 3, resembles a small aquifer. With a length of 2.5 km and a width of 1.5 km, it spans over 3.75 km². The thickness of the aquifer is 20 m. The model considers only the saturated zone, thus leaving out the intricate feedback between surface water hydrology, vegetation, as well as water movement, and nutrient cycling in the vadose zone. Flow is introduced from the top by groundwater recharge with a constant rate of 450 mm a⁻¹, and from the left side, where a constant head boundary down to a depth of 2 m represents an infiltrating river. The remaining left side is considered to be a no-flow boundary. At the right side we consider a constant head boundary. The remaining sides are no-flow boundaries. Figure 3 shows a plan view and a vertical cross-section of the three-dimensional domain.

Two extraction wells are located at $(x_{well,1}, y_{well,1})=(2,000 \text{ m}, 900 \text{ m})$ and $(x_{well,2}, y_{well,2})=(1,610 \text{ m}, 470 \text{ m})$. The first well is screened over the entire depth of the aquifer, whereas the second well is screened only in the upper sediment layer to a depth of 10 m. The fully screened well has a pumping rate of 30 L s⁻¹, and the partially penetrating well of 15 L s⁻¹, respectively. Two groundwater observation wells are located upstream of the two pumping wells at $(x_{obs,1}, y_{obs,1})=(1,800 \text{ m}, 900 \text{ m})$ and $(x_{obs,2}, y_{obs,2})=(1,400 \text{ m}, 470 \text{ m})$.

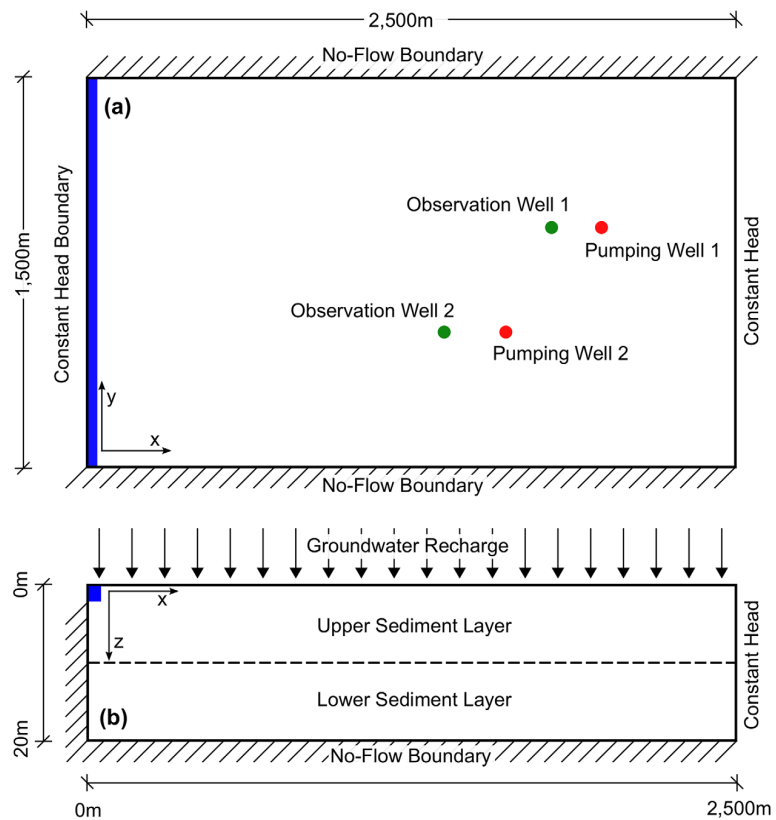


Figure 3. General setup of the three-dimensional application.

Nitrate and oxygen concentrations are introduced by groundwater recharge from the top and by bank infiltration at the left side of the model domain. The recharging water is assumed to have already passed the unsaturated zone above the aquifer. Input concentrations of nitrate and oxygen therefore represent conditions at the bottom of the root zone of intensively cultivated crops. The nitrate and oxygen concentrations in groundwater recharge were set to $50 \text{ mg}(\text{NO}_3^-) \text{ L}^{-1}$ and $10 \text{ mg}(\text{O}_2) \text{ L}^{-1}$, respectively. The nitrate and oxygen concentrations of the infiltrating river water were set to $30 \text{ mg}(\text{NO}_3^-) \text{ L}^{-1}$ and $7 \text{ mg}(\text{O}_2) \text{ L}^{-1}$ (see also Table 2).

The aquifer consists of two heterogeneous sediment layers. They differ in their mean hydraulic conductivity and NOM-content, which also implies differences in their denitrification potential. The upper sediment layer extends from the top of the model domain to a depth of 10 m, the lower from a depth of 10–20 m, where the aquifer is underlain by impervious material. The log-hydraulic conductivity in the two layers is assumed to be independent, autocorrelated, multi-Gaussian random-space functions with parameters listed in Table 2.

The organic-carbon content is assumed to be correlated to the hydraulic conductivity. Areas with a high hydraulic conductivity are assigned a low organic-carbon content, whereas areas with a low hydraulic conductivity are assigned a high organic-carbon content, following the rationale that fines have higher natural-organic-matter concentrations. The organic-carbon content is computed by:

$$c_{NOM} = (\log_{10}(K) + \zeta) \cdot A \tag{28}$$

in which c_{NOM} is the NOM concentration [$\text{M}_C \text{M}_{\text{soil}}^{-1}$], K [LT^{-1}] is the hydraulic conductivity, ζ is an independent multi-Gaussian random field with zero mean, variance of 0.025, and correlation lengths of 30, 20, and 2 m in the x , y , and z direction, respectively. $A = -50 \text{ mol}_C \text{ m}_{\text{soil}}^{-3}$ is a scaling parameter. Figure 4 visualizes the spatially distributed material properties of a single realization. Figure 4a shows the log-hydraulic conductivity, Figure 4b the organic-carbon content, and Figure 4c the corresponding relative reactivity according to equation (27). Because the organic-carbon content is used up over time, the relative reactivity decreases

Table 2
Parameters of the Three-Dimensional Application

Symbol	Meaning	Value
Geometric parameters		
$L \times W \times T$	Length \times width \times depth of domain	2,500 m \times 1,500 m \times 20 m
$n_x \times n_y \times n_z$	Number of cells in x, y, z direction	250 \times 150 \times 20
Hydraulic parameters		
\bar{K}_{lower}	Geometric mean hydraulic conductivity of lower sedimentary layer	1×10^{-2} m/s
\bar{K}_{upper}	Geometric mean hydraulic conductivity of upper sedimentary layer	1×10^{-3} m/s
θ	Porosity	0.35
Geostatistical parameters		
λ_K	Correlation length for log-hydraulic conductivity ($x \times y \times z$)	250 m \times 150 m \times 2 m
$\sigma_{\ln(K)}^2$	Variance of log-hydraulic conductivity	0.8
Inflow concentrations		
	Oxygen (mg/L)	Nitrate (mg/L)
Land surface	10	50
River	7	30

with an intricate pattern reflecting the position of zones with high turnover. Figure 4 shows the initial state of a single realization. The difference in the two sediment layers can be clearly seen. The upper layer is more reactive and has a lower hydraulic conductivity, whereas the lower sedimentary layer has a higher hydraulic conductivity and a lower reactivity.

4.2. Implementation and Numerical Methods

The three-dimensional domain was discretized in 10 m \times 10 m \times 1 m grid cells, leading to a total of 750,000 computational cells. The modeling framework is written in Matlab. We generated realizations of $\ln(K)$ and ξ according to equation (28) using the spectral method of Dietrich and Newsam (1993). Steady-state groundwater heads are calculated with MODFLOW-NWT (Niswonger et al., 2011). We used Pollock's semi-analytical method (Pollock, 1988) for particle tracking in Matlab on the computer's graphics processing unit (GPU) using NVIDIA CUDA (Kirk et al., 2007). The generation of autocorrelated fields of hydraulic conductivity and bioavailable organic-carbon content is also done within Matlab. We back-tracked 10,000 particles in total from the two extraction wells, the two observation wells, and the outflow of the domain. All particles ended either at the top of the model domain or at the river at the left side. Particles starting at the pumping wells were distributed proportional to the discharge around the extraction wells, leading to a nonuniform distribution of particles. Also the extraction rates were set proportional to the transmissivity of the surrounding aquifer, guaranteeing appropriate flux-weighting of individual particles. Particles in the observation well were placed at the same location in every ensemble run. In observation well 1, the particle was released at a depth of $z_{p1} = 15$ m, and in observation well 2 at $z_{p2} = 5$ m.

In each of the 200 ensemble runs, we generated a new random field of hydraulic conductivity and a new random multi-Gaussian field as perturbation of the initial organic-carbon content, using the geostatistical and geometric parameters listed in Table 2. As a consequence, each model run had a different flow field, a different initial NOM distribution, and a different distribution of the relative reactivity, enabling us to study the uncertainty in nitrate breakthrough due to the uncertain spatial variability in the geochemical and hydraulic parameters. In all realizations, the travel-time increment was set to 1 month. The simulation time for every run was 200 years. For the presented three-dimensional problem, the total clock-time on a standard computer (IntelCore i7 CPU @ 3.60 GHz, 16GB RAM) with an NVIDIA GeForce GTX 970 graphics card for a single run was in total approximately 20 min.

4.3. Results

4.3.1. Decreasing Denitrification Potential Along a Single Streamline

Figure 5 shows a single stream line in a single realization. The streamline originates at the surface of the model close to the river and ends in the extraction well at $x_{well,2} = 1,610$ m. The markers indicate travel-time increments of 1 month each. Larger spatial distances between the markers imply lower velocities and shorter distances higher velocities, reflecting differences in hydraulic conductivity or boundary conditions.

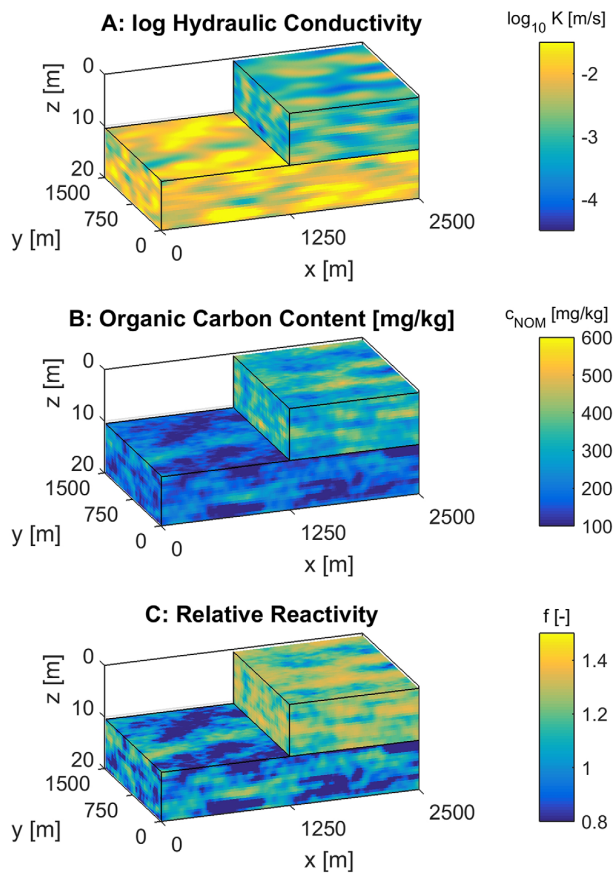


Figure 4. Parameter distribution at the initial time in a single realization of the three-dimensional domain: (a) log-hydraulic conductivity; (b) organic-carbon content; and (c) relative reactivity.

Close to the pumping well the velocity increases significantly. With a travel-time increment of 1 month, the last meters upstream of the well are all in one increment.

Figure 6 shows spatial profiles of concentrations along the streamline shown in Figure 5. The individual lines represent time points that are 25 years apart from each other. Figures 6a–6c depict the organic-carbon content, the dissolved oxygen, and the nitrate concentration, respectively. The gray lines in each plot indicate the travel-time increments. It can be seen that the organic-carbon content is gradually used up with time along the streamline. The first-order rate coefficient of nitrate under reference conditions is so small that at even at early times already $\approx 10 \text{ mg L}^{-1}$ nitrate reaches the well, implying NOM depletion along the entire streamline. Oxygen, by contrast, can only be observed up to a certain distance along the streamline which changes over time.

Note that Figure 6 shows spatial profiles rather than profiles with respect to travel time. The velocity in the first 200 m is particularly slow so that it appears as if the oxygen front is not moving for the first 75 years, when the NOM-concentration in the first section is permanently decreasing. Over this time period, the nitrate profile changes little, too. Once the oxygen front has passed the first low-velocity zone, it moves more quickly along the streamline and the nitrate concentrations in the well starts increasing. There is a second low-velocity region between $\approx 1,000 \text{ m}$ and $\approx 1,500 \text{ m}$ in this realization. At the time when the oxygen front reaches this zone, however, the NOM concentration has already been significantly decreased due to denitrification so that the dissolved-oxygen front is not retarded as strongly as in the initial section. After about 200 years, the bioavailable organic carbon is almost completely gone along the entire streamline, and dissolved oxygen breaks through at the extraction well. The full breakthrough of nitrate is about 25 years earlier. That is, for this particular streamline, the time series of nitrate

in the well is characterized by 75 years of almost constant low values, followed by 100 years of steady increase.

4.3.2. Ensemble Runs

In Figure 7 we present ensemble-based time-series of nitrate and dissolved-oxygen concentrations on three different observation scales: (1) a single observation location (i.e., a point), (2) a pumping well (i.e., a line), and (3) at the outflow of the domain (i.e., a cross section/plane). Figure 7 shows the median over 200 ensemble members as solid red lines, as well as the 5th, 10th, 15th, 20th, 25th, 75th, 80th, 85th, 90th, and 95th percentile. Areas where the percentiles show a higher density have a higher probability whereas areas with a lower density indicate a lower probability. After about 80 years, the percentiles of DO and nitrate

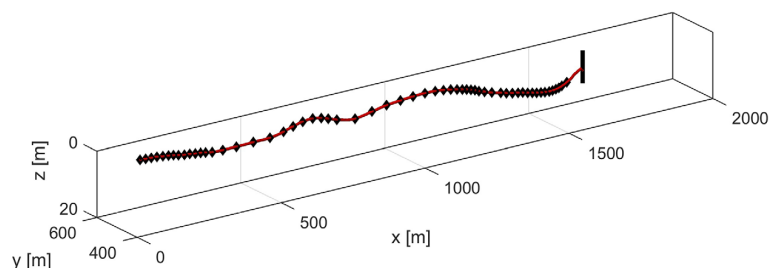


Figure 5. Example of a single streamline (red) in the three-dimensional application. Markers: boundaries of travel-time increments of one month and black line: extraction well.

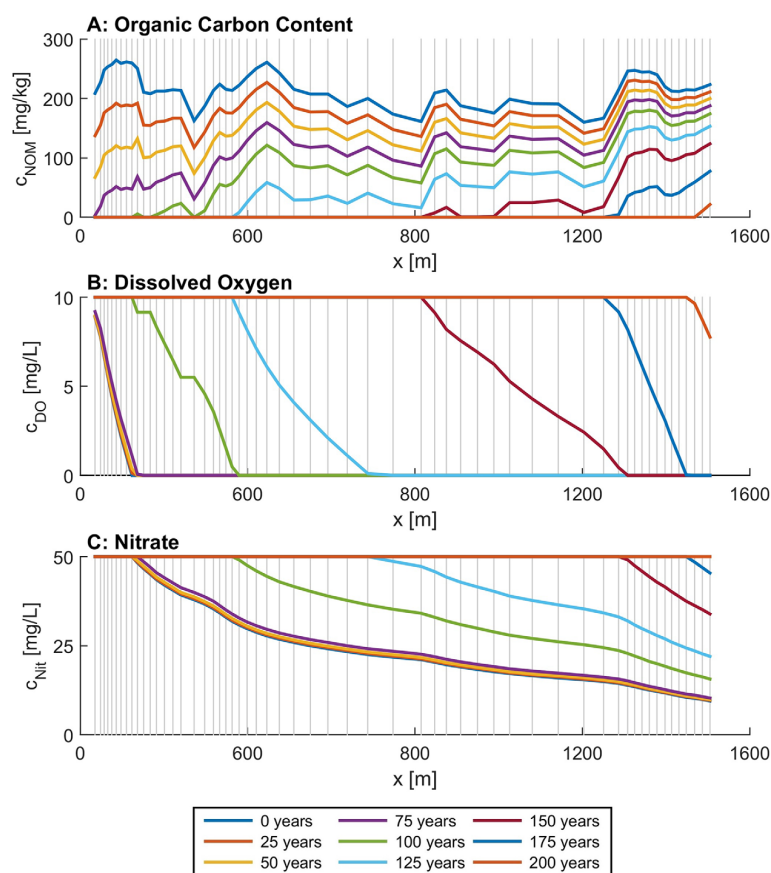


Figure 6. Length profiles of concentrations along the single streamline depicted in Figure 5. (a) Natural organic matter in the aquifer matrix; (b) dissolved oxygen concentration; and (c) nitrate concentration. One concentration profile per 25 years is shown. Gray lines indicate travel time increments of 1 month.

concentration in the observation well (Figures 71 and 7b1) are aligned at $30 \text{ mg}(\text{NO}_3^-) \text{ L}^{-1}$ and $50 \text{ mg}(\text{NO}_3^-) \text{ L}^{-1}$, and $7 \text{ mg}(\text{DO}) \text{ L}^{-1}$ and $10 \text{ mg}(\text{DO}) \text{ L}^{-1}$, respectively. This is due to the point observation in the observation well. The streamline either ends up at the surface or at the river, a concentration in between is not possible. In the pumping well and the outflow, several streamlines are considered leading to a mixed concentration, potentially resulting in a final concentration between the two inflow concentrations.

The uncertainty of concentrations very clearly depends on the observation scale. The concentrations in the observation well are point measurements that are highly sensitive to the spatially variable hydraulic and geochemical parameters. In essence, predictions for such a point measurement are meaningless for practical applications unless the hydraulic and geochemical parameters are constrained by additional information. In case of dissolved oxygen, the chosen uncertainty range covers at $t = 75$ years the entire concentration range between no oxygen and the concentration in the inflow. Also the uncertainty of the nitrate concentration is very large, making useful predictions impossible. The concentrations in the pumping well and the outflow, by contrast, are averaged over a larger volume flux, leading to a significantly smaller uncertainty range. In case of nitrate in the pumping well, the range reaches a maximum of $9 \text{ mg}(\text{NO}_3^-) \text{ L}^{-1}$ between the 15th and 85th percentile. This percentile range is chosen as they are close to the 16th and 84th percentile that represent ± 1 standard deviation in case of a normal distribution. This effect is even more significant when considering the outflow of the domain reaching a maximum range of only $2 \text{ mg}(\text{NO}_3^-) \text{ L}^{-1}$ between the 15th and 85th percentile. Here, the uncertainty range is smaller than in the case of the pumping well. If the averaging scale is large enough, ergodicity is reached and uncertainty due to small-scale spatial variability disappears. This behavior is well known from previous studies (e.g., Schwede

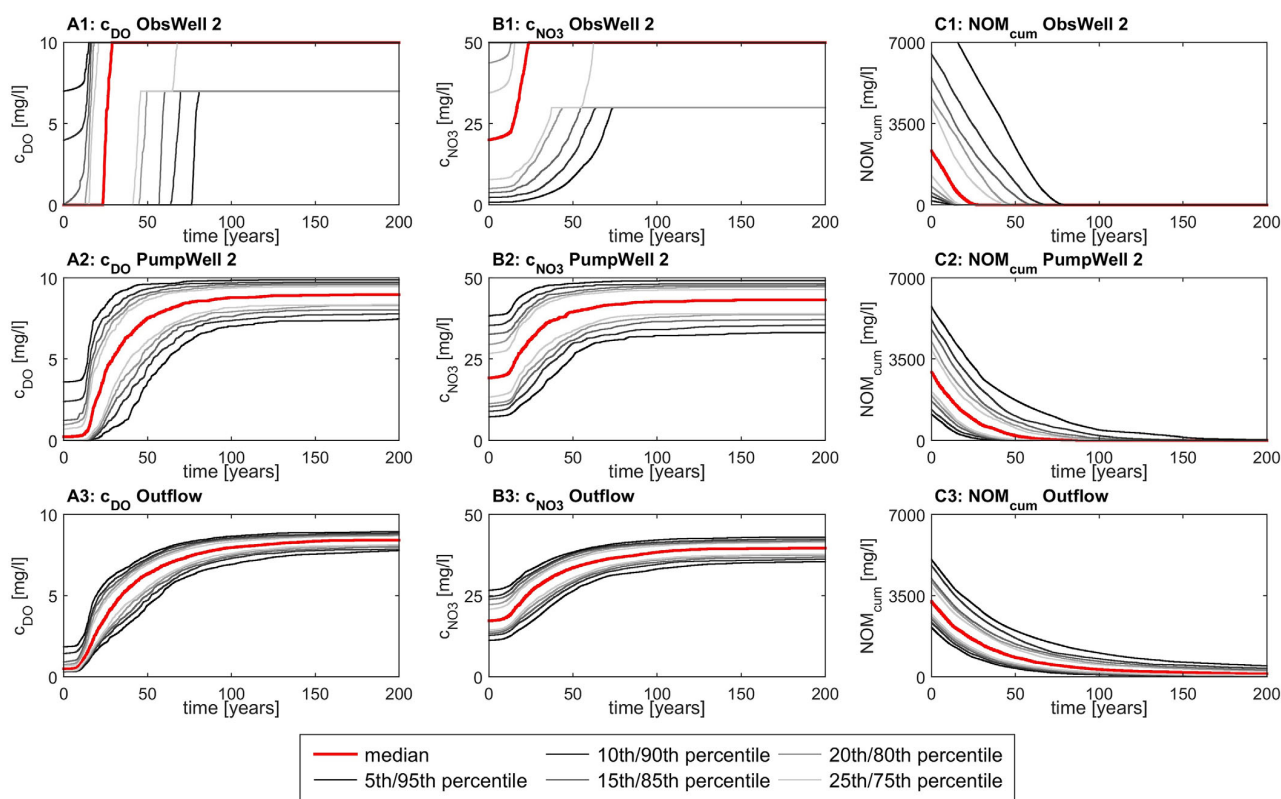


Figure 7. Ensemble time series at different observation points in the three-dimensional application. Red lines: median of 200 ensemble runs; gray lines: 5th, 10th, 15th, 20th, 25th, 75th, 80th, 85th, 90th, 95th percentile. (row 1) Observations in observation well 2 at a depth of 10 m (single point observation); (row 2) observations in pumping well 2 (line observation); (row 3) observations in the outflow plane of the domain (cross section/plane observation). (column A) Dissolved-oxygen (DO) concentration c_{DO} ; (column B) nitrate concentration c_{NO_3} ; and (column C) mean cumulative organic carbon NOM_{cum} along the streamlines leading to point/line/plane of observation.

et al., 2008, and references therein). Of course, the uncertainty of concentrations averaged over intermediate scales, such as those covered by a pumping well, depends on the variance and integral scales of chemical (and hydraulic) heterogeneity, which is rarely assessed in detail.

5. Discussion and Conclusions

The proposed modeling framework accounts for a decreasing pool of reaction partners in the aquifer matrix within a simplified, yet nonlinear, travel-time-based modeling framework of reactive transport. In our application, we consider the reduction of dissolved oxygen and nitrate in reducing aquifers, targeting the breakthrough of nitrate in drinking-water wells, but the framework could also be applied to cases in which constituents of the aquifer matrix act as electron acceptors and the dissolved compounds as electron donors (e.g., oxidation of hydrocarbons by ferric iron (hydr)oxides). The underlying principles would be the same. By implementing several conceptual simplifications, among them the concept of relative reactivity, the framework is computationally so efficient that a stochastic analysis using Monte-Carlo simulations becomes possible without relying on unrealistic first-order decay of nitrate in aquifers. We show the applicability for the concept of cumulative relative reactivity by Loschko et al. (2016). However, the proposed method of discretizing trajectories by travel time increments can also be applied to other streamline-based modeling approaches.

In a one-dimensional test application, we have tested the validity of the conceptual simplifications and obtained a potential functional relationship between organic carbon content C_{NOM}^* and relative reactivity f , which is the key parameter in this study. We have used the function relating the relative

reactivity to the NOM-content, derived in the 1-D application, in a three-dimensional test case. In the latter, we simulated the decreasing denitrification potential of an artificial aquifer over 200 years within a stochastic framework. We could confirm that the predictive capabilities are higher at pumping wells or at the outflow of the domain than at single observation points, because reactive-species concentrations observed in pumping wells and in the outflow plane of the model domain, are flux integrated.

In this study, we derived a potential relation between the organic carbon content and the relative reactivity in the case of aerobic respiration and denitrification. The derived relationship $f(c_{NOM}^*)$ depends on conceptual and parameter choices of the more detailed model used for its calibration, so that we cannot claim generality. For field applications, experimental data on the dependence of the NOM's reactivity on its content in the aquifer matrix would be highly beneficial. Of course, aquifers may contain other electron donors (e.g., ferrous-iron bearing minerals such as pyrite, biotite, siderite, or magnetite) suitable for denitrification that are likely to have a different degradation behavior and will lead to other values of relative reactivity for identical electron content. Thus, the relationship between the electron-donor content of the matrix and the relative reactivity needs to be evaluated in every specific application.

The travel-time-based approach of accounting for a decreasing reaction potential of the aquifer matrix requires that the spatial pattern of travel times does not change in the course of the simulation. This requirement is met if flow is at steady state or a time-invariant velocity field is multiplied with a spatially uniform transient multiplier (Sanz-Prat et al., 2016b; Selroos et al., 2013). If this simplification is not valid, the model problem can only be solved using a spatially fully explicit framework, which comes at higher computational costs and involves issues of numerical dispersion. Accounting for a dynamic change of inflow concentrations, by contrast, poses no challenge to the proposed framework.

For an application to real world problems, we see the biggest challenges in obtaining sufficient data about the aquifer. Apart from the hydraulic parameters, such as hydraulic conductivity, groundwater recharge, and other boundary conditions, the content of the reaction partner in the matrix has to be estimated and linked to the relative reactivity. Data to obtain these values are often scarce and difficult to gather. We are not aware of field studies targeting the spatial variability of the aquifer's organic carbon content or similar reaction partners on the aquifer scale. Several modeling studies have assessed the potential interplay between physical and chemical heterogeneity using educated guesses regarding the chemical heterogeneity and the potential correlation to its physical counterpart. Clearly more field data on the chemical heterogeneity to be expected in certain geological settings are needed. Once at least bounds of uncertainty and correlation scales are known, the presented stochastic framework can be used to project these uncertainties to reactive-species concentrations. We conclude that in general the transfer to a real-world aquifer system is possible once sufficient data are collected, but this is beyond the scope of the present study.

Appendix A: Two-Dimensional Test Case on the Validity of the Approach

To test the validity of the presented travel-time-based approach, we set up a two-dimensional heterogeneous test case. The study domain is $50 \text{ m} \times 25 \text{ m}$ with a resolution of $0.1 \text{ m} \times 0.1 \text{ m}$. The log-hydraulic conductivity was generated as random multi-Gaussian field with an exponential covariance model with variance of 1.0, the geometric mean of hydraulic conductivity was 10^{-3} m/s . The spatial distribution of the immobile NOM concentration was generated by adding a multi-Gaussian random field to the generated hydraulic conductivity with variance of 0.25, correlation length of 5 in both directions and a mean NOM concentration of $0.05 \text{ mol}_C/\text{kg}$. Figure A1a shows the log hydraulic conductivity field and Figure A1d the spatial distribution of immobile NOM. The correlation is visually observable. High values of hydraulic conductivity tend to have lower concentration of immobile NOM and vice versa.

No flow was allowed across the top and bottom boundaries of the domain, whereas the left and right boundaries were assigned fixed hydraulic heads with a total head difference of 0.2 m. Groundwater flow was solved by the finite element method with bilinear elements. We generated a streamline-oriented grid with 250×500 elements by the dual formulation of Frind and Matanga (1985) and Cirpka et al. (1999a) with 250 streamtubes separated into 500 sections each. The resulting flow net is depicted in Figure A1c.

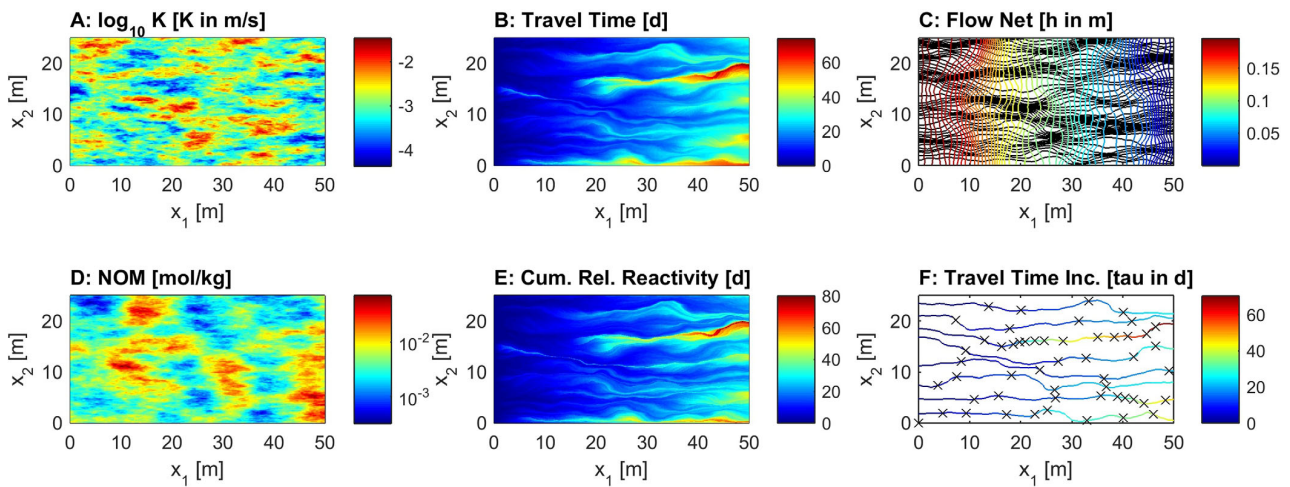


Figure A1. Two-dimensional test case. (a) Spatial distribution of log-hydraulic conductivity; (b) mean groundwater age for strictly advective transport; (c) flow net (colored lines: heads; black lines: streamlines); (d) Spatial distribution of immobile NOM; (e) cumulative relative reactivity for strictly advective transport; (f) selected streamlines with travel time increments (colored lines: streamlines with travel time; crosses: travel time increments of 5 days).

We computed the mean travel time distribution for strictly advective transport with the mean groundwater-age equation of Goode (1996) and the mean cumulative relative reactivity for strictly advective transport using the cell-centered finite volume method on the streamline-oriented grid (Cirpka et al., 1999b). Figure A1b shows the advective travel times and Figure A1e shows the cumulative relative reactivity.

We simulated transient transport involving aerobic respiration and denitrification with two different models. The inflow concentrations were constant (8 mg/L for dissolved oxygen and 62 mg/L for nitrate). The first model solves the spatially explicit advection-dispersion-reaction equation (1) with a fully implicit approach using Newton-Raphson iterations. The pore diffusion coefficient was set to $D_p = 3 \times 10^{-10} \text{ m}^2/\text{s}$, the longitudinal dispersivity $\alpha_l = 0.01 \text{ m}$, and the transverse dispersivity $\alpha_t = 0.001 \text{ m}$. The second model is the simplified model using the cumulative relative reactivity and travel time increments derived in this paper (see section 2.2.3). Figure A1f shows selected streamlines in which the color scale refers to travel time. The marks indicate the travel-time increments of 5 days. The influence of the travel time on the spatial discretization can be seen: streamlines with overall small travel-time values (such as the fifth streamline from the top) have fewer travel-time increments than those with overall large travel-time values (such as the third streamline from the top). The simulation time was 100 years. For the computation of the relative reactivity, we used equation (27).

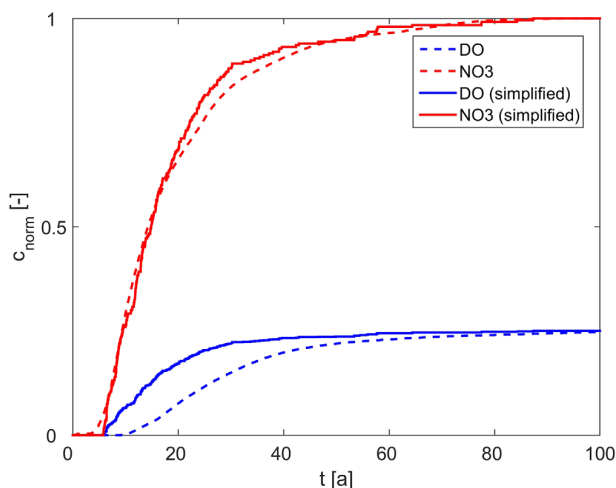


Figure A2. Comparison of the two-dimensional test case. Breakthrough curves of dissolved oxygen and nitrate concentrations in the outflow of the domain for a single realization over 100 years. Dashed lines: spatially explicit advective-dispersive-reactive model. Solid lines: simplified model using cumulative reactive reactivity with travel time increments.

Figure A2 shows the breakthrough curves of dissolved oxygen (blue) and nitrate (red) in the outflow of the domain for the spatially explicit model (dashed lines) and the simplified model (solid lines) for the single realization shown in Figure A1. The simplified model is able to predict the breakthrough of nitrate in the outflow quite well. For dissolved oxygen, the simplified model overestimates the concentration. In both cases, the immobile NOM concentration of the artificial aquifer is totally depleted within 100 years.

This test confirms previous results on the validity of travel and exposure-time-based models Sanz-Prat et al. (2015, 2016a, 2016b) as well as of the concept of cumulative relative reactivity Loschko et al. (2016) for bioactive transport in heterogeneous media.

Acknowledgments

This research was funded by the Deutsche Forschungsgemeinschaft (DFG) in the framework of the Research Training Group GRK1829 "Integrated Hydrosystem Modelling" of the Universities of Tübingen, Hohenheim, and Waterloo. Additional funding is provided by DFG within the Collaborative Research Center SFB 1253 "CAMPOS - Catchments as Reactors". The authors thank Tim Ginn and two anonymous reviewers for their meaningful comments helping to improve the paper. The simulation results of the two test cases are available as matlab binary data files (*.mat) under <https://doi.org/10.6084/m9.figshare.5715571>.

References

- Almasri, M. N., & Kaluarachchi, J. J. (2007). Modeling nitrate contamination of groundwater in agricultural watersheds. *Journal of Hydrology*, 343(3), 211–229. <https://doi.org/10.1016/j.jhydrol.2007.06.016>
- Appelo, C. A. J., & Postma, D. (2004). *Geochemistry, groundwater, and pollution*. Boca Raton, FL: CRC Press. <https://doi.org/10.1201/9781439833544>
- Böhlke, J.-K. (2002). Groundwater recharge and agricultural contamination. *Hydrogeology Journal*, 10(1), 153–179. <https://doi.org/10.1007/s10040-001-0183-3>
- Bourauoi, F., Grizzetti, B., & Aloe, A. (2011). *Long term nutrient loads entering European seas*. Ispra, Italy: European Commission Joint Research Centre, Institute for Environment and Sustainability.
- Bradley, P., Fernandez, M. Jr., & Chapelle, F. (1992). Carbon limitation of denitrification rates in an anaerobic groundwater system. *Environmental Science Technology*, 26(12), 2377–2381. <https://doi.org/10.1021/es00036a007>
- Cirpka, O. A., Frind, E. O., & Helmig, R. (1999a). Streamline-oriented grid generation for transport modelling in two-dimensional domains including wells. *Advances in Water Resources*, 22(7), 697–710. [https://doi.org/10.1016/S0309-1708\(98\)00050-5](https://doi.org/10.1016/S0309-1708(98)00050-5)
- Cirpka, O. A., Frind, E. O., & Helmig, R. (1999b). Numerical methods for reactive transport on rectangular and streamline-oriented grids. *Advances in Water Resources*, 22(7), 711–728. [https://doi.org/10.1016/S0309-1708\(98\)00051-7](https://doi.org/10.1016/S0309-1708(98)00051-7)
- Cirpka, O. A., & Kitanidis, P. K. (2000). An advective-dispersive stream tube approach for the transfer of conservative-tracer data to reactive transport. *Water Resources Research*, 36(5), 1209–1220. <https://doi.org/10.1029/1999WR900355>
- Cvetkovic, V., Cheng, H., & Wen, X.-H. (1996). Analysis of nonlinear effects on tracer migration in heterogeneous aquifers using Lagrangian travel time statistics. *Water Resources Research*, 32(6), 1671–1680. <https://doi.org/10.1029/96WR00278>
- Cvetkovic, V., & Dagan, G. (1994). Transport of kinetically sorbing solute by steady random velocity in heterogeneous porous formations. *Journal of Fluid Mechanics*, 265, 189–215. <https://doi.org/10.1017/S0022112094000807>
- Cvetkovic, V., & Dagan, G. (1996). Reactive transport and immiscible flow in geological media. Part II: Applications. *Proceedings of the Royal Society London Series A: Mathematical, Physical and Engineering Science*, 452(1945), 303–328. <https://doi.org/10.1098/rspa.1996.0017>
- Dagan, G. (2002). An overview of stochastic modeling of groundwater flow and transport: From theory to applications. *EOS, Transactions American Geophysical Union*, 83(53), 621–625. <https://doi.org/10.1029/2002EO000421>
- Dagan, G., & Bresler, E. (1979). Solute dispersion in unsaturated heterogeneous soil at field scale: I. Theory. *Soil Science Society of America Journal*, 43, 461–467. <https://doi.org/10.2136/sssaj1979.03615995004300030008x>
- Dagan, G., & Cvetkovic, V. (1996). Reactive transport and immiscible flow in geological media. i. general theory. *Proceedings of the Royal Society London Series A: Mathematical, Physical and Engineering Science*, 452(1945), 285–301. <https://doi.org/10.1098/rspa.1996.0016>
- D'Haene, K., Moreels, E., Neve, S. D., Daguilar, B. C., Boeckx, P., Hofman, G., et al. (2003). Soil properties influencing the denitrification potential of flemish agricultural soils. *Biology and Fertility of Soils*, 38(6), 358–366. <https://doi.org/10.1007/s00374-003-0662-x>
- Dietrich, C. R., & Newsam, G. N. (1993). A fast and exact method for multidimensional Gaussian stochastic simulations. *Water Resources Research*, 29(8), 2861–2869. <https://doi.org/10.1029/93WR01070>
- Drury, C., McKenney, D., & Findlay, W. (1991). Relationships between denitrification, microbial biomass and indigenous soil properties. *Soil Biology and Biochemistry*, 23(8), 751–755. [https://doi.org/10.1016/0038-0717\(91\)90145-A](https://doi.org/10.1016/0038-0717(91)90145-A)
- DVGW (2015). *DVGW-information Wasser Nr. 85 Stickstoffumsatz im Grundwasser*. Bonn: DVGW
- Eschenbach, W., & Well, R. (2013). Predicting the denitrification capacity of sandy aquifers from shorter-term incubation experiments and sediment properties. *Biogeosciences*, 10(2), 1013–1035. <https://doi.org/10.5194/bg-10-1013-2013>
- Feyen, J., Jacques, D., Timmerman, A., & Vanderborght, J. (1998). Modelling water flow and solute transport in heterogeneous soils: A review of recent approaches. *Journal of Agricultural Engineering Research*, 70(3), 231–256. <https://doi.org/10.1006/jaer.1998.0272>
- Frei, S., & Peiffer, S. (2016). Exposure times rather than residence times control redox transformation efficiencies in riparian wetlands. *Journal of Hydrology*, 543, 182–196. <https://doi.org/10.1016/j.jhydrol.2016.02.001>
- Frind, E. O., & Matanga, G. B. (1985). The dual formulation of flow for contaminant transport modeling 1. Review of theory and accuracy aspects. *Water Resources Research*, 21(2), 159–169. <https://doi.org/10.1029/WR021i002p00159>
- Galloway, J. N., F. J., Dentener, D. G., Capone, E. W., Boyer, R. W., Howarth, S. P., Seitzinger, G. P., et al. (2004). Nitrogen cycles: Past, present, and future. *Biogeochemistry*, 70(2), 153–226. <https://doi.org/10.1007/s10533-004-0370-0>
- Ginn, T. R. (1999). On the distribution of multicomponent mixtures over generalized exposure time in subsurface flow and reactive transport: Foundations, and formulations for groundwater age, chemical heterogeneity, and biodegradation. *Water Resources Research*, 35(5), 1395–1407. <https://doi.org/10.1029/1999WR900013>
- Ginn, T. R. (2000a). On the distribution of multicomponent mixture over generalized exposure time in subsurface flow and reactive transport: Theory and formulations for residence-time-dependent sorption/desorption with memory. *Water Resources Research*, 36(10), 2885–2893. <https://doi.org/10.1029/2000WR900170>
- Ginn, T. R. (2000b). On the distribution of multicomponent mixtures over generalized exposure time in subsurface flow and reactive transport: Batch and column applications involving residence-time distribution and non-Markovian reaction kinetics. *Water Resources Research*, 36(10), 2895–2903. <https://doi.org/10.1029/2000WR900171>
- Ginn, T. R. (2001). Stochastic-convective transport with nonlinear reactions and mixing: Finite stream tube ensemble formulation for multicomponent reaction systems with intra-stream tube dispersion. *Journal of Contaminant Hydrology*, 47(1–2), 1–28. [https://doi.org/10.1016/S0169-7722\(00\)00167-4](https://doi.org/10.1016/S0169-7722(00)00167-4)
- Ginn, T. R., Simmons, C. S., & Wood, B. D. (1995). Stochastic-convective transport with nonlinear reaction: Biodegradation with microbial growth. *Water Resources Research*, 31(11), 2689–2700. <https://doi.org/10.1029/95WR02179>
- Glassley, W. E., Simmons, A. M., & Kercher, J. R. (2002). Mineralogical heterogeneity in fractured, porous media and its representation in reactive transport models. *Applied Geochemistry*, 17(6), 699–708. [https://doi.org/10.1016/S0883-2927\(02\)00031-8](https://doi.org/10.1016/S0883-2927(02)00031-8)
- Goode, D. J. (1996). Direct simulation of groundwater age. *Water Resources Research*, 32(2), 289–296. <https://doi.org/10.1029/95WR03401>
- Green, C. T., Jurgens, B. C., Zhang, Y., Starn, J. J., Singleton, M. J., & Esser, B. K. (2016). Regional oxygen reduction and denitrification rates in groundwater from multi-model residence time distributions, San Joaquin Valley, USA. *Journal of Hydrology*, 543(A, SI), 155–166. <https://doi.org/10.1016/j.jhydrol.2016.05.018>
- Hiscock, K., Lloyd, J., & Lerner, D. (1991). Review of natural and artificial denitrification of groundwater. *Water Research*, 25(9), 1099–1111. [https://doi.org/10.1016/0043-1354\(91\)90203-3](https://doi.org/10.1016/0043-1354(91)90203-3)
- Jang, E., He, W., Savoy, H., Dietrich, P., Kolditz, O., Rubin, Y., et al. (2017). Identifying the influential aquifer heterogeneity factor on nitrate reduction processes by numerical simulation. *Advances in Water Resources*, 99, 38–52. <https://doi.org/10.1016/j.advwatres.2016.11.007>
- Jury, W. A. (1982). Simulation of solute transport using a transfer function model. *Water Resources Research*, 18(2), 363–368. <https://doi.org/10.1029/WR018i002p00363>

- Kaluarachchi, J. J., Cvetkovic, V., & Berglund, S. (2000). Stochastic analysis of oxygen-and nitrate-based biodegradation of hydrocarbons in aquifers. *Journal of Contaminant Hydrology*, 41(3), 335–365. [https://doi.org/10.1016/S0169-7722\(99\)00072-8](https://doi.org/10.1016/S0169-7722(99)00072-8)
- Kinzelbach, W., Schäfer, W., & Herzer, J. (1991). Numerical modeling of natural and enhanced denitrification processes in aquifers. *Water Resources Research*, 27(6), 1123–1135. <https://doi.org/10.1029/91WR00474>
- Kirk, D. (2007). Nvidia CUDA software and GPU parallel computing architecture. In *ISMM* (Vol. 7, pp. 103–104). New York, NY: ACM. <https://doi.org/10.1145/1296907.1296909>
- Korom, S. F. (1992). Natural denitrification in the saturated zone: A review. *Water Resources Research*, 28(6), 1657–1668. <https://doi.org/10.1029/92WR00252>
- Lasserre, F., Razack, M., & Banton, O. (1999). A GIS-linked model for the assessment of nitrate contamination in groundwater. *Journal of Hydrology*, 224(3), 81–90. [https://doi.org/10.1016/S0022-1694\(99\)00130-4](https://doi.org/10.1016/S0022-1694(99)00130-4)
- Ledoux, E., Gomez, E., Monget, J.-M., Viavattene, C., Viennot, P., Ducharme, A., et al. (2007). Agriculture and groundwater nitrate contamination in the seine basin. The STICS–MODCOU modelling chain. *Science of the Total Environment*, 375(1), 33–47. <https://doi.org/10.1016/j.scitotenv.2006.12.002>
- Lohse, K. A., Brooks, P. D., McIntosh, J. C., Meixner, T., & Huxman, T. E. (2009). Interactions between biogeochemistry and hydrologic systems. *Annual Reviews of Environment and Resources*, 34, 65–96. <https://doi.org/10.1146/annurev.enviro.33.031207.111141>
- Loschko, M., Wöhling, T., Rudolph, D. L., & Cirpka, O. A. (2016). Cumulative relative reactivity: A concept for modeling aquifer-scale reactive transport. *Water Resources Research*, 52, 8117–8137. <https://doi.org/10.1002/2016WR019080>
- Luo, J. (2012). Travel-time based reactive transport modeling for in situ subsurface reactor. In *Delivery and mixing in the subsurface* (pp. 117–138). New York, NY: Springer. https://doi.org/10.1007/978-1-4614-2239-6_5
- Mayer, K. U., Frind, E. O., & Blowes, D. W. (2002). Multicomponent reactive transport modeling in variably saturated porous media using a generalized formulation for kinetically controlled reactions. *Water Resources Research*, 38(9), 1174. <https://doi.org/10.1029/2001WR000862>
- Mellage, A., Eckert, D., Grösbacher, M., Inan, A. Z., Cirpka, O. A., & Griebler, C. (2015). Dynamics of suspended and attached aerobic toluene degraders in small-scale flow-through sediment systems under growth and starvation conditions. *Environmental Science Technology*, 49(12), 7161–7169. <https://doi.org/10.1021/es5058538>
- Middelburg, J. J., Soetaert, K., Herman, P. M. J., & Heip, C. H. R. (1996). Denitrification in marine sediments: A model study. *Global Biogeochemistry Cycles*, 10(4), 661–673. <https://doi.org/10.1029/96GB02562>
- Molénat, J., & Gascuel-Oudou, C. (2002). Modelling flow and nitrate transport in groundwater for the prediction of water travel times and of consequences of land use evolution on water quality. *Hydrological Processes*, 16(2), 479–492. <https://doi.org/10.1002/hyp.328>
- Niswonger, R., Panday, S., & Ibaraki, M. (2011). *MODFLOW-NWT: A Newton formulation for modflow-2005* (U.S. Geol. Surv. Tech. Meth., 6-A37, 44 p.). Reston, VA: U.S. Geological Survey.
- Nobile, F., Tempone, R., & Webster, C. G. (2008). A anisotropic sparse grid stochastic collocation method for partial differential equations with random input data. *SIAM Journal on Numerical Analysis*, 46(5), 2309–2345. <https://doi.org/10.1137/060663660>
- Ocampo, C. J., Oldham, C. E., & Sivapalan, M. (2006). Nitrate attenuation in agricultural catchments: Shifting balances between transport and reaction. *Water Resources Research*, 42, W01408. <https://doi.org/10.1029/2004WR003773>
- Pacheco, J., Marín, L., Cabrera, A., Steinich, B., & Escolero, O. (2001). Nitrate temporal and spatial patterns in 12 water-supply wells, Yucatan, Mexico. *Environmental Geology*, 40(6), 708–715. <https://doi.org/10.1007/s002540000180>
- Pätsch, M., Walther, W., Reinstorf, F., & Weller, D. (2003). Research program and development of a suitable tool to minimize nitrogen emissions into groundwater of a pleistocene aquifer, northern low plain of Germany. In *Institut für Grundwasserwirtschaft & Institut für Wasserchemie, Technische Universität Dresden: Diffuse input of chemicals into soil and groundwater-assessment and management, Proceedings Institute of Groundwater Management*, 3, 217–225.
- Pollock, D. W. (1988). Semianalytical computation of path lines for finite-difference models. *Groundwater*, 26(6), 743–750. <https://doi.org/10.1111/j.1745-6584.1988.tb00425.x>
- Prommer, H., Barry, D., Chiang, W., & Zheng, C. (2001). PHT3D: A MODFLOW-MT3DMS-based reactive multicomponent transport model. In H. S. Seo (Eds.), *MODFLOW 2001 and other modeling odysseys* (Vol. 2, pp. 477–483). Golden, CO: International Ground Water Modeling Centre.
- Puckett, L. J., Tesoriero, A. J., & Dubrovsky, N. M. (2011). Nitrogen contamination of surficial aquifers: A growing legacy. *Environmental Science Technology*, 45(3), 839–844. <https://doi.org/10.1021/es1038358>
- Rivett, M. O., Buss, S. R., Morgan, P., Smith, J. W., & Bemment, C. D. (2008). Nitrate attenuation in groundwater: A review of biogeochemical controlling processes. *Water Research*, 42(16), 4215–4232. <https://doi.org/10.1016/j.watres.2008.07.020>
- Sanz-Prat, A., Lu, C., Amos, R. T., Finkel, M., Blowes, D. W., & Cirpka, O. A. (2016a). Exposure-time based modeling of nonlinear reactive transport in porous media subject to physical and geochemical heterogeneity. *Journal of Contaminant Hydrology*, 192, 35–49. <https://doi.org/10.1016/j.jconhyd.2016.06.002>
- Sanz-Prat, A., Lu, C., Finkel, M., & Cirpka, O. A. (2015). On the validity of travel-time based nonlinear bioreactive transport models in steady-state flow. *Journal of Contaminant Hydrology*, 175, 26–43. <https://doi.org/10.1016/j.jconhyd.2015.02.003>
- Sanz-Prat, A., Lu, C., Finkel, M., & Cirpka, O. A. (2016b). Using travel times to simulate multi-dimensional bioreactive transport in time-periodic flows. *Journal of Contaminant Hydrology*, 187, 1–17. <https://doi.org/10.1016/j.jconhyd.2016.01.005>
- Schäfer, W., & Therrien, R. (1995). Simulating transport and removal of xylene during remediation of a sandy aquifer. *Journal of Contaminant Hydrology*, 19(3), 205–236. [https://doi.org/10.1016/0169-7722\(95\)00018-Q](https://doi.org/10.1016/0169-7722(95)00018-Q)
- Schwede, R. L., Cirpka, O. A., Nowak, W., & Neuweiler, I. (2008). Impact of sampling volume on the probability density function of steady-state concentration. *Water Resources Research*, 44, W12433. <https://doi.org/10.1029/2007WR006668>
- Sebilo, M., Mayer, B., Nicolardot, B., Pinay, G., & Mariotti, A. (2013). Long-term fate of nitrate fertilizer in agricultural soils. *Proceedings of the National Academy of Sciences United States of America*, 110(45), 18,185–18,189. <https://doi.org/10.1073/pnas.1305372110>
- Seeboonruang, U., & Ginn, T. R. (2006). Upscaling heterogeneity in aquifer reactivity via exposure-time concept: Forward model. *Journal of Contaminant Hydrology*, 84(3), 127–154. <https://doi.org/10.1016/j.jconhyd.2005.12.011>
- Selroos, J.-O., Cheng, H., Painter, S., & Vidstrand, P. (2013). Radionuclide transport during glacial cycles: Comparison of two approaches for representing flow transients. *Physics and Chemistry of the Earth*, 64, 32–45. <https://doi.org/10.1016/j.pce.2012.10.003>
- Shampine, L. F., & Reichelt, M. W. (1997). The matlab ode suite. *SIAM Journal on Scientific Computing*, 18(1), 1–22. <https://doi.org/10.1137/S1064827594276424>
- Shapiro, A. M., & Cvetkovic, V. D. (1988). Stochastic analysis of solute arrival time in heterogeneous porous media. *Water Resources Research*, 24(10), 1711–1718. <https://doi.org/10.1029/WR024i010p01711>
- Simmons, C. (1982). A stochastic-convective transport representation of dispersion in one-dimensional porous media systems. *Water Resources Research*, 18(4), 1193–1214. <https://doi.org/10.1029/WR018i004p01193>

- Simmons, C. S., Ginn, T. R., & Wood, B. D. (1995). Stochastic-convective transport with nonlinear reaction: Mathematical framework. *Water Resources Research*, 31(11), 2675–2688. <https://doi.org/10.1029/95WR02178>
- Smith, K. (1980). A model of the extent of anaerobic zones in aggregated soils, and its potential application to estimates of denitrification. *Journal of Soil Science*, 31(2), 263–277. <https://doi.org/10.1111/j.1365-2389.1980.tb02080.x>
- Strebel, O., Duynisveld, W., & Böttcher, J. (1989). Nitrate pollution of groundwater in western Europe. *Agriculture, Ecosystems & Environment*, 26(3–4), 189–214. [https://doi.org/10.1016/0167-8809\(89\)90013-3](https://doi.org/10.1016/0167-8809(89)90013-3)
- Tesoriero, A. J., & Puckett, L. J. (2011). O₂ reduction and denitrification rates in shallow aquifers. *Water Resources Research*, 47, W12522. <https://doi.org/10.1029/2011WR010471>
- Thiele, M. R., Batycky, R. P., Blunt, M. J., & Orr, F. M. (1996). Simulating flow in heterogeneous systems using stream tubes and streamlines. *SPE Reservoir Engineering*, 11, 5–12. <https://doi.org/10.2118/27834-PA>
- Wakida, F. T., & Lerner, D. N. (2005). Non-agricultural sources of groundwater nitrate: A review and case study. *Water Research*, 39(1), 3–16. <https://doi.org/10.1016/j.watres.2004.07.026>
- Ward, M. H., deKok, T. M., Levallois, P., Brender, J., Gulis, G., Nolan, B. T., et al. (2005). Workgroup report: Drinking-water nitrate and health: Recent findings and research needs. *Environmental Health perspectives*, 113(11), 1607–1614. <https://doi.org/10.1289/ehp.8043>
- Weyer, P. J., Cerhan, J. R., Kross, B. C., Hallberg, G. R., Kantamneni, J., Breuer, G., et al. (2001). Municipal drinking water nitrate level and cancer risk in older women: The Iowa women's health study. *Epidemiology*, 12(3), 327–338. <https://doi.org/10.1097/00001648-200105000-00013>
- Wisotzky, F. (2012). *Angewandte grundwasserchemie, hydrogeologie und hydrogeochemische modellierung: Grundlagen, anwendungen und problemlösungen*, Berlin, Germany: Springer-Verlag. <https://doi.org/10.1007/978-3-642-17813-9>
- Wolfe, A. H., & Patz, J. A. (2002). Reactive nitrogen and human health: Acute and long-term implications. *Ambio*, 31(2), 120–125. <https://doi.org/10.1579/0044-7447-31.2.120>
- Wriedt, G., & Rode, M. (2006). Modelling nitrate transport and turnover in a lowland catchment system. *Journal of Hydrology*, 328(1), 157–176. <https://doi.org/10.1016/j.jhydrol.2005.12.017>
- Xiu, D., & Hesthaven, J. S. (2005). High-order collocation methods for differential equations with random inputs. *SIAM Journal on Scientific Computing*, 27(3), 1118–1139. <https://doi.org/10.1137/040615201>
- Yabusaki, S. B., Steefel, C. I., & Wood, B. (1998). Multidimensional, multicomponent, subsurface reactive transport in nonuniform velocity fields: Code verification using an advective reactive stream tube approach. *Journal of Contaminant Hydrology*, 30(3), 299–331. [https://doi.org/10.1016/S0169-7722\(97\)00050-8](https://doi.org/10.1016/S0169-7722(97)00050-8)

Research paper/

An Electron-Balance Based Approach to Predict the Decreasing Denitrification Potential of an Aquifer

Matthias Loschko
Center for Applied Geosciences, University of Tübingen, Germany

Thomas Wöhling
Department of Hydrology, Technische Universität Dresden, Germany
Lincoln Agritech Ltd., Ruakura Research Centre, Hamilton, New Zealand

David L. Rudolph
Department of Earth and Environmental Sciences, University of Waterloo, Ontario, Canada

Olaf A. Cirpka
Center for Applied Geosciences, University of Tübingen, Germany

Conflicts of interest: None

Keywords: Reaction Potential, Travel Time, Denitrification, Stochastic Framework

Article Impact Statement: Estimate the time of contaminant breakthrough at a receptor within a stochastic framework without solving reactive transport.

1 **Abstract**

2 Numerical models for reactive transport can be used to estimate the breakthrough of a
3 contaminant at a pumping well or other receptors. However, as natural aquifers are highly
4 heterogeneous with unknown spatial details, reactive transport predictions on the aquifer
5 scale require a stochastic framework for uncertainty analysis. The high computational
6 demand of spatially explicit reactive-transport models hampers such analysis, thus motivating
7 the search for simplified estimation tools. In this work, we suggest performing an electron
8 balance between the reactants in the infiltrating solution and in the aquifer matrix to obtain
9 the hypothetical time of dissolved-reactant breakthrough if the reaction with the matrix was

10 instantaneous. This time we denote the cumulative reaction potential (τ_{pot}). It depends on the
11 amount of the reaction partner present in the matrix, the mass flux of the dissolved reactant,
12 and the stoichiometry. While the shape of the reactive-species breakthrough curve depends
13 on various kinetic parameters, the overall timing scales with τ_{pot} . The latter can be calculated
14 by simple particle tracking or by considering distributions of travel-time and reactive
15 properties. The effort of computing τ_{pot} is so low that stochastic calculations are feasible. We
16 apply the concept to a two-dimensional test case of aerobic respiration and denitrification
17 with a detailed spatially explicit model including microbial dynamics. Scaling the time of
18 point-like breakthrough curves by τ_{pot} decreased the variability of electron-donor
19 breakthrough curves significantly. We conclude that the cumulative reaction potential is an
20 efficient tool to estimate the time over which an aquifer retains its degradation potential.

21 **Introduction**

22 Groundwater resources are at risk by over-exploitation and contamination. Especially the
23 use of fertilizers in agriculture threatens groundwater quality. The intensification of
24 agriculture in the 1960s and 1970s came along with an increase of fertilizer application
25 (Galloway et al., 2004). The most prominent nutrient-turned-to-a-contaminant is nitrate,
26 which originates from both mineral fertilizers and manure. Organic nitrogen is mineralized in
27 the soil to ammonium and oxidized to nitrate, both of which are available to plants. While
28 ammonium is bound relatively strongly to the soil, nitrate is highly soluble in water and does
29 not form insoluble minerals that can precipitate. Consequently, nitrate that has not been used
30 by plants will be leached from the soil. The excess nitrate is transported out of the root zone
31 with seepage water to the saturated zone, from where it is transported further to surface and
32 coastal waters (Puckett et al., 2010). Even though nitrate is a regulated compound (drinking-
33 water standards: 50 mg/L total nitrate in the European Union, 10 mg/L nitrate-N = 44 mg/L
34 total nitrate in the U.S.), the release of nitrate into groundwater cannot fully be prevented or

35 prohibited by laws. Especially in regions with intensive agriculture, nitrate levels in
36 groundwater remain at elevated levels (Strebel et al., 1989; Pacheco et al., 2001; Wakida and
37 Lerner, 2005).

38 In contrast to the increased loading of nitrate due to the continuous use of fertilizer, an
39 increase of nitrate in wells has not always been observed even though other compounds may
40 have indicated an anthropogenic influence on groundwater quality (Wisotzky, 2012). This is
41 so because some aquifers can naturally degrade nitrate by microbial activity, a reduction
42 process known as denitrification. For denitrification to occur, an electron donor needs to be
43 present, which in aquifers is often natural organic matter (NOM). While in the bioactive soil
44 zone the organic material is renewed by degrading plant material, the organic carbon in
45 aquifers typically originates from organic materials deposited with the sediments and is thus
46 non-renewable. Continuous loading of aquifers with nitrate and other electron acceptors leads
47 to the consumption of the electron donors in the matrix during denitrification (Korom, 1992),
48 a decrease of the natural denitrification potential of aquifers, and finally the breakthrough of
49 nitrate in pumping wells or surface-water bodies, the so-called receptors (Wisotzky, 2012).
50 The depletion of the denitrification potential, however, may be rather slow and might take
51 several decades or even centuries (Korom, 1992). If the nitrate concentrations in the pumped
52 groundwater exceed the drinking water standards, the well might be shut down, as treatment
53 of nitrate is costly. In practice, nitrate-rich water is often diluted with less polluted water to
54 meet the standards. For water supply companies and other stakeholders it is therefore of
55 utmost importance to estimate how long the natural degradation potential of an exploited
56 aquifer endures. The extent to which the nitrogen loads from previous actions, such as
57 intensive agriculture, will continue to increase in the future is known as “load to come” (Vant
58 and Smith, 2004). A belated increase of nitrate is also known as “time lag”, which describes
59 the delay between the implementation of management changes and an improvement in

60 groundwater quality (Vero et al., 2018). For policy makers it is necessary to consider the
61 current fertilizer input as well as previous inputs that will arrive at receptors with some delay.

62 Computational models of aquifer-scale reactive transport can help determining and
63 evaluating the fate of nitrate in aquifers and predict the decreasing denitrification potential.
64 However, setting up a model for the catchment of a drinking-water well is costly, time
65 consuming, and challenging, because the hydraulic and biogeochemical properties and
66 boundary conditions of natural aquifers are heterogeneous and uncertain. These uncertainties
67 may be addressed by putting the simulations into a stochastic framework, in which parameter
68 values are considered random variables with an assumed statistical distribution, and
69 predictions are thus also statistical distributions. With the exception of a few simplified cases,
70 in which stochastic-analytical expressions have been derived, the computational effort of
71 obtaining probabilistic predictions of reactive transport within a stochastic framework is
72 considerably higher than that of associated deterministic predictions because multiple model
73 runs are to be performed.

74 Conventional reactive solute transport models rely on spatially explicit descriptions of
75 all properties (e.g., hydraulic conductivity, porosity, organic-carbon content) and state
76 variables (hydraulic head, concentrations) and consider multi-dimensional advective-
77 dispersive-reactive transport. While such models can account for all processes assumed
78 relevant at any desired level of detail, they require spatially distributed parameters, which are
79 difficult to obtain and thus uncertain, and they come at high computational costs leading to
80 extensive run times. This puts modelers into the ironic situation that a spatially explicit,
81 detailed, reactive-transport model requires a stochastic description because the parameter
82 fields are highly uncertain, while at the same time the associated computational effort is so
83 high that a probabilistic treatment involving multiple model runs is prohibited. Hence,

84 simplifications that reduce the computational effort without losing the conceptual
85 understanding of the system are required.

86 A widely used, efficient approach to simplify solute transport in hydrological systems is
87 to link the reactive-species concentrations to the time that the water has stayed in the system
88 (Rubin et al., 1994). Travel-time based models were first introduced by Todorovic (1970) and
89 further developed by Shapiro and Cvetkovic (1988). These models yield a suitable
90 representation of the system if flow is in steady state and dispersion can be neglected
91 altogether. This is most likely the case if contaminants are introduced over large areas which
92 is the case for nitrate leaching into groundwater. Without transverse dispersion, transport
93 becomes one-dimensional along independent streamlines, and the spatially variable velocity
94 vector simplifies to a “velocity” of unity in travel-time coordinates (e.g., Feyen et al., 1998).
95 In previous studies dispersive mixing both along and between streamlines has often been
96 neglected. These methods consider advective transport only (e.g., Ginn et al., 1995; Atchley
97 et al., 2013). Under these conditions, solving a single set of ordinary differential equations for
98 one set of inflow concentrations is sufficient if the reaction-rate coefficients are constant
99 along the streamline. In so-called stochastic-convective reactive models, advection and thus
100 travel times were considered random variables (Cvetkovic et al., 1996; Simmons et al., 1995).
101 While such models can address spreading by macrodispersion, they cannot simulate reactions
102 that are controlled by dispersive mixing. Extensions of streamline-methods that allow for
103 dispersive mixing in the longitudinal direction are straightforward (e.g., Ginn, 2001).
104 However, differential advection and local transverse mixing causes macroscopic longitudinal
105 mixing between invading and receding solutions that must be accounted for by appropriate
106 parameterizations if such mixing exerts a major control on the reactions (e.g., Cirpka and
107 Kitanidis, 2000; Sanz-Prat et al., 2015).

108 By switching from a spatially explicit modeling approach towards a spatially non
109 explicit framework, the computational effort is reduced so much that a stochastic analysis,
110 using for example Monte Carlo simulations, becomes feasible (e.g., Atchley et al., 2013;
111 Diem et al., 2013). Other studies showed that travel times alone are insufficient predictors of
112 reactive transport, and the exposure time to particular conditions should additionally be
113 considered (Lohse et al., 2009; Ocampo et al., 2006; Sanz-Prat et al., 2016).

114 The biogeochemical conditions of an aquifer commonly vary in space and time within an
115 aquifer. Loschko et al. (2016) extended the exposure-time based modeling framework by
116 implementing the so-called “relative reactivity”. The dimensionless relative reactivity
117 parameterizes the intensity of a specific reaction at every location in the domain. Loschko et
118 al. (2018) expanded the latter approach to account for the decreasing reaction potential of the
119 aquifer matrix along streamlines without returning to a fully spatially explicit description.

120 Most of the streamline-based methods discussed above are based on solving advective-
121 (dispersive)-reactive transport along streamlines. While the restriction to one-dimensional
122 transport along a single or multiple streamlines significantly reduces the computational effort
123 in comparison to multi-dimensional simulations, the models still require an extended set of
124 reactive parameters, which are often uncertain in practical applications. In this work we
125 present a simplified approach to estimate the time of breakthrough of a contaminant at a
126 receptor, such as a pumping well or an outflow plane, without rigorous reactive transport
127 simulations. We perform an electron balance between the infiltrating solution and the aquifer
128 matrix to compute after which time the infiltrating reactants would break through if the
129 reaction with the aquifer matrix was instantaneous. This time we denote the cumulative
130 reaction potential (τ_{pot}). Evaluating τ_{pot} does not require solving reactive transport equations.
131 We claim that breakthrough curves of complex reactive-transport simulations actually scale

132 with τ_{pot} in time and demonstrate this for the reactive case of coupled aerobic respiration and
133 denitrification.

134 In a two-dimensional test case with a heterogeneous hydraulic conductivity and a
135 heterogeneous distribution of organic carbon, we compare the results of breakthrough of
136 nitrate from a spatially explicit model to the prediction from the cumulative reaction
137 potential. We demonstrate that an estimate of τ_{pot} is possible with derived distribution
138 functions of travel time and organic carbon concentration and without the use of a numerical
139 model at all.

140 We like to emphasize that our methodology is not restricted to the case of denitrification
141 and aerobic respiration, but we apply it to this case as it is of practical relevance and
142 comparably well understood.

143 The remainder of this paper is organized as follows: The theoretical considerations of
144 aerobic respiration and denitrification, the spatially explicit model and the derivation of the
145 cumulative reaction potential are discussed in Section 2. The conceptual model of the
146 spatially explicit test case is presented in Section 3. Section 4 shows the results and the
147 comparison with the cumulative reaction potential. We close with concluding remarks in
148 Section 5.

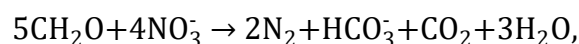
149 **Theory**

150 In this section we elucidate the principles of aerobic respiration and denitrification in
151 groundwater as our chosen example of the reactive system. We derive the underlying
152 principles of the detailed spatially-explicit model and define the cumulative reaction potential
153 τ_{pot} . The detailed model serves as a reference model ('virtual truth') and the timing of solute
154 breakthrough predicted by this model will be compared to the cumulative reaction potential.
155 We later show how the probability density function (*pdf*) of τ_{pot} is related to the *pdf* of travel

156 time and the *pdf* of natural organic matter (NOM), which is the depleting, matrix-bound
 157 reaction partner in our case.

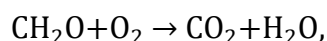
158 **Denitrification and Aerobic Respiration**

159 Many aquifers, that are exposed to nitrate have the capability to reduce nitrate by the
 160 process of denitrification, which is defined as the microbial reduction of nitrate (NO_3^-) and
 161 nitrite (NO_2^-) via nitric oxide (NO) and nitrous oxide (N_2O) to molecular nitrogen (N_2)
 162 (Knowles, 1982). Denitrification is a major factor in the global nitrogen cycle and a common
 163 process in anoxic subsurface environments. Denitrification requires the oxidation of an
 164 electron donor, which in aquifers is usually provided by the matrix. The net stoichiometry of
 165 heterotrophic-chemoorganotrophic denitrification, with organic carbon as electron donor, is:



166 in which CH_2O is the simplified chemical composition of natural organic matter (NOM), NO_3^-
 167 is nitrate, N_2 is molecular nitrogen, HCO_3^- is bicarbonate, CO_2 is carbon dioxide, and H_2O is
 168 water. The reduction process involves several intermediates, but molecular nitrogen is the
 169 predominant reaction product.

170 Denitrification stands in competition to aerobic respiration. Oxygen, which competes
 171 with nitrate as an electron acceptor in the energy metabolism of cells, is an important
 172 inhibitor of denitrification. Nitrate reduction is not observed at an oxygen concentration
 173 above 0.2 mg/L (Skerman and MacRae, 1957). Taking organic matter as the electron donor,
 174 the net stoichiometry of aerobic respiration is:



175 in which O_2 denotes molecular oxygen.

176 Other inhibiting compounds like hydrogen sulfide and acetylene play only minor roles in
177 natural denitrification. Facultative anaerobic, denitrifying bacteria are able to use nitrogen
178 oxides as electron acceptors in place of oxygen when exposed to anaerobic conditions. After
179 the consumption of oxygen, they rely on nitrate to generate energy via cellular respiration
180 (Foth et al., 1991).

181 Denitrification rates vary depending on the ambient conditions in the aquifer. There is a
182 broad variety of factors controlling denitrification. The most important one is the organic
183 carbon content, as the availability of electrons in organic carbon compounds is one of the
184 most important factors controlling the activity of the denitrifying heterotrophic bacteria (Van
185 Kessel, 1978). However, the electron donor is not limited to organic materials. Reduced
186 sulfur compounds, ferrous iron (Fe^{2+}), molecular hydrogen, assimilating dissolved CO_2 , or
187 pyrite (FeS_2) can act as electron donor and lead to denitrification. In the present work we
188 focus on organic carbon in the form of NOM as electron donor. Rather than considering
189 direct utilization of NOM by denitrifying bacteria, we assume that matrix-bound NOM
190 releases dissolved organic carbon (DOC), which can be incorporated by the microbes.

191 **Detailed, Spatially Explicit Reactive-Transport Model**

192 We have set up a detailed spatially explicit reference model for aerobic respiration and
193 denitrification ('virtual truth'). This model will be compared to estimates based on the
194 cumulative reaction potential, defined below. The reference model considers the growth and
195 decay of biomass of an immobile facultative anaerobic microbial community. Natural organic
196 matter (NOM) is the source of the electron donor in the matrix. The NOM releases dissolved
197 organic carbon (DOC) which then can be utilized by the microorganisms. Nitrate and
198 dissolved oxygen are the competing electron acceptors introduced by groundwater recharge.

199 We start our analysis with the spatially explicit multi-dimensional advection-dispersion-
 200 reaction equation involving mobile and immobile species:

$$\frac{\partial c_i}{\partial t} + \mathbf{v} \cdot \nabla c_i - \nabla \cdot (\mathbf{D} \nabla c_i) = r_i(\mathbf{c}(\mathbf{x}, t), \mathbf{c}^*(\mathbf{x}, t)), \quad (1)$$

$$\frac{\partial c_i^*}{\partial t} = r_i^*(\mathbf{c}(\mathbf{x}, t), \mathbf{c}^*(\mathbf{x}, t)), \quad (2)$$

201 in which t [T] is time, $\mathbf{v} = \frac{\mathbf{q}}{\theta}$ [LT⁻¹] is the linear-average-velocity vector, which is the
 202 specific-discharge vector \mathbf{q} [LT⁻¹] divided by the flow-effective porosity θ [-], \mathbf{D} [L²T⁻¹] is the
 203 dispersion tensor, \mathbf{x} [L] is the vector of spatial coordinates, r_i [mol L⁻³T⁻¹] and r_i^* [mol
 204 M_{soil}⁻¹T⁻¹] are the reaction rates for the mobile- and immobile-phase compound i , respectively,
 205 and \mathbf{c} [mol L⁻³] and \mathbf{c}^* [mol M_{soil}⁻¹] are the concentration vectors of all dissolved and
 206 immobile-phase compounds, respectively, c_i and c_i^* being associated to the individual
 207 compound i .

208 The reaction rates r_i of the specific compounds i are expressed as:

$$r_{DO} = -\frac{\mu_{DO}}{Y_{DO}} \cdot \frac{\rho_b}{\theta}, \quad (3)$$

$$r_{Nit} = -\frac{\mu_{Nit}}{Y_{Nit}} \cdot \frac{\rho_b}{\theta}, \quad (4)$$

$$r_{DOC} = r_{DOC}^{rel} - \left(\frac{Y_{DO} \cdot \mu_{DO}}{Y_{DO}} + \frac{Y_{Nit} \cdot \mu_{Nit}}{Y_{Nit}} \right) \cdot \frac{\rho_b}{\theta}, \quad (5)$$

$$r_{NOM}^* = \left(r_{dec}^* - r_{DOC}^{rel} \cdot \frac{\theta}{\rho_b} \right), \quad (6)$$

$$r_{bio}^* = (\mu_{DO} + \mu_{Nit}) \cdot \left(1 - \frac{c_{bio}^*}{c_{bio}^{*max}} \right) - r_{dec}^*, \quad (7)$$

209 with:

$$\mu_{DO} = \frac{c_{DO}}{c_{DO} + K_{DO}} \cdot \frac{c_{DOC}}{c_{DOC} + K_{DOC}} \cdot \mu_{max}^{aer} \cdot c_{bio}^* \quad (8)$$

$$\mu_{Nit} = \frac{c_{DOC}}{c_{DOC} + K_{DOC}} \cdot \frac{c_{Nit}}{c_{Nit} + K_{Nit}} \cdot \frac{K_{DO}^{inh}}{K_{DO}^{inh} + c_{DO}} \cdot \mu_{max}^{Nit} \cdot c_{bio}^* \quad (9)$$

$$r_{dec}^* = k_{dec} (c_{bio}^* - c_{bio}^{*min}), \quad (10)$$

210 in which $\mu_{DO}(\mathbf{x},t)$ [$\text{mol}_{\text{C}_{\text{bio}}} \text{M}_{\text{soil}}^{-1} \text{T}^{-1}$] and $\mu_{Nit}(\mathbf{x},t)$ [$\text{mol}_{\text{C}_{\text{bio}}} \text{M}_{\text{soil}}^{-1} \text{T}^{-1}$] are the growth rates due to
 211 aerobic respiration and denitrification, respectively, and μ_{max}^{aer} [T^{-1}] and μ_{max}^{Nit} [T^{-1}] are the
 212 corresponding maximum specific growth rates. Y_{DO} [$\text{mol}_{\text{C}_{\text{bio}}} \text{mol}_{\text{DO}}^{-1}$] and Y_{Nit} [$\text{mol}_{\text{C}_{\text{bio}}} \text{mol}_{\text{Nit}}^{-1}$]
 213 are the yield coefficients related to aerobic respiration and denitrification. $c_{DO}(\mathbf{x},t)$
 214 [$\text{mol}_{\text{DO}} \text{L}^{-3}$], $c_{Nit}(\mathbf{x},t)$ [$\text{mol}_{\text{Nit}} \text{L}^{-3}$], and $c_{DOC}(\mathbf{x},t)$ [$\text{mol}_{\text{C}} \text{L}^{-3}$] refer to the concentrations of
 215 dissolved oxygen, nitrate, and dissolved organic carbon, respectively, $c_{bio}^*(\mathbf{x},t)$ [$\text{mol}_{\text{C}_{\text{bio}}} \text{M}_{\text{soil}}^{-1}$]
 216 denotes the mass-related concentration of the immobile biomass in the aquifers matrix, and
 217 c_{bio}^{*max} [$\text{mol}_{\text{C}_{\text{bio}}} \text{M}_{\text{soil}}^{-1}$] is the maximum biomass concentration. ρ_b [$\text{M}_{\text{soil}} \text{L}^{-3}$] is the dry bulk
 218 mass density of the aquifer material and θ [-] the volumetric water content. γ_{Nit} [$\text{mol}_{\text{C}} \text{mol}_{\text{Nit}}^{-1}$]
 219 and γ_{DO} [$\text{mol}_{\text{C}} \text{mol}_{\text{DO}}^{-1}$] are the stoichiometric coefficients between DOC and the electron
 220 acceptors nitrate and oxygen, respectively. K_i [$\text{mol} \text{L}^{-3}$] is the Monod constant of compound i ,
 221 and K_{DO}^{inh} [$\text{mol} \text{L}^{-3}$] is the inhibition constant of oxygen in denitrification. k_{dec} [T^{-1}] denotes
 222 the rate coefficient of biomass decay. The biomass concentration c_{bio}^* cannot fall
 223 below the threshold concentration c_{bio}^{*min} [$\text{mol}_{\text{C}_{\text{bio}}} \text{M}_{\text{soil}}^{-1}$] to provide a seed.

224 The release rate of dissolved organic carbon from the aquifer matrix $r_{DOC}^{rel}(\mathbf{x},t)$
 225 [$\text{mol}_{\text{C}} \text{T}^{-1} \text{L}^{-3}$] is modeled as a first-order mass-transfer process:

$$r_{DOC}^{rel} = k_{DOC}^{rel,eff} \cdot (c_{DOC}^{sat} - c_{DOC}), \quad (11)$$

226 with:

$$k_{DOC}^{rel,eff} = k_{DOC}^{rel,max} \cdot \left(\frac{c_{NOM}^*}{c_{NOM}^{*init}} \right)^{\frac{2}{3}}, \quad (12)$$

227 in which $k_{DOC}^{rel,eff}$ [T⁻¹] is the effective rate coefficient of DOC release with its maximum of
 228 $k_{DOC}^{rel,max}$ [T⁻¹] obtained at the initial concentration c_{NOM}^{*init} [mol_CM_{soil}⁻¹] of NOM. c_{DOC}^{sat} [mol_CL⁻³]
 229 is the saturation concentration of DOC, and c_{NOM}^* [mol_CM_{soil}⁻¹] denotes the mass-related
 230 concentration of the natural organic matter in the aquifers matrix. The release rate of DOC
 231 changes with changing concentration of NOM. At early times, the microorganisms can utilize
 232 the easily available NOM. With progressing dissolution of NOM, the surface area of
 233 bioavailable NOM decreases. Assuming spherical NOM particles and a release rate that is
 234 proportional to the surface area, we arrive at the power-law dependence of the release rate to
 235 the NOM concentration with an exponent of 2/3 in equation 12.

236 **Damköhler Analysis**

237 The rate-limiting step in the reactive system described above is often the release of the
 238 electron donor from the matrix. This defines an intrinsic time-scale related to the average rate
 239 coefficient of DOC release $k_{DOC}^{rel,eff}$. We can compare the mass-transfer related time scale to
 240 the advective travel time τ_{adv} to reach the receptor, resulting in a Damköhler number:

$$Da = \tau_{adv} \overline{k_{DOC}^{rel,eff}} = \tau_{adv} k_{DOC}^{rel,max} \cdot \int_0^1 c_{rel}^{\frac{2}{3}} dc_{rel} = \tau_{adv} \frac{3}{5} k_{DOC}^{rel,max}, \quad (13)$$

241 in which the overbar denotes an average, and $c_{rel} = c_{NOM}^*/c_{NOM}^{*init}$ is the NOM-content at any
 242 given time scaled by the initial value. For Damköhler numbers $Da \gg 1$, the overall timing of
 243 a reactant's breakthrough is controlled by advection and equilibrium considerations of the
 244 reactions rather than by kinetics.

245 **Electron Balance along a Streamline**

246 We now analyze the limiting case in which reaction kinetics and dispersive mixing are
 247 neglected. Then, the oxygen and nitrate introduced with the infiltrating water would
 248 instantaneously react with the NOM in the aquifer matrix. Assuming a continuous input of
 249 the electron acceptors with groundwater recharge, a sharp reaction front would move through
 250 the domain with a propagation velocity proportional to the mean linear velocity. The space
 251 increment Δx over which the front moves within a time increment Δt can be computed by the
 252 electron balance:

$$\Delta x \cdot \rho_b \cdot c_{NOM}^* = q \cdot \Delta t \cdot (\gamma_{DO} \cdot c_{in,DO} + \gamma_{Nit} \cdot c_{in,Nit}), \quad (14)$$

253 in which $c_{in,DO}$ [$\text{mol}_{DO}\text{L}^{-3}$] and $c_{in,Nit}$ [$\text{mol}_{Nit}\text{L}^{-3}$] are the concentrations of oxygen and
 254 nitrate in the inflow, respectively, and $q = \|\mathbf{q}\|_2$ is the absolute value of specific discharge.
 255 We may rearrange equation 14 to obtain the time increment Δt of the moving reaction front
 256 in comparison to the advective travel-time increment $\Delta \tau = \Delta x/v$ with $v = q/\theta$:

$$\Delta t = \frac{\Delta \tau \cdot \rho_b \cdot c_{NOM}^*}{\theta \cdot (\gamma_{DO} \cdot c_{in,DO} + \gamma_{Nit} \cdot c_{in,Nit})}, \quad (15)$$

257 which finally leads to a characteristic time of solute breakthrough at a given observation
 258 location \mathbf{x}_{obs} , which we denote the cumulative reaction potential τ_{pot} [T]. The interpretation
 259 of the cumulative reaction potential is the time that is needed for a breakthrough of dissolved
 260 oxygen and nitrate if the reaction with the NOM in the aquifer matrix was instantaneous.

$$\tau_{pot}(\mathbf{x}_{obs}) = \frac{1}{\gamma_{DO} \cdot c_{in,DO} + \gamma_{Nit} \cdot c_{in,Nit}} \cdot \int_0^{\tau(\mathbf{x}_{obs})} \frac{\rho_b \cdot c_{NOM}^*}{\theta} d\tau, \quad (16)$$

261 in which $\tau(\mathbf{x}_{obs})$ [T] is the travel time at this location, and the integration is performed along
 262 the streamline leading to the observation point. Equation 16 may also be expressed by an
 263 Eulerian conservation law:

$$\mathbf{q} \cdot \nabla \tau_{pot} = \frac{\rho_b \cdot c_{NOM}^*}{\gamma_{DO} \cdot c_{in,DO} + \gamma_{Nit} \cdot c_{in,Nit}}. \quad (17)$$

264 The cumulative reaction potential τ_{pot} depends on the hydraulics of the aquifer, the
 265 distribution of the bioavailable NOM mass, and the electron-acceptor load in the inflow. As
 266 hydraulic and geochemical properties of aquifers are spatially variable and uncertain, the
 267 cumulative reaction potential τ_{pot} at an observation point, well, or plane is also uncertain. For
 268 a spatially distributed observation in a well or plane, τ_{pot} is a distribution rather than a single
 269 value even without uncertainty because different streamlines leading to the same target have
 270 been exposed to a different NOM mass over a different time. Note, however, that computing
 271 the integral over travel time in equation 16 is a linear operation, for which a first-order
 272 stochastic solution in heterogeneous, stationary media with uniform-in-the-mean velocity
 273 exists (Cvetkovic et al., 1998).

274 If we account for reaction kinetics and dispersion, we don't expect a perfect step-like
 275 reaction front to move through the system, but it is reasonable to assume that the timing of
 276 the electron-acceptor breakthrough scales with the virtual breakthrough time of the front for
 277 an instantaneous reaction, at least for Damköhler numbers well above unity. If the variability
 278 of the flow field and the bioavailable NOM-content is large, the overall width of the electron-
 279 acceptor breakthrough curves in an observation well will be controlled by the variability of
 280 τ_{pot} among the streamlines leading to the well. The same arguments hold for the predictive
 281 uncertainty of electron-acceptor breakthrough at an individual point.

282 In order to compute the cumulative reaction potential τ_{pot} , we need to calculate the
283 groundwater velocity field by solving the groundwater-flow equation, determine particle
284 trajectories to obtain the travel time $\tau(\mathbf{x}, t)$ and the cumulative NOM content along the
285 streamlines, compute the electron demand by the inflow concentrations c_{in} of all dissolved
286 electron acceptors and perform the integration of equation 16 along all trajectories leading to
287 the receptor of interest. Heterogeneous distribution of hydraulic conductivity and bioavailable
288 NOM content can be accounted for. We later show that we may obtain a rough estimate of
289 τ_{pot} by using known or derived distribution functions of travel times and cumulative NOM.
290 In the latter approach, there is no need to calculate the exact spatial distribution of
291 groundwater velocities with a *pde*-based groundwater-flow model.

292 **Conceptual Model of a Virtual Example Application**

293 To test the predictive power of the cumulative reaction potential we have set up a virtual,
294 two-dimensional, spatially explicit test case. We simulated steady-state flow and transient
295 reactive transport of aerobic respiration and denitrification with constant inflow
296 concentrations by solving the spatially explicit advection-dispersion-reaction equation
297 introduced in the Section ‘Detailed, Spatially Explicit Reactive-Transport Model’ above. We
298 denote this model as ‘virtual truth’. The flow field stays constant throughout the time of
299 simulation, whereas the reaction rates change over time with changing concentrations (see
300 Equations 3 to 7). For the same conceptual model we calculated the cumulative reaction
301 potential according to Equation 16. Note that for the calculation of the cumulative reaction
302 potential only the velocity field and the distribution of NOM are necessary.

303 *Table 1: Reactive parameters used in the two-dimensional test case.*

Symbol	Meaning	Value
μ_{max}^{DO}	Maximum specific growth rate based on oxygen	1/86400 1/s
μ_{max}^{Nit}	Maximum specific growth rate based on nitrate	1/86400 1/s
K_{DO}	Monod coefficient of oxygen	11.4 $\mu\text{mol/L}$
K_{Nit}	Monod coefficient of nitrate	70 $\mu\text{mol/L}$
K_{DOC}	Monod coefficient of DOC	20 $\mu\text{mol/L}$
K_{DO}^{inh}	Inhibition coefficient of oxygen in denitrification	10 $\mu\text{mol/L}$
Y_{DO}	Yield coefficient of oxygen	0.25 mol(DO) ^{bio} /mol(C)
Y_{Nit}	Yield coefficient of nitrate	0.25 mol(Nit) ^{bio} /mol(C)
k_{dec}	Decay coefficient of bacteria	0.05/86400 1/s
K_{DOC}^{relmax}	Rate constant of DOC release	0.2/86400 1/s
c_{DOC}^{sat}	Saturation concentration of DOC	10/12000 mol/L
c_{bac}^{max}	Maximum biomass concentration	$10^{-3}/12$ mol(C)/L
c_{bac}^{min}	Minimum biomass concentration	$10^{-6} \cdot c_{bac}^{max}$ mol(C)/L

304 The two-dimensional domain has a size of 50m \times 25m and is discretized for flow by a
305 regular 0.1m \times 0.1m grid. The top and bottom boundaries are no-flow boundaries, whereas
306 the left and the right boundaries were assigned a fixed head with a head difference of 0.2m.
307 We generated an ensemble of 100 realizations of hydraulic conductivity and NOM content,
308 using an exponential covariance function for log-hydraulic conductivity with a geometric
309 mean of the conductivity of 10^{-3} m/s. The variance of $\ln(K)$ was set to 1.0. The correlation
310 length was 4m in the x -direction and 1m in the y -direction, respectively. The NOM content is
311 correlated with hydraulic conductivity. High values of hydraulic conductivity result in low
312 values of NOM and vice versa, following the rationale that fines have higher natural-organic-

313 matter concentrations. The geometric mean NOM concentration was set to
 314 $c_{NOM,g} = 0.05 \text{ mol}_C/\text{kg}$ based on literature values of sedimentary carbon content (Avnimelech
 315 et al., 2001, Nieuwenhuize et al., 1993, Schultz et al., 1999). The concentration of NOM was
 316 then calculated by:

$$c_{NOM} = \left(\frac{K}{K_g} \right)^{-0.5 \cdot R_{NOM} \cdot c_{NOM,g}}, \quad (18)$$

317 in which K is the local value of hydraulic conductivity, K_g is the geometric mean of hydraulic
 318 conductivity, and R_{NOM} is a multi-Gaussian random field with a geometric mean of 1,
 319 correlation length of 5m in both directions, and a variance of 0.25. Figure 1A shows the
 320 hydraulic conductivity and Figure 1C depicts the distribution of NOM for an arbitrarily
 321 selected individual realization. The general groundwater flow direction is from left to right
 322 and the resulting head field is depicted in Figure 1B.

323 We then solved for stream function values, and generated streamline-oriented grids
 324 with 250 streamtubes and 500 sections per streamtube (Frind and Matanga, 1985; Cirpka et
 325 al., 1999). Figure 1D shows the resulting flow net for the selected realization. Reactive
 326 transport was calculated on the streamline-oriented grid using a cell-centered finite volume
 327 method for spatial discretization (Cirpka et al., 1999). In the spatially explicit model, the
 328 longitudinal dispersivity was set to $\alpha_l = 0.01 \text{ m}$ and the transverse dispersivity to $\alpha_t = 0.001 \text{ m}$.
 329 The pore diffusion coefficient was $D_p = 3 \times 10^{-10} \text{ m}^2/\text{s}$. We assumed spatially uniform
 330 values of porosity, $\theta = 0.3$, and dry bulk density of the aquifer material, $\rho_b = 1.855 \text{ kg/L}$.
 331 While in real aquifers, these coefficients may be non-uniform, their variability is typically
 332 much smaller than that of hydraulic conductivity or organic-carbon content. The reactive
 333 parameters of the two-dimensional test case are listed in Table 1.

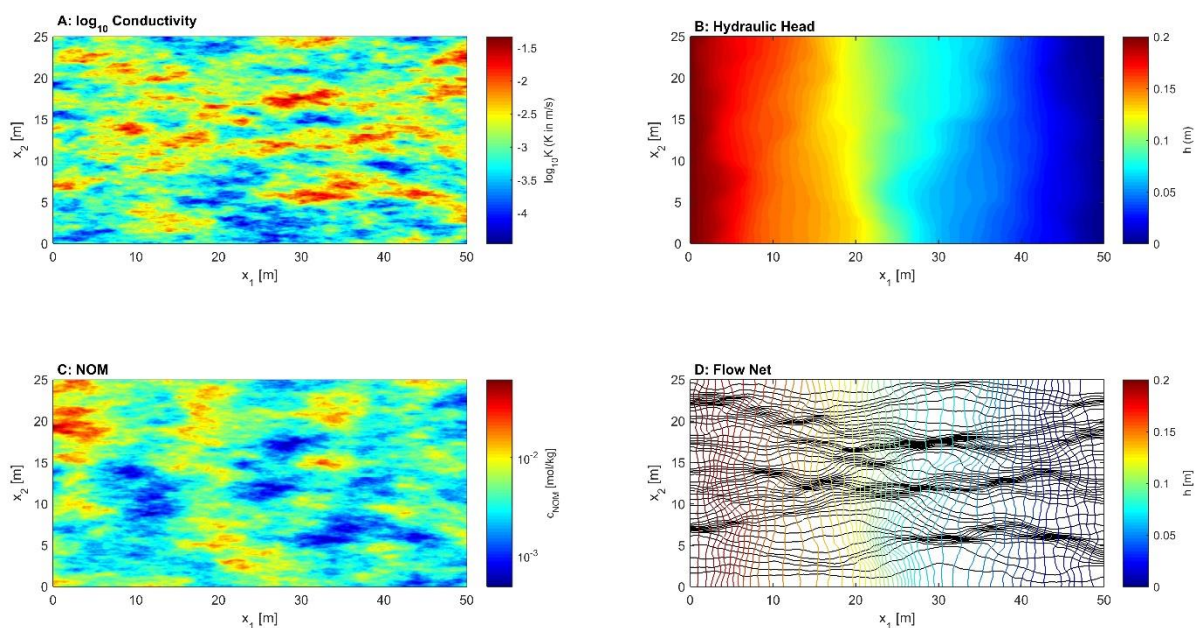
334 Nitrate and oxygen were introduced at the left side of the domain with constant inflow
 335 concentrations of 62 mg/l for nitrate and 8 mg/l for oxygen. Reactive transport considering
 336 the detailed, spatially explicit, kinetic description was solved using a fully implicit approach
 337 with Newton-Raphson iterations. For a more robust comparison we computed 100 fields of
 338 hydraulic conductivity, subsequently referred to as realizations, and performed the spatially
 339 explicit reactive transport simulation for each of them. We simulated reactive transport
 340 including the loss of NOM in the aquifer matrix over 100 years. In addition to the detailed
 341 model we calculated the cumulative reaction potential according to equation 16 for every
 342 streamline in each realization.

343 The model code was implemented in Matlab. A single run of the spatially explicit
 344 model took on average 4.5 hours on a standard desktop PC (IntelCore i7 CPU @ 3.60 GHz,
 345 16GB RAM). The calculation of the cumulative reaction potential took less than 10 seconds.

346 With the given coefficients, we can compute an average Damköhler number $Da =$

347 $\frac{3}{5} \frac{L^2 \theta}{K_g \Delta h} k_{DOC}^{rel,max} = 5.2$, indicating that the average electron-donor supply by the matrix is

348 quicker than advection over the entire domain. Under such conditions we would expect that
 349 the cumulative reaction potential should be a good indicator for the timing of the reactants'
 350 breakthrough at the outflow end of the domain.

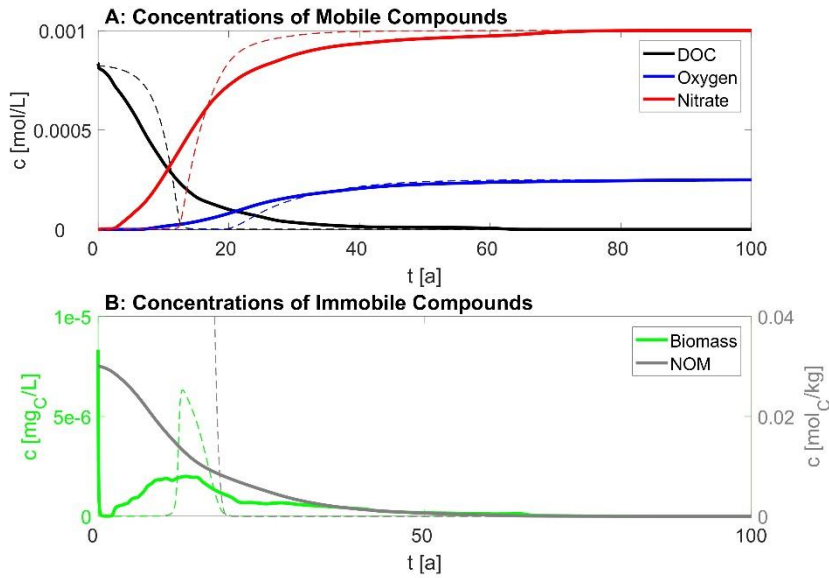


351

352 *Figure 1: Example realization of the two-dimensional test case. (A) Spatial distribution of log-*
 353 *hydraulic conductivity; (B) spatial distribution of hydraulic head; (C) spatial distribution of initial*
 354 *bioavailable NOM content of the matrix; (D) flow net (colored lines: heads; black lines: streamlines)*

355 Results

356 Figure 2 shows the mean concentrations of all dissolved compounds (dissolved organic
 357 carbon, dissolved oxygen, nitrate, Figure 2A) in the outflow of the domain and the mean
 358 concentrations of immobile compounds (biomass, natural organic matter, Figure 2B) in the
 359 last right-hand side cells of the domain for the single realization shown in Figure 1. Because
 360 denitrification is inhibited by elevated oxygen concentrations, the breakthrough of dissolved
 361 oxygen in the outflow is delayed in comparison to that of nitrate. It takes about two years for
 362 the nitrate and seven years for the oxygen to reach the outflow plane. In the first two years
 363 the aquifer reduces the entire incoming flux of oxygen and nitrate.



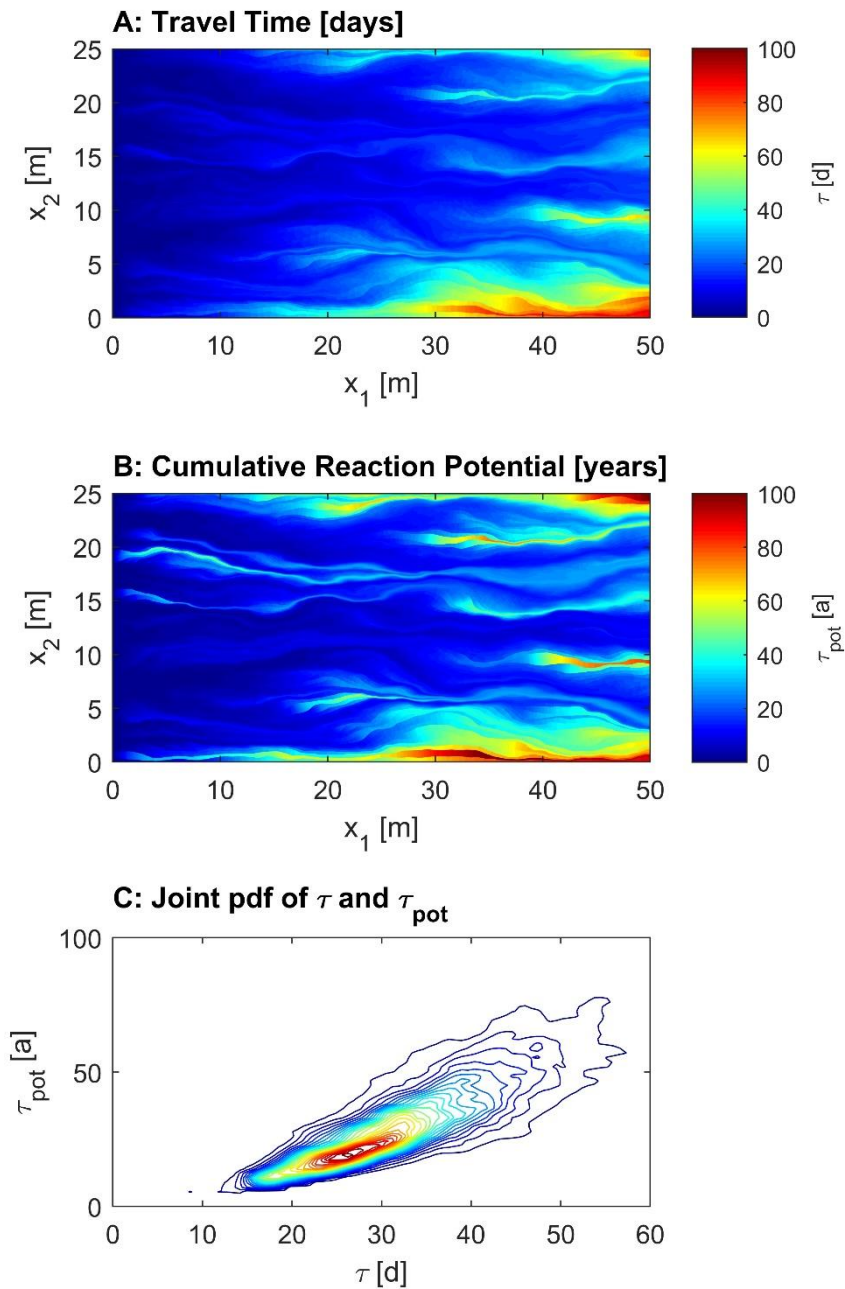
364

365 *Figure 2: Flux-averaged concentration in the outflow of the domain or in the last elements before the*
 366 *outflow, calculations of a single realization. A: dissolved oxygen (blue), nitrate (red), and DOC*
 367 *(black) in the outflow; B: biomass (green) and NOM (gray) at the end of the domain. Dashed lines*
 368 *show the result of a single streamline.*

369 The long tailing of the nitrate and oxygen breakthrough curves is caused by
 370 heterogeneity. This can be seen by comparing the breakthrough curves for the entire domain
 371 to the breakthrough curves of at a single point (dotted lines in Figure 2). Here the tailing is
 372 much less pronounced. The velocity of the oxidation front is slow in zones with high original
 373 bioavailable NOM content and low hydraulic conductivity (see Figures 1A&C). In the
 374 example it takes about 75 years until the aquifer lost its entire denitrification potential and the
 375 breakthrough of nitrate in the outflow is complete. After half of the full simulation time, 90%
 376 breakthrough is reached. It takes about 50 years for almost 95% of the initial NOM to react
 377 with dissolved oxygen or nitrate, respectively. Again, the long tailing is associated with small
 378 regions of high initial NOM concentrations and low hydraulic conductivity.

379 The biomass concentrations close to the outlet of the domain increase slowly with
 380 increasing concentrations of the electron acceptors and reach a maximum value at about 10
 381 years. After that the concentration stays about constant for five years and then slowly
 382 decreases with a simultaneous decrease of the electron donor DOC (respectively NOM). Note

383 that if we would increase the mean initial NOM concentration, the breakthrough would show
384 the same behavior but would be delayed. The time of no nitrate and oxygen in the outflow
385 would be longer whereas the time to reach the maximum values of nitrate and oxygen,
386 respectively, would be similar. Basically the breakthrough curves would be expanded in time
387 without changing their shape.



388

389 *Figure 3: A: Spatial distribution of the mean groundwater age for advective-dispersive transport for*
 390 *the single realization shown in Figure 1. B: cumulative reaction potential for the same realization.*
 391 *C: Joint distribution of travel time and cumulative reaction potential over all 100 realizations.*

392 Figure 3A shows the mean groundwater age as computed by the groundwater-age
 393 equation of Goode (1996) for advective-dispersive transport in a single realization of the two-
 394 dimensional test case shown in Figure 1, whereas Figure 3B shows the associated cumulative
 395 reaction potential. Flow is from left to right. Because of mixing, the groundwater age at a

396 point in a single realization is a distribution of which we only show the mean. The cumulative
397 reaction potential was calculated by equation 16, which neglects local-scale dispersion,
398 whereas the mean groundwater age is smoothed by this process. The comparison between
399 Figure 3A and 3B shows that high cumulative reaction potentials can be found along
400 streamlines with large travel times that additionally pass areas with high concentrations of
401 initial NOM. This effect can be observed at the streamlines starting at about $x_1=15\text{m}$ and
402 $x_2=20\text{m}$. Even though the travel times are comparatively low (about 20 days), the cumulative
403 reaction potential is very high already at the beginning of the streamline (about 50 years).
404 This is caused by the high initial concentrations of NOM at this location (compare Figure
405 1C).

406 Figure 3C shows the joint distribution of the cumulative reaction potential and the travel
407 time for all of the 100 realizations as a distribution plot. The cumulative reaction potential
408 τ_{pot} and the travel time τ are positively correlated, because water parcels that have been
409 longer in the system have also been exposed longer to the aquifers matrix, but the dependence
410 is not deterministic. The negative correlation between hydraulic conductivity and NOM
411 content increases the probability that an old water parcel has experienced particularly high
412 NOM contents so that a fitted dependence of τ_{pot} on τ would most likely be quadratic rather
413 than linear. Note that this relationship depends on the assumptions made for the relationship
414 between hydraulic conductivity and NOM content.

415 The left column of Figure 4 shows the local breakthrough curves of nitrate (red) and
416 oxygen (blue) at the outflow plane on the right side of the domain for all 250 streamtubes of
417 the single realization depicted in Figure 1. This is contrasted by the breakthrough curves
418 integrated over the outflow plane for 100 realizations shown in the right column. The lightly
419 colored areas show the 2%-98% and the 16%-84% quantile, respectively, whereas the bold
420 lines are the medians over all realizations. In case of a Gaussian distribution, these quantiles

421 would represent the mean plus/minus one and two standard deviations. The thick black
422 vertical line indicates the mean cumulative reaction potential of all 250 streamtubes. Figure
423 4A and 4B show the normalized concentration as function of simulated time, whereas Figure
424 4E shows the same breakthrough curves as Figure 4A, obtained by the detailed, spatially
425 explicit, kinetic model, but now time is scaled by the cumulative reaction potential of each
426 streamtube. The breakthrough curves based on the cumulative reaction potential are shown in
427 Figure 4C and 4D. Again the lightly colored areas show the 2%-98% and the 16%-84%
428 quantiles. Note that the framework of the cumulative reaction potential cannot distinguish
429 between the breakthrough times of nitrate and dissolved oxygen so that only the distribution
430 of a single value is depicted.

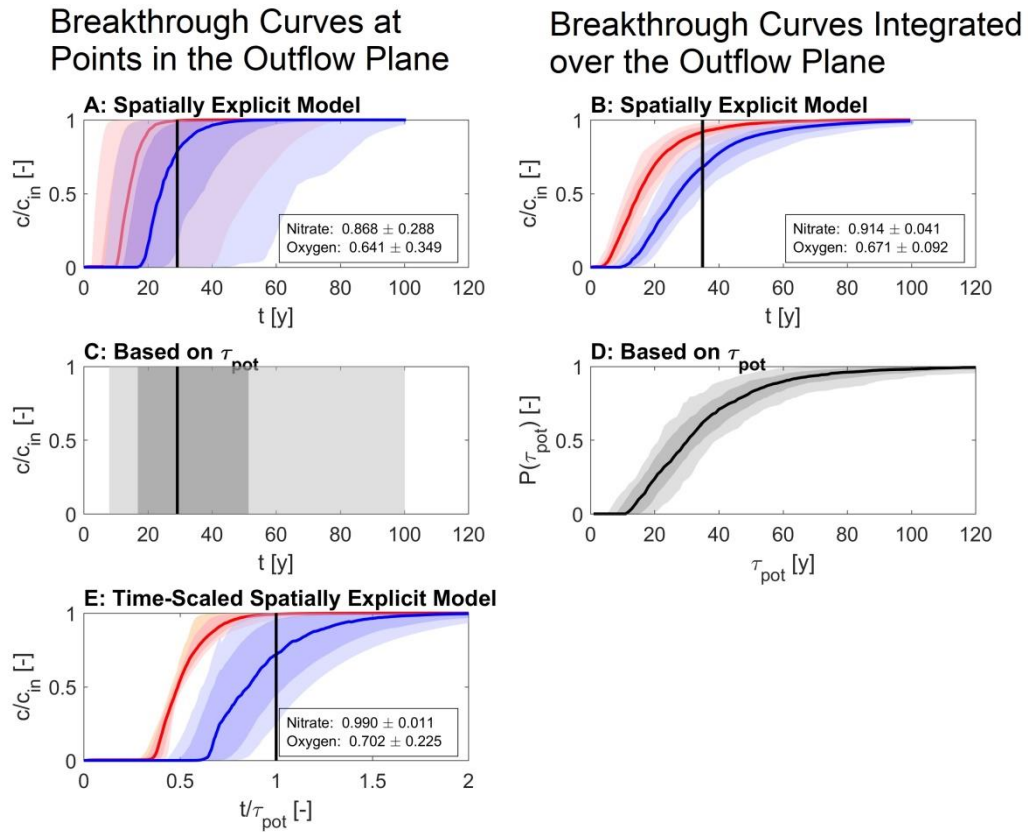
431 The quantiles of the breakthrough curves in real time (Figure 4A) are widely spread. For
432 nitrate the total breakthrough time in an individual streamtube ranges between approximately
433 5 and 75 years across the outflow plane. The large spread is caused by the heterogeneity of
434 hydraulic conductivity and the reaction parameters: The individual travel paths of water
435 parcels differ greatly in velocity and exposure to NOM. The distribution of the cumulative
436 reaction potential (Figure 4B) is also wide spread as there is a high variety among the
437 streamlines of a single simulation run. In Figure 4C, where the simulated time of every
438 streamtube is scaled with the corresponding cumulative reaction potential, the range of
439 normalized concentrations for a given scaled time is considerably narrower. This indicates
440 that the variation in the timing of the solute breakthrough can largely be explained by the
441 variation in the cumulative reaction potential.

442 In case of an instantaneous reaction of NOM with the dissolved electron acceptors, both
443 oxygen and nitrate would break through at the time of the cumulative reaction potential if
444 physical transport was restricted to advection. In Figure 4E the idealized curves would show
445 a step at unity. With the scaling by τ_{pot} it becomes now clearer that nitrate breaks through

446 prior to oxygen. Please note also that the cumulative reaction potential τ_{pot} is formulated for
447 the entire electron-acceptor load so that the target time is that of the oxygen breakthrough.
448 The observed spread around this time is an indicator of reaction kinetics and dispersive
449 mixing.

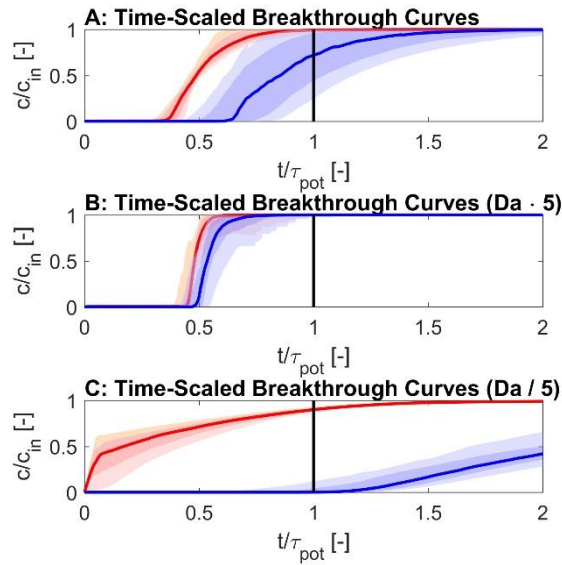
450 Mean values and standard deviations of the solute concentrations at the time of the
451 cumulative reaction potential are depicted in the upper left corners of Figures 4A, 4B, and 4E,
452 respectively.

453 The spread of the quantiles in Figure 4B is narrower, which means a more reliable
454 prediction of the breakthrough is possible. However, obtaining these breakthrough curves
455 comes with a high computational effort. Figure 4D shows the prediction of the joint
456 breakthrough of oxygen and nitrate as predicted from the *cdf* of the local τ_{pot} -values over the
457 cross-section. The quantiles are related to the 100 realizations. Computing this breakthrough
458 curve does not require solving a spatially explicit reactive transport model. The shape agrees
459 quite well with the oxygen breakthrough curve of the detailed model.



460

461 *Figure 4: Left column: Breakthrough curves at points in the outflow plane considering for a single*
 462 *realization. Right column: Breakthrough curves integrated over the outflow plane for 100*
 463 *realizations. (A) and (B): Breakthrough curves of nitrate (red) and dissolved oxygen (blue) as a*
 464 *function of simulated time. (C) and (D): Breakthrough curves based on the cumulative reaction*
 465 *potential. (E): every curve from (A) scaled by the corresponding cumulative reaction potential of the*
 466 *streamline. Thick red and blue line in (A), (B) and (C): median breakthrough curves of nitrate and*
 467 *dissolved oxygen; light and medium colored areas: 2%-98% and 16%-84% quantiles; thick black line*
 468 *in (A) and (B): mean cumulative reaction potential of all streamlines; boxes in (A), (B) and (C): mean*
 469 *and standard deviation of nitrate and dissolved oxygen at the black line in (A), (B) and (C). All*
 470 *concentrations are scaled with the respective inflow concentration.*



471

472 *Figure 5: Breakthrough curves of nitrate (red) and dissolved oxygen (blue) of all streamlines at the*
 473 *outflow end of the domain, considering a single realization of the spatially explicit model as a*
 474 *function of simulated time. All concentrations are scaled with the respective inflow concentration. All*
 475 *curves are scaled by the corresponding cumulative reaction potential of the streamline. Thick red and*
 476 *blue lines resembles the median breakthrough curves of nitrate and dissolved oxygen respectively. A:*
 477 *same as Figure 4C. B: five times higher Damköhler number. C: five times lower Damköhler number.*
 478 *Light red and blue areas show the 2%-98% and the 16%-84% quantile, respectively.*

479 To test the influence of reaction kinetics on the predictive power of the cumulative
 480 reaction potential, we performed calculations with five-fold increased and decreased
 481 Damköhler number by multiplying the velocity fields of all realizations by corresponding
 482 factors. We could as well have achieved larger Damköhler numbers by increasing the domain
 483 rather than decreasing the velocity. For these modified scenarios, Figure 5 shows the
 484 breakthrough curves of nitrate and dissolved oxygen for all streamlines of a single realization
 485 of the spatially explicit model scaled with the corresponding cumulative reaction potential.
 486 Figure 5A is identical to Figure 4C. In Figure 5B, the Damköhler number is 26 and thus five
 487 times higher whereas in Figure 5C the Damköhler number is 1.0 and thus reduced by a factor
 488 of five.

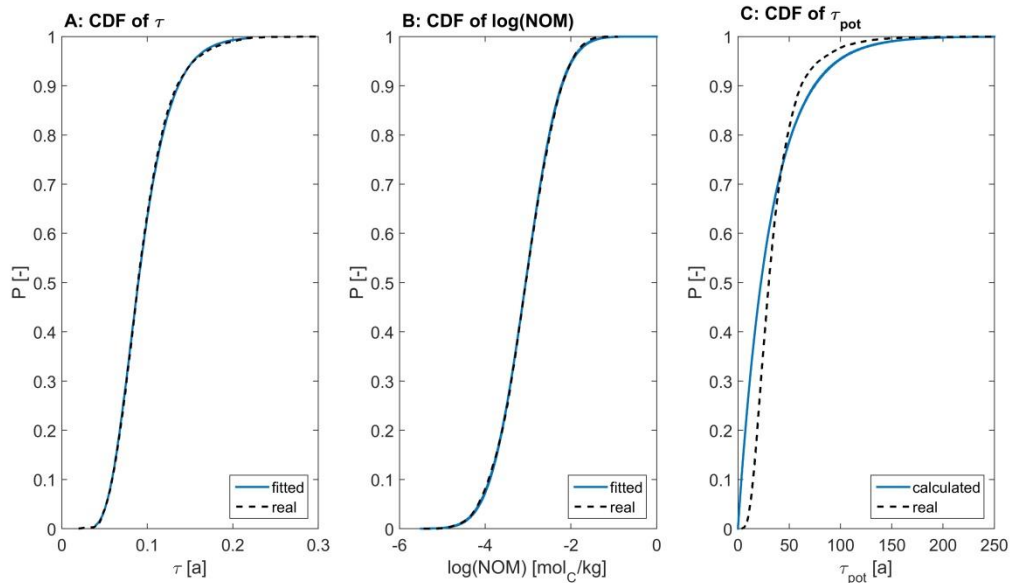
489 It appears that the relative breakthrough is earlier with increasing Damköhler number.

490 However, in real time the breakthrough is later because of the reduced velocity. The

491 cumulative reaction potential is supposed to mark the complete breakthrough of both
492 electron acceptors. For the case with $Da = 26$, this is indeed the case even though a large
493 fraction of the breakthrough occurs earlier. For the case with $Da = 1.0$, the reaction kinetics
494 cause a much earlier relative initial breakthrough, which is considerably wider. The
495 breakthrough of dissolved oxygen just starts at $t \approx \tau_{pot}$. In both cases the quantiles are
496 closely spread around the median value, indicating that the cumulative reaction potential can
497 explain a large fraction of the variability in the breakthrough of the electron acceptors. As
498 expected, τ_{pot} is a better predictor for the time of complete breakthrough if the Damköhler
499 number is high.

500 Figures 6A and 6B depict the cumulative distribution function (*cdf*) of the travel time
501 and the log-concentration of the initial NOM, respectively. The dashed lines are derived from
502 the 100 model realizations of the two-dimensional model described earlier. We fitted
503 distributions of travel time and initial NOM concentration. The travel time distribution could
504 be fitted by a normal distribution with a mean of 0.0944 years and a standard deviation of
505 0.0322 years. The initial NOM concentration was fitted by a log-normal distribution with a
506 geometric mean of $4.70 \times 10^{-2} \text{ mol}_C/\text{kg}$ and a standard deviation of the log-concentration of
507 0.654. The fitted distributions are plotted as blue solid lines in Figures 6A and 6B. It can be
508 seen that they very well match the distribution from the example test case. With only these
509 two fitted distribution functions, the *cdf* of the cumulative reaction potential can be easily
510 estimated when the travel time and initial NOM concentration are assumed to be
511 uncorrelated. To do so, we drew one million random numbers from each of the two fitted
512 distributions and calculated the cumulative reaction potential according to equation 14 using
513 the entire travel time and a constant NOM-concentration. The resulting distribution is shown
514 as blue solid line in Figure 6C. For comparison, Figure 6C also shows the *cdf* of the
515 cumulative reaction potential from the 100 model runs as dashed line. The roughly estimated

516 mean cumulative reaction potential is 32.3 years whereas the mean cumulative reaction
 517 potential of 100 model realizations of the two-dimensional test case is 35.7 years. That is, the
 518 simple estimate gives an approximately good mean estimate. Albeit, it overestimates the
 519 variance. Note that the *cdf* of cumulative reaction potential is calculated without any
 520 numerical model but just with the *cdfs* of travel time and initial NOM concentration.



521

522 *Figure 6: Cumulative distribution functions (cdf) of flux-averaged travel time in the outflow (A), log-*
 523 *concentration of NOM (B), and the flux-averaged cumulative reaction potential in the outflow (C)*
 524 *over 100 realizations. Solid lines: fitted parametric and predicted cdf; dashed lines: empirical cdf of*
 525 *the 100 realizations of the two-dimensional test case.*

526 Discussion and Conclusions

527 In this study we performed a simple electron balance to estimate at which time the
 528 electron-acceptor load of groundwater recharge would break through at an observation point,
 529 a control plane, or in an extraction well, if the reaction with electron donors within the aquifer
 530 matrix was instantaneous and transport was strictly advective. We denoted this quantity the
 531 cumulative reaction potential τ_{pot} . While the exact shape of the breakthrough curves of
 532 reactive species in a spatially explicit complex model showed spreading that could not be
 533 explained with the distribution of τ_{pot} , the overall timing correlated very well with the
 534 cumulative reaction potential. Both when considering the spatial variability of the

535 breakthrough in extended control planes and when performing a stochastic analysis over the
536 control-plane averaged concentration, the variability of τ_{pot} was a good predictor for the
537 variability in the time of electron-acceptor breakthrough. In the given example application of
538 nitrate transport, the breakthrough of elevated nitrate concentrations is largely controlled by
539 the mass of bioavailable electron donors in the matrix and the load of electron acceptors in
540 groundwater recharge, which is essentially a statement of electron balance. If the reaction
541 kinetics are slow in comparison to physical transport, the breakthrough of electron acceptors
542 will start earlier and be completed later than predicted by the cumulative reaction potential. If
543 the kinetics are comparably fast, the cumulative reaction potential marks the completion of
544 the electron-acceptor breakthrough. We have presented a way of computing the associated
545 Damköhler number. In any case, scaling of time with the cumulative reaction potential
546 significantly decreased the uncertainty in predicting solute breakthrough.

547 The computational effort to compute the cumulative reaction potential τ_{pot} is minimal.
548 For a single aquifer, the computer time needed is on the order of seconds. In the given two-
549 dimensional example, the average runtime of the spatially explicit, complex model was about
550 4.5 hours for a single realization on a standard personal computer. The runtimes for the
551 complex reactive-transport models would dramatically increase in three-dimensional
552 simulations of aquifer systems. Incorporating more processes in the detailed model (e.g.,
553 transport of microbes or competition among different microbial groups) would further
554 increase the computational effort and the number of uncertain parameters. Thus, we consider
555 analyzing the spatially explicit model by rigorous stochastic methods as unfeasible, even
556 though the uncertainty of the associated parameters would call for such an analysis. By
557 contrast, a stochastic analysis of the cumulative reaction potential τ_{pot} can be performed fast.
558 As no reaction equations are solved when evaluating τ_{pot} , no reactive parameters beyond the
559 stoichiometry are needed and no knowledge about their non-uniform distribution is

560 necessary. Instead only the travel time and the distribution of a reaction partner in the aquifer
561 matrix is necessary for the calculation of the cumulative reaction potential. The travel time
562 can be easily obtained by simple particle tracking, also on the aquifer scale in three-
563 dimensional domains, which may be further expedited by performing the particle tracking on
564 the graphics processing unit of a computer (e.g., Loschko et al., 2016). If no numerical model
565 is available, travel time distributions can often be estimated or are known from tracer tests.

566 In addition, the content of organic carbon, or other relevant reaction partners in the
567 aquifers matrix, is needed to compute the cumulative reaction potential τ_{pot} . In our example
568 calculation we assumed an anti-correlation of hydraulic conductivity and NOM content of the
569 aquifer based on the reasoning that the fines of the aquifer material typically contain more
570 organic carbon than the coarse material. While this anti-correlation influences the mean value
571 and spread of the cumulative reaction potential (see Cvetkovic et al., 1998 for first-order
572 expressions in stationary fields) it does not affect the overall principle of the approach.

573 If distributions of travel time and NOM content can be estimated, and correlations
574 among them are neglected, the cumulative reaction potential can be computed without any
575 numerical model at all. Average concentrations are often easier to predict than spatially
576 explicit NOM fields. A mean value for a sedimentary layer may be a good estimate. By
577 estimating a distribution of NOM content, there is no need to spatially resolve the
578 geochemical heterogeneity, which was identified as one of the limiting factors of numerical
579 models, as data about the chemical heterogeneity of aquifers are often scarce. Without any
580 numerical model we were able to predict the cumulative distribution function (*cdf*) of the
581 cumulative reaction potential relatively well compared to the full spatially explicit model.
582 Our proposed approach is extremely fast and easy to compute and can be seen as a quick first
583 estimate of the lasting reaction potential of an aquifer. With the cumulative reaction potential
584 time, the “load to come” can be accounted for when making policy decisions. However, our

585 results indicate that the cumulative reaction potential marks the time of total breakthrough,
586 which is not when the breakthrough starts. For realistic cases of high Damköhler numbers, we
587 recommend a safety factor of two in the assessment of nitrate breakthrough. Note that travel
588 times and concentrations of NOM or any other reaction partners are also necessary for other
589 models, including spatially explicit models and travel-time based models.

590 In reality, the reactions of dissolved oxygen and nitrate with an electron donor provided
591 by the matrix are of course not instantaneous. Reaction kinetics smear out the electron-
592 acceptor fronts and the competition between oxygen and nitrate lead to a separation of fronts
593 on the local scale. In particular, there is an earlier rise of the nitrate concentration than
594 predicted by τ_{pot} and a long tail. If the target quantity is not the first arrival of nitrate but a
595 significant breakthrough, the cumulative reaction potential is a conservative estimation for
596 breakthrough and the “load to come” and can serve as a predictive tool for management
597 implications.

598 In this work we performed all simulations using a rather small virtual test aquifer. This
599 had two reasons. First, the computational effort of the spatially explicit model is reduced, and
600 second, the results are more illustrative than this would be the case for a three-dimensional
601 model. However, evaluating the cumulative reaction potential for a large scale, three
602 dimensional model is not a challenge as no (reactive) transport model needs to be set up. All
603 that is needed is a velocity field to do particle tracking and the spatial distribution of the
604 reaction partner in the matrix. Even if one of them is not present, we showed a possibility to
605 calculate the cumulative reaction potential without any numerical model at all by using *cdfs*
606 of travel time and the distribution of the reaction partner in the matrix.

607 Our approach relies on the assumption of steady state flow. As the cumulative reaction
608 potential is meant for catchment scale applications with a run time of several years to
609 decades, this assumption is justifiable.

610 In our application we considered organic carbon as electron donor in the matrix.
611 However, other electron donors might be present (such as pyrite or biotite) that can be
612 utilized in denitrification. For the purpose of computing τ_{pot} , all bioavailable electron donors
613 would be added up. Therefor the choice of a different electron donor will not limit the
614 applicability of the method presented. Finally, we have restricted our analysis to the saturated
615 zone of an aquifer. Coupled water, carbon, and nitrogen cycling in the active soil zone is
616 more complex, and need to be addressed by models including more feedbacks.

617 The cumulative reaction potential τ_{pot} does not replace a working numerical model as its
618 validity is limited to the decreasing reaction potential. However, the concept is a quick and
619 easy to implement tool for the estimation of the lasting decreasing reaction potential of an
620 aquifer undergoing contaminant loading by groundwater recharge. We see the biggest
621 advantage of our proposed approach that the cumulative reaction potential can be calculated
622 without solving any numerical or reactive models at all. Distributions of travel times and
623 organic carbon content (or other electron donors) are sufficient to calculate the τ_{pot} . The
624 cumulative reaction potential can serve as an important and valuable tool for water suppliers,
625 consultants and other stakeholders to quickly estimate the lasting time of the natural
626 denitrification potential of groundwater aquifers and prevent them from a rude awakening.

627 **Acknowledgements**

628 This research was funded by the Deutsche Forschungsgemeinschaft (DFG) in the framework
629 of the International Research Training Group GRK1829 “Integrated Hydrosystem
630 Modelling” of the Universities of Tübingen, Hohenheim, and Waterloo. Additional funding is

631 provided by DFG within the Collaborative Research Center SFB 1253 “CAMPOS -
632 Catchments as Reactors”.

633 **References**

- 634 Atchley, A.L., R.M. Maxwell, and A.K. Navarre-Sitchler (2013), Using streamlines to
635 simulate stochastic reactive transport in heterogeneous aquifers: Kinetic metal release
636 and transport in CO₂ impacted drinking water aquifers, *Advances Water Resour.*, 52, 93–
637 106, doi:10.1016/j.advwatres.2012.09.005.
- 638 Avnimelech, Y., G. Ritvo, L. Meijer, and M. Kochba, Water content, organic carbon and dry
639 bulk density in flooded sediments, *Aquacult. Eng.*, 25, 25-33, doi:10.1016/S0144-
640 8609(01)00068-1
- 641 Cirpka, O.A., E.O. Frind, and R. Helmig (1999a), Streamline-oriented grid generation for
642 transport modelling in two-dimensional domains including wells, *Advances Water*
643 *Resour.*, 22(7), 697–710, doi:10.1016/S0309-1708(98)00050-5.
- 644 Cirpka, O.A., E.O. Frind, and R. Helmig (1999b), Numerical methods for reactive transport
645 on rectangular and streamline-oriented grids, *Advances in Water Resources*, 22(7), 711–
646 728, doi:10.1016/S0309-1708(98)00051-7.
- 647 Cirpka, O.A., P.K. Kitanidis (2000), An advective-dispersive streamtube approach for the
648 transfer of conservative tracer data to reactive transport, *Water Resour. Res.*, 36(5),
649 1209-1220.
- 650 Cvetkovic, V., H. Cheng, and X.-H. Wen (1996), Analysis of nonlinear effects on tracer
651 migration in heterogeneous aquifers using lagrangian travel time statistics, *Water Resour.*
652 *Res.*, 32(6), 1671–1680, doi:10.1029/96WR00278.

- 653 Cvetkovic, V., G. Dagan, and H. Cheng (1998), Contaminant transport in aquifers with
 654 spatially variable hydraulic and sorption properties, *Proc. Royal Soc. A - Math. Phys.*
 655 *Eng. Sci.*, 454(1976), 2173–2207, doi:10.1098/rspa.1998.0254.
- 656 Diem, S., O.A. Cirpka, and M. Schirmer (2013), Modeling the dynamics of oxygen
 657 consumption upon riverbank filtration by a stochastic–convective approach, *J. Hydrol.*,
 658 505, 352–363, doi:10.1016/j.jhydrol.2013.10.015.
- 659 Feyen, J., D. Jacques, A. Timmerman, and J. Vanderborght (1998), Modelling water flow and
 660 solute transport in heterogeneous soils: A review of recent approaches, *J. Agric. Eng.*
 661 *Res.*, 70(3), 231–256, doi:10.1006/jaer.1998.0272.
- 662 Foth, H.D., et al. (1991), *Fundamentals of soil science.*, Ed. 8, John Wiley and Sons, Inc.
- 663 Frind, E.O., and G.B. Matanga (1985), The dual formulation of flow for contaminant
 664 transport modeling 1. review of theory and accuracy aspects, *Water Resour. Res.*, 21(2),
 665 159–169, doi:10.1029/WR021i002p00159.
- 666 Galloway, J. N., F. J. Dentener, D. G. Capone, E. W. Boyer, R. W. Howarth, S. P. Seitzinger,
 667 G. P. Asner, C. Cleveland, P. Green, E. Holland, et al. (2004), Nitrogen cycles: past,
 668 present, and future, *Biogeochem.*, 70(2), 153–226, doi:10.1007/s10533-004-0370-0.
- 669 Ginn, T.R. (2001), Stochastic-convective transport with nonlinear reactions and mixing: finite
 670 streamtube ensemble formulation for multicomponent reaction systems with intra-
 671 streamtube dispersion. *J. Contam. Hydrol.* 47(1-2), 1-28, doi: 10.1016/S0169-
 672 7722(00)00167-4.
- 673 Ginn, T.R., C.S. Simmons, B.D. Wood (1995), Stochastic-convective transport with
 674 nonlinear reaction: biodegradation with microbial growth. *Water Resour. Res.* 31 (11),
 675 2689-2700, doi: 10.1029/95WR02179

- 676 Goode, D. J. (1996), Direct simulation of groundwater age. *Water Resour. Res.* 32(2), 289-
677 296, doi: 10.1029/95WR03401.
- 678 Hickel, W., P. Mangelsdorf, and J. Berg (1993), The human impact in the german bight:
679 Eutrophication during three decades (1962–1991), *Helgoländer Meeresuntersuchungen*,
680 47(3), 243, doi:10.1007/BF02367167.
- 681 Knowles, R. (1982), Denitrification., *Microbiol. Rev.*, 46(1), 43–70.
- 682 Korom, S. F. (1992), Natural denitrification in the saturated zone: a review, *Water Resour.*
683 *Res.*, 28(6), 1657–1668, doi:10.1029/92WR00252.
- 684 Lohse, K. A., P. D. Brooks, J. C. McIntosh, T. Meixner, and T. E. Huxman (2009),
685 Interactions between biogeochemistry and hydrologic systems, *Ann. Rev. Environ.*
686 *Resour.*, 34, 65–96, doi:10.1146/annurev.enviro.33.031207.111141.
- 687 Loschko, M., T. Wöhling, D.L. Rudolph, and O.A. Cirpka (2016), Cumulative relative
688 reactivity: A concept for modeling aquifer-scale reactive transport, *Water Resour. Res.*,
689 52(10), 8117–8137, doi:10.1002/2016WR019080.
- 690 Loschko, M., T. Wöhling, D.L. Rudolph, and O.A. Cirpka (2018), Accounting for the
691 decreasing reaction potential of heterogeneous aquifers in a stochastic framework of
692 aquifer-scale reactive transport, *Water Resour. Res.*, 54(1), 442–463,
693 doi:10.1002/2017WR021645.
- 694 Nieuwenhuize, J., Y. Maas, and J. Middelburg, Rapid analysis of organic carbon and nitrogen
695 in particulate materials, *Marine Chem.*, 45, 217-224, doi: 10.1016/0304-4203(94)90005-
696 1

- 697 Ocampo, C.J., C.E. Oldham, and M. Sivapalan (2006), Nitrate attenuation in agricultural
698 catchments: Shifting balances between transport and reaction, *Water Resour. Res.*, 42(1),
699 doi:10.1029/2004WR003773.
- 700 Pacheco, J., L. Marín, A. Cabrera, B. Steinich, and O. Escolero (2001), Nitrate temporal and
701 spatial patterns in 12 water-supply wells, yucatan, mexico, *Environ. Geol.*, 40(6), 708–
702 715, doi:10.1007/s002540000180.
- 703 Puckett, L. J., A. J. Tesoriero, and N. M. Dubrovsky (2010), Nitrogen contamination of
704 surficial aquifers - a growing legacy, *Environ. Sci. Technol.*, 45 (3), 839–844,
705 doi:10.1021/es1038358.
- 706 Rubin, Y., M. Cushey, and A. Bellin (1994), Modeling of transport in groundwater for
707 environmental risk assessment, *Stoch. Hydrol. Hydraulics*, 8(1), 57–77,
708 doi:10.1007/BF01581390.
- 709 Sanz-Prat, A., C. Lu, M. Finkel, and O.A. Cirpka (2015), On the validity of travel-time based
710 nonlinear bioreactive transport models in steady-state flow, *J. Contam. Hydrol.*, 175, 26-
711 43, doi: 10.1016/j.jconhyd.2015.02.003.
- 712 Sanz-Prat, A., C. Lu, R.T. Amos, M. Finkel, D.W. Blowes, and O.A. Cirpka (2016),
713 Exposure-time based modeling of nonlinear reactive transport in porous media subject to
714 physical and geochemical heterogeneity, *J. Contam. Hydrol.*, 192, 35-49, doi:
715 10.1016/j.jconhyd.2016.06.002.
- 716 Schultz, M.K., S. Biegalski, K. Inn, L. Yu, W. Burnett, J. Thomas, and G. Smith (1999),
717 Optimizing the removal of carbon phases in soils and sediments for sequential chemical
718 extractions by coulometry, *J. Environ. Monit.*, 1, 183-190, doi: 10.1039/A900534J

- 719 Shapiro, A.M., and V.D. Cvetkovic (1988), Stochastic analysis of solute arrival time in
720 heterogeneous porous media, *Water Resour. Res.*, 24(10), 1711–1718,
721 doi:10.1029/WR024i010p01711.
- 722 Simmons, C. S., T. R. Ginn, and B. D. Wood (1995), Stochastic-convective transport with
723 non-linear reaction: Mathematical framework, *Water Resour. Res.*, 31(11), 2675–2688,
724 doi: 10.1029/95WR02178.
- 725 Skerman, V., and I. MacRae (1957), The influence of oxygen availability on the degree of
726 nitrate reduction by *seudomonas denitrificans*, *Can. J. Microbiol.*, 3(3), 505–530,
727 doi:10.1139/m57-055.
- 728 Smolders, A. J., E. C. Lucassen, R. Bobbink, J. G. Roelofs, and L. P. Lamers (2010), How
729 nitrate leaching from agricultural lands provokes phosphate eutrophication in
730 groundwater fed wetlands: the sulphur bridge, *Biogeochem.*, 98(1-3), 1–7,
731 doi:10.1007/s10533-009-9387-8.
- 732 Strebel, O., W. Duynisveld, and J. Böttcher (1989), Nitrate pollution of groundwater in
733 western europe, *Agr. Ecosyst. Environ.*, 26(3-4), 189–214, doi:10.1016/0167-
734 8809(89)90013-3.
- 735 Todorovic, P. (1970), A stochastic model of longitudinal diffusion in porous media, *Water*
736 *Resour. Res.*, 6(1), 211–222, doi:10.1029/WR006i001p00211.
- 737 Van Kessel, J. (1978), Gas production in aquatic sediments in the presence and absence of
738 nitrate, *Water Res.*, 12(5), 291–297.
- 739 Vant, W., and P. Smith (2004), *Nutrient concentrations and water ages in 11 streams flowing*
740 *into Lake Taupo* (Revised), Technical Report 2002/18R, Environment Waikato,
741 Ngaruawahia, New Zealand.

- 742 Vero, S. E., N.B. Basu, K. van Meter, K.G. Richards, P.-E. Mellander, M.G. Healy, and O.
743 Fenton (2018), the environmental status and implications of the nitrate time lag in
744 Europe and North America, *Hydrogeol. J.*, 26(1), 7–22, doi:10.1007/s10040-017-1650-9.
- 745 Wakida, F.T., and D.N. Lerner (2005), Non-agricultural sources of groundwater nitrate: a
746 review and case study, *Water Res.*, 39(1), 3–16, doi:10.1016/j.watres.2004.07.026.
- 747 Ward, M. H., et al. (2005), Workgroup report: drinking-water nitrate and health - recent
748 findings and research needs, *Environ. Health Persp.*, 113(11), 1607,
749 doi:10.1289/ehp.8043.
- 750 Weyer, P.J., J.R. Cerhan, B.C. Kross, G.R. Hallberg, J. Kantamneni, G. Breuer, M.P. Jones,
751 W. Zheng, and C.F. Lynch (2001), Municipal drinking water nitrate level and cancer risk
752 in older women: the iowa women’s health study, *Epidemiology*, 12(3), 327–338,
753 doi:10.1097/00001648-200105000-00013.
- 754 Wisotzky, F. (2012), *Angewandte Grundwasserchemie, Hydrogeologie und*
755 *hydrogeochemische Modellierung: Grundlagen, Anwendungen und Problemlösungen,*
756 Springer-Verlag, Heidelberg, doi:10.1007/978-3-642-17813-9.
- 757 Wolfe, A.H., and J.A. Patz (2002), Reactive nitrogen and human health: acute and long-term
758 implications, *AMBIO*, 31(2), 120–125, doi:10.1579/0044-7447-31.2.120.